Development and Characterization of Recyclable Elastomers via Covalent Adaptable Network

by

Maher Abdulrahman Alraddadi

A thesis submitted to the University of Birmingham for the degree of

Doctor of Philosophy

School of Chemistry

College of Engineering and Physical Sciences

University of Birmingham

February 2023

ABSTRACT

The inherently high strength, thermal and solvent stability of thermoset is a consequence of the permanent crosslinking between the polymer chains. However, this permanent crosslink is a doubtful advantage; it does provide strength and thermal stability to the polymeric material, but it also makes the material so thermally stable that it cannot be thermally reprocessed. As a result, new type of crosslink has been developed and implemented into polymeric materials, namely dynamic covalent bonding. The use of dynamic covalent bonds in the crosslinking of polymeric material provides the highly sought-after strength, thermal and solvent resistance as a consequence of crosslinking the chains. Furthermore, the dynamic nature of these crosslinks is added to the reprocessability feature to the polymeric materials as a result of the chemically reversible exchange of these bonds. Ultimately, the implementation of the dynamic bond into the crosslinking of polymers create another type of polymer network that are responsive to their environment, commonly known as covalent adaptable networks (CANs).

CANs have been implemented widely to improve some polymer networks properties such as reprocessability, recyclability, and self-healability. However, there is still room for improvement in the field of CANs, especially in tuning their mechanical properties *i.e*., improving tensile strength and elongation while maintaining good dynamicity. In this the dissertation, a fundamental study of the dynamicity of thiol-yne based small molecule models was executed. Furthermore, novel CANs with controllable thermomechanical properties were successfully synthesised and characterised.

Finally, a series of novel bio-based CANs with tunable thermomechanical properties were also successfully synthesised and characterised.

ACKNOWLEDGEMENTS

First and foremost, I would like to express my deepest gratitude to Allah subhanahu wa ta'ala (SWT) for his uncountable blessings.

I can’t thank enough my supervisor Professor Andrew Dove for all his guidance and support. I’m thankful for all the opportunities you gave me to improve my scientific and leadership skills. I’m really honoured to be in your research group and to work closely with you.

I must also thank the Royal Commission for Jubail and Yanbu for funding my PhD.

Next, I would like to thank all my friends and colleagues from both Dove and O’Reilly group. Special thanks to Dr. Josh C. Worch, Bossman. I really appreciate your mentorship. You were always there advising and helping me improve both my technical and theoretical knowledge throughout my PhD journey.

Special thanks go to Dr. Viviane Chiaradia the “full of life” and Dr. Natalia Reis for your professional proofreading of my work, Dr. Connor Stubbs and Ms. Anissa Khalfa for all the lab support and Pleasant chat, Ms. Ana Àlvarez for being very kind with everyone and for all the well-deserved coffee breaks with “full of life”, Dr. Cinzia Clamor I will always remember your help and support especially when I first arrived to the group, Mr. Lukmanul Samada for his support and enjoyable chats, Dr. Marjolaine Thomas for spreading positive vibes wherever you go. I would also like to thank Ms. Tessa Kintail

for being the contact point to solving all my admin issues, Ms. Julia Valverde for your friendship and for being the contact point for many lab issues.

Finally, I want to express my deepest appreciation to my parents for your unconditional love and invaluable support and encouragement. To my brothers and sisters, thank you for being the best siblings ever, I know you all missed me as much I do. Lastly, none of these would happen without my wife, Maria, who takes good care of me and our kids. You are truly behind all the achievements we have. Your love, supports, and encouragements make my entire life much happier and easier. Of course, I can't forget to thank my sons Abdulrahman and Kenan, my best buddies, for being patient with me during my tough and busy time and for being such a wonderful and talented kids.

TABLE OF CONTENTS

LIST OF FIGURES

LIST OF TABLES AND EQUATIONS

LIST OF ABBREVIATIONS

3-D	3 dimensional
CAN	Covalent adaptable network
$CDCl_3$	Deuterated chloroform
cm	Centimeter
d	doublet
DBU	1,8-diazabicyclo[5.4.0]undec-7-ene
DCC	dynamic covalent chemistry
DCM	Dichloromethane
DCvC	Dynamic covalent chemistry
DEA	Diethylamine
DMA	Dynamic mechanical analysis
DMAP	4-dimethylaminopyridine
DMPP	Dimethylphenylphosphine
DMSO-d_6	Deuterated dimethylsulfoxide
DSC	Differential Scanning Calorimetry
E	Young’s modulus

E’	Storage modulus (in longitudinal deformation)
E”	Loss modulus (in longitudinal deformation)
ESI MS	Electrospray ionisation mass spectrometry
Et	Ethyl
EtOAc	Ethyl acetate
FT-IR	Fourier-transform infrared
G’	Shear Storage modulus
G”	Shear Loss modulus
GC-MS	Gas chromatography mass spectrometry
HA	Hexylamine
HDPE	High density polyethylene
J	Joule
kPa	Kilopascals
LDPE	Low density polyethylene
m	meter
$MgSO_4$	Magnesium sulfate
MIM	1-methylimidazole
mm	Millimeter
MPa	Megapascals

mW	Milliwatt
N	Newtons
NMM	N-methyl morpholine
NMR	Nuclear magnetic resonance
Pa	Pascals
pH	Potential hydrogen
q	quartet
qu	quintet
ROP	Ring-opening polymerization
s	singlet
SBS	Poly(styrene-butadiene-styrene)
t	triplet
tan δ	The tangent of the phase angle (δ)
T_c	Crystallisation Temperature
TEA	Triethylamine
T_g	Glass Transition Temperature
THF	Tetrahydrofuran
T_m	Melting Transition Temperature
U_T	Toughness

UTS	Ultimate tensile strength
UV	Ultraviolet
v/v %	Volume percentages of two components
δ	Chemical shift
ΔH_c	Enthalpy of crystallisation
ΔH_m	Enthalpy of melting
ε	Elongation
ε_b	Elongation at break
μ	Viscosity
σ	Uniaxial stress
τ	Shear stress

LIST OF LESS COMMON NOMENCLATURE

Name	Generic Structure
Ynone	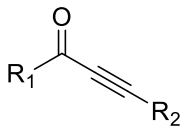
Enone	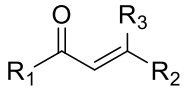
Thiyl	
Thiolate	
Gutta-Percha (trans-1,4-polyisoprene)	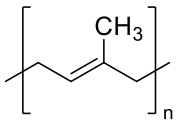
Natural rubber (cis-1,4-polyisoprene)	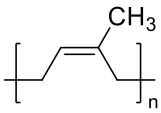
β-sulfido-α,β-unsaturated carbonyl	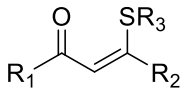
Lipoic acid	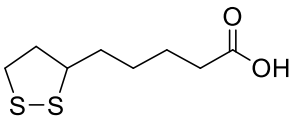
1-Ethyl-3-(3-dimethylaminopropyl)carbodiimide (EDC)	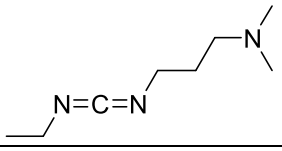

LIST OF PUBLICATIONS

1. **Maher A Alraddadi**, Viviane Chiaradia, Connor J Stubbs, Joshua C Worch, Andrew P Dove, Renewable and recyclable covalent adaptable networks based on bio-derived lipoic acid, *Polym. Chem.*, (2021),12, 5796-5802

2. Ivan Djordjevic, Gautama Wicaksono, Juhi Singh, Manisha Singh, Elizabeth G Ellis, **Maher A Alraddadi**, Andrew P Dove, Terry WJ Steele, Hybrid polymer networks of carbene and thiol ene, *Eur. Polym. J.*, (2022) 178, 111502

DECLARATION OF AUTHORSHIP

This thesis is submitted to the University of Birmingham in support of my application for the degree of Doctor of Philosophy. The material contained in this thesis has not been submitted in any previous application for any degree at any institute.

Parts of this thesis have been published as open access articles in peer-reviewed journal or are displayed in a format suitable for publication in peer-reviewed journal, as outlined in the University of Birmingham alternative thesis format guidelines. The work presented in this thesis (including data generated and data analysis, materials characterisation, writing and figure design) was performed by myself, except for co-author contributions which are outlined below and before each chapter.

Chapter 2 - Manuscript Prepared: Maher A. Alraddadi, Joshua C. Worch, Andrew P. Dove, Super tough and reprocessable elastomers based on thiol-yne covalent adaptable networks, *Manuscript Prepared.*

Dr Josh Worch (University of Birmingham) provided technical and synthetic guidance and editing of this manuscript. Prof. Andrew P. Dove (University of Birmingham) supervised in addition to providing guidance and editing the manuscript.

Chapter 3 - Manuscript Prepared: Maher A. Alraddadi, Joshua C. Worch, Andrew P. Dove, Using composition to tune thermomechanical properties of thiol-yne covalent adaptable networks, *Manuscript Prepared.*

Dr Josh Worch (University of Birmingham) provided technical and synthetic guidance and editing of this manuscript. Prof. Andrew P. Dove (University of Birmingham) supervised in addition to providing guidance and editing the manuscript.

Chapter 4 - Reprinted with permission from: Maher A. Alraddadi‡, Viviane Chiaradia‡, Connor J. Stubbs, Joshua C. Worch and Andrew P. Dove, Renewable and recyclable covalent adaptable networks based on bio-derived lipoic acid

‡denotes equal contribution

Dr. Connor J. Stubbs (University of Birmingham) performed TGA and FTIR analysis. Dr. Viviane Chiaradia (University of Birmingham) synthesised the networks and performed rheology, DSC, and tensile experiments. Dr. Josh C. Worch (University of Birmingham) and Prof. Andrew P. Dove (University of Birmingham) conceived the material synthesis and designed the project idea. The manuscript was written through contributions of J. C. W and A. P. D.

CHAPTER 1: INTRODUCTION

1.1 Polymer structure-property relationships

Polymers, which are well-known large molecules that are built up by chemically bonded smaller molecules known as monomers, are used as dominant materials in many industries. The extensive industrial use of polymers is a consequence of their versatile properties and low cost, allowing them to be used in widespread application.

In contrast to other materials, most polymers have tuneable and “custom-made” properties, especially thermomechanical properties like thermal processability, stiffness, and strength. When tailoring such properties to specific applications, the interaction between the polymer chains needs to be considered carefully, as it will greatly affect these properties.[1] For example, increasing the degree of branching in the polymer chains, at constant molecular weight, will increase the free volume, which is the empty space between chains. Consequently, this will increase the freedom of movement (chains mobility) which decreases the thermal transition temperature and stiffness of the polymer.[2] In contrast, linear polymer chains with no branching tend to cause an increase in packing of polymer chains which reduce the mobility of the chains, increases the chance of crystallinity, and increases the overall stiffness of the polymer. The chain packing effect can be seen clearly in polyethylenes, where the low-density polyethylene (LDPE) has a lower thermal transition temperature than its functionally analogous high-density polyethylene (HDPE) as a consequence of the higher degree of branching in LDPE.[3, 4] Similarly, increasing the chance of cross-linking the polymer chains lead to restricting the mobility of polymer chains and increase the thermal transition and stiffness of the polymer.[5, 6]

Likewise, the choice of the monomers (building blocks) and their compositions should also be considered since it controls the type of interactions between polymer chains and their significance. For example, the use of polymers containing aliphatic carbon-carbon double bond as opposed to fully saturated polymer is believed to increase the stiffness and thermal transition temperature of the polymer as a consequence of the higher internal rotation barrier at the molecular level for the unsaturated monomer restricting the polymer chains flexibility.[7] On the other hand, the use of a monomer that contains etheric carbon-oxygen bond (flexible group) is known to reduce the stiffness and lower the thermal transition of a polymer as a consequence of the effect of the carbon-oxygen bond which work as a swivelling group promoting torsional mobility to the polymer chains.[8, 9] This fundamental understanding of polymer structure-property relationship has led to many innovative contributions, especially to the field of polymer sustainability.

Polymers have been classified under different categories as a consequence of their complex structure, applications, and behaviours. For example, Polymers have been classified based on their source of availability, structure, type of polymerisation, and others. However, the most common and simple classification of polymers is based on the polymer structure, polymers are conventionally classified as linear polymers (thermoplastics) or cross-linked polymers (thermosets).

1.2 Thermoplastics and Thermosets

Thermoplastics consist of linear “uncross-linked” polymeric chains. The lack of cross-linking allows these linear chains to slide freely past each other upon heating to a specific temperature. This free movement of individual chain causes an overall reduction of the material’s viscosity (μ), and the material will eventually flow physically.[10] The flow behaviour of thermoplastic polymers does not involve any chemical reactions, and it is the most significant advantage of thermoplastic over thermoset polymers. Indeed, the fact that these materials can flow upon exposure to sufficient heat makes them reprocessable, reshapable, and recyclable.

On the other hand, thermosets consist of a 3-dimensional network where the linear chains are permanently cross-linked to each other by covalent bonds. The cross-liking of the polymeric chains renders the thermosets valuable properties like solvent resistance and thermal stability.

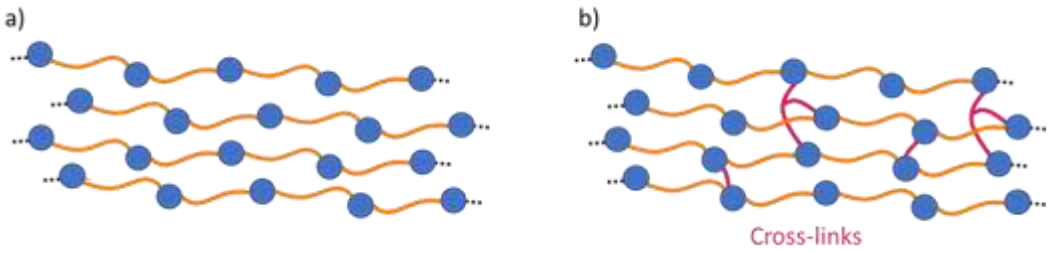

Figure 1.2.1 Illustration of a) linear polymer chains of thermoplastic b) 3-D cross-linked structure of thermosets.

The thermal stability of thermoset materials, which is conferred by the covalent networks, prevents a significant reduction of the material’s viscosity (μ) and hence they can’t be thermally reprocessed. This resistance to flow is one of the major drawbacks of thermoset polymers, as they cannot be thermally reprocessed even at high

temperatures, as the polymer degrades. To overcome these challenges, new types of cross-links are being investigated.

Table 1 Summary of the most important properties differences between thermoplastics and thermosets.

Table 1 Properties comparison between thermoplastics and thermosets

Properties	**Thermoplastics**	**Thermosets**
Thermal stability	Low	High thermal resistance, the presence of cross-links prevents flowing and melting
Solvent resistance	Soluble in a good solvent.	Insoluble, showed swelling behaviour in a good solvent
Fatigue resistance	Low resistance to repetitive deformation	Good
Creep resistance	Low	High
Recyclability	Easier - lower thermal and solvent resistance	Difficult because of the high solvent and thermal resistance.

1.3 Dynamic Covalent Chemistry

The need to improve the recyclability of polymers, especially thermosets, has initially led to the use of dynamic non-covalent bonds in polymeric materials, also called supramolecular polymers, to furnish the highly sought-after properties like self-healability and reprocessability. However, the dynamic nature of the supramolecular polymers makes them unstable and susceptible to the environment, which impedes them from being used in some applications where robustness and stability are required.[11] As a result, dynamic covalent chemistry (DCvC) was evolved to fulfil the requirement of robustness and stability in polymers while maintaining controllable dynamicity.[12] Unlike supramolecular systems, which are based on the dynamicity of "weak" non-covalent bonding, dynamic covalent chemistry is based on covalent bonding, which renders the system the robustness and stability required. Furthermore, these covalent bonds are dynamic and may undergo reversible reactions over time or upon exposure to the right stimuli i.e. light, heat, and others.[13-15]

The dynamic behaviour in polymer networks was reported by pioneering works of Tobolsky's research group in mid 1940s.[16] They discovered an unusual stress relaxation of polysulfide cross-linked rubbers during their study of the viscoelasticity of rubber. Even though this observation was a phenomenal theoretical discovery, it is only recently that this concept received attention in the literature as a result of the need to improve the sustainability of polymeric materials, especially thermosets. This interest has led to re-implementing DCvC into polymer networks as an inevitable consequence of the development of the chemistries and characterisation techniques of DCvC.[17] Consequently, reversible networks were brought to light again, often referred to as covalent adaptable networks (CANs).

1.4 Covalent Adaptable Networks (CANs)

CANs were first defined by Bowman and co-workers as the networks that contain enough number and topology of dynamic “reversible” covalent bonds, which makes the network structure chemically responsive to an applied stimulus.[18] As the cross-linking enhances the polymeric material’s strength and solvent resistance, the use of CANs will also improve the strength and solvent resistance of polymeric material. On the other hand, the dynamic nature of these networks promotes flowability resembling thermoplastic which paves the way to reprocessability and recyclability of these networks. Furthermore, the fact that some of these dynamic bonds break and reform only in response to stimulus should provide some greatly sought-after features to these networks, like self-healability and environmental responsiveness features, which help create smart polymeric materials that are responsive to their environment.[18, 19]

1.4.1 Types of Dynamic Covalent Bonds Used in CANs

In addition to the structure-property relationships discussed above, the choice of dynamic bond and its activating stimuli is crucial for the success or failure of CANs to meet a specific requirement. For example, it is most common to trigger the dynamic reaction of hydrogels by changing the pH, temperature, light exposure, and other stimuli.[19, 20] Whereas, certain disulfide-based CANs, use only heat[21] or ultraviolet (UV)[22] to trigger the exchange. Furthermore, the type of dynamic bond plays an important role in the final thermomechanical properties of CANs as it controls the rate and mechanisms at which the dynamic reaction occurs. Generally, many types of dynamic chemistries could be used in CANs. For simplicity; however, they were conventionally been grouped into two main categories, dissociative and associative

chemistries, based on the mechanism of their dynamic reaction, Figure 1.4.1.[23] The dynamic reaction of the dissociative chemistry follows a bond-breaking, bond-forming sequence. As a result, this type of mechanism usually shows a loss in the overall cross-link density and result in reduction of the mechanical properties after reprocessing.[24-27] Examples of common dynamic chemistries that follow dissociative mechanism includes disulfides, thiol-Michael, Diels-Alder exchange, beside others.

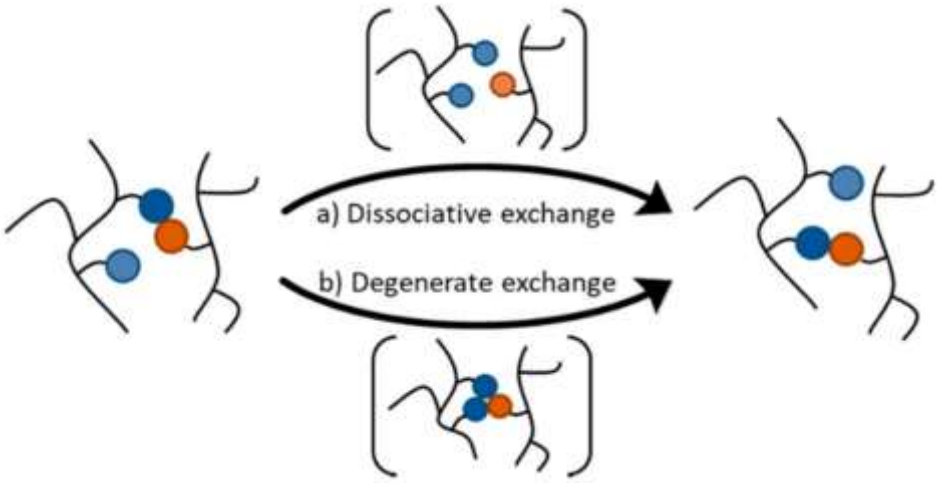

Figure 1.4.1 Dynamic bond exchange mechanisms a) Dissociative exchange: available bond is broken before new one is formed. b) Associative "degenerate" exchange: new bond is formed before existing bond is broken. Reproduced under Creative Commons Attribution License from *Polymers*, 2021, **13**, 396. Ref.26.

On the other hand, the associative mechanism follows a bond-forming, bond-breaking order, which means the overall cross-link density is maintained throughout the dynamic reaction and is sometimes referred to as reversible exchange rearrangement. As a result of preserving the cross-link density throughout the dynamic exchange, this type of mechanism tends to maintain the mechanical properties after reprocessing.[24-28] Common chemistries that follow the associative mechanism include

disulfides, thiol-thioester exchange, transesterification, and others.[19] Only relevant chemistries to the work conducted in this thesis are highlighted below.

1.4.1.1 Disulfide

Disulfide dynamic bond was heavily studied for a long time, and the thermal dynamicity of disulfide was, in the beginning, considered an unpleasant reaction that affects the thermal stability of vulcanised rubber.[19] However, in the early 1990s, Tesoro and Sastri synthesised reversible epoxy networks using a disulfide-containing cross-linker, demonstrating that the network could be broken down by reduction and then reformed by oxidation.[29] This pioneering work has led to a rapid increase in the implementation of disulfide into polymer networks. Furthermore, the versatility of the disulfide bond, which enables it to be cleaved using a variety of conditions, such as thermal scission, mechanical stresses, or photoirradiation, has also contributed to this noticeable increase in the implementation of disulfide bond in polymer networks.

Regardless of the conditions by which the cleavage occurs, disulfide cleaves into either thiolate anions or thiyl radicals, both of which are capable of participating in a molecular rearrangement.[30] In general, the mechanism at which the disulfide exchange is initiated involves three suggested pathways; disulfide homolysis (through the formation of thiyl radical), disulfide nucleophilic substitution, and disulfide metathesis, Figure 1.4.2.[31, 32] Typical reported triggers for disulfide exchange include UV light, heat, redox conditions, and others.[33-35] Furthermore, some aromatic disulfide exchanges was reported to proceed without any external stimuli at room temperature and thus are very useful for incorporating the self-healing feature into polymers.[33]

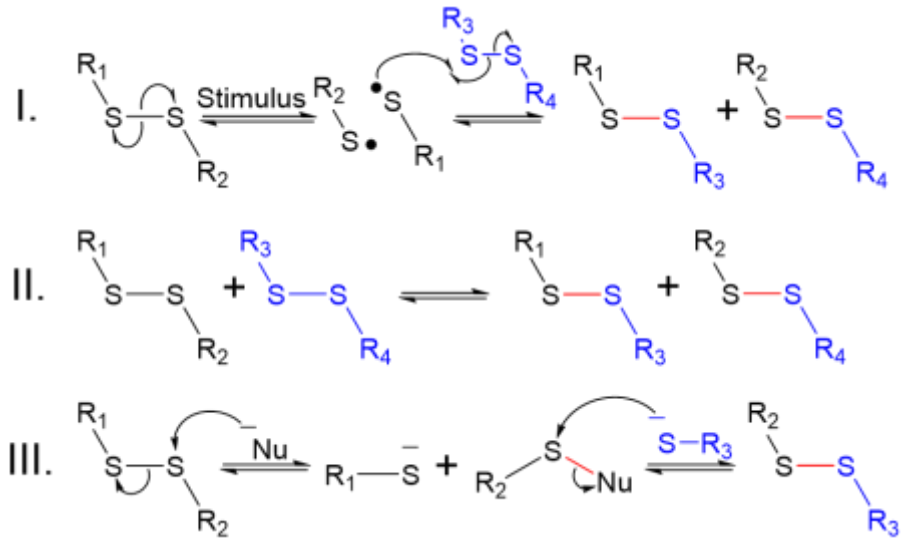

Figure 1.4.2 Disulfide dynamic exchange mechanisms I) radical pathway "homolysis cleavage". II) Metathesis exchange pathway. III) Nucleophilic exchange pathway.

Thiol-disulfide exchange is one of the most used dynamic reactions in polymer networks. The rapid interchange between thiol and disulfide happens at moderate to basic conditions (pH ≥ 7), and the formed bond is stable in acidic conditions (pH < 5). The chemoselectivity of this exchange, where only the thiol-disulfide can exchange despite of the presence of other functional groups, and the ability to perform under organic and aqueous mediums are some of the advantages of this thiol-disulfide exchange.[36, 37] The exchange is a three-step reaction where thiol first deprotonated to form a thiolate anion, the reacting species[38] that attacks the disulfide, forming a new disulfide bond and creating a new thiolate anion. Finally, the new thiolate anion attacks another disulfide and propagates the reaction, Figure 1.4.3.[39, 40]

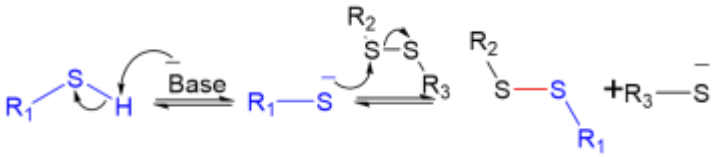

Figure 1.4.3 Thiol-disulfide dynamic exchange mechanism.

1.4.1.2 Thiol-yne Michael Adducts

Michael addition, named after Arthur Michael for his discovery of this type of addition reaction, is the 1,4-conjugate nucleophilic addition to an α,β-unsaturated carbonyl. Thia-Michael addition or Thiol-Michael addition is, therefore, the 1,4-conjugate nucleophilic addition of sulfur containing species, thiolate anion in particular (Michael donor), to alkene ketone "enone" or alkyne ketone "ynone" (Michael acceptor).[41] The dynamic nature of the thiol-Michael addition has been known since the early 1960s[42-44]; however, it has been known that the reaction required a long time to achieve equilibrium. Anslyn and co-workers have shown a faster thiol exchange in a series of small molecules of thiol-alkynone single adduct and thiol-alkynone double adducts.[45] This recent discovery has contributed to the rapid interest in the dynamicity of thiol-ene adducts, which led to the successful employment of these bonds into polymer chemistry by Konkolewicz and co-workers, Figure 1.4.4.[46, 47]

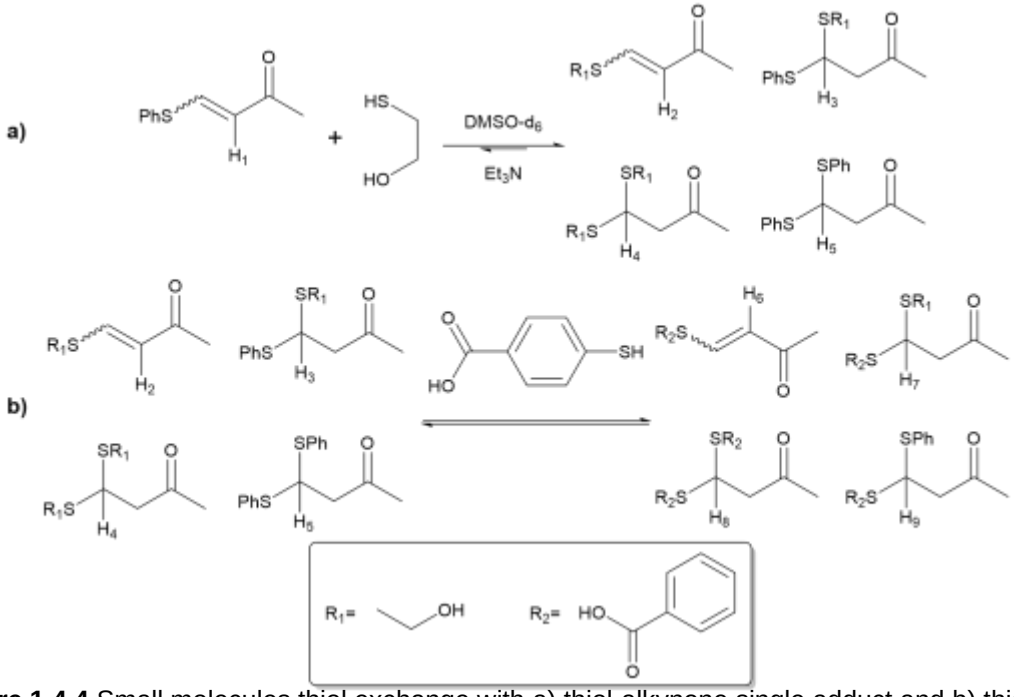

Figure 1.4.4 Small molecules thiol exchange with a) thiol-alkynone single adduct and b) thiol-alkynone double adducts. Reprinted with permission from *Org. Lett.* 2012, 14, 18, 4714-4717. Copyright 2012 American Chemical Society. Ref.45.

Even though thiol-yne Michael addition reaction is dynamic under various conditions [42, 45, 48], it has received less attention than thiol-ene reaction in the polymer field, especially in CANs. In 2020, Du prez and co-workers unprecedently explored a series of activated alkyne species used as a dynamic cross-linker that created a promising platform for designing reversible networks. [47]

1.4.2 Characterisation of CANs

Conventionally, dynamic covalent chemistries are characterised first in small molecules using techniques such as nuclear magnetic resonance (NMR), gas chromatography mass spectrometry (GC-MS), Fourier-transform infrared spectroscopy (FT-IR), and other small molecule characterisation techniques to reveal important information like the dynamicity of the bonds, functionality, thermal stability, among others. These characterisation tests are usually used when constructing the CANs to serve as a proof of concept as well as to help select the best components for CANs.[49] Subsequently, the bulk properties of CANs are characterised, such as mechanical properties, thermal transitions, rheology, dynamic mechanical analysis (DMA), and others.

1.4.2.1 Mechanical Properties

The relationship between stress and strain in a polymeric system denote its mechanical properties.[50] Since the polymeric materials are used in a wide range of applications that require specific responses to stress or strain, the mechanical properties of these systems are essential to determine their suitability for such applications. Another factor to consider when testing the quality and suitability of a

polymeric material for a certain application is the mode of the prospective applied stress or strain. Generally, two main types of stresses could be exerted on a polymeric object, namely normal or shear stress. Normal stress (σ) is the stress resulting from applying a force perpendicular to the cross-sectional area of the polymeric material. Shear stress (τ), on the other hand, is created when a force is exerted parallel to the surface of the polymeric object. It is worth mentioning that there are other stress modes like compressive, torsional, bending, tensile stress and others that consist of normal or shear stress or a combination of both, Figure 1.4.5.

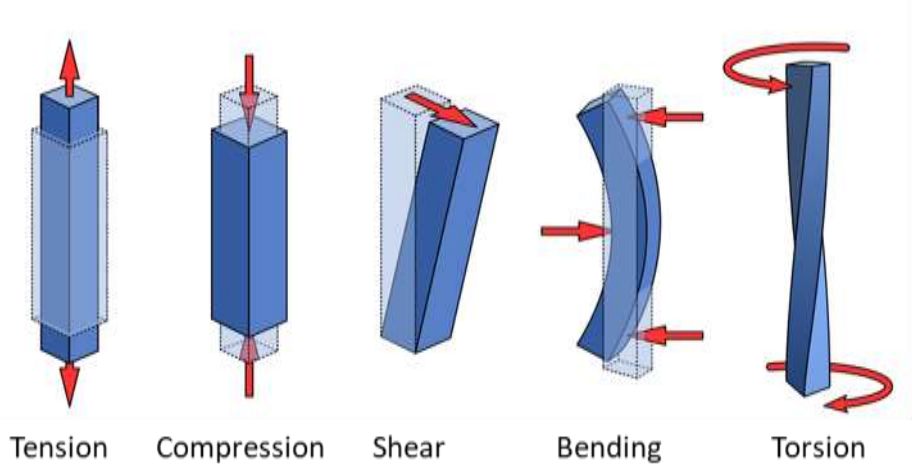

Figure 1.4.5 Illustration of the different types of mechanical stresses.

Tensile testing is an ideal method that widely used to characterise the tensile strength and overall stress-strain relationship in polymers, where a normal force is applied to a material in a tension mode. During the tensile test, a sample of polymeric material with a known dimension is placed under a determined force, and the stress that is exerted on the sample is calculated (N m^{-2} or Pascal). The strain percentage is also calculated from the sample extension by knowing the initial and final length of the material. The following are some relevant values and characteristics for the interpretation of a tensile curve (Figure 1.4.6), Equations 1.1 to 1.4:

$$\textbf{Stress}\ (\boldsymbol{\sigma}) = \frac{Force\ (N)}{Cross-sectional\ area\ (m^2)}$$

Equation 1. 1 Engineering stress is defined as the ratio the force applied to the cross-sectional area of a sample reported in N m^{-2} or pascal (Pa).

$$\textbf{Strain}\ (\boldsymbol{\varepsilon}) = \frac{Final\ length - initial\ length}{Initial\ length} \times 100$$

Equation 1. 2 Engineering strain is the change of one dimension of a sample length reported in percentage.

$$\textbf{Young's modulus}\ (\boldsymbol{E}) = \frac{Change\ in\ stress}{Change\ in\ strain}$$

Equation 1. 3 Young's Modulus, the ratio of stress to strain within the elastic proportional limit of the polymeric material reported in Pacal (Pa).

Ultimate tensile strength (UTS) is the maximum stress that a material can resist before it breaks.

Strain at break (ε_b) is the maximum strain that a sample reaches when it breaks.

$$\textbf{Toughness}\ (\mathbf{U_T}) = \int_0^{\varepsilon_b} \sigma\, d\varepsilon$$

Equation 1. 4 Toughness is the ratio of energy of the deformation to the unit volume that is required to break the material.

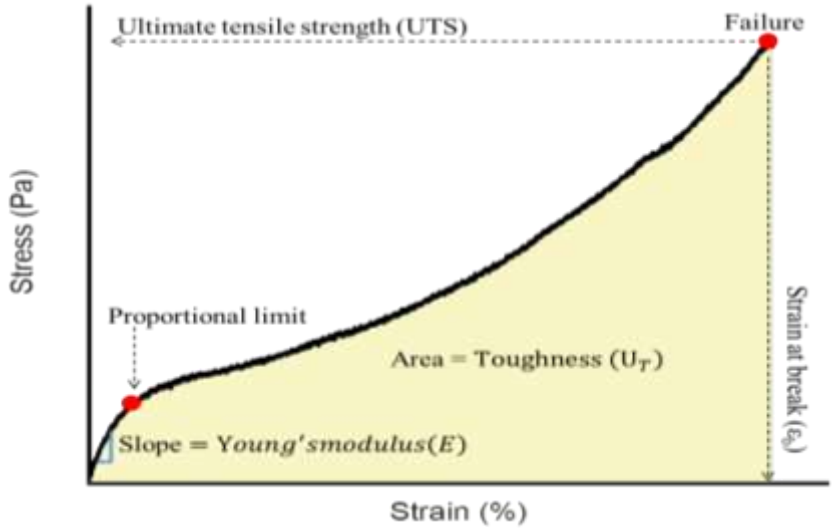

Figure 1.4.6 Illustration of typical tensile curve features and values.

1.4.2.2 Rheology and Dynamic Mechanical Properties

While a typical tensile test reveals important information about the polymer's mechanical properties, it measures the overall material response to an applied deformation. However, CANs as viscoelastic materials, consist of viscous component and elastic component, it is therefore important to have an advanced testing technique that is capable of differentiate between the responses of these two components. In fact, the ability to distinguish the response of each component, viscous and elastic component, grants a deeper understanding of the material's chemistry and microstructure.[51] Fortunately, rheology and dynamic mechanical analysis (DMA) meets these needs. Using the principle of rheology, one can separate viscous response from elastic response by applying a sinusoidal deformation to the material using either a rheometer or a dynamic mechanical analyser. The elastic component of a viscoelastic material is responsible for storing the energy of deformation elastically and is indicated by storage modulus (*G'* for shear deformation or *E'* for longitudinal deformation). On the other hand, the viscous component is responsible for dissipating the energy of deformation and is thus indicated by loss modulus (*G"* or *E"* for shear and longitudinal deformation, respectively). The ratio of loss modulus to storage modulus is called tan δ, which is an indicator of the energy dissipation potential and thus often used to identify thermal transitions such as glass transition temperature T_g.[52]

The rheometer and the DMA can also be used to find the gelation time for a polymeric resin by applying a dynamic deformation while the sample experiences a cross-linking process. The rheometer can also measure the viscosity at different shear rates. Besides their ability to perform sinusoidal deformation using a dynamic mode,

the rheometer and the DMA can be used to test single “static” normal or shear deformation like the stress relaxation of a material.

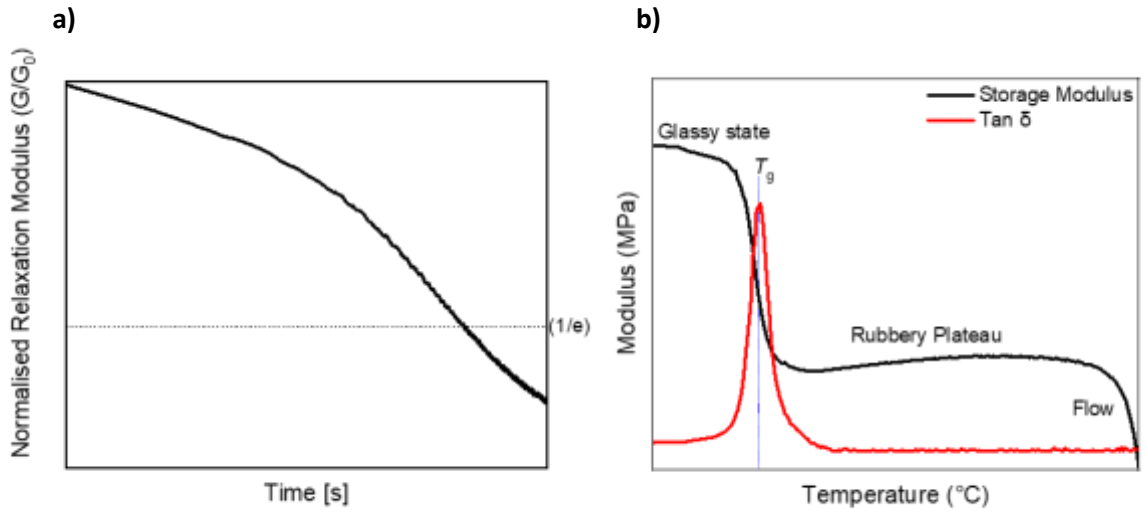

Figure 1.4.7 a) Typical stress relaxation curve for dynamic network by rheometer (static ramp). b) Typical DMA temperature sweep curve (dynamic ramp).

A stress relaxation measurement is a well-known test, especially in the field of CANs, to distinguish between dynamic and permanent cross-links and compare the dynamicity of different systems. Under constant strain and elevated temperature, permanently cross-linked polymers are thermally stable and show no relaxation or softening, while the dynamic cross-linked polymer softens and relieves the stress.[53] This macroscopic stress relaxation in CANs, which could lead to a complete flow of material, is a consequence of the microscopic molecular rearrangement caused by the thermal activation of the dynamic bonds. Thus, the ability to relieve the stress under constant strain is a key feature of CANs and an important indicator of the cross-link’s dynamicity, the more dynamic the bonds, the faster it relaxes.

1.4.2.3 Thermal Transitions

Although other instruments could measure the thermal transition of CANs (*i.e.,* DMA), differential scanning calorimetry (DSC) is a simple yet powerful instrument to identify and quantify thermal transitions in CANs. The DSC instrument heats two pans, one empty used as a reference and another with the desired sample and maintain a constant heat rate. The thermal transitions are identified by the change in the heat consumption of the sample pan as a consequence of the change in the heat capacity of the sample.[54] Furthermore, the magnitude of the transition could be quantified by integrating the area under the transition peak, which represents the amount of latent heat or the enthalpy (ΔH), the energy used to change the phase of the material without changing the material's temperature.[55, 56] Melting transition temperature (T_m), as a first-order transition, involving both latent heat and a change in the heat capacity of a sample, is often observed in a crystalline or semi-crystalline CANs. Another first-order transition observed in CANs is crystallisation temperature (T_c) which is not suitable for diagnosing the crystallinity of CANs since it mainly depends on the cooling rate.[57]

A second-order transition detected by DSC is the glass transition temperature (T_g), involving only change in the heat capacity of the sample with no latent heat observed. It is associated with the amorphous region of the polymeric material; thus, it is observed only on the amorphous or semi-crystalline material. T_g is the temperature at which the material changes from a glassy and rigid material to a soft and rubbery like material. As a result, it is one of the most important parameters used to identify suitable application and service temperature of a polymeric material, Figure 1.4.8.

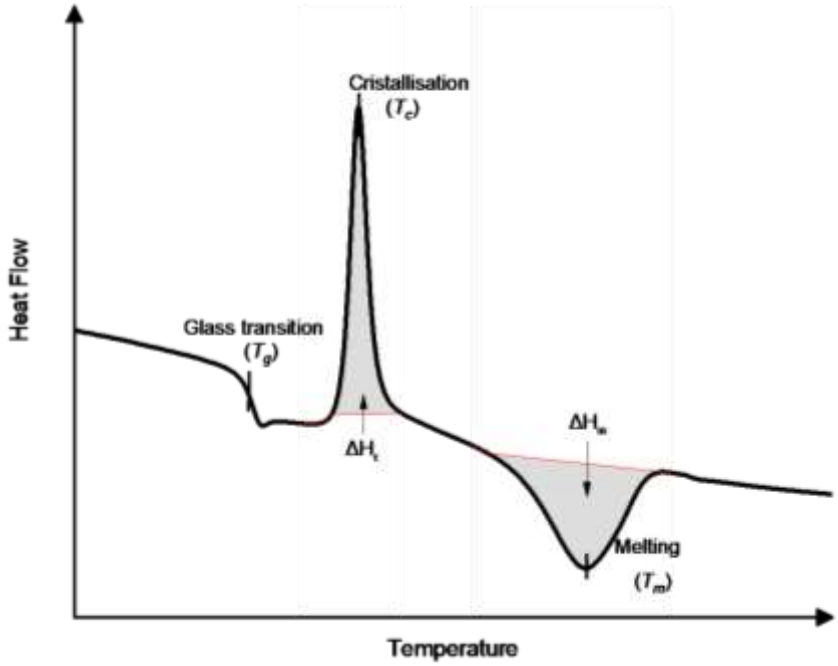

Figure 1.4.8 Typical DSC thermogram of a heating run for semi-crystalline polymer.

1.5 Thiol-yne Click Reactions

The thiol-yne reaction, or alkyne hydrothiolation, is a powerful and relatively simple way to produce alkenyl sulfides, which have significant importance in many applications such as pharmaceuticals, biological science, polymer materials and others.[58, 59] Generally, the nucleophilic thiol-yne reactions inherently possess most of the characteristics of a “click reaction” reported by Sharpless and co-workers[60] owing to the fact that the reaction occurs under mild conditions, it does not produce by-products, and it gives high yields.[48] Even though thiol-ene and thiol-yne additions, are very similar reactions, the thiol-yne addition provides wider application than its thiol-ene counterparts as it allows double thiol addition to alkyne which could be utilised to create highly functional monomers or for increasing the cross-link density.[61-66]

Like thiol-ene, thiol-yne addition reactions occur through one of the two mechanisms, nucleophilic or radical mechanisms. Thiol-yne reactions therefore are a general term used to describe the thiol-yne addition *via* the radical pathway (radical-mediated) or the nucleophilic pathway. Radical-mediated thiol-yne addition required the use of unhindered alkyne, thiol moiety, UV light and an initiator to form radicals. While the nucleophilic thiol-yne addition required an electron-deficient alkyne, thiol moiety, and a catalyst.[67, 68]

1.5.1 Radical-Mediated Thiol-yne

The radical-mediated thiol-yne reaction, similar to its counterpart radical thiol-ene reaction, in principle is efficient coupling chemistry and more versatile, tolerating a wider range of functional groups, thus more common in post-polymerisation modification techniques as well as highly cross-linked[63] and hyperbranched materials[69]. The suitability of radical-mediated thiol-yne for these range of applications is a consequence of the natural abundance of functional groups and the mild reaction conditions used.[61, 62, 67]

The mechanism of the radical thiol-yne begins with forming a thiyl radical, thermally, photochemically, or using photoinitiators, which then attacks the alkyne to form a radical vinyl thioether. In a chain transfer reaction, the radical vinyl thioether abstracts a hydrogen from another thiol species to form vinyl thioether and another active thiyl radical. Unlike thiol-ene reaction, this second thiyl radical is capable of attacking a new alkyne or a vinyl thioether as a second addition to form dithioether radical that will undergo a similar chain transfer reaction to form dithioether species, Figure 1.5.1.[63, 70]

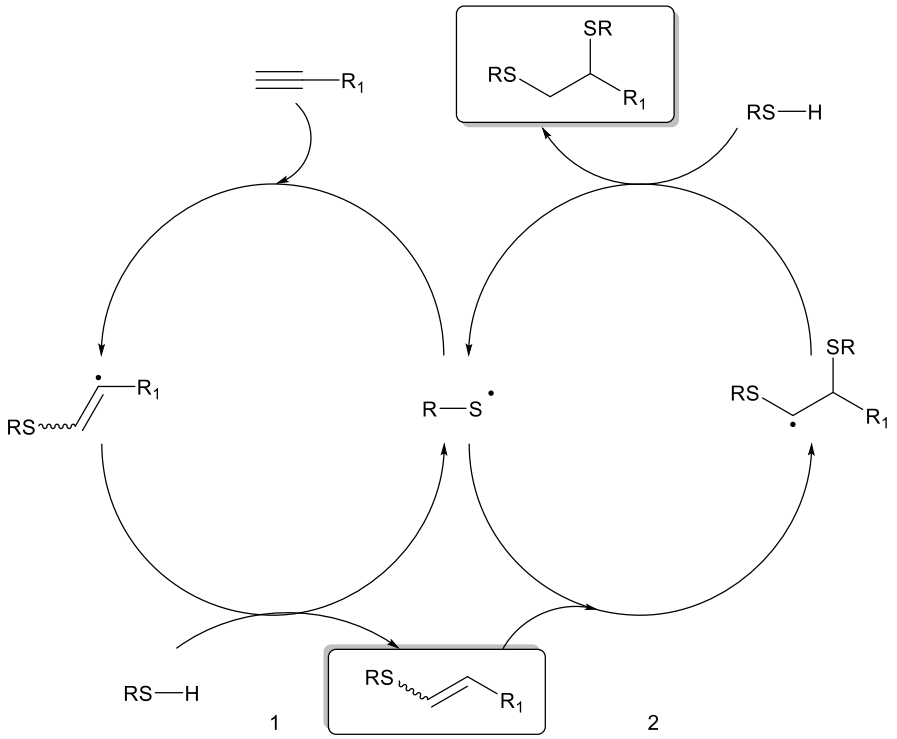

Figure 1.5.1 Mechanism of the radical thiol-yne reaction. Reproduced with permission from *Chem. Mater.* 2009, 21, 8, 1579-1585. Copyright 2009 American Chemical Society.Ref.70.

Despite the fact that the radical thiol-yne addition is a modular reaction with a very high conversion, it should be noted that it is less controllable than the nucleophilic thiol-yne reaction as the second thiol addition to the vinyl sulfide is faster than the first thiol addition to the alkyne in the radical pathway.[71] As a result, radical thiol-yne reaction can give different possible products.

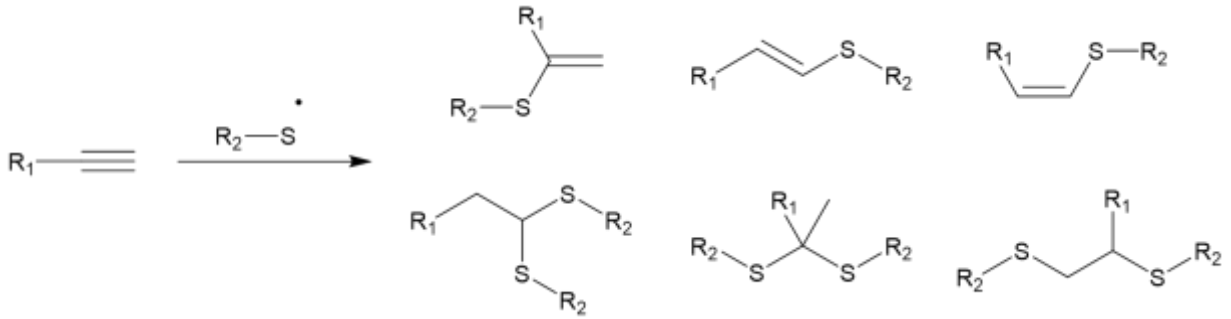

Figure 1.5.2 Possible products of radical mediated thiol-yne reaction. Reproduced under Creative Commons Attribution License from *Chem. Rev.*, 2021, **121**, 6744-6776.

The fact that radical thiol-yne reaction could produce different side products, beside the demolishing of its stereospecificity and regiospecificity, disqualifies the radical thiol-yne reaction from “click reaction” categories.

1.5.2 Nucleophilic Thiol-yne

Unlike the radical-mediated thiol-yne reactions, nucleophilic thiol-yne reactions do not require the use of heat or light, instead they can be proceed using a variety of catalysts. However, it is important to note that since alkyne and thiol moieties are both inherently nucleophilic, it is crucial to activate one or both of them to produce the desired vinyl sulfide through the use of electron-deficient alkyne along with suitable catalyst. [72] In general, the nucleophilic thiol-yne reaction produces variety of possible

Markovnikov and anti-Markovnikov products of different stereoisomers when one equivalent of thiol is used, or dithioether when two equivalent of thiol are used. [73]

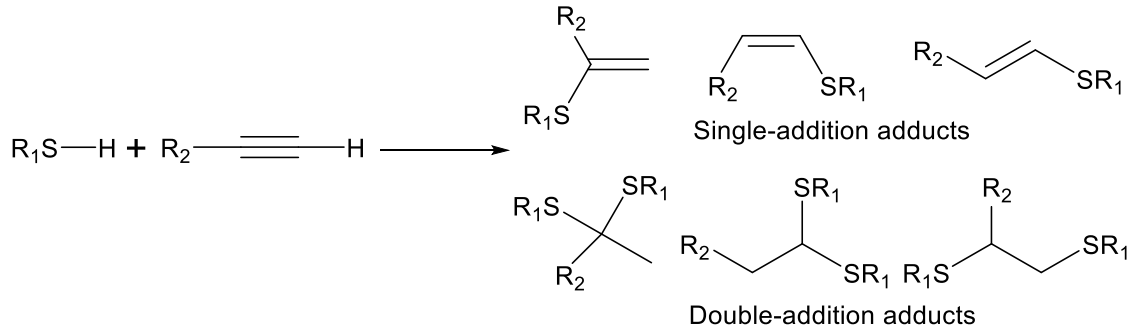

Figure 1.5.3 Possible products for nucleophilic thiol-yne reaction.

The nucleophilic addition of thiol to alkyne was known since early 1950s by the work of Cristol *et. al.*[74] as well as Truce and Simms[75,.67, 76-78] In this latter work, Truce and Simms have reported an extensive studies of the stereochemistry of the vinyl thioether resulted from the thiol addition to the alkyne. Specifically, they have studied the base-catalysed addition of *p*-toluenethiol in ethanol to three different alkynes, namely, phenylacetylene, 2-butyne, and 1-hexyne. They have observed that all reactions formed a mono-addition product. They have also observed that phenylacetylene produced one isomer resulting from the *cis* addition exclusively and that 2-butyne produced only one isomer resulting from the *trans* addition, while 1-hexyne produced two isomers resulting from the *cis* and *trans* addition. The study highlighted the importance of the structure of the starting alkyne on the resultant vinyl sulfide.

While there is a lack of prior research that detail the mechanism of nucleophilic thiol-yne addition reaction, its analogous nucleophilic thiol-ene reaction has been greatly studied for decades. As a result, the long-accepted reaction mechanism of nucleophilic thiol-ene was revisited back in 2010 by Bowman and co-workers.[79] In their

study, the authors showed that, on its simple accepted form, the mechanism of thia-Michael addition proceeds through the deprotonation of thiol by a stronger base (catalyst) forming thiolate anion. This thiolate anion is a strong nucleophile that reacts readily and is added into the activated double or triple bond, forming another enolate intermediate capable of deprotonating another thiol in a propagation step. However, the authors argued that the deprotonation of thiol to form a thiolate anion could be achieved by two distinguished pathways. The first one is a base-initiated pathway which is a simple acid-base reaction between thiol as a Brønsted acid and the catalyst as a Brønsted base (Figure 1.5.5a). The second pathway is a nucleophilic-initiated mechanism in which the catalyst behaves as a nucleophile and attacks the activated alkyne (Michael acceptor). This nucleophilic attack will form an enolate intermediate, a strong base, that could deprotonate a thiol and form a thiolate anion (Figure 1.5.5b). The thiolate anion that was formed by either pathway can deprotonate another thiol and propagate the reaction (Figure 1.5.5c).

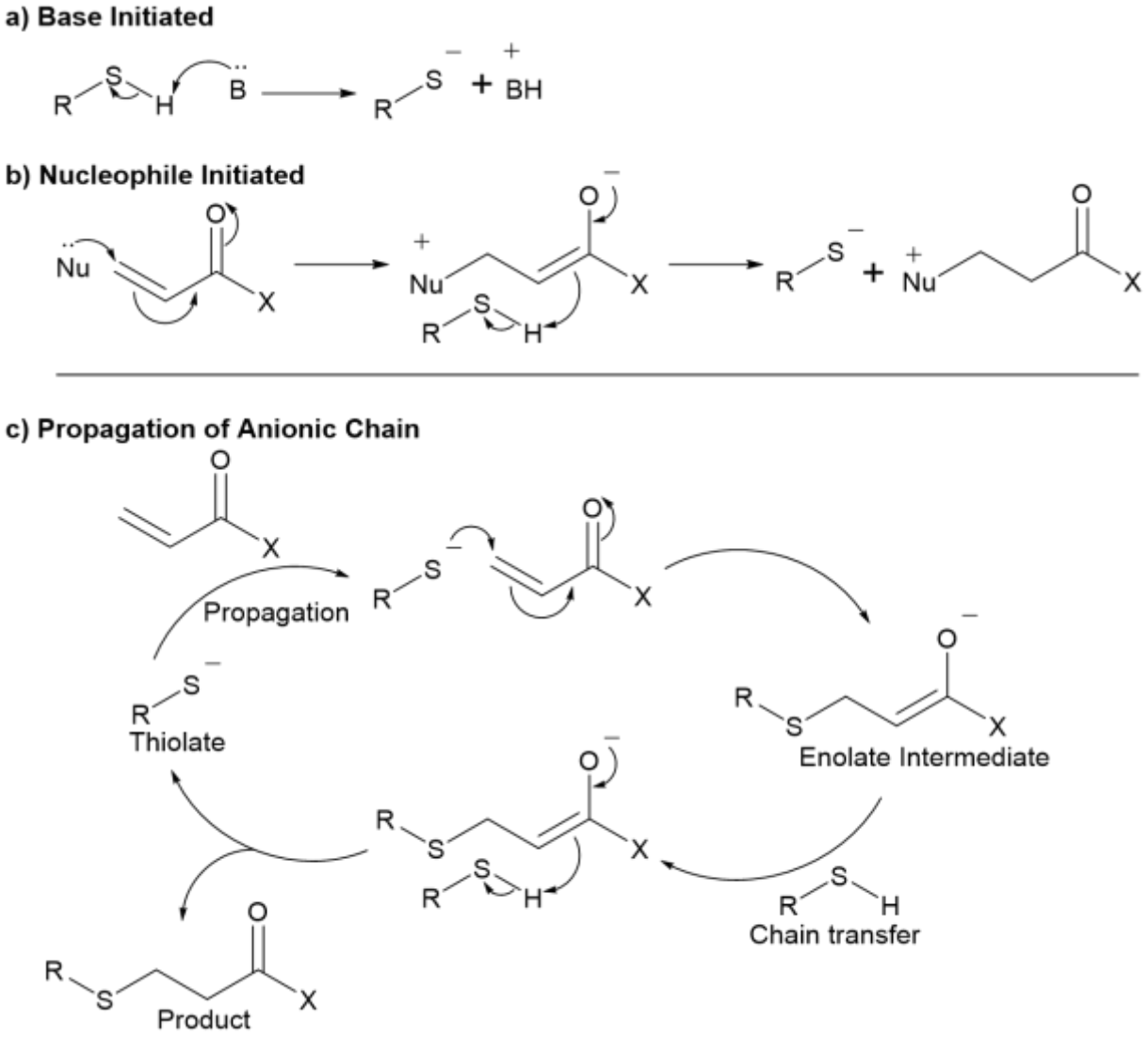

Figure 1.5.4 a) Mechanism of thiol deprotonation to form thiolate anion by base-initiated pathway, b) Thiol deprotonation mechanism by nucleophile-initiated pathway, c) The catalytic cycle of the thia-Michael addition.

Analogous to the nucleophilic thiol-ene Michael reaction, the catalyst in the catalysed thiol-yne Michael reaction can act as a base and deprotonate the thiol, or as a nucleophile and attack the alkyne forming an allene enolate intermediate, which deprotonate the thiol (Figure 1.5.6).

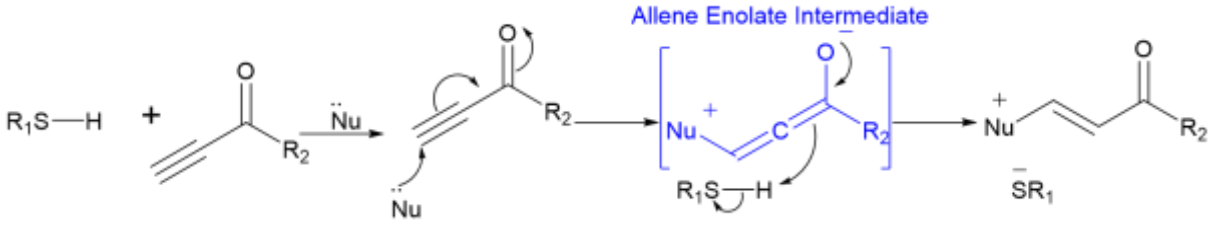

Figure 1.5.5 Catalysed thiol-yne reaction mechanism following a nucleophilic initiated pathway.

Since the nucleophilic-initiated mechanism proceeds *via* the addition of the nucleophile initiator (catalyst) into the unsaturated bond to form a nucleophile-enolate intermediate, the stability and persistence of this intermediate will limit the reaction yield. In fact, rational concerns about the use of high nucleophilic loading, which may lead to the accumulation of unwanted products from nucleophilic-Michael adducts, have been reported.[79-82] However, Northrop and co-workers have evaluated the likelihood of forming stable nucleophile byproducts in thiol-methyl acrylate reaction.[83] In their studies, they have deliberately used three different initiators, which known to promote the reaction mainly *via* the nucleophilic pathway, namely, dimethylphenylphosphine (DMPP), hexylamine (HA), and diethylamine (DEA). Monitoring the formation of the nucleophile byproducts in a reaction of model thiol-methyl acrylate system by ^{1}H-NMR spectroscopy revealed minimal formation of nucleophile byproduct <4%. They have concluded that the formation of nucleophile byproduct is negligible and that thia-Michael adducts are more stable. They've also added that the extent of the byproducts depends on the type and loading of the initiator as well as the reaction type and the solvent used.

A further extended study, including the most commonly used catalysts in thiol-Michael reaction, has also been reported by Northrop and co-workers.[84] In this later report, the

authors studied the reactivity of methyl 3-mercaptoproprionate with three commonly used aprotic amines, 4-dimethylaminopyridine (DMAP), 1-methylimidazole (MIM), and 1,8-diazabicyclo[5.4.0]undec-7-ene (DBU), which may initiate the reaction *via* the nucleophilic pathway.

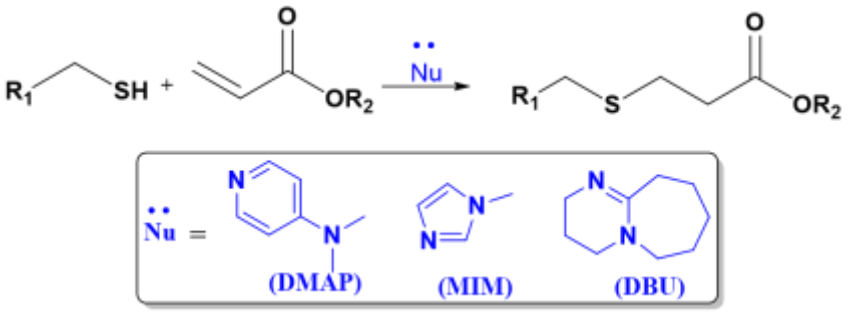

Figure 1.5.6 Representation of the reactivity study of methyl 3-mercaptoproprionate using DMAP, MIM, and DBU as nucleophiles.

The study showed that the byproducts are not persistent and react with the methyl 3-mercaptoproprionate completely to form the desired thiol-Michael adducts. The study has also highlighted the difference between aprotic versus protic amines to promote thiol-Michael addition. It showed that the use of protic amine, like hexylamine or diethylamine, creates a persistent aza-Michael adduct byproduct. The aza-Michael byproducts, which were created by aprotic amines, are generally reactive and are further converted to the desire thiol-Michael adducts in the presence of thiolate.

1.6 Application of Thiol-yne in Polymer Materials

Thiol-ene reactions have been extensively explored in polymer materials, while the thiol-yne reactions have received comparatively less attention.[68] However, the capability of the triple bonds of the alkyne to be utilised has helped leverage and increase the interest of implementing thiol-yne in polymer materials. In fact, since controlling the mono-addition of thiol to alkyne *via* nucleophilic addition is easier than radical addition, the nucleophilic thiol-yne addition has gathered special attention in the literature, especially in polymer applications. This special attention is due to the fact that the nucleophilic mono-addition of thiol to alkyne produces vinyl thioether, which contains unreactive double bonds that could be utilised for further functionalisation and tunning the thermomechanical properties of a polymer by controlling the stereochemistry of the vinyl thioether monomers. Also, the simplicity of preparation, its ability to proceed in organic or aqueous media and the availability of a large library of suitable catalysts have helped leverage the nucleophilic thiol-yne reaction.[48, 85] Moreover, the nucleophilic addition of dithiols to electron-deficient alkyne occurs faster than many other functional groups reported.[86, 87] While there are many applications of thiol-yne reactions in general, the present work will focus on the most relevant reports that used nucleophilic thiol-yne reactions in both linear and network polymers.

1.6.1 Thiol-yne Based Linear Polymers

The synthesis of linear polymers *via* step growth polymerisation is one of the earliest direct implementations of thiol-Michael addition.[88] The inherently “click” behaviour of this reaction as well as the wide range of suitable Michael acceptors, help spread the use of thiol-yne Michael additions in polymer materials. The earliest

examples of using thiol-yne addition in polymerisation were the polymerisation of ynones with dithiol creating linear polymers.[89-91] Bass *et al.* reported a poly(enone sulfide) series by polymerising different aromatic dithiols with different aryl internal ynones using N-methyl morpholine (NMM) as a catalyst at a temperature range of 25 °C to 40 °C. While the poor solubility of some of these polymers has limited their full characterisation, the solvent casting of other polymers have shown relatively high glass transition temperature (107 °C to 156 °C) with an outstanding tensile strength of 78 MPa.[89] Dix *et al.* have also synthesised a linear poly(enone-sulfide) polymer by polymerising aryl internal ynones monomer with aliphatic dithiol. The resulting polymer incorporate both *Z/E* isomers in a 60/40 *Z:E* ratio.[91] Controlling the structure of the starting alkyne, the strength of the base catalyst and the polarity of the solvent helps to control the reaction stereochemistry and thus improve the thermomechanical properties of the resultant polymers.[92] In fact, the influence of stereochemistry of unsaturated polymers in their thermomechanical properties has been a topic of interest for many years inspired by the well-known natural example of natural rubber (*cis*-1,4-polyisoprene) and Gutta-Percha (*trans*-1,4-polyisoprene). For example, Bell *et al.* have recently synthesised a series of linear polymers by polymerising dipropiolate monomers with commercially available aliphatic dithiols *via* thiol-yne Michael addition.[85] In this work, they have used combinations of different solvents and organo-base catalysts to alter the stereoisomers in the polymers' backbone. As a result, the bulk thermomechanical properties of the polymers were successfully tuned (Figure 1.6.1). Polymers with higher *cis* content showed higher degree of crystallinity confirmed by the presence of melting transitions and higher glass transition temperatures about -2 °C, while polymers with lower *cis* content are completely

amorphous with low glass transition temperature, below -15 °C. Furthermore, polymers with high *cis* content showed high tensile strength (<40 MPa) and comparatively lower elongation (< 1400%), while low *cis* content polymers have shown lower tensile strength (>3 MPa), but exceptionally higher elongation (<2900%).

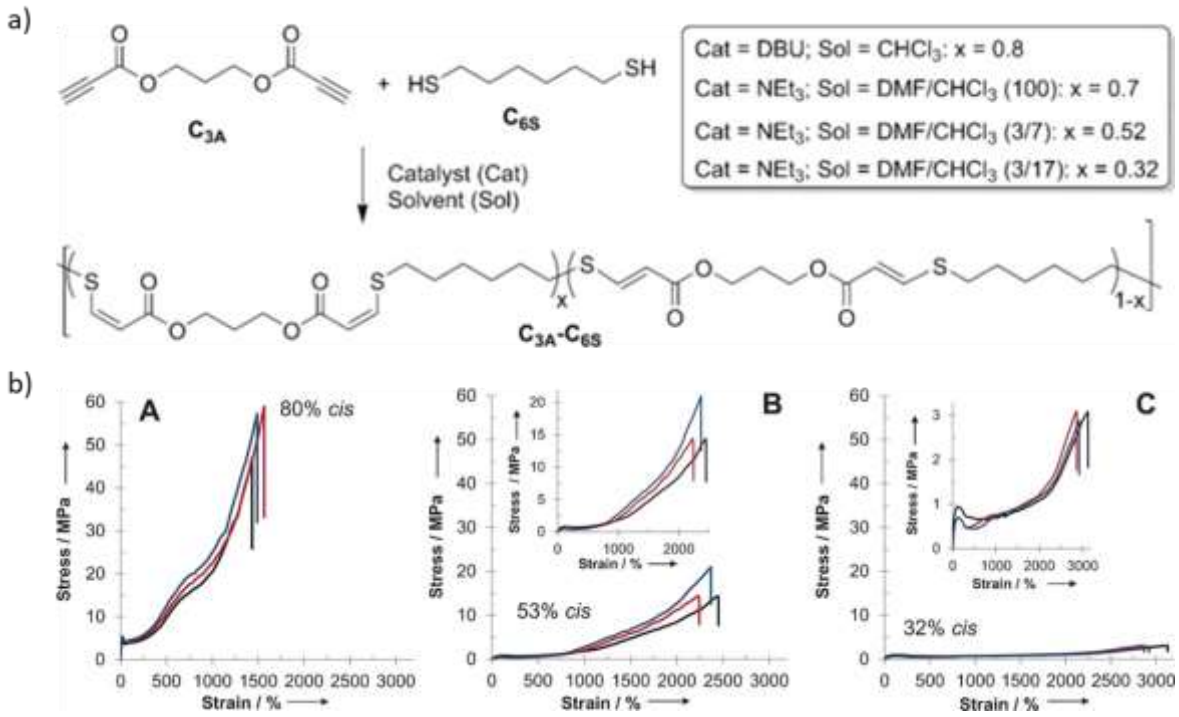

Figure 1.6.1 a) Synthesis of thiol-yne polymers from dialkyne (dipropiolate) and dithiol precursors. b) Change of mechanical properties of thiol-yne polymers with different *cis* content A=80% *cis*, B=53% *cis*, and C=32% *cis*. Reproduced under Creative Commons Attribution License from *Angew. Chem. Int. Ed.* **2016**, *55*, 13076. Ref.85.

1.6.2 Thiol-yne Based Network

It has been shown that the nucleophilic thiol-yne addition chemistry is a very efficient crosslinking reaction in aqueous media. As a result, the reaction is

heavily employed in the synthesis of hydrogels.[87, 93-99] Furthermore, thiol-yne based hydrogels have shown self-healability behaviour as a consequence of the dynamicity of thiol-yne reactions, which makes thiol-yne reaction a better option for cross-linking hydrogels. Fan *et al*. have recently synthesised hydrogels with self-healing properties.[100] By altering the concentration of commercially available precursors, they have successfully tuned the mechanical properties of the hydrogels. Furthermore, the dynamic nature of thiol-yne reaction has furnished excellent self-healability and shear thinning, allowing the hydrogel to be easily injected through a medical syringe as well as rapidly heal itself after being cut. These excellent properties endow by the dynamic behaviour of thiol-yne reaction, demonstrate a promising future for hydrogels, especially in biomedical applications.

Another recent example of using the thiol-yne addition reactions in the synthesis of polymer networks is the pioneering work reported by Du Prez and co-workers in which they synthesised covalent adaptable networks (CANs) using thiol-yne reaction.[47] They have demonstrated the dynamicity of thiol-yne reaction using kinetic studies on small molecules model compounds as well as stress relaxation studies on polymer networks. More importantly, the exchange rates of thiol were successfully controlled by varying the substituents on the activated alkyne (or ynone). Beyond that, a clear trend between the thiol exchange rate and the substituents on the aromatic scaffold (the phenylpropynone) was observed, in which the use of electron withdrawing, or donating, groups increased, or decreased, the exchange rate, respectively (Figure 1.6.2). As a consequence of the dynamicity of the thiol-alkynone reaction, the availability of the precursors,

and the ability to control the exchange rate, the thiol-alkynone reaction could be developed further in the preparation of dynamic network

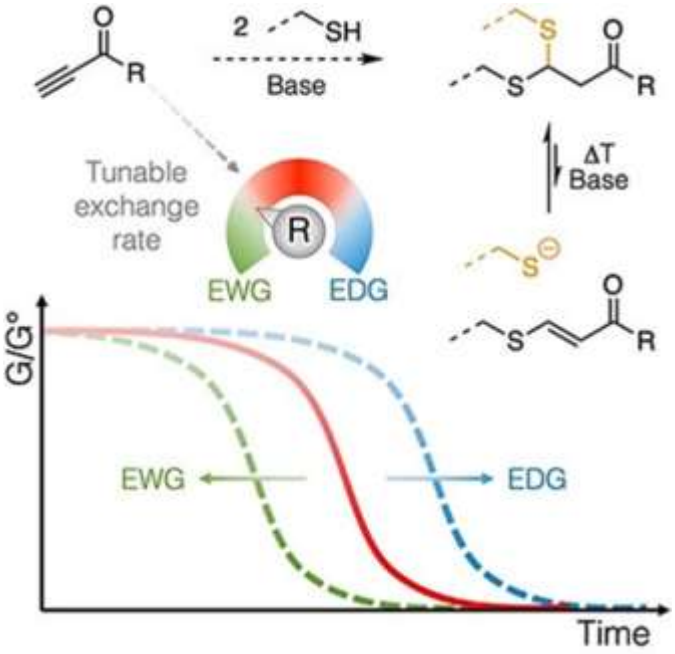

Figure 1.6.2 Controlling the second thiol exchange by varying the electronic differences of the substituents on activated alkyne between electron withdrawing group (EWG) and electron donating group (EDG). Reproduced with permission from Ref.14. Copyright 2020 John Wiley and Sons.

1.7 Summary

Conventional cross-linking of polymer material provides many advantages, including the improvement of thermal stability, mechanical properties, chemical resistance, and others. However, these advantages have always come at the expense of the recyclability of these conventional irreversible cross-links. The implementation of dynamic bonds in the synthesis of polymer networks led to the discovery of new reversible networks, coined covalent adaptable networks (CANs). Besides the advantages of the conventional “irreversible” network, these CANs are recyclable and could create smart and reconfigurable networks responsive to their environment. Nonetheless, CANs is, without a doubt, a trending topic that is still under development, and a major challenge so far is to replicate the outstanding thermal and mechanical properties of conventional networks. This introductory chapter highlights the relevant concepts for developing and testing of covalent adaptable networks that possess outstanding thermomechanical properties superior to most conventionally cross-linked thermosets. Initially, the structure-properties relationship in the polymeric material was introduced, highlighting the advantages and disadvantages of thermosets and thermoplastics. Then, a brief presentation of the dynamic covalent chemistry was highlighted, focusing on their application towards solving the recyclability issue of thermosets. This study was followed by a detailed outline of the covalent adaptable networks (CANs) highlighting the dynamic disulfide exchange and the thiol-yne Michael addition as the relevant chemistries to the work conducted in this thesis. The most relevant analyses used to characterise CANs and polymers, in general, were outlined. Finally, recent applications of thiol-yne reactions in the linear polymer as well as networks were highlighted.

1.8 Project aims

The aim of this thesis is to investigate methods and techniques for improving the recyclability of crosslinked elastomers by the implementation of covalent adaptable networks (CANs). It was envisioned that the use of thiol-yne chemistries in the construction of the polymer network would afford network recyclability as a consequence of the dynamicity of the second thiol-yne addition. Likewise, the use of thiol-yne reaction would provide unsaturation in the polymer's backbone, this unsaturation was accountable for increasing the polymer's robustness in previously reported hydrogels by the Dove group.[1] Therefore, the first step in the present work was to synthesise small molecule models of the proposed alkynes, ynones in specific, as a consequence of their synthesis versatility and exceptional reactivity, followed by testing their dynamicity. Subsequently, monomers of the same chemical structure were synthesised and polymerised with commercially available dithiols to provide unsaturated prepolymer, which were later cross-linked with a multivalent thiol to construct the dynamic network. Finally, the thermomechanical properties were tested and tuned by altering the dithiol:cross-linker ratio, and changing the length and structure of the ynone monomers.

While thiol-yne dynamic chemistry was the main focus in the present work, the implementation of bio-based dynamic reactions such as disulfide-thiol exchange was also explored to construct alternative bio-based dynamic networks with tunable thermomechanical properties. However, these networks are known to have low to moderate thermomechanical properties compared to the non-bio-based alternatives. Even though the thermomechanical properties of these bio-based CANs are less than

the thiol-yne CANs, a successful control over the thermomechanical properties of these CANs is reported.

References

1. M. Gilbert, in *Brydson's Plastics Materials (Eighth Edition)*, ed. M. Gilbert, Butterworth-Heinemann, 2017, DOI: https://doi.org/10.1016/B978-0-323-35824-8.00004-9, pp. 59-73.
2. X. Luo, S. Xie, J. Liu, H. Hu, J. Jiang, W. Huang, H. Gao, D. Zhou, Z. Lü and D. Yan, *Polym. Chem.*, 2014, **5**, 1305-1312.
3. G. Sarkhel, A. Banerjee and P. Bhattacharya, *Polym Plast Technol Eng.*, 2006, **45**, 713-718.
4. Q. Fu, Y. Men and G. Strobl, *Polymer*, 2003, **44**, 1927-1933.
5. H. C. Jung, S. J. Kang, W. N. Kim, Y.-B. Lee, K. H. Choe, S.-H. Hong and S.-B. Kim, *J. Appl. Polym. Sci.*, 2000, **78**, 624-630.
6. S. Desai, I. M. Thakore, B. D. Sarawade and S. Devi, *Eur. Polym. J.*, 2000, **36**, 711-725.
7. T. F. Garrison, M. R. Kessler and R. C. Larock, *Polymer*, 2014, **55**, 1004-1011.
8. C. S. Wang and T. S. Leu, *J. Appl. Polym. Sci.*, 1999, **73**, 833-839.
9. M. Sava, C. Gaina, V. Gaina and D. Timpu, *Macromol. Chem. Phys.*, 2001, **202**, 2601-2605.
10. N. S. Muralisrinivasan, *Introduction to Polymer Compounding: Raw Materials, Volume 1*, Smithers Rapra, 2014.
11. T. Maeda, H. Otsuka and A. Takahara, *Prog. Polym. Sci.*, 2009, **34**, 581-604.
12. C. N. Bowman and C. J. Kloxin, *Angew. Chem., Int. Ed.*, 2012, **51**, 4272-4274.
13. W. Zhang and Y. Jin, 2017.
14. W. Lu, X. Pan, Z. Zhang, J. Zhu, N. Zhou and X. Zhu, *Polym. Chem.*, 2017, **8**, 3874-3880.
15. Y. Jin, C. Yu, R. J. Denman and W. Zhang, *Chem. Soc. Rev.*, 2013, **42**, 6634-6654.
16. M. D. Stern and A. V. Tobolsky, *J. Chem. Phys.*, 1946, **14**, 93-100.
17. M. K. McBride, B. T. Worrell, T. Brown, L. M. Cox, N. Sowan, C. Wang, M. Podgorski, A. M. Martinez and C. N. Bowman, *Annu. Rev. Chem. Biomol. Eng.*, 2019, **10**, 175-198.
18. C. J. Kloxin, T. F. Scott, B. J. Adzima and C. N. Bowman, *Macromolecules*, 2010, **43**, 2643-2653.

19. C. J. Kloxin and C. N. Bowman, *Chem. Soc. Rev.*, 2013, **42**, 7161-7173.
20. J. S. Kahn, Y. Hu and I. Willner, *Acc. Chem. Res.*, 2017, **50**, 680-690.
21. A. Takahashi, T. Ohishi, R. Goseki and H. Otsuka, *Polymer*, 2016, **82**, 319-326.
22. B. T. Michal, C. A. Jaye, E. J. Spencer and S. J. Rowan, *ACS Macro Lett.*, 2013, **2**, 694-699.
23. G. M. Scheutz, J. J. Lessard, M. B. Sims and B. S. Sumerlin, *J. Am. Chem. Soc.*, 2019, **141**, 16181-16196.
24. M. Podgórski, N. Spurgin, S. Mavila and C. N. Bowman, *Polym. Chem.*, 2020, **11**, 5365-5376.
25. W. Zou, J. Dong, Y. Luo, Q. Zhao and T. Xie, *Adv. Mater.*, 2017, **29**, 1606100.
26. L. Hammer, N. J. Van Zee and R. Nicolaÿ, *Polymers*, 2021, **13**, 396.
27. J. M. Winne, L. Leibler and F. E. Du Prez, *Polym. Chem.*, 2019, **10**, 6091-6108.
28. N. Zheng, Y. Xu, Q. Zhao and T. Xie, *Chem. Rev.*, 2021, **121**, 1716-1745.
29. G. Tesoro and V. Sastri, *J. Appl. Polym. Sci.*, 1990, **39**, 1425-1437.
30. U. Lafont, H. Van Zeijl and S. Van Der Zwaag, *ACS Appl. Mater. Interfaces*, 2012, **4**, 6280-6288.
31. S. Nevejans, N. Ballard, J. I. Miranda, B. Reck and J. M. Asua, *Phys. Chem. Chem. Phys.*, 2016, **18**, 27577-27583.
32. D.-I. Lee, S.-H. Kim and D.-S. Lee, *Molecules*, 2019, **24**, 1492.
33. Y. Yao, M. Xiao and W. Liu, *Macromol. Chem. Phys.*, 2021, **222**, 2100002.
34. Y. Wang, Y. Li, J. Bai, Z. Li and G. Hu, *Macromol. Chem. Phys.*, 2019, **220**, 1900340.
35. A. Shaabani and R. Sedghi, *Polymer*, 2021, **223**, 123694.
36. O. Ramström and J.-M. Lehn, *ChemBioChem*, 2000, **1**, 41-48.
37. S. Otto, R. L. E. Furlan and J. K. M. Sanders, *J. Am. Chem. Soc.*, 2000, **122**, 12063-12064.
38. P. A. Fernandes and M. J. Ramos, *Chem. Eur. J.*, 2004, **10**, 257-266.
39. Z. Q. Lei, H. P. Xiang, Y. J. Yuan, M. Z. Rong and M. Q. Zhang, *Chem. Mater.*, 2014, **26**, 2038-2046.
40. J. Houk and G. M. Whitesides, *J. Am. Chem. Soc.*, 1987, **109**, 6825-6836.
41. D. P. Nair, M. Podgórski, S. Chatani, T. Gong, W. Xi, C. R. Fenoli and C. N. Bowman, *Chem. Mater.*, 2014, **26**, 724-744.
42. B. Zhang, P. Chakma, M. P. Shulman, J. Ke, Z. A. Digby and D. Konkolewicz, *Org. Biomol. Chem.*, 2018, **16**, 2725-2734.
43. C. F. H. Allen, J. O. Fournier and W. J. Humphlett, *Can. J. Chem.*, 1964, **42**, 2616-2620.
44. C. F. H. Allen and W. J. Humphlett, *Can. J. Chem.*, 1966, **44**, 2315-2321.

45. G. Joshi and E. V. Anslyn, *Org. Lett.*, 2012, **14**, 4714-4717.

46. B. Zhang, Z. A. Digby, J. A. Flum, P. Chakma, J. M. Saul, J. L. Sparks and D. Konkolewicz, *Macromolecules*, 2016, **49**, 6871-6878.

47. N. Van Herck, D. Maes, K. Unal, M. Guerre, J. M. Winne and F. E. Du Prez, *Angew. Chem., Int. Ed.*, 2020, **59**, 3609-3617.

48. J. C. Worch, C. J. Stubbs, M. J. Price and A. P. Dove, *Chem. Rev.*, 2021, **121**, 6744-6776.

49. A. B. Lagron, B. M. El-Zaatari and L. S. Hamachi, *Front. Mater.*, 2022, **9**, 915296.

50. J. J. Aklonis, *J. Chem. Educ.*, 1981, **58**, 892.

51. J. Meissner, *Annu. Rev. Fluid Mech.*, 1985, **17**, 45-64.

52. P. Sharma, U. Chauhan, S. Kumar and K. Sharma, *Int. J. Appl. Eng. Res.*, 2018, **13**, 363-368.

53. M. Podgórski, B. D. Fairbanks, B. E. Kirkpatrick, M. McBride, A. Martinez, A. Dobson, N. J. Bongiardina and C. N. Bowman, *Adv. Mater.*, 2020, **32**, 1906876.

54. R. L. Blaine, *TA123*, 2010.

55. J. H. Flynn, *Thermochim. Acta*, 1993, **217**, 129-149.

56. H. Bitter and S. Lackner, *Chem. Eng. J.*, 2021, **423**, 129941.

57. J. E. K. Schawe, *J. Therm. Anal. Calorim.*, 2014, **116**, 1165-1173.

58. N. Velasco, C. Virumbrales, R. Sanz, S. Suárez-Pantiga and M. A. Fernández-Rodríguez, *Org. Lett.*, 2018, **20**, 2848-2852.

59. A. Kausar, S. Zulfiqar and M. I. Sarwar, *Polym. Rev.*, 2014, **54**, 185-267.

60. H. C. Kolb, M. G. Finn and K. B. Sharpless, *Angew. Chem., Int. Ed.*, 2001, **40**, 2004-2021.

61. A. B. Lowe, C. E. Hoyle and C. N. Bowman, *J. Mater. Chem.*, 2010, **20**, 4745-4750.

62. R. Hoogenboom, *Angew. Chem., Int. Ed.*, 2010, **49**, 3415-3417.

63. B. D. Fairbanks, T. F. Scott, C. J. Kloxin, K. S. Anseth and C. N. Bowman, *Macromolecules*, 2009, **42**, 211-217.

64. R. J. Amir, L. Albertazzi, J. Willis, A. Khan, T. Kang and C. J. Hawker, *Angew. Chem., Int. Ed.*, 2011, **50**, 3425-3429.

65. G. Chen, J. Kumar, A. Gregory and M. H. Stenzel, *Chem. Commun.*, 2009, DOI: 10.1039/B910340F, 6291-6293.

66. B. D. Fairbanks, E. A. Sims, K. S. Anseth and C. N. Bowman, *Macromolecules*, 2010, **43**, 4113-4119.

67. A. B. Lowe, *Polymer*, 2014, **55**, 5517-5549.

68. B. Yao, J. Sun, A. Qin and B. Z. Tang, *Chin. Sci. Bull.*, 2013, **58**, 2711-2718.

69. D. Konkolewicz, A. Gray-Weale and S. Perrier, *J. Am. Chem. Soc.*, 2009, **131**, 18075-18077.

70. J. W. Chan, H. Zhou, C. E. Hoyle and A. B. Lowe, *Chem. Mater.*, 2009, **21**, 1579-1585.

71. A. Massi and D. Nanni, *Org. Biomol. Chem.*, 2012, **10**, 3791-3807.

72. F. Nador, J. Mancebo-Aracil, D. Zanotto, D. Ruiz-Molina and G. Radivoy, *RSC Adv.*, 2021, **11**, 2074-2082.

73. V. X. Truong and A. P. Dove, *Angew. Chem., Int. Ed.*, 2013, **52**, 4132-4136.

74. S. J. Cristol, A. Begoon, W. P. Norris and P. S. Ramey, *J. Am. Chem. Soc.*, 1954, **76**, 4558-4561.

75. W. E. Truce and J. A. Simms, *J. Am. Chem. Soc.*, 1956, **78**, 2756-2759.

76. E. Blasco, M. B. Sims, A. S. Goldmann, B. S. Sumerlin and C. Barner-Kowollik, *Macromolecules*, 2017, **50**, 5215-5252.

77. S. Nurhanna Riduan, J. Y. Ying and Y. Zhang, *Org. Lett.*, 2012, **14**, 1780-1783.

78. J. Liu, J. W. Y. Lam and B. Z. Tang, *Chem. Rev.*, 2009, **109**, 5799-5867.

79. J. W. Chan, C. E. Hoyle, A. B. Lowe and M. Bowman, *Macromolecules*, 2010, **43**, 6381-6388.

80. A. B. Lowe, *Polym. Chem.*, 2014, **5**, 4820-4870.

81. G.-Z. Li, R. K. Randev, A. H. Soeriyadi, G. Rees, C. Boyer, Z. Tong, T. P. Davis, C. R. Becer and D. M. Haddleton, *Polym. Chem.*, 2010, **1**, 1196-1204.

82. G. B. Desmet, M. K. Sabbe, D. R. D'Hooge, P. Espeel, S. Celasun, G. B. Marin, F. E. Du Prez and M.-F. Reyniers, *Polym. Chem.*, 2017, **8**, 1341-1352.

83. S. H. Frayne and B. H. Northrop, *J. Org. Chem.*, 2018, **83**, 10370-10382.

84. V. Drogkaris and B. H. Northrop, *ChemPlusChem*, 2020, **85**, 2466-2474.

85. C. A. Bell, J. Yu, I. A. Barker, V. X. Truong, Z. Cao, A. V. Dobrinyin, M. L. Becker and A. P. Dove, *Angew. Chem., Int. Ed.*, 2016, **55**, 13076-13080.

86. O. Daglar, S. Luleburgaz, E. Baysak, U. S. Gunay, G. Hizal, U. Tunca and H. Durmaz, *Eur. Polym. J.*, 2020, **137**, 109926.

87. L. J. Macdougall, V. X. Truong and A. P. Dove, *ACS Macro Lett.*, 2017, **6**, 93-97.

88. B. D. Mather, K. Viswanathan, K. M. Miller and T. E. Long, *Prog. Polym. Sci.*, 2006, **31**, 487-531.

89. R. G. Bass, E. Cooper, P. M. Hergenrother and J. W. Connell, *J. Polym. Sci., Part A: Polym. Chem.*, 1987, **25**, 2395-2407.

90. J. M. Wilbur Jr. and B. A. Bonner, *J. Polym. Sci., Part A: Polym. Chem.*, 1990, **28**, 3747-3759.

91. L. R. Dix, J. R. Ebdon and P. Hodge, *Eur. Polym. J.*, 1995, **31**, 653-658.

92. L. J. Macdougall, M. M. Pérez-Madrigal, J. E. Shaw, J. C. Worch, C. Sammon, S. M. Richardson and A. P. Dove, *Angew. Chem., Int. Ed.*, 2021, **60**, 25856-25864.

93. M. M. Pérez-Madrigal, J. E. Shaw, M. C. Arno, J. A. Hoyland, S. M. Richardson and A. P. Dove, *Biomater. Sci.*, 2020, **8**, 405-412.

94. L. J. Macdougall, M. M. Pérez-Madrigal, M. C. Arno and A. P. Dove, *Biomacromolecules*, 2018, **19**, 1378-1388.

95. L. J. Macdougall, M. M. Pérez-Madrigal, J. E. Shaw, M. Inam, J. A. Hoyland, R. O'Reilly, S. M. Richardson and A. P. Dove, *Biomater. Sci.*, 2018, **6**, 2932-2937.

96. L. Racine, G. Costa, E. Bayma-Pecit, I. Texier and R. Auzély-Velty, *Carbohydr. Polym.*, 2017, **170**, 166-175.

97. X. Y. Cai, J. Z. Li, N. N. Li, J. C. Chen, E.-T. Kang and L. Q. Xu, *Biomater. Sci.*, 2016, **4**, 1663-1672.

98. V. X. Truong, M. P. Ablett, S. M. Richardson, J. A. Hoyland and A. P. Dove, *J. Am. Chem. Soc.*, 2015, **137**, 1618-1622.

99. L. An, J. Chen, J. W. Heo, J. W. Kim, H. Mo Jeong, D. H. Youn and Y. S. Kim, *J. Wood Chem. Technol.*, 2022, DOI: 10.1080/02773813.2022.2120898, 1-11.

100. B. Fan, K. Zhang, Q. Liu and R. Eelkema, *ACS Macro Lett.*, 2020, **9**, 776-780.

CHAPTER 2: SUPER TOUGH AND REPROCESSABLE ELASTOMERS BASED ON THIOL-YNE COVALENT ADAPTABLE NETWORKS

2.1 Manuscript and overview

Title: Super tough and reprocessable elastomers based on thiol-yne covalent adaptable networks

Authors: **Maher A. Alraddadi**[1], Joshua C. Worch[1], Andrew P. Dove[1]*

Affiliations: [1] School of Chemistry, The University of Birmingham, Edgbaston, Birmingham, B15 2TT, UK.

Manuscript Prepared

Co-author contributions: Dr Josh Worch (University of Birmingham) provided technical and synthetic guidance and editing of this manuscript. Prof. Andrew P. Dove (University of Birmingham) supervised in addition to providing guidance and editing the manuscript.

Overview:

The objective of this chapter was to explore the reversibility of nucleophilic thiol-yne addition reaction as a suitable platform to synthesis covalent adaptable networks (CANs) that will improve the recyclability of elastomers.

The use of dynamic covalent bonds to crosslink polymer instead of typical non-dynamic covalent bonds created reversible cross-links between polymer chains which is commonly refer to as covalent adaptable networks (CANs). These CANs has helped improve the reprocessability and recyclability of thermosets. However, most CAN

materials are underperform compared to those with networks constructed from non-dynamic.

In our attempt to investigate this issue, we used thiol-yne addition reaction to synthesise a series of CANs with tunable properties. We initially, explore the dynamicity between vinyl thioether moieties, single-addition adducts of thiol addition to unsaturated internal ynone, in small molecules study.

After successfully confirmed the dynamicity of the proposed thiol-yne system, prepolymers, constructed from the addition of dithiol to diynone monomer, was further cross-linked using multivalent thiol to afford dynamic network composed of mainly α,β-unsaturated thioether moieties. Furthermore, a large range of properties were easy accessed by changing the crosslink density in CANs as well as varying the dithiol used to prepare the prepolymer. Most of all, CAN with outstanding mechanical properties (ultimate tensile strength above 23 MPa and elongation at break near 1000%) was successfully synthesised and characterised. Our study highlighted how varying the cross-linking density in CAN materials as well as changing the prepolymer structure can lead to changes in the thermomechanical properties of the resultant CAN materials.

Super tough and reprocessable elastomers based on thiol-yne covalent adaptable networks

Maher A. Alraddadi[§], Joshua C. Worch[§], Andrew P. Dove[*§]

[§]School of Chemistry, University of Birmingham, Edgbaston, Birmingham, B15 2TT (UK)

Abstract Synthesizing robust elastomeric materials using covalent adaptable networks (CANs) seeks to address historical challenges facing the waste management of rubbers by imparting inherent reprocessability into such systems. However, these highly sought-after properties usually come with a trade-off in mechanical properties and many elastomeric CAN materials underperform compared to those with permanent networks such as vulcanized rubbers. We report the synthesis of super tough, reprocessable CANs based on the dynamic thiol-yne reaction between thiols and internal ynones. Small molecule model studies confirmed the reversibility of the organobased-catalyzed reaction. Prepolymer linear oligomers were first formed from dithiol and diynone monomers and subsequently cross-linked using a multi-valent thiol to afford a dynamic network. A large range of material properties were easily accessed by changing the crosslinking density. Moreover, some of our CANs displayed outstanding mechanical properties that are superior to commercially available elastomers, with the best performing material possessing an ultimate tensile strength > 23 MPa, elongation at break near 1000%, and toughness exceeding 9543 $J \cdot m^{-2}$.

Introduction

Elastomeric materials are vital commodity resources due to their excellent chemical or thermal stabilities and their inherent ability to undergo reversible deformation. However, these features are usually reliant on their permanently cross-linked network architecture which hinders reprocessability and ultimately contributes to waste management concerns.[1] Recent efforts to improve the sustainability of elastomers have turned toward creating materials with reversible chemical cross-links between polymer chains based on dynamic covalent bonds, commonly referred to as covalent adaptable networks (CANs), instead of traditional materials with permanent crosslinks.[2-5] These dynamic networks can often mimic some of the desirable properties of conventional elastomers, namely their reversible deformation behaviour, but with the

added feature of reprocessability, including mechanical recyclability and/or self-healing behaviour, which also paves the way to so-called 'smart' materials that are responsive to their environment.[6, 7]

Natural rubber (NR), which is largely unprossessable as post-consumer waste due to vulcanization, is the archetypical elastomeric material. Although there exist many formulations of natural rubber-based materials (such as composite structures) that possess varied properties, these materials are generally renowned for their remarkably high toughness due to good elongation at break coupled with high tensile strength, which is related to a unique strain-induced hardening behaviour.[8, 9] Synthetic efforts to find surrogates that reproduce the favourable property profile of natural rubber have been ongoing for years, yet it still remains as a leading industrial material.[10-12] Similarly, many innovative CAN elastomers are inferior to conventional rubbers in terms of toughness, i.e. the materials may possess good tensile strength or high elongation at break but not usually both attributes. This trade-off in material performance is intimately tied to the nature of the overall material composition including, but not limited to, bond-exchange processes[3] and/or crosslinking density[13-15]. For example, highly cross-linked systems can afford materials with excellent mechanical strength and behaviour that is more typical of conventional, hard thermosets such as epoxy. On the other hand, many lightly crosslinked materials (and/or those with glass transition temperatures below working temperature) are often evocative of softer, thermoplastic elastomers such as styrene-butadiene-styrene (SBS) rubber, especially as it relates to their material processing.[3, 16] Thus, the development of elastomers that are both mechanically competitive and reprocessable remains a significant challenge in the field.

Herein, we report the straightforward synthesis of responsive CANs based on thiol-yne chemistry (reaction between a thiol and ynone) that are mechanically superior to many commercial rubbers. Du Prez and co-workers have recently reported an analogous thiol-yne CAN featuring tuneable exchange rates, according to the electronic environment of the ynone moiety.[17] However, in that work the materials exploited the exchange between the double-addition and single-addition reaction products of the thiol to the activated alkyne to afford a fully 'saturated' network and the resultant material has elongation at break < 100% and tensile strengths < 20 MPa. Alternatively, our approach relies on the single thiol conjugate addition to maintain unsaturation in the material architecture which we have previously employed to afford robust thiol-

yne hydrogels[18, 19] and linear step-growth polymers[20, 21]. Furthermore, we constructed networks with high toughness by first forming oligomeric prepolymers[22], based on the organobase-catalyzed reaction between internal diynone monomers with commercially available dithiols, and then crosslinking with a multivalent thiol to furnish a hyperbranched CAN architecture that possessed double bonds in the polymeric chains between crosslink sites. Finally, the mechanical properties of materials were optimized by altering the crosslinking density (i.e. varying dithiol:multivalent thiol ratio) to afford a super tough elastomer that displayed good recyclability, albeit with some deterioration of mechanical properties, likely due to residual catalyst in the network to facilitate bond exchange reactions.

Results and Discussion

We began our investigation by examining the reaction between model substituted (internal) ynone substrates and monofunctional thiols in order to determine the reversibility of the reaction. In particular, we were interested in the reversibility of the single-addition products since it is comparatively understudied next to the double/single-addition exchange reactions.[23] We employed 1,8-diazabicyclo(5.4.0)undec-7-ene (DBU) to catalyse the addition of 1 equivalent of a unique thiol (thiophenol) to a β-sulfido-α,β-unsaturated single-adduct formed from a different thiol (ethanethiol). The reaction was monitored by ^{1}H-NMR spectroscopy and indicated that the double-substituted mixed species was the predominant product, *i.e.* a second conjugate addition reaction was favourable, as evidenced by the diagnostic resonance at δ = 3.4 ppm. However, we also observed the appearance of new reaction products with similar, but distinct, resonances compared to the initial single-addition adduct, which suggested that the single-addition product is dynamic under these conditions (Figure 1a). Specifically, the resonances at δ = 6.38 ppm, δ = 7.08 ppm and δ = 3.37 ppm correspond to the thiophenol single and double adduct species, respectively (Supplementary Information Figure S7,S9). To further corroborate this observation, we then mixed two single-addition reaction products (each formed from unalike ynones and thiols) which we suggest is representative of the exchange processes expected in an idealized network (alkyne:thiol 1:1) where free thiol would be initially absent. We observed a complex mixture of products with resonances attributable to new compounds at δ = 5.67 ppm, δ = 6.31 ppm, δ = 6.64 ppm and δ = 7.00 ppm that indicate exchange

between single-addition adducts occurs (Figure 1b, Supplementary Information Figure S11,S17). However, in the absence of free thiol, the exchange reactions only proceeded at elevated temperature (140 °C). Unsurprisingly, additional experiments also corroborate existing exchange processes among double-addition and single-addition species (Supplementary Information Figure S20). Finally, (*E/Z)* isomerism of the unsaturated thiol-Michael adduct[24] was observed at ambient temperature in a catalyst-free solution, further highlighting the dynamic nature of this bond (Supplementary Information, Figure S26).

Anslyn and co-workers have previously investigated the reversibility of the thiol-ynone reaction employing terminal ynone substrates where they reported dynamic exchange between thioacetals (double-addition adducts) and β-sulfido-α,β-unsaturated carbonyl moieties (single-addition adducts).[23, 25] A similar exchange between double- and single-addition adducts was also observed for substituted ynone substrates.[17] However, a previous study revealed that the first conjugate addition reaction was irreversible when employing a butyl-substituted internal ynone, *i.e.* free thiol and ynone were not evolved under the reported reaction conditions.[26] In contrast, our results suggest that the single-addition products resulting from the addition of thiols to methyl-substituted internal ynones are reversible (albeit less dynamic than the thioacetal species) and thus capable of dynamic exchange reactions (Figure 1a).

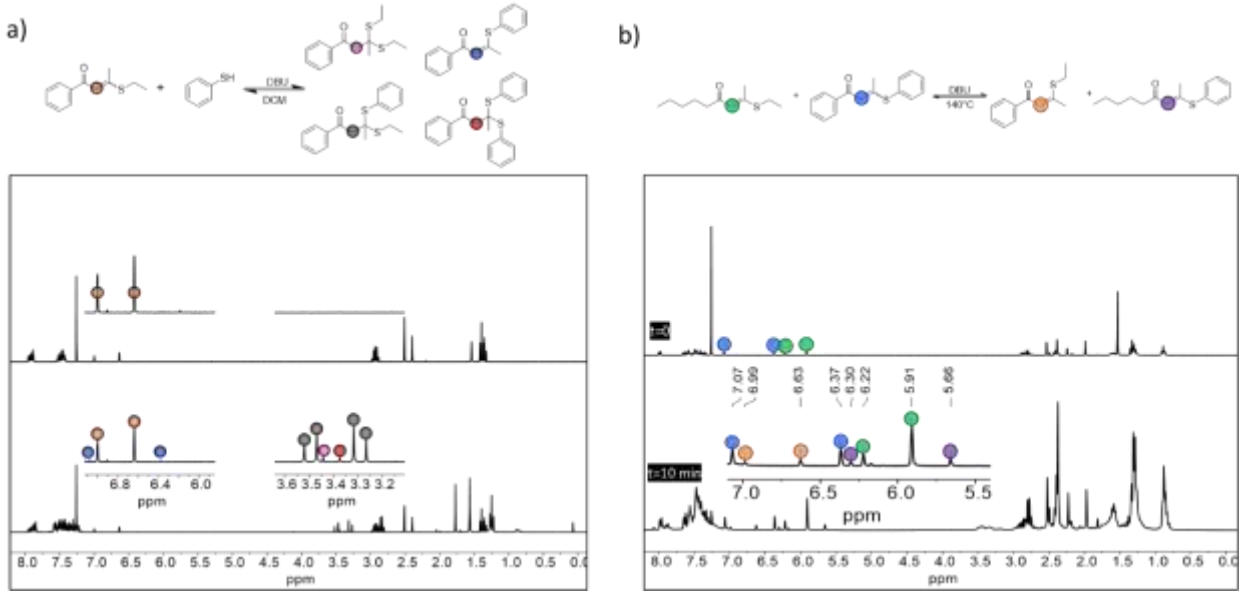

Figure 1. ^{1}H-NMR spectrum ($CDCl_3$, 298 K) for a) Thiol exchange between β-sulfido-α,β-unsaturated carbonyl and free thiol. b) Intermolecular thiol exchange of two different β-sulfido-α,β-unsaturated carbonyl with reference ^{1}H-NMR spectrum for starting material and expected products.

After confirming the dynamic behaviour of the unsaturated model compounds, we synthesized crosslinked network materials to probe the reversibility of the reaction on a macroscopic level. We employed a straightforward, two-step synthesis reacting commercially available dithiols with a diynone in molar excess to generate unsaturated, linear pre-polymers that were terminated with ynone functionalities. The pre-polymers were then cross-linked with a multivalent thiol (where the overall thiol:ynone ratio in the material was kept at 1:1 among each formulation) to afford a network architecture composed of predominantly α,β-unsaturated thioether moieties (Figure 2).

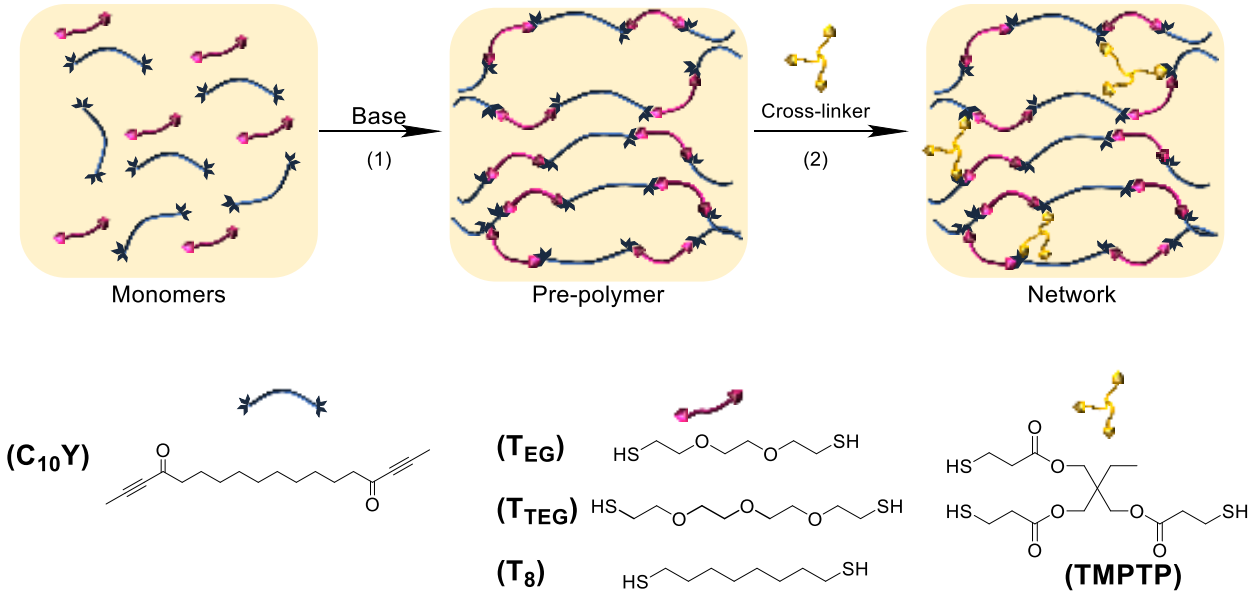

Figure 2. Synthesis of linear prepolymers (1) using the base-catalysed addition between dithiols and a diynone substrate, followed by the formation of covalent adaptable networks (CANs) (2) after cross-linking with a second multi-valent thiol.

We initially screened 2,2′-(ethylenedioxy)diethanethiol (T_{EG}) with an alkyl-based diynone, $C_{10}Y$, to afford the prepolymers and crosslinked the respective structures with trimethylolpropane tris(3-mercaptopropionate) (TMPTP). Initially, we synthesized densely crosslinked networks (T_{EG}:TMPTP ratio 0.37:0.45) and observed modest mechanical properties (UTS = 2.20 MPa, elongation at break = 265%) when the materials were assessed using uniaxial tensile testing (Figure 3a). This behaviour is likely related to the high cross-link density, and specifically the short-chain oligomers that are formed during the prepolymer step. We then optimized the mechanical properties of the networks by varying the molar ratio of dithiol (T_{EG}) and cross-linker (TMPTP) while maintaining (1:1) overall ratio of alkyne:thiol to avert a second thiol addition to the

unsaturated thioether unit. By increasing the ratio of dithiol to multivalent thiol crosslinker, this affords higher molecular weight prepolymers and an overall lower cross-linking density, which should improve the elasticity and strain at break. As this ratio was increased, the material toughness dramatically improved, reaching a maximum at a dithiol:crosslinker ratio of 0.85:0.10 with ultimate tensile strength above 23 MPa and near 1000% elongation and these values exceed those of commonly used elastomers like natural rubber (tensile strength about 19.7 MPa and elongation near 900±100%)[27], styrene butadiene rubber (SBR), and Ethylene Propylene Diene Monomer (EPDM), both of which show tensile strength below 2 MPa and elongation below 150%).[28] Compared to some of the commonly used elastomer such as NR, SBR, and EPDM, our CAN ($C_{10}Y$-T_{EG} at dithiol:crosslinker ratio of 0.85:0.10) showed very high toughness. However, the strength and elongation decreased when the cross-linking density was lowered further. We hypothesize that this may be due to the fact that the material has a mostly linear architecture above this threshold and thus exhibits thermoplastic-like behaviour as evidenced by a yielding event in the tensile curve for a ratio of 0.94:0.4. Nevertheless, a large range of material properties were accessed simply by varying the ratio of dithiol and crosslinkers in the CANs (Figure 3a). There is a rather large standard deviation in material properties that we can attribute to sample inhomogeneity associated with limitations in preparing films *in situ* from the cross-linking step. Since the cross-linking step is so rapid, the reaction mixture gelled almost instantaneously, even at low temperatures (e.g. around 0 °C) and often caused wrinkling of the film surface. The formation of the network was confirmed in all CANs by performing swelling experiments at room temperature using Tetrahydrofuran (THF). Representative CAN ($C_{10}Y$-T_{EG} with 0.85:0.10 dithiol:trithiol ratio) has shown a swelling ratio of 120±16% and soluble fraction of 3.7±0.3%.

Next, we replaced the T_{EG} thiol with a more flexible tetra(ethylene glycol) dithiol (T_{TEG}) to assess the effect of dithiol structure on the mechanical properties of CANs. We formulated a material containing T_{TEG} at the optimal dithiol:crosslinker ratio (0.85:0.10) that was observed for the previous formulation and assessed the mechanical properties. The resultant CAN displayed slightly improved elongation at break compared to the T_{EG} analogue (1200 vs 1000% respectively) which may be attributable to the increasing number of ethereal carbon-oxygen bonds which promote torsional mobility and material flexibility. To manifest the effect of the ethereal carbon-oxygen bonds, a third dithiol (T_8), which has similar architecture to T_{EG} with carbon-carbon

bonds instead of the ethereal carbon-oxygen bonds. The result clearly shows lower elongation at break compared to both T_{EG} and T_{TEG} (Figure 3b).

Thermal analysis of CANs using Differential Scanning Calorimetry (DSC) showed that the glass transition temperature (T_g) increased as the molar ratio of dithiol (T_{EG}) to cross-linker (TMPTP) increased, from −25 °C (0.45/0.37) to 0 °C (0.91/0.06). However, the T_g again decreased as the crosslinker amount was lowered further and the material approached a more linear form (Figure 3c). In addition, DSC analysis among the materials possessing different dithiols clearly shows the importance of the composition on properties. For example, without ether moieties in the monomer (i.e. T_8, octanedithiol) a semi-crystalline CAN was obtained with T_g of −10 °C and melting temperature (T_m) of 63 °C (Figure 3d).

Table 1. Summary of thermal and mechanical properties for all CANs

Dithiol	Dithiol/trithiol	T_g (°C)	Youngs Modulus (MPa)	UTS (MPa)	Elongation at break (%)
T_{EG}	0.45/0.37	−25	2.03±0.47	2.20±0.20	265±22
T_{EG}	0.70/0.20	−22	8.42±3.73	6.95±1.53	458±34
T_{EG}	0.78/0.15	−15	0.61±0.43	8.88±4.02	1016±78
T_{EG}	0.85/0.10	−10	4.10±0.34	23.56±6.12	992±138
T_{EG}	0.91/0.06	0	17.43±5.96	15.30±6.91	792±232
T_{EG}	0.94/0.04	−20	25.64±4.11	12.84±2.82	733±119
T_{EG}	1.00/0.00	−20	5.21±1.60	3.38±1.36	404±145
T_{TEG}	0.85/0.10	−23	0.83±0.17	4.07±0.93	1270±159
T_8	0.85/0.10	−10	17.58±5.86	12.95±2.58	470±103
NR[a]	-	-	-	19.69	900±100

[a] Representative mechanical properties for vulcanized natural rubber.[27] The reported results are average value of 3 samples, and uncertainty taken as standard deviation (n = 3).

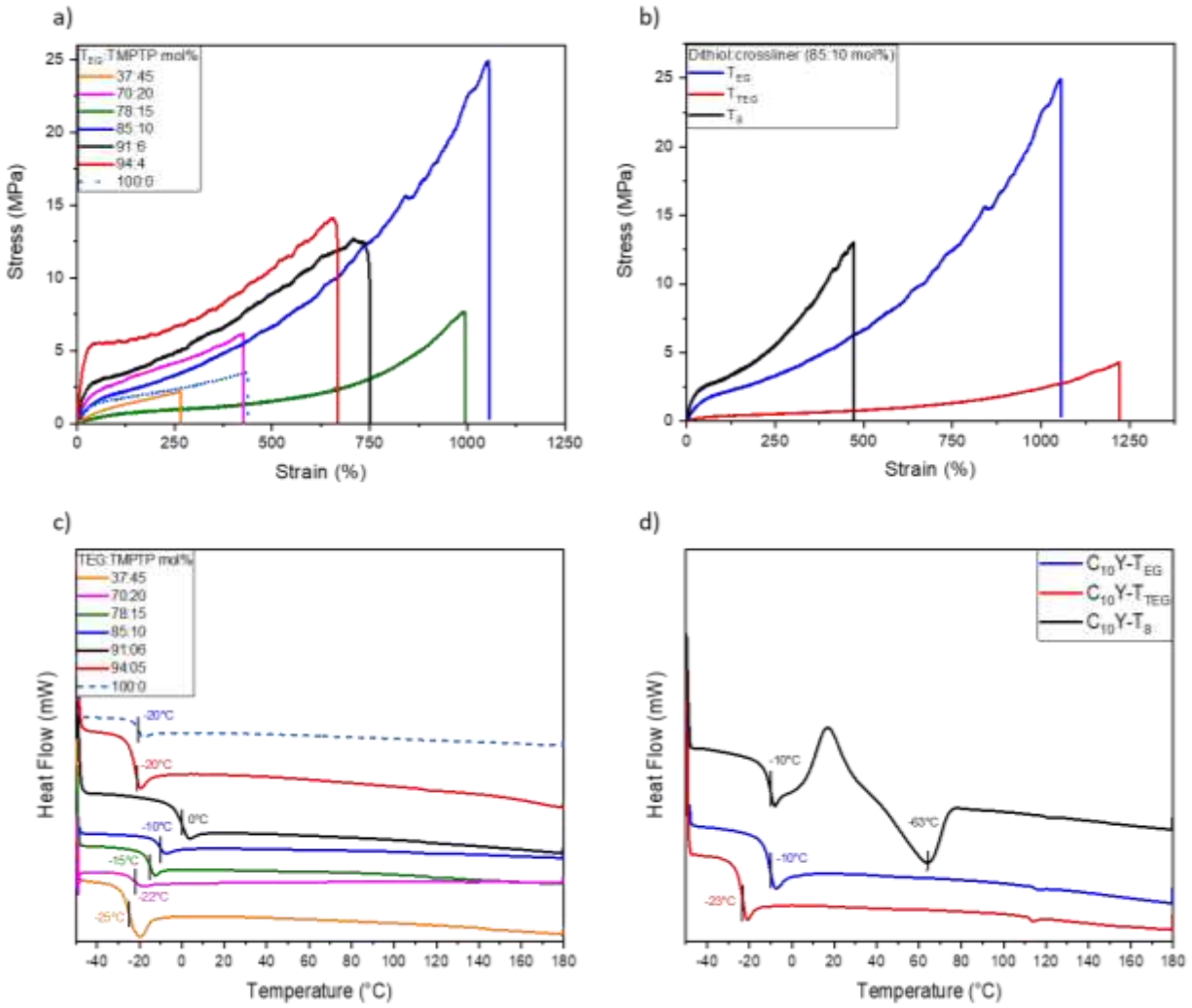

Figure 3. a) Representative tensile curves of different CANs formulated from the reaction of $C_{10}Y$ with T_{EG} at various cross-linking densities (n ≥ 3). b) Representative tensile curves of CANs based on different dithiols at the optimal dithiol:crosslinker ratio (n ≥ 3). c) Representative DSC curves "2nd heating cycle" of different CANs formulated from the reaction of $C_{10}Y$ with T_{EG} at various cross-linking densities. d) Representative DSC curves "2nd heating cycle" of CANs based on different dithiols at the optimal dithiol:crosslinker ratio.

Relaxation moduli of the materials as a function of time were obtained at 140 °C and 80 °C with a constant applied strain of 1% for $C_{10}Y$-T_{EG} and $C_{10}Y$-T_{TEG} (Supplementary Information Figure S31, S32). Full stress relaxation is observed for both CANs at best ratio as a result of the dynamic bond exchange. Moreover, $C_{10}Y$-T_{EG} shows relaxation time of *c.a.* 43 s, which is determined to be the time correspond to (1/e) or ~37% of the initial stress value on normalized relaxation modulus (G/G_0) based on Maxwell model.[29, 30] On the other hand, $C_{10}Y$-T_{TEG} shows rapid relaxation time of 6 s which could be attributed to the lower glass

transition temperature and overall improved flexibility of the material (Figure 4a). Together, these data suggest that the material should be dynamic and thus reprocessable. Both CANs were subjected to 3 reprocessing cycles using thermal compression moulding at 140 °C for 10 minutes (Figure 4b). It is worth noting; however, that the design of the dynamic bonds within the prepolymer led to limitation in preserving not only the crosslink density, but also the original chain lengths of the prepolymer. As a result, the mechanical properties of the reprocessed CANs were diminished compared to the original composition. On the other hand, an additional benefit of having these dynamic bonds within the prepolymer is that both the linear prepolymer as well as the networks are dynamic which permit readily blending of different CANs. For example, a new CAN was successfully obtained by blending $C_{10}Y\text{-}T_{EG}$ and $C_{10}Y\text{-}T_{TEG}$ in a 50:50 ratio.

Unlike other reported dissociative CANs, our networks have shown robust mechanical properties at room temperature while maintaining relatively fast relaxation time and rapid decrease in viscosity at elevated temperature i.e. 140 °C. In fact, due to the poor mechanical properties of reported dissociative CANs and the gradual viscosity decrease in associative CANs, caused by the network conservation, they have not been largely implemented in many industrial “fast” processing techniques which required good mechanical properties and rapid decrease in viscosity to allow for easier and faster processing.[31]

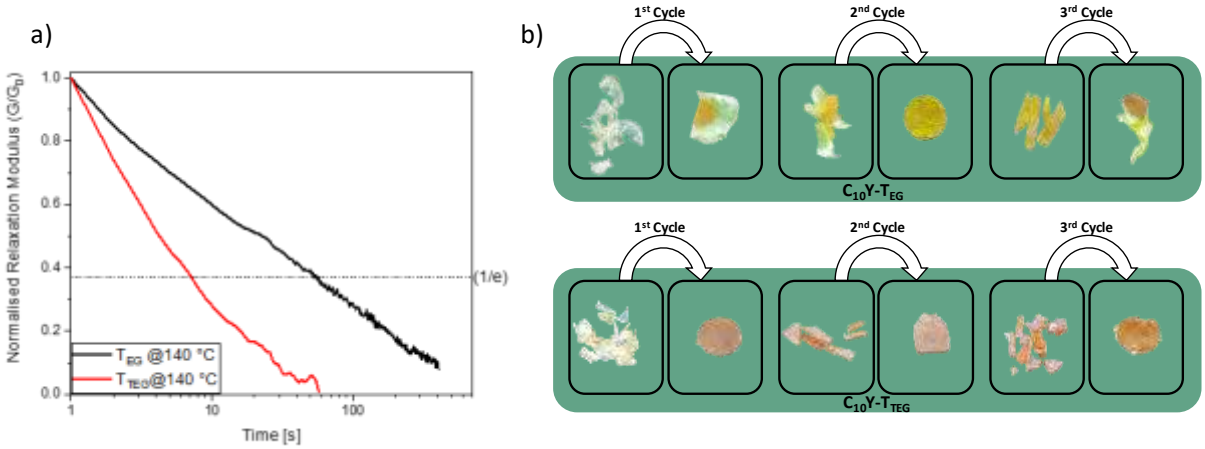

Figure 4. a) Stress-relaxation measurement of $C_{10}Y\text{-}T_{EG}$ and $C_{10}Y\text{-}T_{TEG}$ at 140 °C. b) Thermal reprocessing cycles for $C_{10}Y\text{-}T_{EG}$ and $C_{10}Y\text{-}T_{TEG}$ CANs.

Conclusion

In this work, we described the synthesis of mechanically robust elastomeric materials based on thiol-yne covalent adaptable networks (CANs). The dynamic nature of the materials was first established in small molecule model reactions in order to assess the reversibility of the reaction before extrapolating to material synthesis. The resultant materials displayed outstanding mechanical properties (with one formulation featuring an ultimate tensile strength above 23 MPa and elongation at break near 1000%) and good reprocessability at reasonable working temperatures (140 °C). This particular "super-tough" formulation ($C_{10}Y$-T_{EG} with 0.85:0.10 dithiol:trithiol ratio) has higher tensile strength and elongation than most commonly used elastomers such as NR, SBR, and EPDM. Also, maintaining unsaturation in the material backbone in this work has greatly enhanced the thermomechanical properties of CANs compared to fully saturated material architecture that was reported by Du Prez *et al*. Importantly, our synthesized materials have also shown full stress-relaxation at elevated temperature with rapid relaxation time (as low as 6 s) which is indicative of their facile reprocessability. However, there are still limitations with the presented approach since the reprocessed samples deteriorate in mechanical strength which we believe is due to loss of the defined prepolymer architecture in the as-synthesized material. We are currently developing and investigating a more robust formulation method to improve the network integrity by designing a material with regioselective exchange processes via tuning of the ynone functionality. A more exhaustive material library is also being constructed by varying the ynone and thiol precursors since we observed a wide range of thermomechanical properties even using a restricted monomer pool. Still, the fact that these thiol-yne networks are reprocessable while also mechanically strong, at least in their initial composition, positions these materials as some of the toughest dynamic materials to date. We envision reprocessable materials such as CANs to feature in the next-generation materials economy and contribute to the alleviating of waste management issues associated with our current portfolio of materials.

References

1. A. Fazli and D. Rodrigue, *Materials*, 2020, **13**, 782.
2. M. Delahaye, J. M. Winne and F. E. Du Prez, *J. Am. Chem. Soc.*, 2019, **141**, 15277-15287.
3. G. M. Scheutz, J. J. Lessard, M. B. Sims and B. S. Sumerlin, *J. Am. Chem. Soc.*, 2019, **141**, 16181-16196.
4. P. Chakma and D. Konkolewicz, *Angew. Chem., Int. Ed.*, 2019, **58**, 9682-9695.
5. N. Zheng, Y. Xu, Q. Zhao and T. Xie, *Chem. Rev.*, 2021, **121**, 1716-1745.
6. C. J. Kloxin and C. N. Bowman, *Chem. Soc. Rev.*, 2013, **42**, 7161-7173.
7. C. J. Kloxin, T. F. Scott, B. J. Adzima and C. N. Bowman, *Macromolecules*, 2010, **43**, 2643-2653.
8. C. W. M. Bunn, *Proc. R. Soc. A*, 1942, **180**, 40-66.
9. C. W. M. Bunn, *Proc. R. Soc. A*, 1942, **180**, 82-99.
10. J. Hu, R. Mo, X. Sheng and X. Zhang, *Polym. Chem.*, 2020, **11**, 2585-2594.
11. Z.-H. Chen, S.-T. Fan, Z.-J. Qiu, Z.-J. Nie, S.-X. Zhang, S. Zhang, B.-J. Li and Y. Cao, *Polym. Chem.*, 2021, **14**, 3142-3152.
12. W. Wang, W. Zhang, Z. Liu, Y. Xue, X. Lei, G. Gong and Q. Zhang, *J. Mater. Chem. C .* 2021, **9**, 6241-6250.
13. Y. Spiesschaert, C. Taplan, L. Stricker, M. Guerre, J. M. Winne and F. E. Du Prez, *Polym. Chem.*, 2020, **11**, 5377-5385.
14. R. L. Snyder, C. A. L. Lidston, G. X. De Hoe, M. J. S. Parvulescu, M. A. Hillmyer and G. W. Coates, *Polym. Chem.*, 2020, **11**, 5346-5355.
15. Y. Liu, Z. Tang, J. Chen, J. Xiong, D. Wang, S. Wang, S. Wu and B. Guo, *Polym. Chem.*, 2020, **11**, 1348-1355.
16. W. Denissen, J. M. Winne and F. E. Du Prez, *Chem. Sci.*, 2016, **7**, 30-38.
17. N. Van Herck, D. Maes, K. Unal, M. Guerre, J. M. Winne and F. E. Du Prez, *Angew. Chem., Int. Ed.*, 2020, **59**, 3609-3617.
18. L. J. Macdougall, V. X. Truong and A. P. Dove, *ACS Macro Lett.*, 2017, **6**, 93-97.
19. M. M. Pérez-Madrigal, J. E. Shaw, M. C. Arno, J. A. Hoyland, S. M. Richardson and A. P. Dove, *Biomater. Sci.*, 2020, **8**, 405-412.
20. C. A. Bell, J. Yu, I. A. Barker, V. X. Truong, Z. Cao, A. V. Dobrinyin, M. L. Becker and A. P. Dove, *Angew. Chem., Int. Ed.*, 2016, **55**, 13076-13080.
21. J. C. Worch, A. C. Weems, J. Yu, M. C. Arno, T. R. Wilks, R. T. R. Huckstepp, R. K. O'Reilly, M. L. Becker and A. P. Dove, *Nat. Commun*, 2020, **11**, 3250.
22. R. L. Snyder, C. A. Lidston, G. X. De Hoe, M. J. Parvulescu, M. A. Hillmyer and G. W. Coates, *Polym. Chem.*, 2020, **11**, 5346-5355.
23. G. Joshi and E. V. Anslyn, *Org. Lett.*, 2012, **14**, 4714-4717.
24. R. K. Dieter, L. A. Silks, J. A. Fishpaugh and M. E. Kastner, *J. Am. Chem. Soc.*, 1985, **107**, 4679-4692.
25. G. Joshi and E. V. J. O. l. Anslyn, *Org. Lett.*, 2012, **14**, 4714-4717.

26. H.-Y. Shiu, T.-C. Chan, C.-M. Ho, Y. Liu, M.-K. Wong and C.-M. Che, *Chem. Eur. J.*, 2009, **15**, 3839-3850.

27. T. Xie, F. Wang, C. Xie, S. Lei, S. Yu, J. Liu and D. Huang, *Materials*, 2019, **12**, 1863.

28. T. M. Nair, M. G. Kumaran and G. Unnikrishnan, *J. Appl. Polym. Sci.*, 2004, **93**, 2606-2621.

29. B. M. El-Zaatari, J. S. Ishibashi and J. A. Kalow, *Polym. Chem.*, 2020, **11**, 5339-5345.

30. N. Obaid, M. T. Kortschot and M. Sain, *Materials*, 2017, **10**, 472.

31. C. Taplan, M. Guerre, J. M. Winne and F. E. Du Prez, *Mater. Horiz.*, 2020, **7**, 104-110.

2.2 Supporting Information

Super tough and reprocessable elastomers based on thiol-yne covalent adaptable networks

Maher A. Alraddadi[§], Joshua C. Worch[§], Andrew P. Dove[*§]

[§]School of Chemistry, University of Birmingham, Edgbaston, Birmingham, B15 2TT (UK)

Table of Contents

General Materials and Methods

Materials: Unless otherwise stated, all chemicals and solvents used were purchased from Sigma-Aldrich, VWR Chemicals, Apollo Scientific, or Fisher Scientific and used as received without further purifications. All air sensitive compounds were synthesised under a dry nitrogen atmosphere using standard Schlenk techniques. Dry THF was used directly from a drying and degassing solvent tower.

NMR Spectroscopic Analysis: All NMR experiments were performed on a Bruker DPX-300 and DPX-400 spectrometer. All chemical shifts were reported in ppm and referenced to the solvent signal $CDCl_3$, δ = 7.26 ppm and ^{13}C NMR spectra are referenced to the solvent signal (δ = 77.16 for $CDCl_3$). The multiplicity of the peaks was characterized as s = singlet, d = doublet, t = triplet, q = quartet, qu = quintet, m = multiplet.

Mass Spectrometry: High Resolution Electrospray Ionization Mass Spectrometry was performed in the School of Chemistry at University of Birmingham on a Waters Xevo G2-XS QTof Quadrupole Time-of-Flight mass spectrometer.

Fourier-transform Infared spectroscopy (FTIR)

All FTIR analysis were performed on an Agilent Technologies Cary 630 FTIR spectrometer.

At a resolution of 4 cm^{-1}, 16 Scans from 600 to 4000 cm^{-1} were preformed and the spectra were corrected for background absorbance.

Differential scanning calorimetry (DSC): All thermal transitions include glass transition temperature (T_g) and melting temperature (T_m) were determined using Mettler-Toledo STARe system DSC3+. All samples were tested under nitrogen at heating rate of 10 °C/min for two heating/cooling cycles, unless otherwise stated. The glass transition temperature was taken from the inflection point of the second heating cycle.

Rheology: The flow characteristics of the polymers were studied using Anton Paar MCR302 rheometer with Peltier controlled heating. All tests were performed using parallel plates on disk-shape samples of 8 mm in diameter. Unless otherwise specified, stress relaxation experiments were performed at 1% constant strain which is within the linear viscoelastic region of polymer at 140 °C. For frequency sweep measurement, the frequency was varied from 100 Hz to 0.01 Hz. For strain sweep measurements, strain was varied between 0.1% to 10%.

Tensile testing: All uniaxial tensile testing was performed on a Testometric M350-5CT tensometer fitted with a load cell of 5 kgF. All measurements were performed at room temperature and strain rate of 10 mm/min. Polymer films were cut into dumbbell-shaped samples with custom ASTM Die D-638 Type 5 (Neck dimensions 7.11 × 1.70) and a hand press. The sample width about 1.7 mm and thickness about 0.2 mm with the gauge length set to 7.1 mm. Unless otherwise stated, a minimum of n = 3 specimens were tested for each polymer film with average values and standard deviation reported.

Swelling experiments: Swelling experiments were performed on disks (diameter = 8 mm, thickness = 2 mm). The initial weights of the samples were taken, then the samples were submerged into a 10 mL of Tetrahydrofuran (THF) in a 20 mL glass vial. The samples were left at room temperature for 3 days. The swollen weight was then taken, and the sample were left to dry overnight in a vacuum oven at 40 °C. The swelling ratio and the soluble fraction were calculated using the formulas:

$$\text{Swelling ratio} = \frac{swollen\ weight - dried\ weight}{dried\ weight}$$

$$\text{Soluble fration} = \frac{initial\ weight - dried\ weight}{initial\ weight}$$

The reported result is an average of 3 measurements (n = 3).

Film casting: a 20 mL glass vial charged with the respective prepolymer was cooled to −70 °C (dry ice/acetone bath) for 30 seconds. The proper amount of crosslinker was added to the vial and stirred for 5 seconds. The vial was then removed from the cooling bath and rotated in a rotary evaporator for about 30 seconds, ensuring the polymer mixture was covering the wall of the glass vial. The vial was then removed from the rotary evaporator and placed inside a fume hood to allow solvent evaporation overnight. Note: better film with smoother surface was casted when the solvent evaporation process was slow down by placing the vial under an inverted beaker “upside-down”. The vial was then placed into a dry ice/acetone bath for about 30 seconds to reduce tackiness of the film to the glass, then the film was pulled out from the vial’s wall and cut (Figure S34).

Synthesis

General procedure for Weinreb amide synthesis

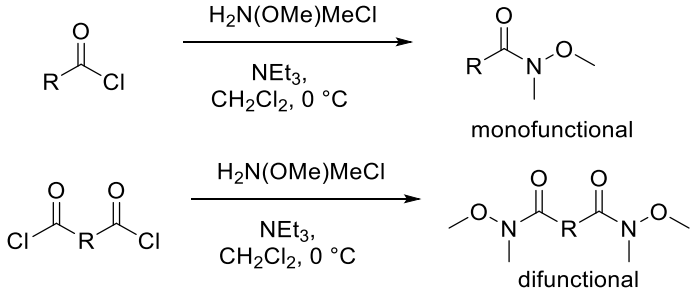

The procedure was adapted from literature.[1, 2] The stoichiometry in this procedure are used for the synthesis of a mono-functional Weinreb amide, twice the molar equivalent should be used in the synthesis of a difunctional Weinreb amide. Into a 3-neck round-bottom flask equipped with magnetic stirrer and attached to a dropping funnel, (1 equiv.) of the acid chloride of interest, or diacid chloride for difunctional amide, and dichloromethane were added to make a 1 M solution. The reaction mixture was cooled to −10 °C (brine-ice bath) and (1.1 equiv.) of N,O-dimethylhydroxylamine hydrochloride was added to the reaction mixture. (2.2 equiv.) of triethylamine was transferred to the dropping funnel and slowly added to the reaction mixture (dropwise, over 20−30 minutes). The reaction is exothermic and a white precipitate (ammonium salt by-product) was produced. After the addition of the triethylamine, the reaction mixture was removed from the cooling bath and stirred at ambient temperature for 1 h. The reaction mixture was diluted with dichloromethane (20% v/v) and transferred to a separatory funnel. The organic layer was washed with 1 M HCl, saturated $NaHCO_3$, water, and brine, respectively. The combined organic layer was dried over magnesium sulfate and concentrated using a rotary evaporator.

Synthesis of N-methoxy-N-methylbenzamide

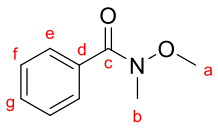

Using the general procedure and employing benzoyl chloride, a transparent light-yellow oil (33.0 g, 86% yield) was obtained. ^{1}H NMR (300 MHz, Chloroform-*d*) δ 7.70 – 7.62 (m, 2H, H^{e}), 7.50 – 7.35 (m, 3H, H^{f,g}), 3.55 (s, 3H, H^{a}), 3.35 (s, 3H, H^{b}). ^{13}C NMR (75 MHz, $CDCl_3$) δ 169.89 (C^{c}), 134.07 (aromatic C), 130.48 (aromatic C), 128.06(aromatic C), 127.94 (aromatic C), 60.96 (C^{a}), 33.72 (C^{b}). FTIR: 1633 cm^{-1} (C=O Amide). HRMS (TOF MS ES+) (m/z): [M + H]$^{+}$ calculated for $C_9H_{11}NO_2$, 166.0868; found, 166.0874. Anal. Calcd for $C_9H_{11}NO_2$: C, 65.44; H, 6.71; N, 8.48. Found: C, 65.69; H, 6.59; N, 8.69. FT-IR: 1633 cm^{-1} (C=O amide). The spectra are in accordance with a previous report.[1]

Synthesis of N-methoxy-N-methylhexanamide

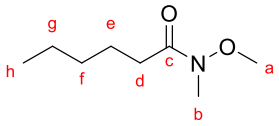

Using the general procedure and employing hexanoyl chloride, a transparent light-yellow oil of (9.4 g, 80% yield) was obtained after purification by silica gel column chromatography (hexane/ethyl acetate 3/1, R_f = 0.8). ^{1}H NMR (300 MHz, Chloroform-d) δ 3.67 (s, 3H, H^{a}), 3.17 (s, 3H, H^{b}), 2.40 (t, J = 7.6 Hz, 2H, H^{d}), 1.62 (qu, J = 7.4 Hz, 2H, H^{e}), 1.39 – 1.26 (m, 4H, H^{f-g}), 0.89 (t, J = 6.9 Hz, 3H, H^{h}). ^{13}C NMR (101 MHz, $CDCl_3$) δ 174.99 (C^{C}), 61.30 (C^{a}), 32.27 (C^{b}), 31.98 (C^{d}), 31.74 (C^{e}), 24.46 (C^{f}), 22.59 (C^{g}), 14.07 (C^{h}). HRMS (TOF MS ES+) (m/z): [M + H]$^{+}$ calculated for $C_8H_{17}NO2$, 160.1338; found, 160.1345. Anal. Calcd for $C_8H_{17}NO_2$: C, 60.34; H, 10.76; N,8.80; S,0. Found: C, 60.15; H, 10.61; N,8.79; S,0. FT-IR: 1659 cm^{-1} (C=O amide). The spectrum are in accordance with a previous report.[2]

General procedure for ynone/diynone synthesis

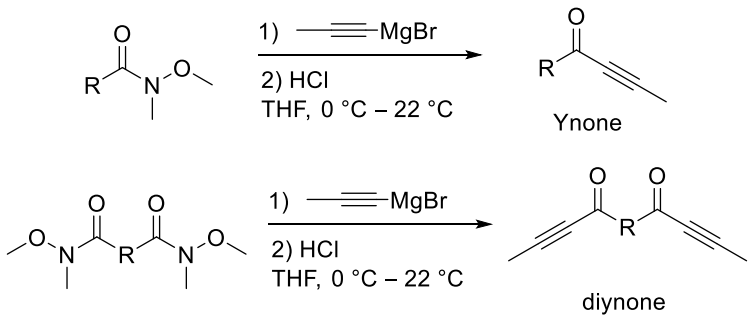

The following stoichiometry used in this procedure are for the synthesis of ynone, twice the molar equivalent should be used when synthesising diynone. In dried glassware and under Schlenk conditions, (1 equiv.) of the mono-functional Weinreb amide (di-functional Weinreb amide for diynone synthesis) is added to a 3-neck round bottom flask with a dropping funnel attached. It was then diluted to 1 M using dry THF via cannula transfer. Then, (1.4 equiv.) of 1-propynylmagnesium bromide solution (0.5 M in THF) was cannula transferred into the dropping funnel and the reaction mixture was cooled to −10 °C (brine-ice bath). After the solution cooled, the 1-propynylmagnesium bromide solution was added to the reaction mixture slowly (over 30 min). The reaction mixture was then stirred for 30 min in the cooling bath and then warmed to room temperature to react overnight (c.a. 16 h). The reaction mixture was cooled back to 0 °C. After the mixture is cooled, it was quenched with 1 M HCl (25% v/v) dropwise at first, then in excess. The crude mixture was transferred to a separatory funnel and purified using aqueous extraction with ethyl acetate. The organic layer was washed with brine. The combined organic layer was dried over magnesium sulfate and concentrated using a rotary evaporator and purified using silica gel column chromatography.

Synthesis of 1-phenylbut-2-yn-1-one

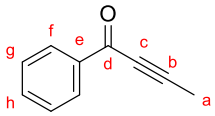

A transparent light-yellow oil was obtained in (5.2 g, 70% yield) after purification by silica gel column chromatography (hexane/ethyl acetate 4/1, R_f = 0.5). ^{1}H NMR (300 MHz, Chloroform-*d*) δ 8.21 – 8.10 (m, 2H, H^{f}), 7.66 – 7.42 (m, 3H, $H^{g,h}$), 2.16 (s, 3H, H^{a}). ^{13}C NMR (75 MHz, Chloroform-d) δ 178.21 (C^{d}), 136.80 (aromatic C), 133.90 (aromatic C), 129.57 (aromatic C), 128.47 (aromatic C), 92.46 (C^{b}), 78.98 (C^{c}), 4.32 (C^{a}). FT-IR: 1633 cm^{-1} (C=O ketone), 2198 cm^{-1} (C≡C). HRMS (TOF MS CI+) (m/z): $[M + H]^{+}$ calculated for $C_{10}H_8O$, 145.07; found, 145.06. Anal. Calcd for $C_{10}H_8O$: C, 83.31; H, 5.59; N,0; S,0. Found: C, 86.75; H, 6.36; N,0; S,0. The NMR spectra are in accordance with a previous report. [3]

Synthesis of non-2-yn-4-one

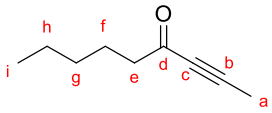

The product was isolated as a transparent yellow liquid (3.7 g, 78% yield) after purification by silica gel column chromatography (hexane/ethyl acetate 8/1, R_f = 0.6).

^{1}H NMR (300 MHz, Chloroform-d) δ 2.50 (t, J = 7.4 Hz, 2H, H^{e}), 2.01 (s, 3H, H^{a}), 1.65 (qu, J = 7.4 Hz, 2H, H^{f}), 1.37 – 1.18 (m, 4H, $H^{g,h}$), 0.94 – 0.83 (t, J= 6.9 Hz, 3H, H^{i}). ^{13}C NMR (75 MHz, Chloroform-d) δ 188.46 (C^{d}), 89.75 (C^{b}), 80.21 (C^{c}), 45.37 (C^{e}), 31.09 (C^{f}), 23.70 (C^{g}), 22.33 (C^{h}), 13.83 (C^{i}), 3.99 (C^{a}). FT-IR: 1667 cm^{-1} (C=O ketone), 2213 cm^{-1} (C≡C). HRMS (TOF MS CI+) (m/z): $[M + NH_4]^{+}$ calculated for $C_9H_{18}NO$, 156.1388; found, 156.1388. Anal. Calcd for $C_9H_{14}O$: C, 78.21; H, 10.21; N,0; S,0. Found: C, 63.57; H, 7.48; N,0; S,0.

Synthesis of octadeca-2,16-diyne-4,15-dione Monomer ($C_{10}Y$)

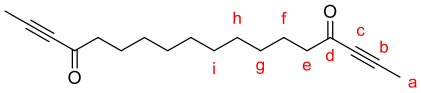

The product was isolated as a white powder in (9.1 g, 80% yield) after purification by silica gel column chromatography (hexane/ethyl acetate 4/1, R_f = 0.6). ^{1}H NMR (400 MHz, Chloroform-*d*) δ 2.54 – 2.48 (t, *J* = 7.4 Hz, 4H, H^e), 2.01 (s, 6H, H^a), 1.64 (qu, *J* = 7.2 Hz, 4H, H^f), 1.33 – 1.23 (m, 12H, $H^{g\text{-}i}$).^{13}C NMR (101 MHz, $CDCl_3$) δ 188.45 (C^d), 89.76 (C^b), 80.21 (C^c), 45.39 (C^e), 29.28 (C^f), 28.90 (C^g), 23.99 (C^h), 4.01 (C^a). FT-IR: 1650 cm^{-1} (C=O ketone), 2211 cm^{-1} (C≡C). Anal. Calcd for $C_{18}H_{26}O_2$: C, 78.79; H, 9.55; N,0; S,0. Found: C, 36.90; H, 4.51; N,0; S,0.

General procedure for thiol-yne single and double addition

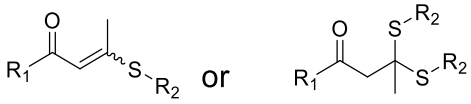

To a round bottom flask, (1 equiv.) of thiol, for single addition or (2 equiv.) for double addition, is added to (1 equiv.) of the ynone. The substrates were cooled in an ice bath. After the mixture was cooled down, (0.01 equiv.) of 1,8-Diazabicyclo[5.4.0] undec-7-ene (DBU) was added to the mixture and stirred at room temperature for 3 hours. The crude reaction mixture was then analysed by TLC and purified using silica gel column chromatography.

Synthesis of 3-(ethylthio)-1-phenylbut-2-en-1-one

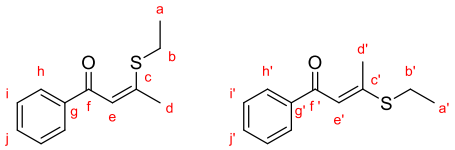

A mixture of *E/Z* isomers, in ratio of 0.61:0.39 *E* to *Z* isomer, as a yellow powder product of (0.90 g, 60% yield) was obtained after purification by silica gel column chromatography using (hexane/ethyl acetate 3/1, R_f = 0.5).

^{1}H NMR (300 MHz, Chloroform-d) δ 8.02 – 7.81 (m, 4H, H^{h}, *E/Z*-isomers), 7.62 – 7.33 (m, 6H, $H^{i,j}$, *E/Z*-isomers), 7.00 (d, J = 1.1 Hz, 1H, H^{e}, Z-isomer), 6.64 (d, J = 1.1 Hz, 1H, $H^{e'}$, E-isomer), 3.01-2.86 (m, 4H, H^{b}, *E/Z*-isomers), 2.51 (d, J = 1.1 Hz, 3H, $H^{C'}$, *E*-isomer), 2.40 (d, J = 1.1 Hz, 3H, H^{C}, *Z*-isomer), 1.45-1.30 (m, 6H, H^{a}, *E/Z*-isomers). ^{13}C NMR (101 MHz, $CDCl_3$) δ (188.45, 188.00, $C^{f/f'}$), (162.32, 161.64, $C^{C/C'}$), (140.15, 139.01, $C^{g/g'}$), (132.17, 132.05, $C^{j/j'}$), (128.65, 128.61, $C^{i/i'}$), (128.11, 128.04, $C^{h/h'}$), (116.76, 113.54 $C^{e/e'}$), (26.09, 25.06, $C^{b/b'}$), (24.64, 22.21, $C^{d/d'}$), (14.10, 12.87, $C^{a/a'}$). FT-IR: 1617 cm^{-1} (C=O ketone), 726 cm^{-1} (C=CH). HRMS (TOF MS ASAP+) (m/z): $[M + H]^{+}$ calculated for $C_{12}H_{15}OS$, 207.0844; found, 207.0848. Anal. Calcd for $C_{12}H_{15}OS$: C, 69.52; H, 7.29; N,0; S,15.47. Found: C, 69.98; H, 7.08; N,0; S,15.66. The NMR spectra are in accordance with literature[4].

Synthesis of 3,3-bis(ethylthio)-1-phenylbutan-1-one

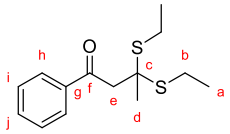

The product was obtained as a light-yellow viscous oil in (0.90 g, 50% yield) after purification by silica gel column chromatography using (hexanes/ethyl acetate 8/1, R_f = 0.5). ^{1}H NMR (300 MHz, Chloroform-d) δ 8.05 – 7.89 (m, 2H, H^{h}), 7.71 – 7.40 (m, 3H, $H^{i,j}$), 3.44 (s, 2H, H^{e}), 2.67 (q, J = 7.5, 4H, H^{b}), 1.79 (s, 3H, H^{d}), 1.21 (t, J = 7.5 Hz, 6H, H^{a}).^{13}C NMR (101 MHz, $CDCl_3$) δ 196.76 (C^{f}), 133.23 (C^{g}), 128.72 (aromatic C), 128.49 (aromatic C), 57.57 (C^{e}), 48.70 (C^{C}), 28.18 (C^{d}), 24.06 (C^{b}), 13.99 (C^{a}). FT-IR: 1625 cm^{-1} (C=O ketone). HRMS (TOF MS ASAP+) (m/z): $[M + H]^{+}$ calculated for $C_{14}H_{20}OS_2$, 207.0844; found, 207.0851. Anal. Calcd for $C_{14}H_{20}OS_2$: C, 62.64; H, 7.51; N,0; S,23.89. Found: C, 69.41; H, 6.88; N,0; S,15.66.

Synthesis of 1-phenyl-3-(phenylthio)but-2-en-1-one

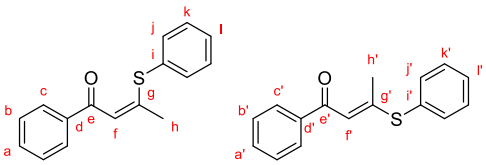

A mixture of *E/Z* isomers, in ratio of 0.31:0.69 *E* to *Z* isomer, as an orange powder in (1.8 g, 70% yield) after purification by silica gel column chromatography using (hexanes/ethyl acetate 4/1, R_f = 0.6)

^{1}H NMR (300 MHz, Chloroform-d) δ 8.10 – 7.91 (m, 8H, H^c, *E/Z*-isomers), 7.73 – 7.31 (m, 12H, $H^{a,b}$, *E/Z*-isomers), 7.08 (q, J = 1.1 Hz, 1H, H^f,*Z*-isomers), 6.38 (q, J = 1.0 Hz, 1H, $H^{f'}$, *E*-isomers), 2.54 (d, J = 1.0 Hz, 3H, $H^{h'}$, *E*-isomers), 1.99 (d, J = 1.1 Hz, 3H, H^h,*Z*-isomers). ^{13}C NMR (101 MHz, $CDCl_3$) δ 161.96 ($C^{g/g'}$), (135.92, 135.69, 132.27, 130.18, 129.97, 129.64, 129.25, 128.65, 128.53, 128.13, 128.04, aromatic C), (116.43, 115.66, $C^{f/f'}$), (26.00, 21.27, $C^{h/h'}$). FT-IR: 1625 cm^{-1} (C=O ketone), 701 (C=CH). HRMS (TOF MS ASAP+) (m/z): $[M + H]^+$ calculated for $C_{16}H_{14}OS$, 255.0844; found, 255.0850. Anal. Calcd for $C_{16}H_{14}OS$: C, 75.56; H, 5.55; N,0; S,12.61. Found: C, 76.62; H, 5.95; N,0; S,12.71.

Synthesis of 1-phenyl-3,3-bis(phenylthio)butan-1-one

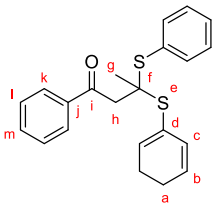

The compound was isolated as a light yellow viscous liquid in (1.3 g, 50% yield) after purification by silica gel column chromatography using (hexanes/ethyl acetate 3/1, R_f = 0.6). ^{1}H NMR (300 MHz, Chloroform-*d*) δ 7.80 – 7.62 (m, 6H, $H^{c,k}$), 7.56 – 7.29 (m, 9H, $H^{a,b,l,m}$), 3.38 (s, 2H, H^h), 1.71 (s, 3H, H^g).^{13}C NMR (101 MHz, $CDCl_3$) δ 196.46 (C^i), (137.37, 133.18, 131.73, 129.58, 128.85, 128.66, 128.25, aromatic C), 61.24 (C^g), 47.80 (C^b), 28.12 (C^a). HRMS (TOF MS ES+) (m/z): [M + Na] calculated for $C_{22}H_{20}OS_2$, 387.0853; found, 387.0852. Anal. Calcd for

$C_{22}H_{20}OS_2$: C, 72.49; H, 5.53; N,0; S,17.59. Found: C, 72.50; H, 5.55; N,0; S,17.38. FT-IR: 1676 cm^{-1} (C=O ketone).

Synthesis of 2-(ethylthio)non-2-en-4-one

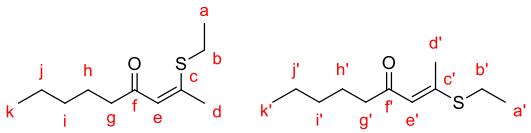

The product was afforded as a transparent yellow liquid in (0.5 g, 70% yield) after purification by silica gel column chromatography (hexane/ethyl acetate 5/1, R_f = 0.5). ^{1}H NMR (300 MHz, Chloroform-*d*) δ 6.23 (q, *J* = 1.1 Hz, 1H,H^e, *Z*-isomers), 5.92 (d, *J* = 1.1 Hz, 1H, $H^{e'}$, *E*-isomers), 2.87 (q, *J* = 7.5, 4H, $H^{b/b'}$,*E/Z*-isomers-Overlap), 2.45 – 2.36 (m, 8H, $H^{e/e',f/f'}$, *E/Z*-isomers), 2.24 (d, *J* = 1.1 Hz, 3H, $H^{d'}$, *E*-isomers), 2.17 (s, 3H, H^d, *Z*-isomers), 1.34 – 1.27 (m, 14H, $H^{a/a',j/j',\ i/l'}$, *E/Z*-isomers), 0.92 – 0.85 (m, 6H, $H^{k/k'}$, *E/Z*-isomers). ^{13}C NMR (101 MHz, $CDCl_3$) δ (197.75, 197.75, $C^{f/f'}$), (158.83, 158.47, $C^{c,c'}$), (120.13, 116.29, $C^{e/e'}$), 44.52 ($C^{g/g'}$), 43.21, ($C^{i/i'}$), (31.66, 31,69, $C^{b/b'}$), (25.76, 24.74, $C^{h/h'}$), (24.45, 23.90, $C^{d/d'}$), (22.67, 21.69, $C^{j/j'}$), 14.10 ($C^{a/a'}$), 12.77 ($C^{k/k'}$). FT-IR: 1650 cm^{-1} (C=O ketone), 723 (C=CH). HRMS (TOF MS ASAP+) (m/z): $[M + H]^+$ calculated for $C_{11}H_{20}OS$, 201.1313; found, 201.1316. Anal. Calcd for $C_{11}H_{20}OS$: C, 65.95; H, 10.06; N,0; S,16. Found: C, 66.86; H, 9.66; N,0; S,16.80.

Synthesis of 2-(phenylthio) non-2-en-4-one

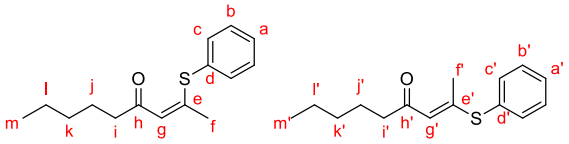

The compound was obtained as a transparent yellow liquid in (0.5 g, 60% yield) after purification by silica gel column chromatography (hexane/ethyl acetate 3/1, R_f = 0.7)

^{1}H NMR (300 MHz, Chloroform-d) δ 7.60 – 7.31 (m, 10H, $H_{E/Z\ \text{aromatic}}$), 6.31 (d, J = 1.2 Hz, 1H, H^g), 5.67 (d, J = 1.0 Hz, 1H, $H^{g'}$), 2.48 (d, J = 7.3 Hz, 2H, H^i), 2.41 (d, J = 1.0 Hz, 3H, $H^{f'}$), 2.22 (t, J = 7.5 Hz, 2H, $H^{i'}$), 1.83 (d, J = 1.1 Hz, 3H, H^f), 1.66 (qu, J = 7.3 Hz, 2H, H^l), 1.47 (qu, J =

7.5 Hz, 2H,$H^{l'}$), 1.38 – 1.12 (m, 8H, $H^{k/k,j/j'}$), 0.95 – 0.80 (m, 6H, $H^{m/m'}$).^{13}C NMR (101 MHz, $CDCl_3$) δ (199.23, 198.33, $C^{h/h'}$), (159.39, 158.18, $C^{e/e'}$), (135.95, 135.56, $C^{d/d'}$), (131.52, 129.94, 129.80, 129.50, 129.13, aromatic C), (119.71, 118.43, $C^{g/g'}$), (44.37, 43.30, $C^{i/i'}$), (31,69, 31.48, $C^{k/k'}$), 25.26 $C^{j/j'}$, (24.38, 24.11, $C^{f/f'}$), (22.66, 22.57, $C^{l/l'}$), (14.08, 14.02, $C^{m/m'}$). FT-IR: 1659 cm^{-1} (C=O ketone), 752 (C=CH). Anal. Calcd for $C_{15}H_{20}OS$: C, 72.53; H, 8.12; N,0; S,12.91. Found: C, 72.64; H, 8.16; N,0; S,12.17.

Synthesis of 2,2-bis(phenylthio)nonan-4-one

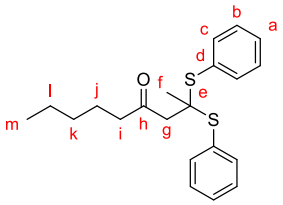

The product was isolated as a transparent yellow liquid in (0.5 g, 50% yield) after purification by silica gel column chromatography (hexane/ethyl acetate 5/1, R_f = 0.5) ^{1}H NMR (300 MHz, Chloroform-d) δ 7.71 – 7.58 (m, 4H, H^c), 7.52 – 7.27 (m, 6H, $H^{a,b}$), 2.82 (s, 2H, H^g), 2.34 (t, J = 7.3 Hz, 2H, H^i), 1.60 (s, 3H, H^f), 1.51 (p, J = 7.3 Hz, 2H, H^j), 1.36 – 1.16 (m, 4H, $H^{k,l}$), 0.88 (t, J = 7.0 Hz, 3H, H^m). ^{13}C NMR (101 MHz, $CDCl_3$) δ 207.16 (C^h), (137.16, 135.99, 135.59, 131.76, 129.55, 129.16, 128.86, 127.66, 127.30, aromatic C), 60.71 (C^g), 52.50 (C^e), 45.03 (C^i), 31.39 (C^k), 27.96 (C^f), 23.29 (C^l), 22.60 (C^j), 14.06 (C^m). HRMS (TOF MS ASAP+) (m/z): $[M + H]^+$ calculated for $C_{21}H_{26}OS_2$, 249.1313; found, 249.1313. Anal. Calcd for $C_{21}H_{26}OS_2$: C, 70.35; H, 7.31; N,0; S,17.88. Found: C, 72.49; H, 7.87; N,0; S,17.53.

Representative synthesis of $C_{10}Y$-T_{EG} Prepolymer

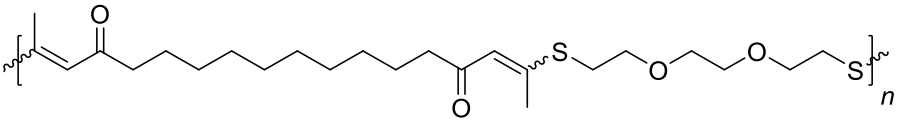

The following stoichiometry is for the synthesis of $C_{10}Y$-T_{EG} at the best dithiol:cross-linker ratio. (1 equiv.) of diynone monomer ($C_{10}Y$) was added into a flask and dissolved in dichloromethane

(30 wt%). Next, (0.85 equiv.) of the 2,2′-(ethylenedioxy)diethanethiol (T_{EG}) was added to the mixture. The reaction mixture was stirred for 5 minutes and cooled to −70 °C (dry ice/acetone bath). (0.05 equiv.) of 1,8-diazabicyclo[5.4.0]undec-7-ene (DBU) was added, then the reaction mixture was removed from the cooling bath and stirred at ambient temperature for 1 h. The reaction mixture was then cooled to −70 °C (dry ice/acetone bath) before the addition of trimethylolpropane tris(3-mercaptopropionate) (0.10 equiv.). The reaction mixture was then removed from the cooling bath and stirred for 30 seconds, then the polymer film was casted.

Representative Synthesis of $C_{10}Y$-T_{TEG} Prepolymer

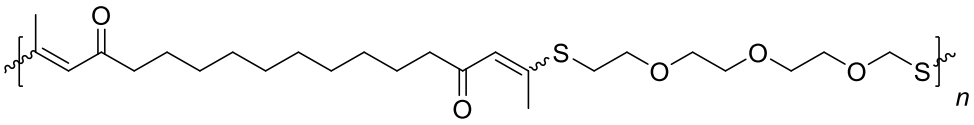

The following stoichiometry is for the synthesis of $C_{10}Y$-T_{TEG} at the best dithiol:cross-linker ratio. (1 equiv.) of diynone monomer ($C_{10}Y$) was added into a flask and dissolved in dichloromethane (30 wt%). Next, tetra(ethylene glycol) dithiol (T_{TEG}) (0.85 equiv.) was added to the mixture. The reaction mixture was stirred for 5 minutes and cooled to −70 °C (dry ice/acetone bath). (0.05 equiv.) of 1,8-diazabicyclo[5.4.0]undec-7-ene (DBU) was added then the reaction mixture was removed from the cooling bath and stirred at ambient temperature for 1 h. The reaction mixture was then cooled to −70 °C (dry ice/acetone bath), before the addition of trimethylolpropane tris(3-mercaptopropionate) (0.10 equiv.). The reaction mixture was then removed from the cooling bath and stirred for 30 seconds, then the polymer film was casted.

NMR Spectra

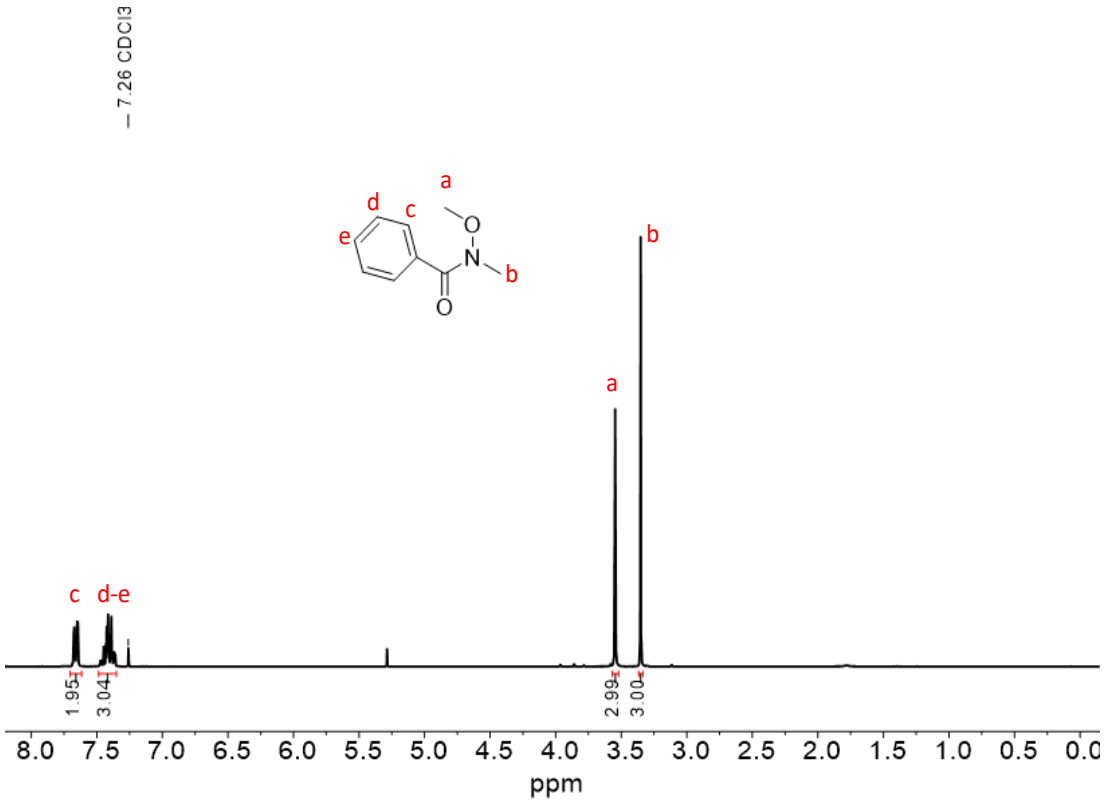

Figure S1. N-methoxy-N-methylbenzamide ^{1}H NMR Spectrum (300 MHz, 298 K,$CDCl_3$).

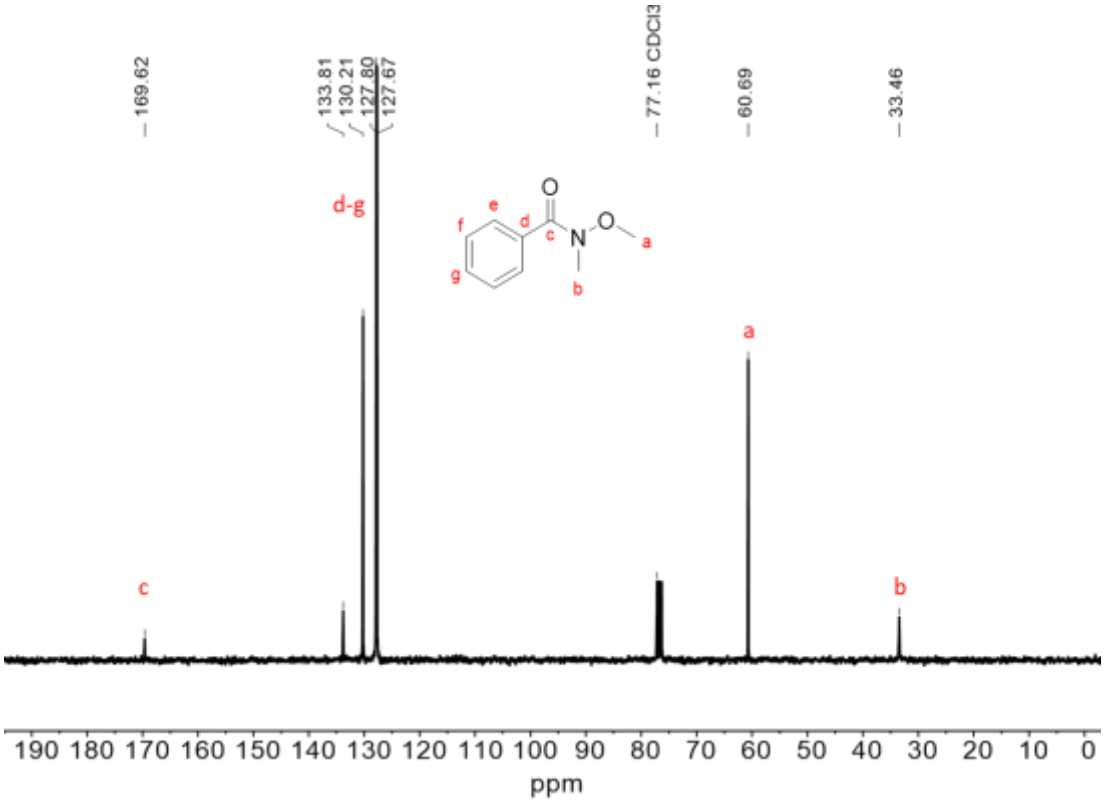

Figure S2. N-methoxy-N-methylbenzamide ^{13}C NMR Spectrum (75 MHz, 298 K, $CDCl_3$).

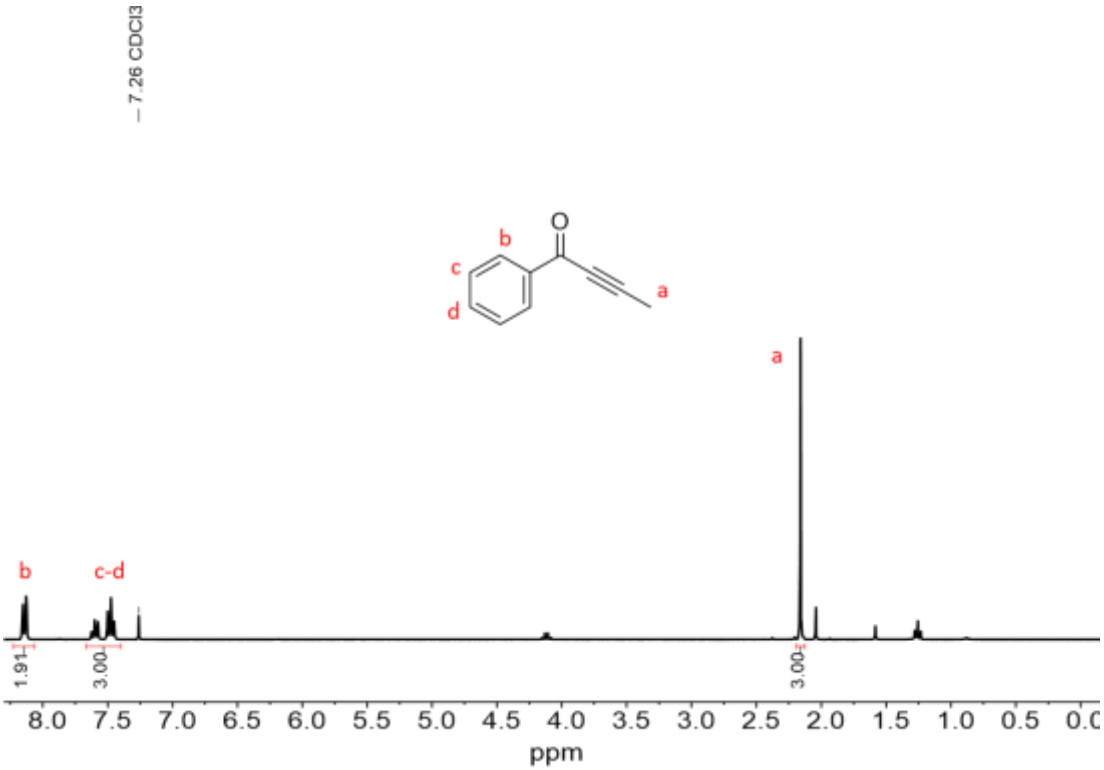

Figure S3. 1-phenylbut-2-yn-1-one ^{1}H NMR Spectrum (300 MHz, 298 K, $CDCl_3$).

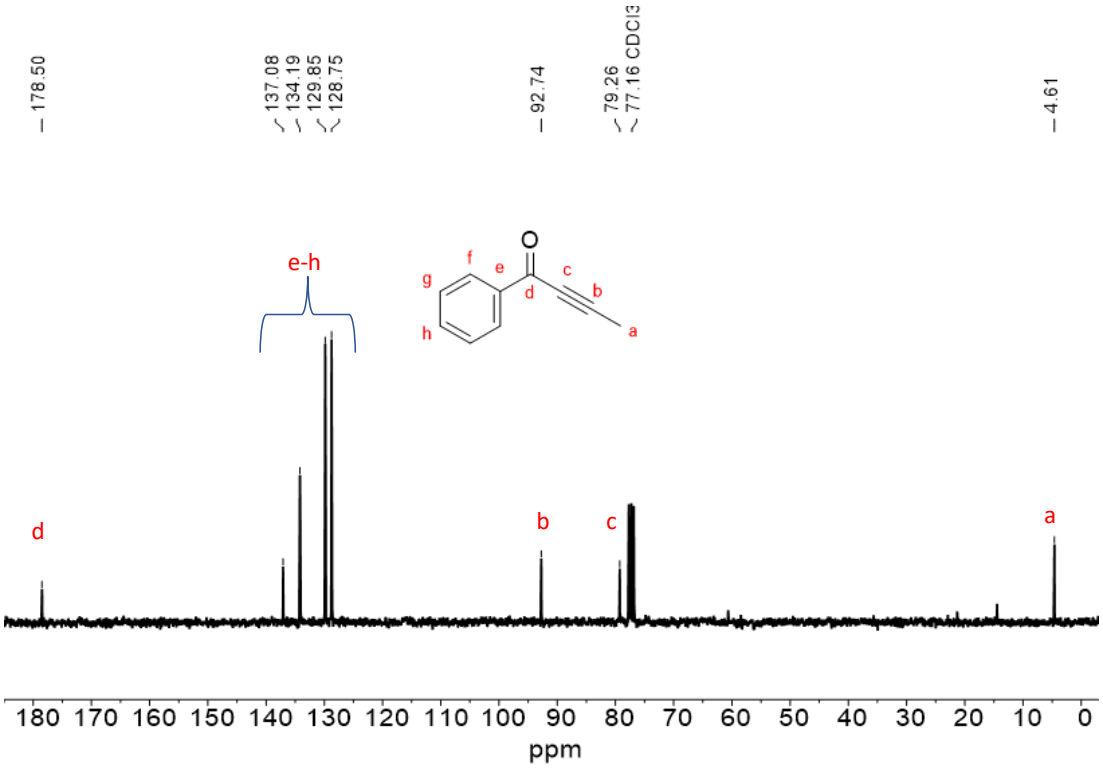

Figure S4. 1-phenylbut-2-yn-1-one ^{13}C NMR Spectrum (75 MHz, 298 K, $CDCl_3$).

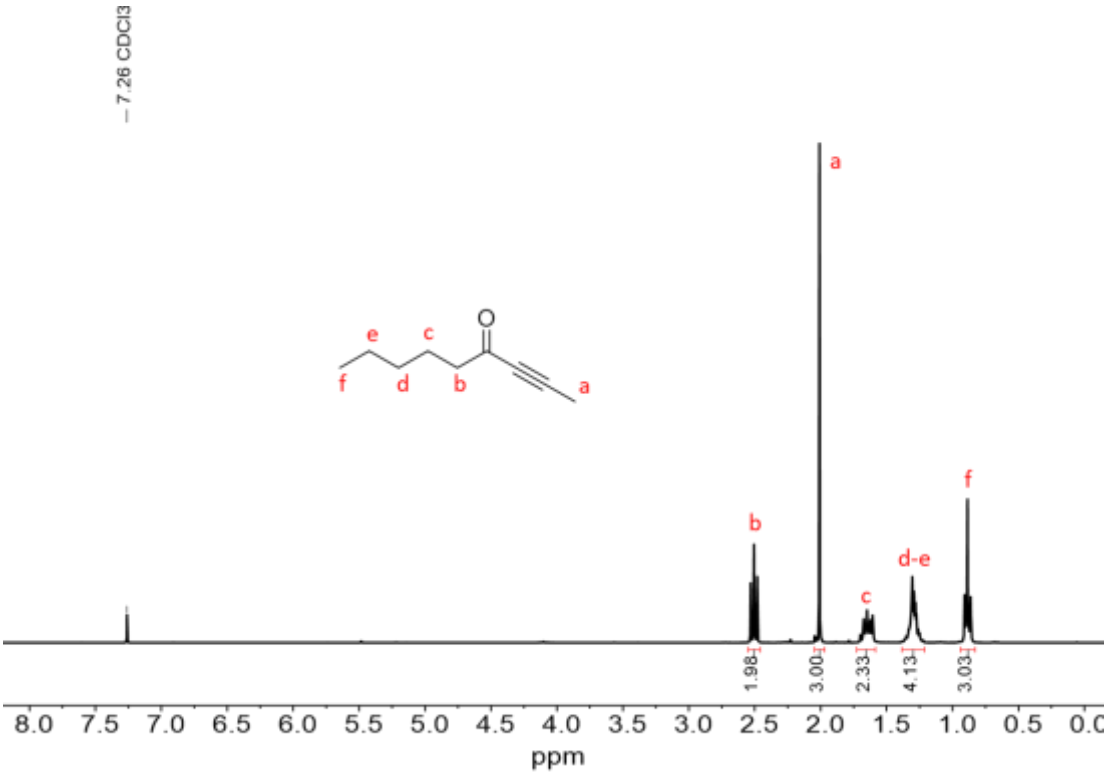

Figure S5. non-2-yn-4-one ^{1}H NMR Spectrum (300 MHz, 298 K, $CDCl_3$).

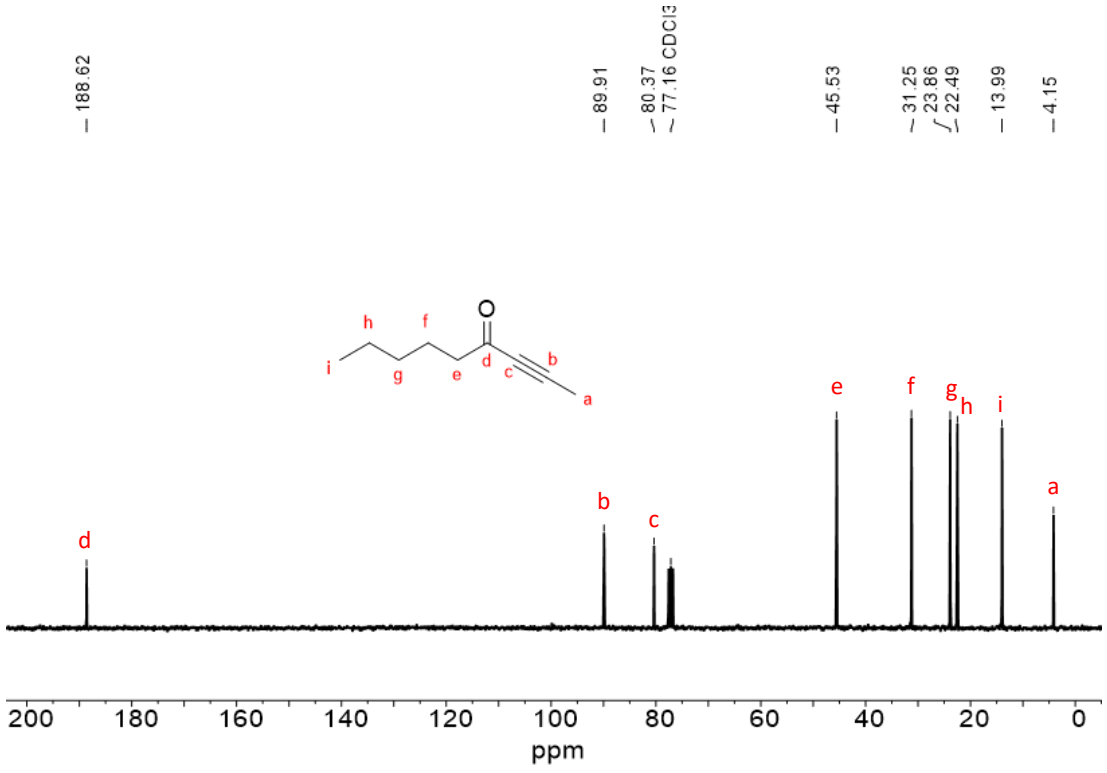

Figure S6. non-2-yn-4-one ^{13}C NMR Spectrum (75 MHz, 298 K, $CDCl_3$).

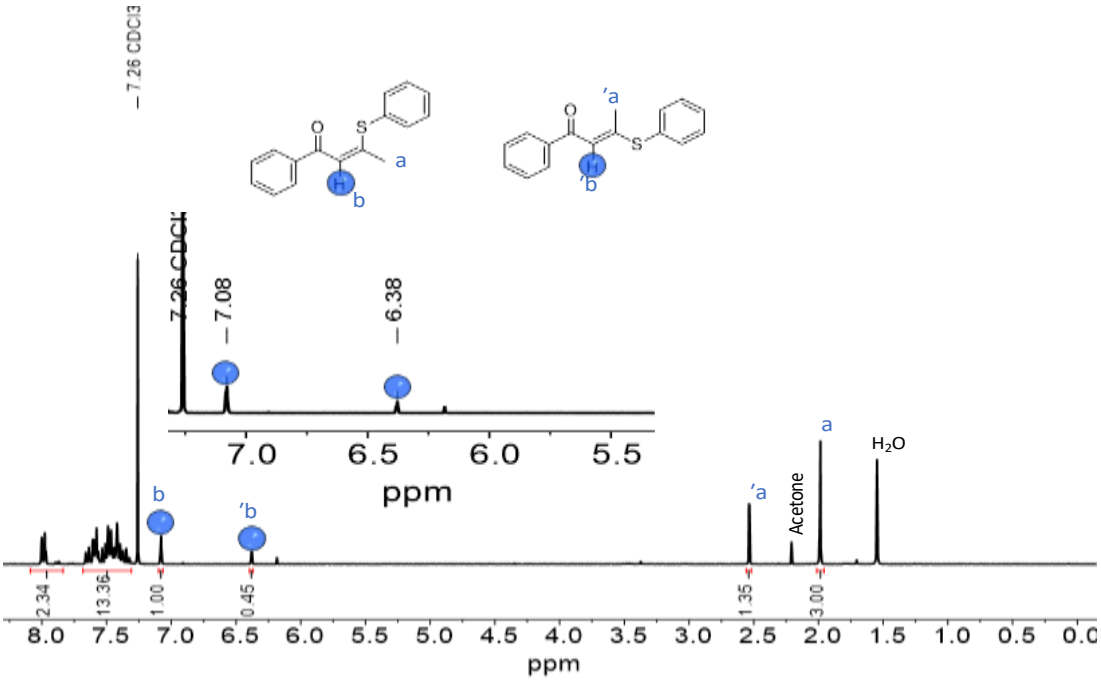

Figure S7. 1-phenyl-3-(phenylthio)but-2-en-1-one ^{1}H NMR Spectrum (300 MHz, 298 K, $CDCl_3$) *E/Z* isomers assignment in accordance with literature Ref.4.

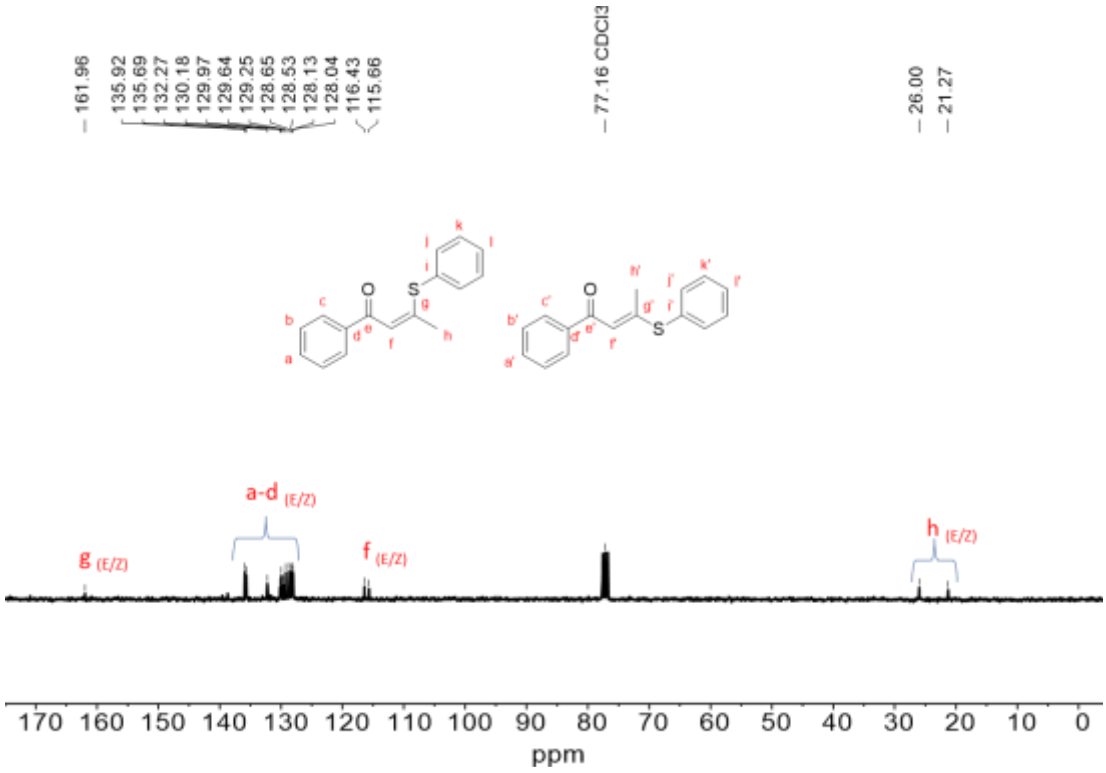

Figure S8. 1-phenyl-3-(phenylthio)but-2-en-1-one ^{13}C NMR Spectrum (101 MHz, 298 K, $CDCl_3$).

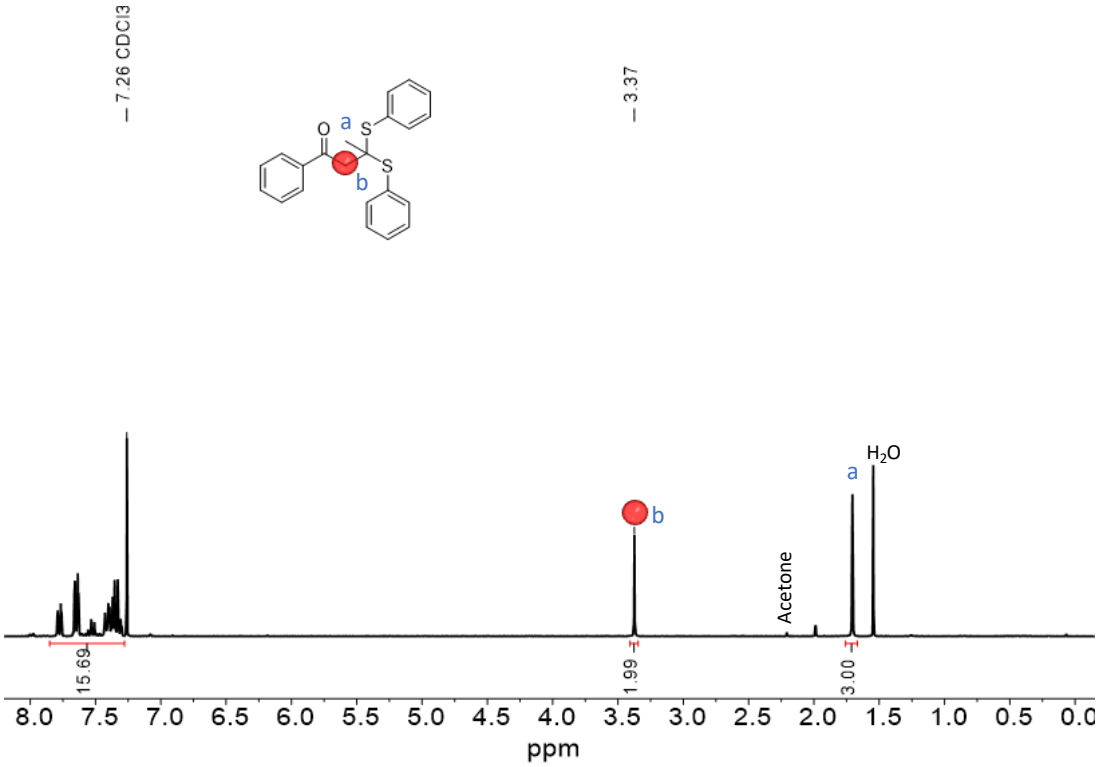

Figure S9. 1-phenyl-3,3-bis(phenylthio)butan-1-one ^{1}H NMR Spectrum (300 MHz, 298K, $CDCl_3$).

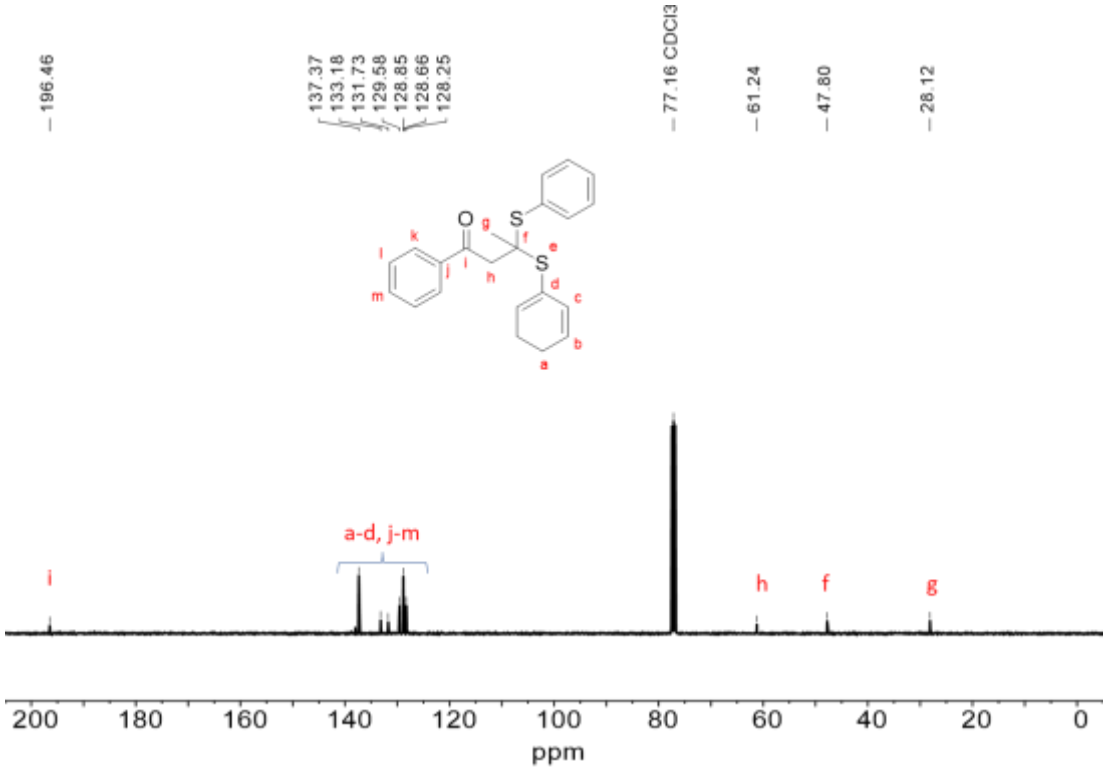

Figure S10. 1-phenyl-3,3-bis(phenylthio)butan-1-one ^{13}C NMR Spectrum (101 MHz, 298 K, $CDCl_3$).

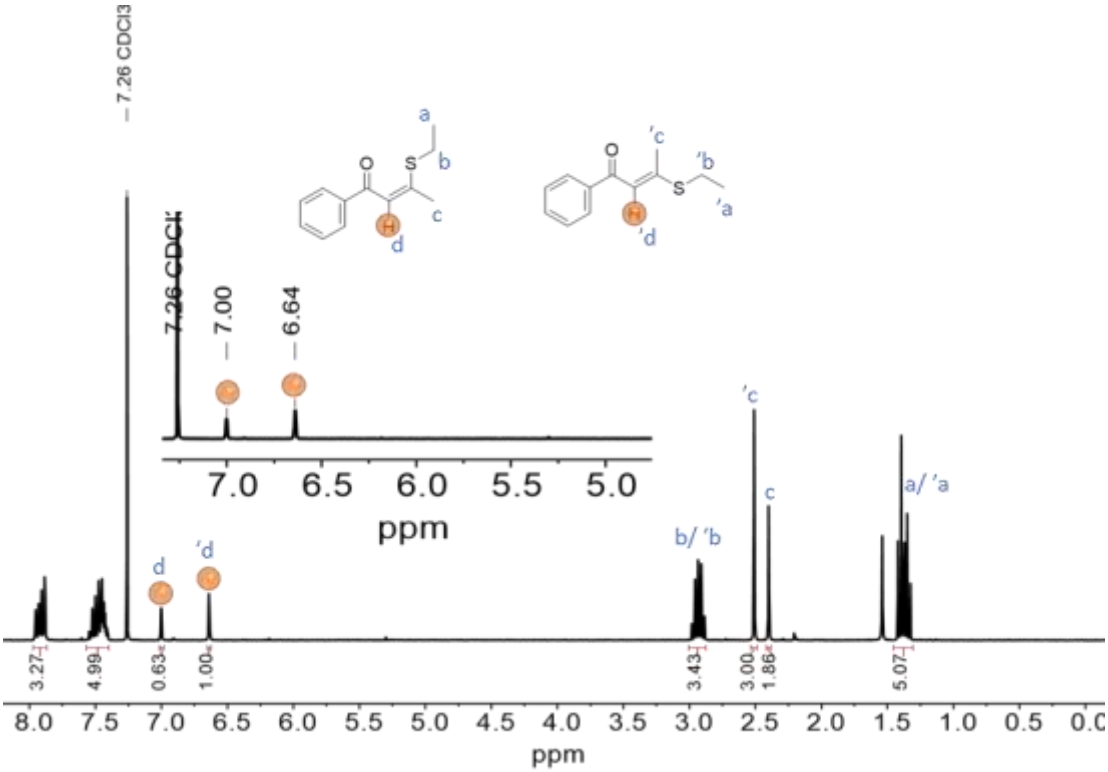

Figure S11. 3-(ethylthio)-1-phenylbut-2-en-1-one ^{1}H NMR Spectrum (300 MHz, 298 K, $CDCl_3$)*E/Z* isomers assignment in accordance with literature. Ref.4.

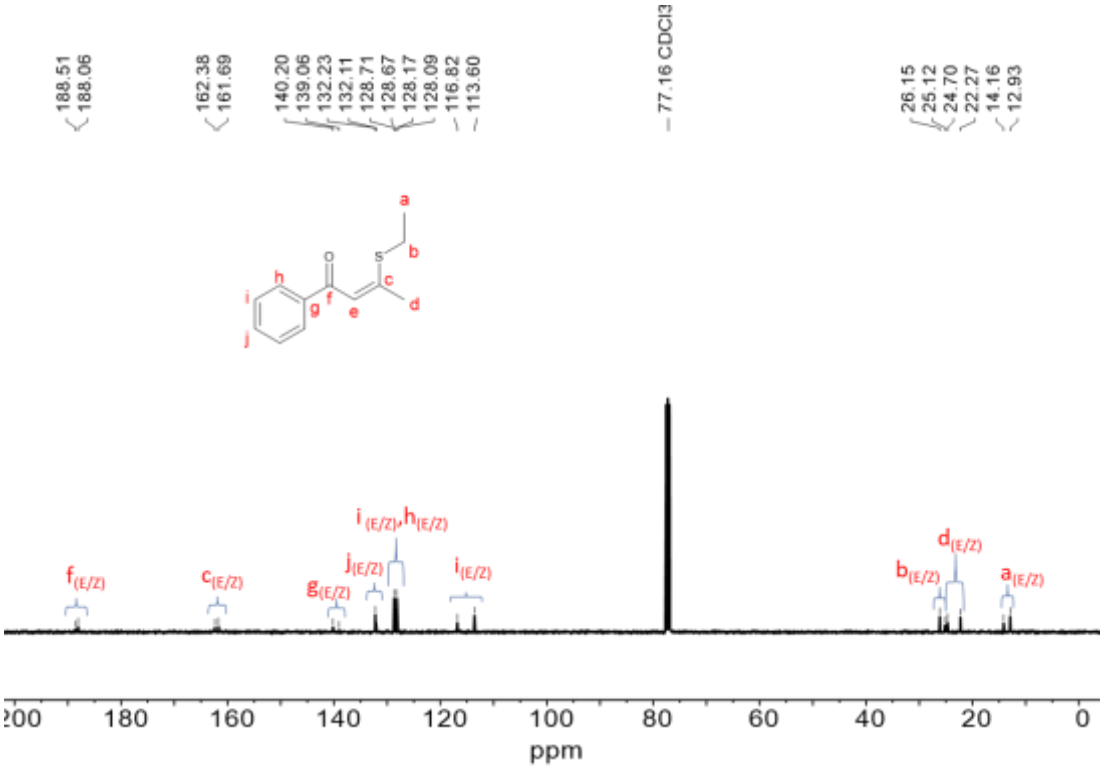

Figure S12. 3-(ethylthio)-1-phenylbut-2-en-1-one ^{13}C NMR Spectrum (101 MHz, 298 K, $CDCl_3$).

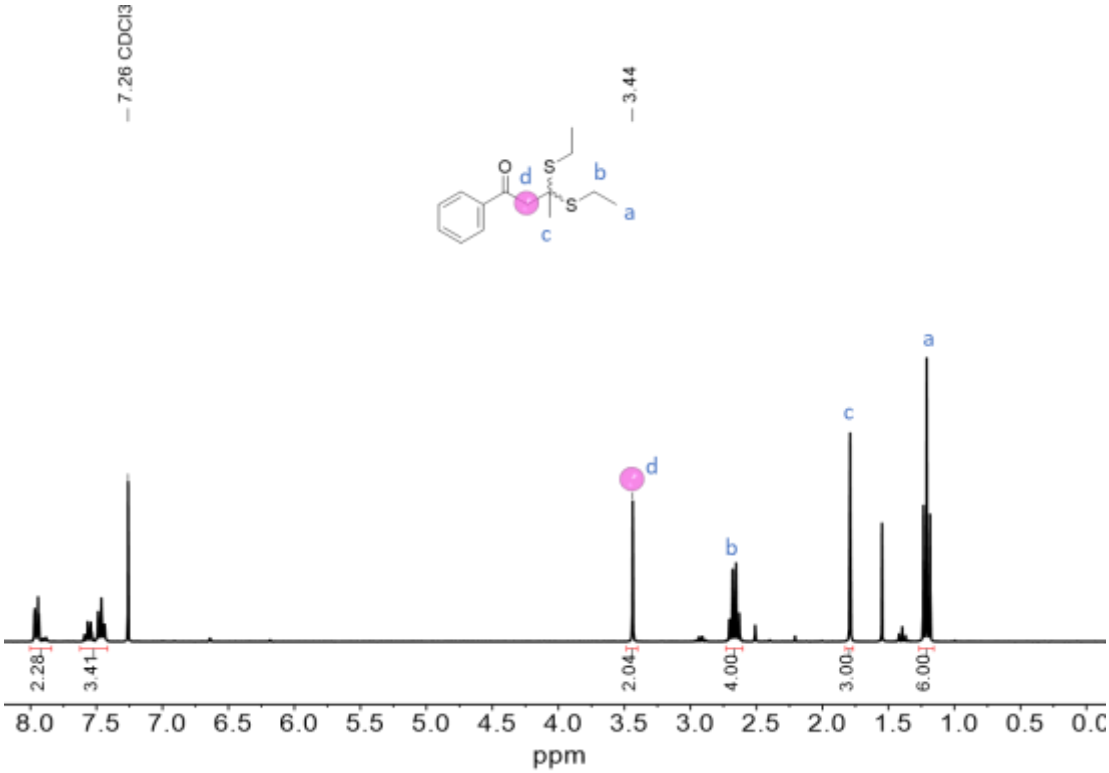

Figure S13. 3,3-bis(ethylthio)-1-phenylbutan-1-one ^{1}H NMR Spectrum (300 MHz, 298 K, $CDCl_3$).

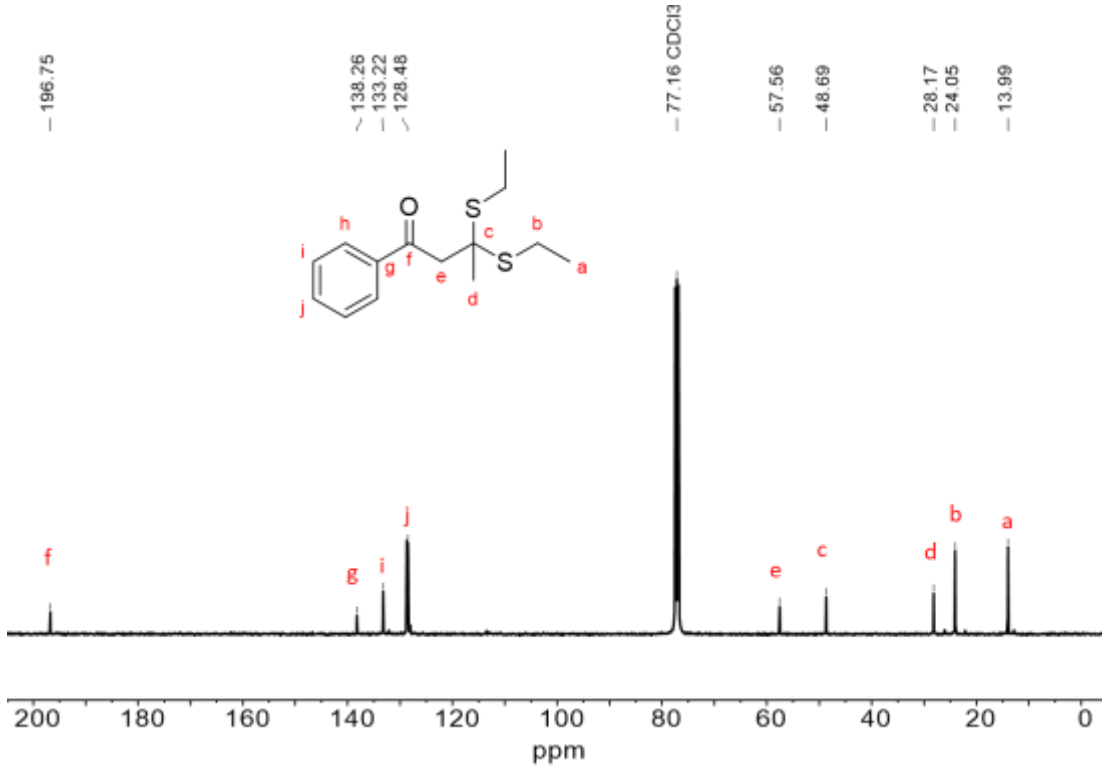

Figure S14. 3,3-bis(ethylthio)-1-phenylbutan-1-one ^{13}C NMR Spectrum (101 MHz, 298 K, $CDCl_3$).

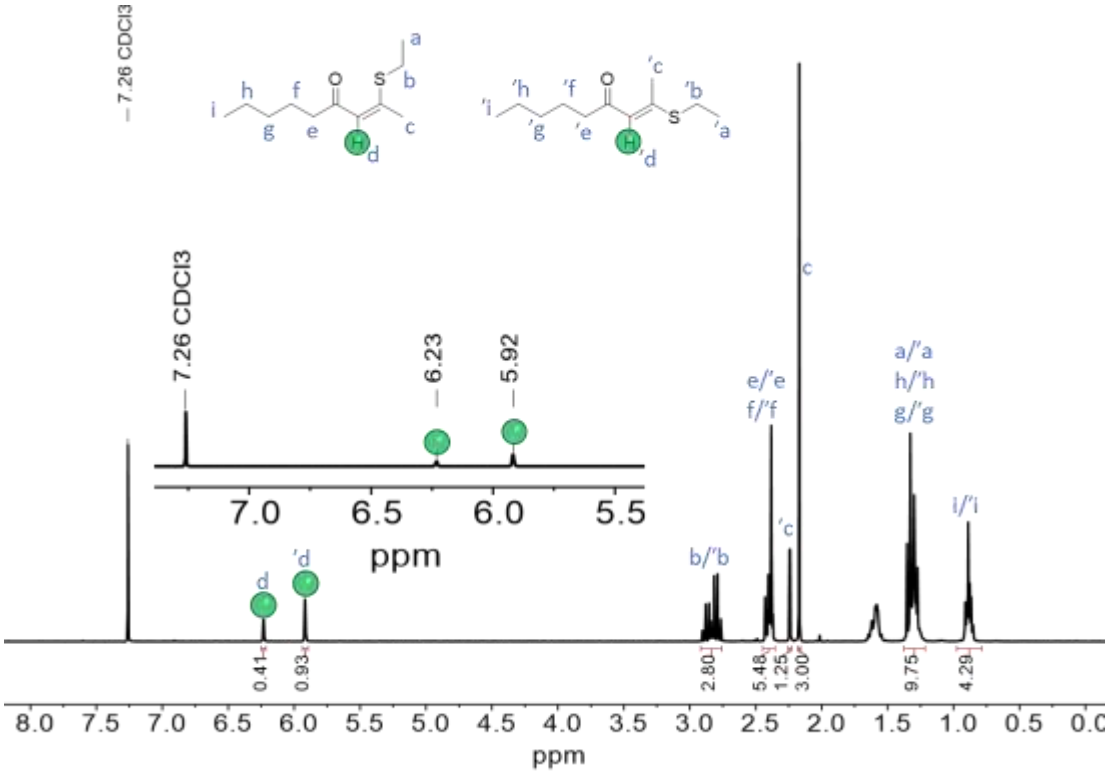

Figure S15. 2-(ethylthio)non-2-en-4-one ^{1}H NMR Spectrum (300 MHz, 298 K, $CDCl_3$).

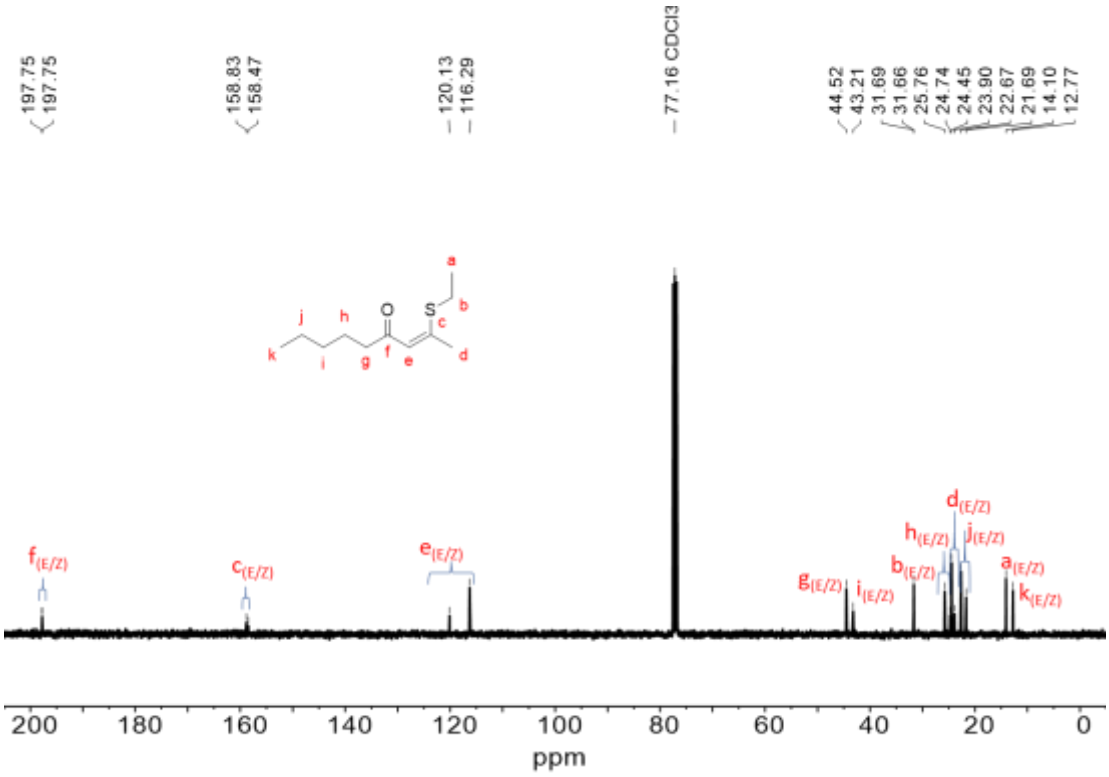

Figure S16. 2-(ethylthio)non-2-en-4-one ^{13}C NMR Spectrum (101 MHz, 298 K, $CDCl_3$).

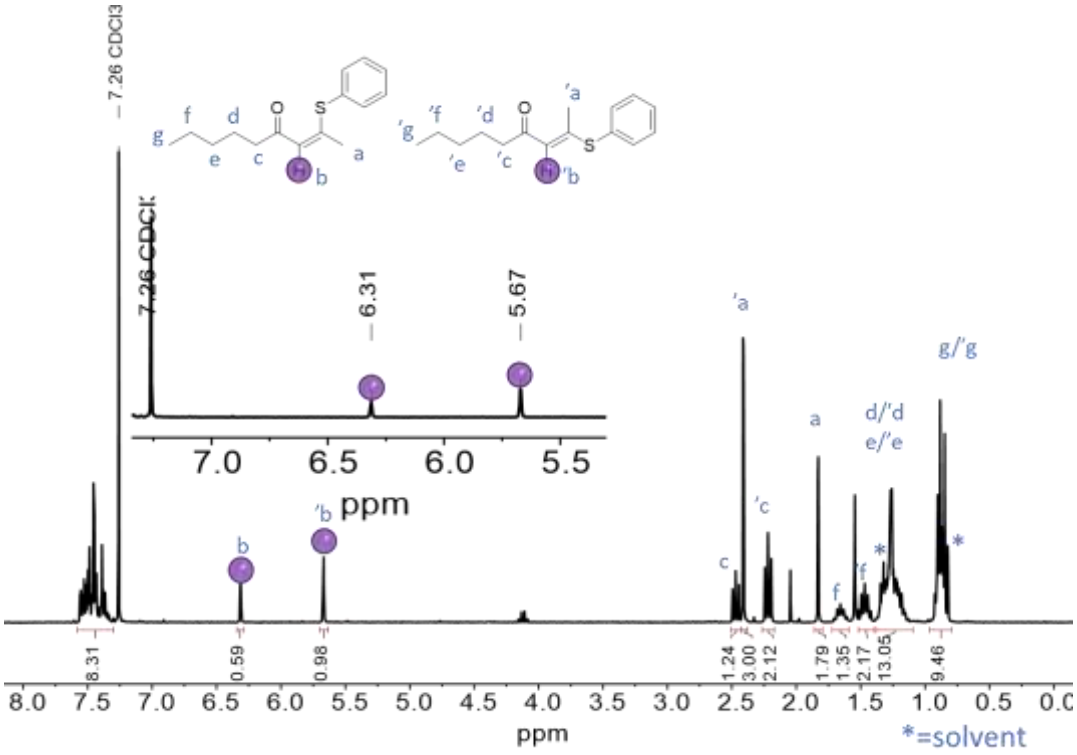

Figure S17. 2-(phenylthio)non-2-en-4-one ^{1}H NMR Spectrum (300 MHz, 298 K, $CDCl_3$).

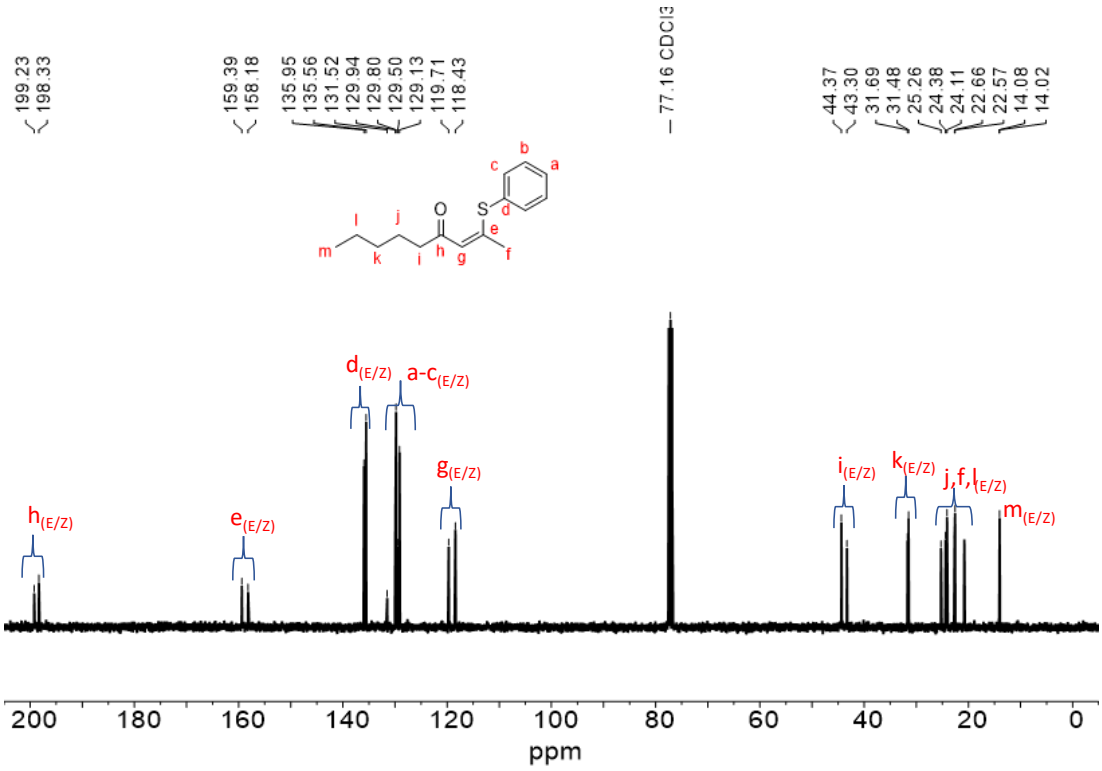

Figure S18. 2-(phenylthio)non-2-en-4-one ^{13}C NMR Spectrum (101 MHz, 298 K, $CDCl_3$).

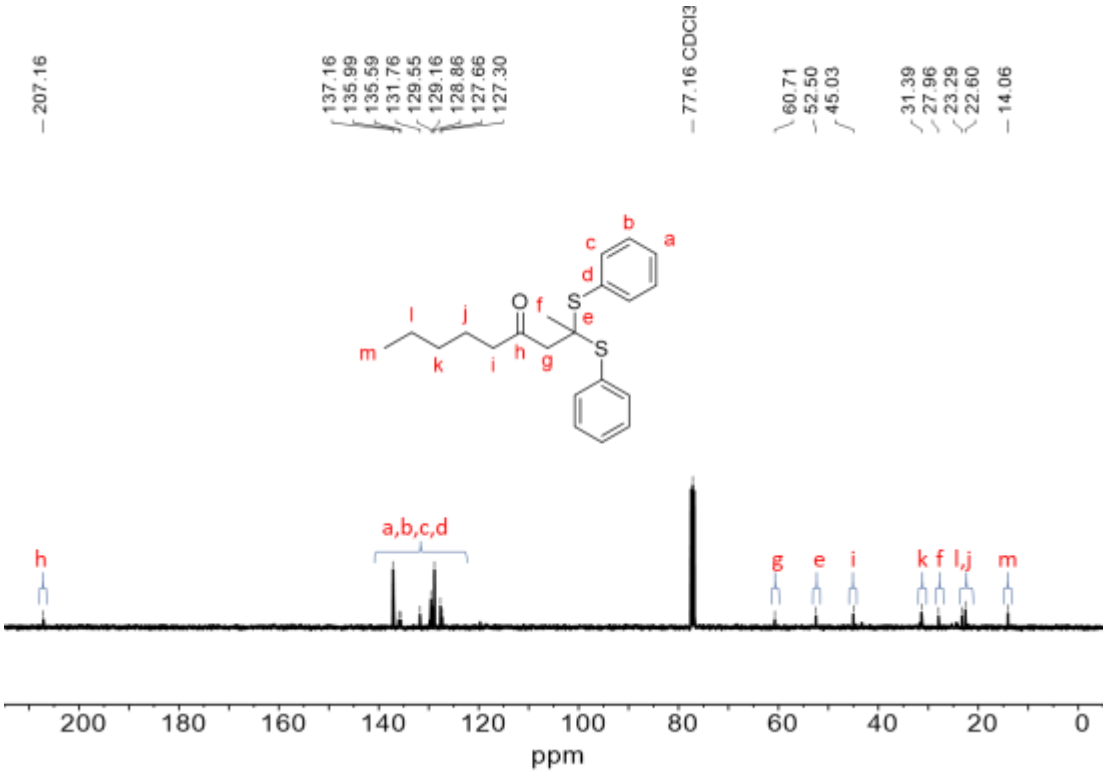

Figure S19. 2,2-bis(phenylthio)nonan-4-one ^{13}C NMR Spectrum (300 MHz, 298 K, $CDCl_3$).

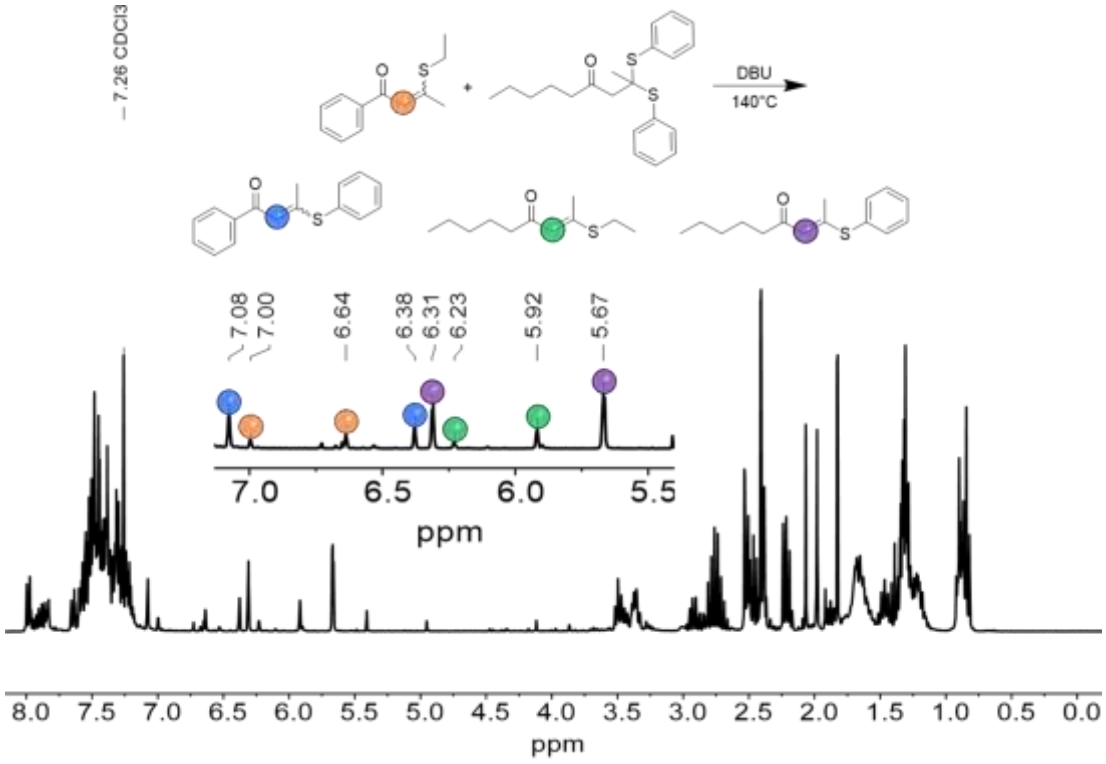

Figure S20. Thiol dynamic exchange between thioacetals (double-addition adducts) and β-sulfido-α,β-unsaturated carbonyl moieties (single-addition adducts). ^{1}H NMR Spectrum (300 MHz, 298 K, $CDCl_3$).

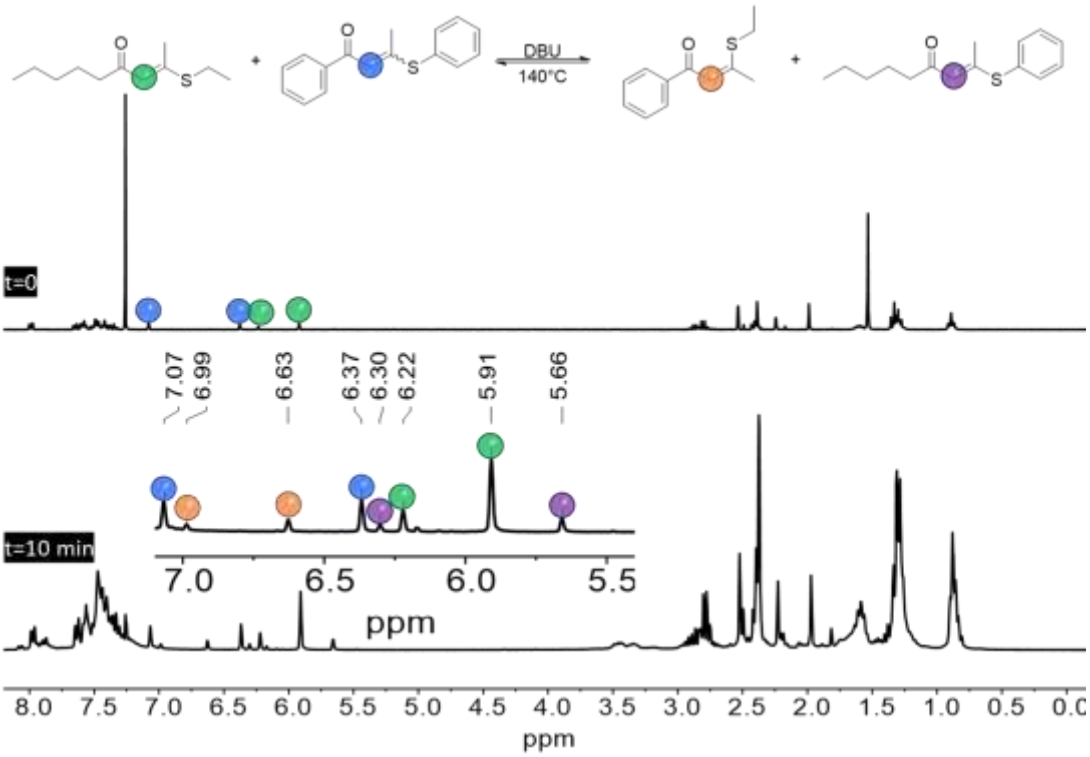

Figure S21. Thiol dynamic exchange between single-addition species (each formed from different ynones and thiols) ^{1}H NMR Spectrum (300 MHz, 298 K, $CDCl_3$).

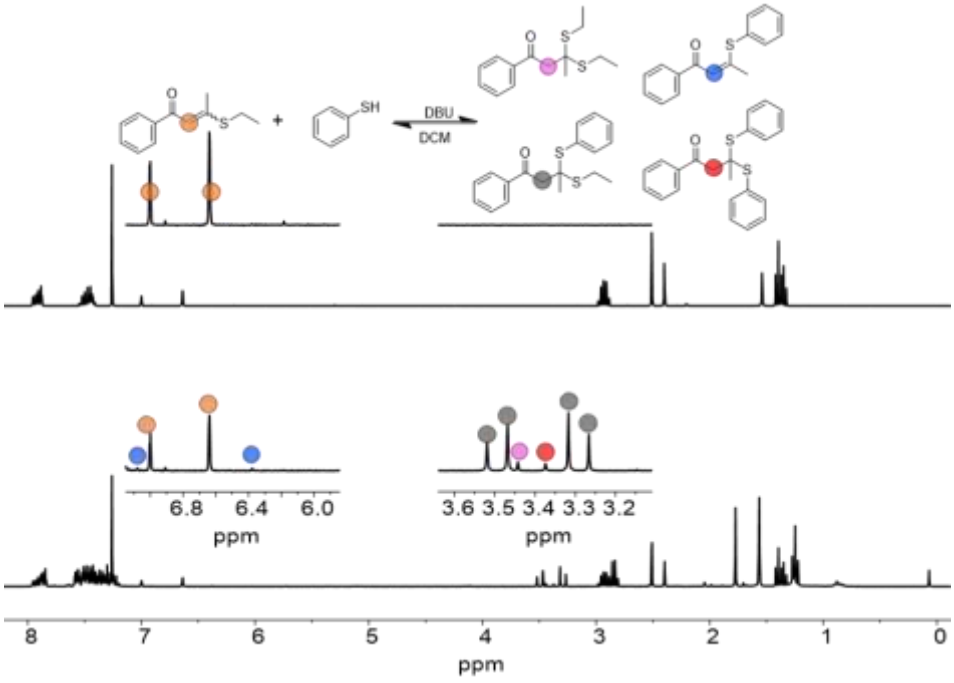

Figure S22. Thiol dynamic exchange between single-addition adducts and free thiol ^{1}H NMR Spectrum (300 MHz, 298 K, $CDCl_3$).

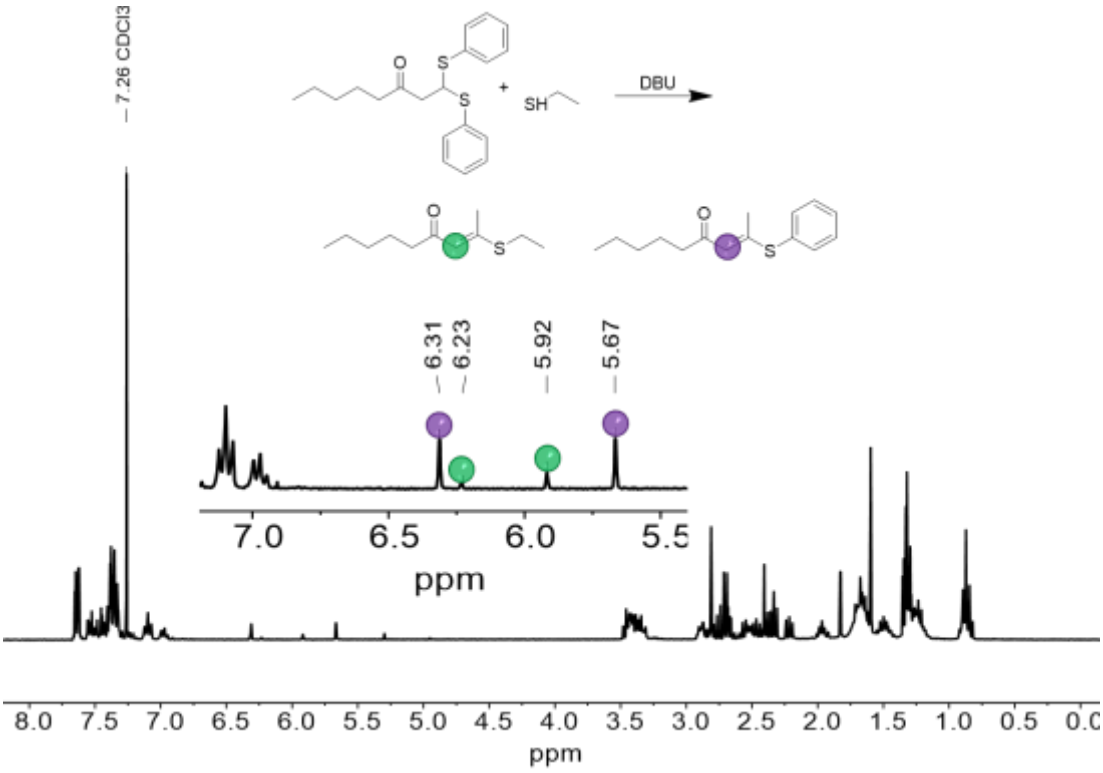

Figure S23. Thiol dynamic exchange between double-addition adducts and free thiol ^{1}H NMR Spectrum (300 MHz, 298 K, $CDCl_3$).

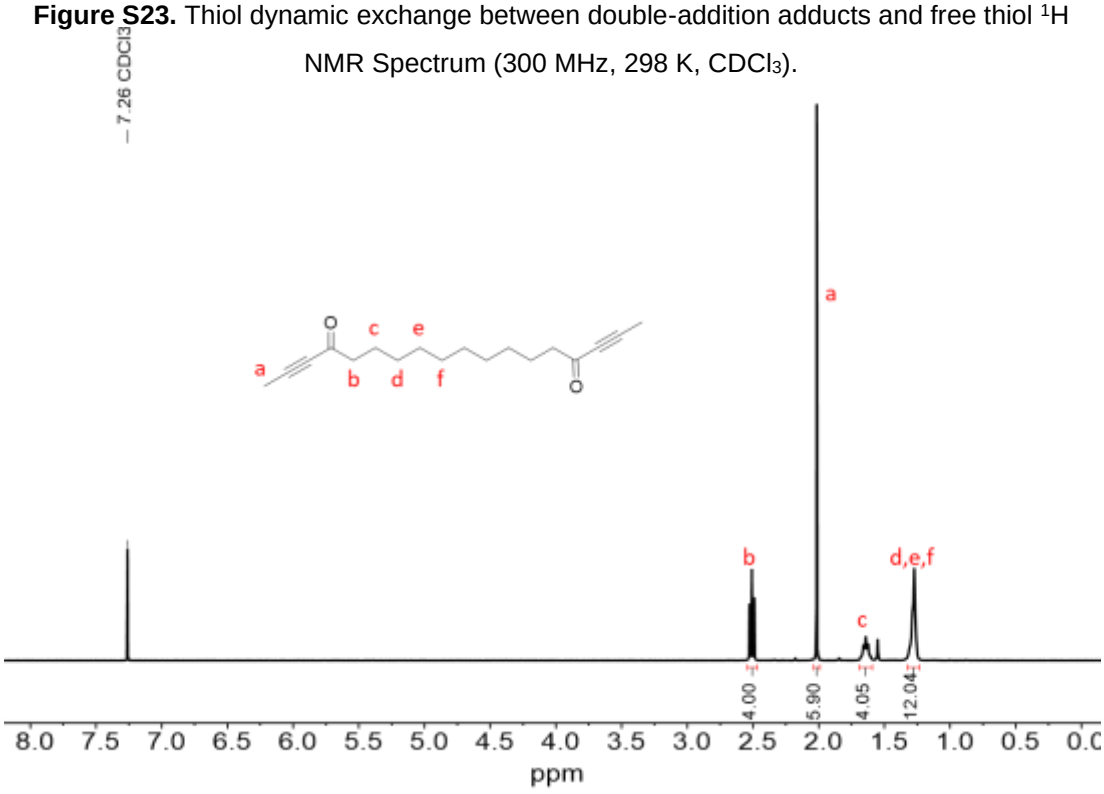

Figure S24. octadeca-2,16-diyne-4,15-dione Monomer ($C_{10}Y$) ^{1}H NMR Spectrum (400 MHz, 298 K, $CDCl_3$).

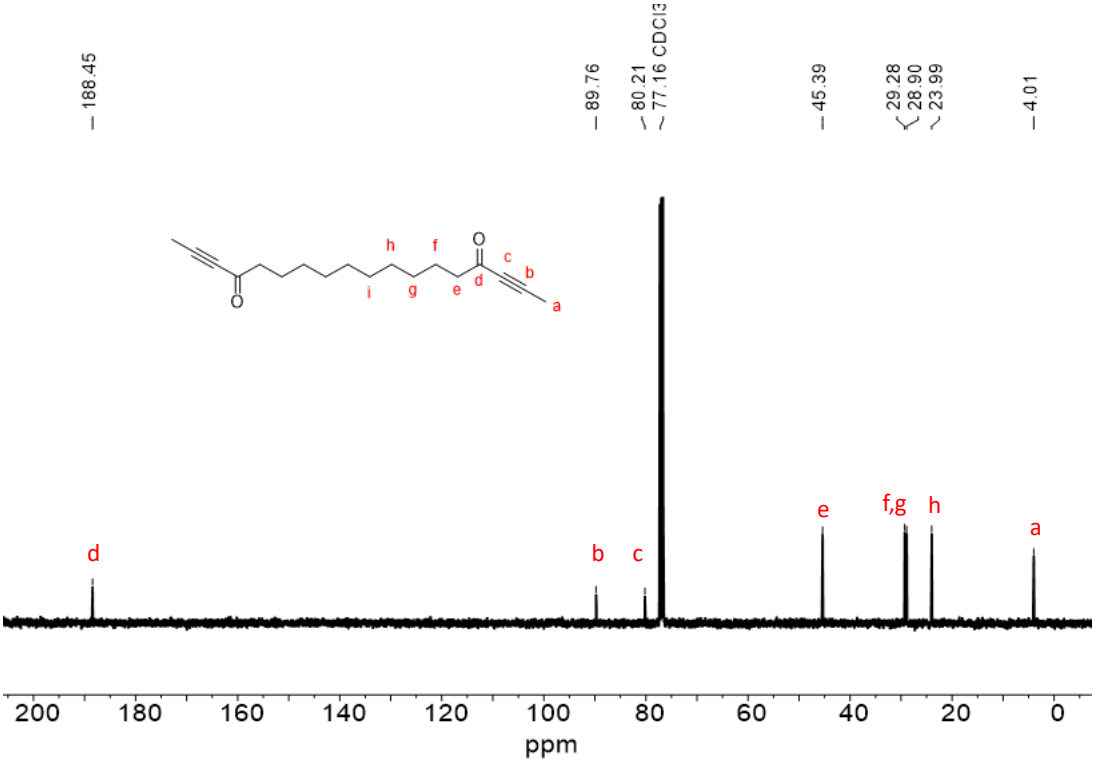

Figure S25. octadeca-2,16-diyne-4,15-dione Monomer ($C_{10}Y$) ^{13}C NMR Spectrum (101 MHz, 298 K, $CDCl_3$).

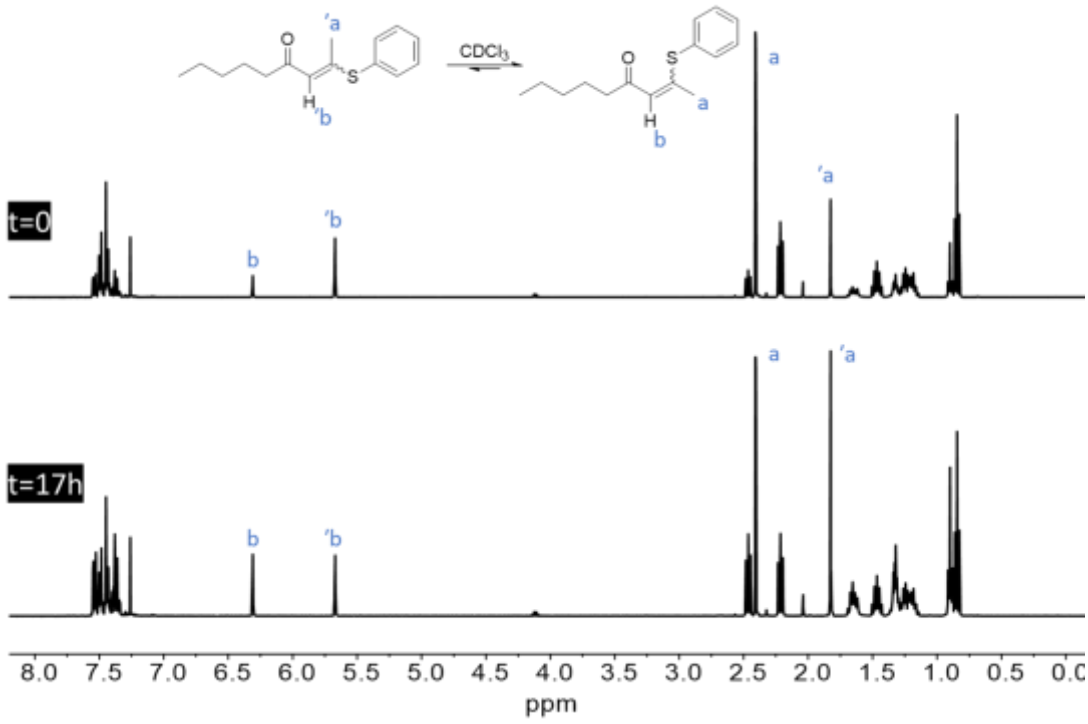

Figure S26. (*E/Z*) equilibrium of 2-(phenylthio)non-2-en-4-one at ambient temperature in catalyst-free solution ^1H NMR Spectrum (400 MHz, 298 K, $CDCl_3$)

Thermal Analysis

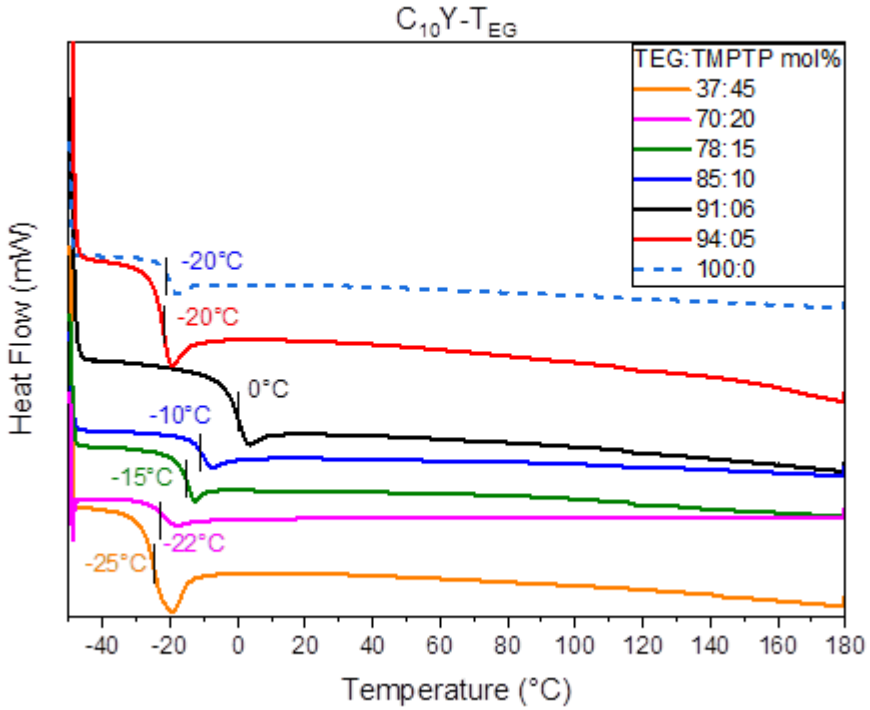

Figure S27. DSC thermograms of 2nd heating cycle for $C_{10}Y\text{-}T_{EG}$ with different dithiol ratio.

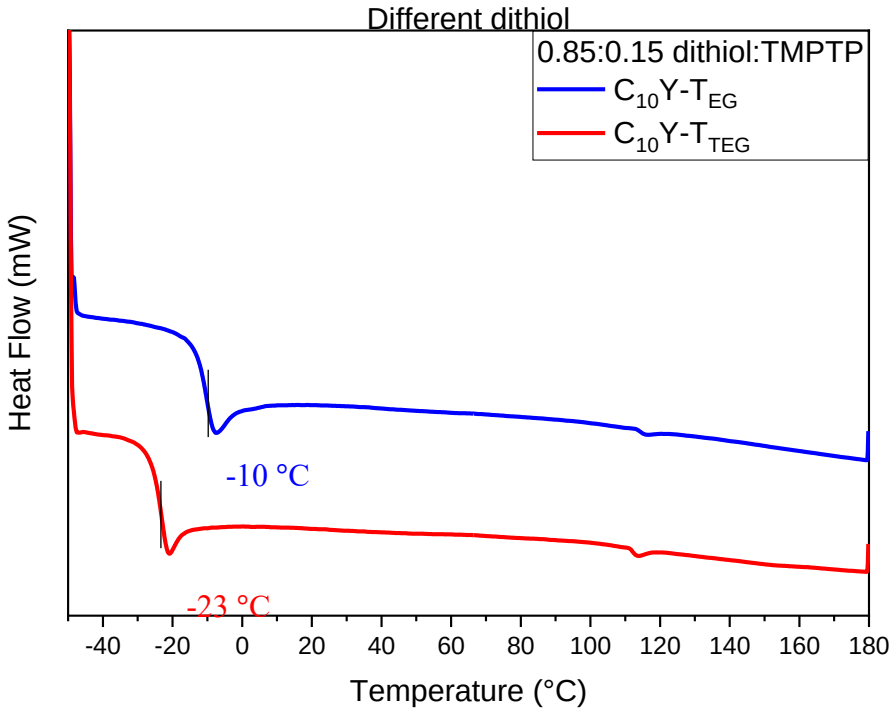

Figure S28. DSC thermograms of 2nd heating cycle for $C_{10}Y\text{-}T_{EG}$ and $C_{10}Y\text{-}T_{TEG}$ at the optimized dithiol:crosslinker ratio (0.85:0.10).

Tensile Testing

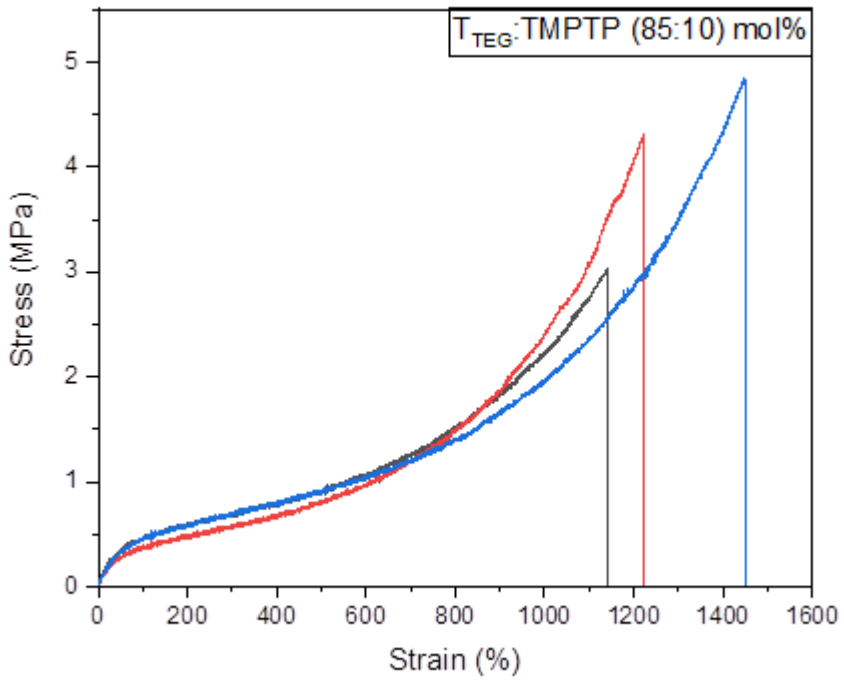

Figure S29. Stress vs strain curve of $C_{10}Y$-T_{TEG} polymer at optimized dithiol:crosslinker ratio (85:10) at 10 mm min^{-1} strain rate.

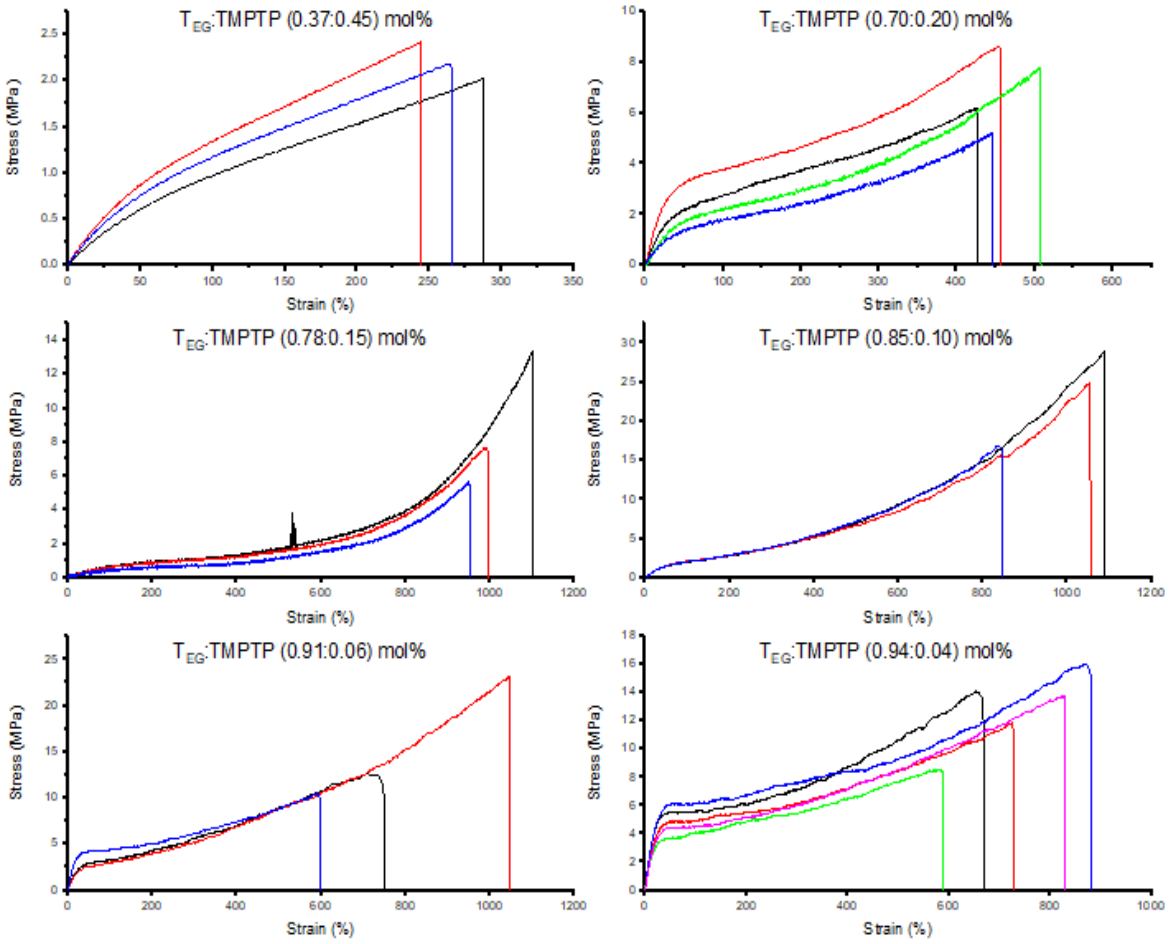

Figure S30. Stress vs strain curve of $C_{10}Y$-T_{EG} polymer with various dithiol:crosslinker (T_{EG}:TMPTP) ratios at 10 mm min^{-1} strain rate.

Rheological Analysis

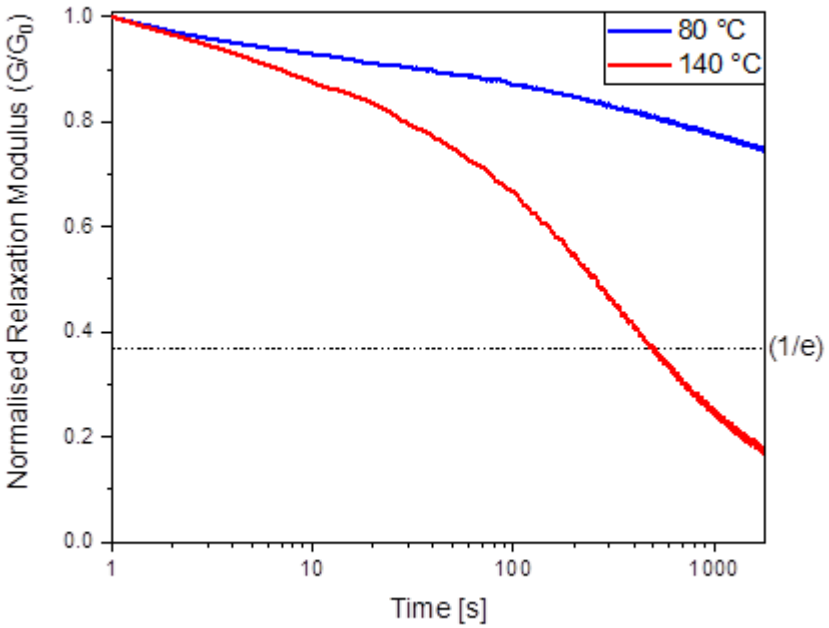

Figure S31. Stress relaxation at 80 °C and 140 °C for $C_{10}Y\text{-}T_{EG}$ CAN at optimal dithiol:crosslinker ratio (0.85:0.10).

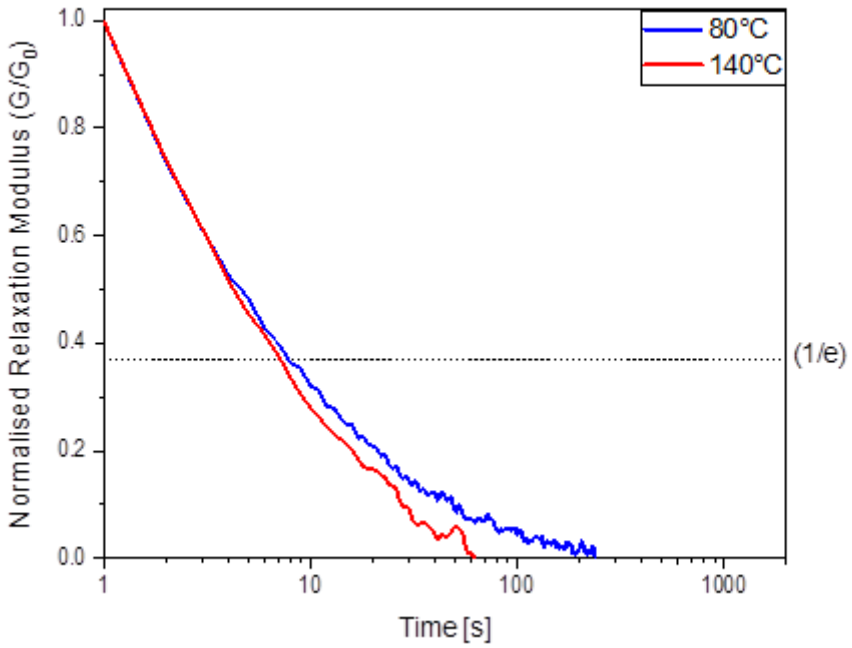

Figure S32. Stress relaxation at 80 °C and 140 °C for $C_{10}Y\text{-}T_{TEG}$ CAN at optimal dithiol:crosslinker ratio (0.85:0.10).

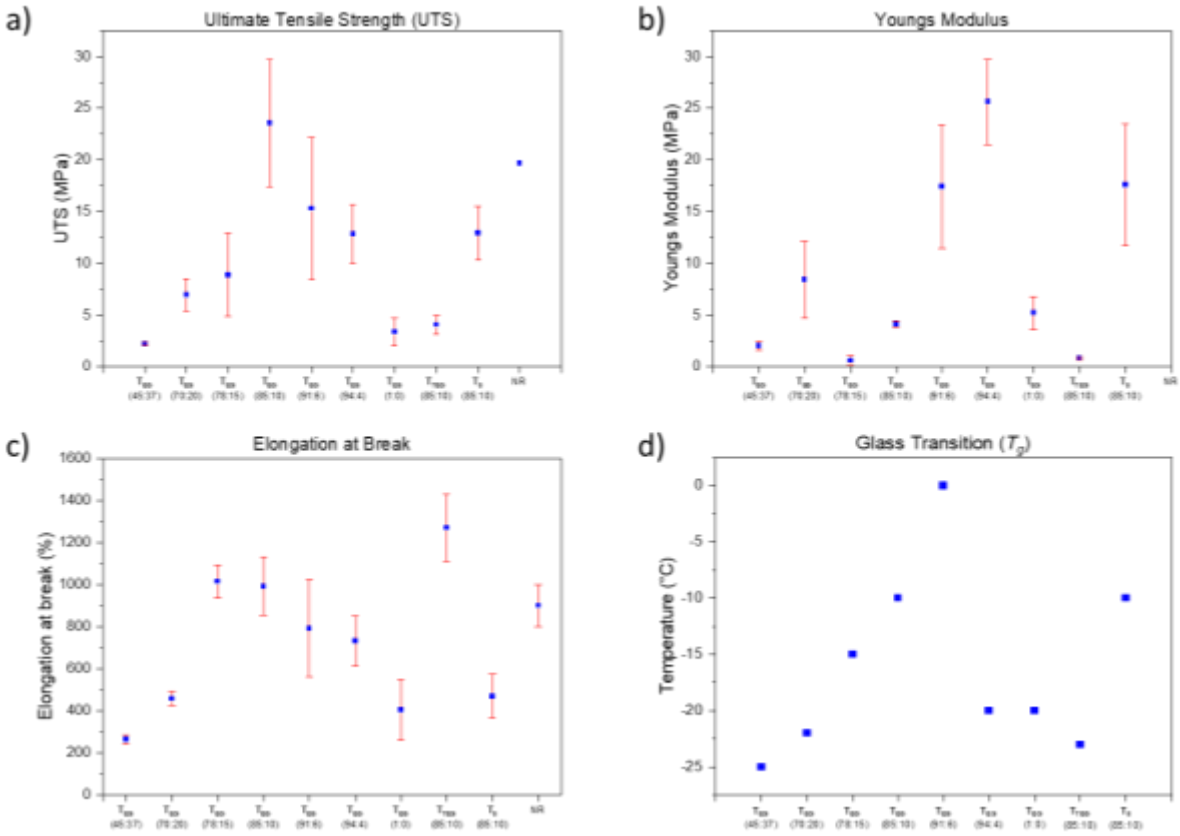

Figure S33. Thermomechanical properties of all CANs. a) Ultimate tensile strength. b) Youngs modulus. c) Elongation at break. d) Glass transition temperature (T_g).

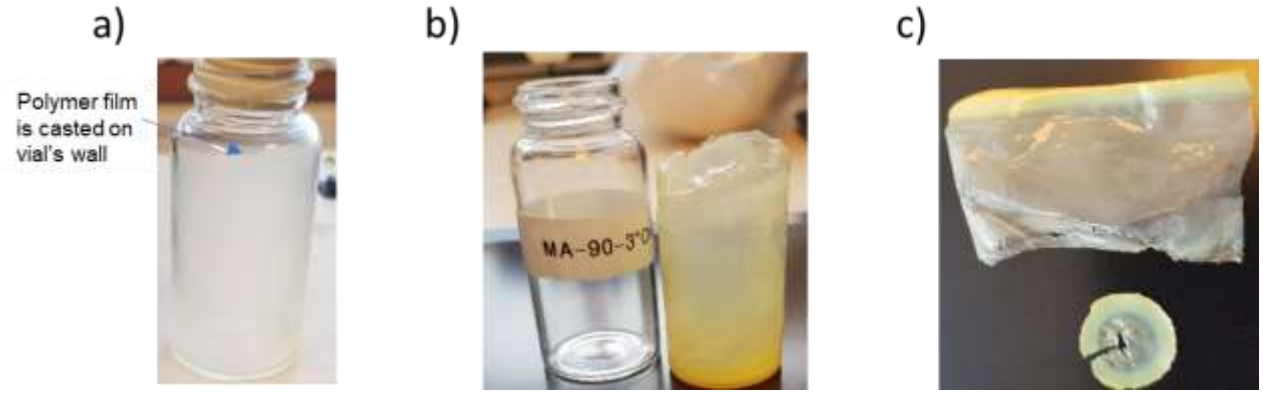

Figure S34. Film casting process a) Glass vial after rotated on rotary evaporator showing the polymeric mixture covering the vial's wall. b) The film after cooled down and pulled out of the vial. c) The film is cut and opened ready to be cut into a dog-bone shape for tensile testing.

References

1. F. Pilathottathil, D. Vineet Kumar and A. Kaliyamoorthy, *Synth. Commun.*, 2020, **50**, 1622-1632.
2. S. J. Wagh, R. Chowdhury, S. Mukhopadhyay and S. K. Ghosh, *J. Label. Compd. Radiopharm.*, 2013, **56**, 649-654.
3. S. González Granda, D. Méndez Sánchez, I. Lavandera García and V. Gotor Fernández, *ChemCatChem*, 2020.
4. T. Nishio and Y. Omote, *J. Chem. Soc., Perkin Trans. 1*, 1981, 934-938.

CHAPTER 3: USING COMPOSITION TO TUNE THERMOMECHANICAL PROPERTIES OF THIOL-YNE COVALENT ADAPTABLE NETWORKS

3.1 Manuscript and overview

Title: Using composition to tune thermomechanical properties of thiol-yne covalent adaptable networks

Authors: **Maher A. Alraddadi**[1], Joshua C. Worch[1], Andrew P. Dove[1]*

Affiliations: [1] School of Chemistry, The University of Birmingham, Edgbaston, Birmingham, B15 2TT, UK.

Manuscript Prepared

Co-author contributions: Dr Josh Worch (University of Birmingham) provided technical and synthetic guidance and editing of this manuscript. Prof. Andrew P. Dove (University of Birmingham) supervised in addition to providing guidance and editing the manuscript.

Overview:

Following on from Chapter 2, we want to investigate the effect of changing the monomer composition of the prepolymer on the thermomechanical properties of the resulting CANs. Several reports have shown strong dependency of the prepolymer architecture and the resulting CANs thermomechanical properties for CANs that are assembled directly from prepolymers. We adapted thiol-yne addition reaction used in Chapter 2 to construct prepolymers by reacting diynone and commercially available dithiol, then further cross-links these prepolymer with multivalent thiol to construct

desired CANs. Our aim is to vary the prepolymer composition by changing the length of aliphatic ynone monomer as well as using an aromatic ynone monomer. To this end, diynones containing different length aliphatic monomer (6 and 8 carbons) were as well diynone containing aromatic monomer were synthesised and copolymerised with three different dithiols. As expected, a range of thermomechanical properties was easily access by altering the prepolymer composition. In general, increasing the aliphatic length of the prepolymer increased the flexibility of the resulting CANs which led to lower glass transition temperatures and higher toughness. Whilst the incorporation of aromatic structure increased the stiffness of the CANs. More importantly, one CAN material has showed excellent mechanical properties (Ultimate tensile strength = 26 ± 0.8 MPa, elongation at break = 965.3 ± 34%).

Using composition to tune thermomechanical properties of thiol-yne covalent adaptable networks

Maher A. Alraddadi§, Joshua C. Worch§, Andrew P. Dove*§

§School of Chemistry, University of Birmingham, Edgbaston, Birmingham, B15 2TT (UK)

Abstract Improving the mechanical properties of covalent adaptable networks (CANs) while maintaining a reasonable bond dynamicity is a big challenge within the dynamic chemistry field. Despite advances in this area, a detailed understanding of how the structure of CANs can affect their properties remains elusive. Recently, our group demonstrated a simple approach to improve the mechanical properties of CANs using thiol-yne chemistry. In particular, reacting commercially available dithiols with alkyl-based diynone to form a prepolymer which was then crosslinked using a multivalent thiol. Capitalizing on this finding, here we investigate how the monomer composition can affect the thermomechanical properties of different CANs. To this end, monomers containing different length alkyl spacers, as well as different chemical structures were copolymerized with different commercially available dithiols to form linear prepolymers, which were further crosslinked with a multivalent thiol. The resulting CANs exhibited tuneable thermomechanical properties, with networks built from longer aliphatic spacers displaying lower glass transition temperatures and higher ultimate tensile strengths than those containing shorter spacers. Differences in monomer composition also afforded CANs with widespread thermomechanical properties; one CAN showed incredible mechanical properties surpassing the strength and elongation of currently reported CANs (ultimate tensile strength > 26 MPa and elongation at break > 900%).

Introduction

Thermoset elastomers, which are polymeric materials formed by permanent covalent networks, have widespread application in many industries *i.e.* medical, automotive, painting and coating, and others as consequence of their outstanding strength and extensibility.[1, 2] Even though these permanent crosslinks render the elastomers with excellent properties, such as reversible deformation as well as chemical and thermal resistance, they hinder the processability and recyclability of thermosets.[3] Several efforts to improve the sustainability of elastomers have been dedicated to the use of dynamic covalent chemistry (DCC) into the elastomer crosslink sites. This has led to the development of a new class of dynamic networks, known as covalent adaptable networks (CANs).[4, 5] CANs provide elastomers with sought-after

properties *i.e.* reversible deformation as well as chemical and thermal resistance, while the dynamic nature of these networks allow the material to flow like typical thermoplastics upon activation.[6] Consequently, a controlled activation/deactivation of these networks creates smart and responsive materials that are also reprocessable, recyclable, and self-healable.[7, 8]

The well-known trade-off between the reversibility of CANs and their mechanical performance has initiated significant research interest in improving the thermal and mechanical properties of CANs whilst maintaining good reversibility of the dynamic bonds.[9] To help tackle these issues, research has been focused on the use of reactive and nonreactive fillers[10, 11], multiple crosslinking system in a single CAN[12,13], CANs with different crosslink density[14, 15], and the effect of monomer composition on CAN properties[16-19]. Additionally, several reports have shown that the prepolymer architecture strongly affects the thermal and rheological properties of CANs that are assembled directly from prepolymers.[20-22] The effect of the prepolymer "spacer" length on the thermal and mechanical properties have been studied in non-aqueous gels. For example, Mrozek *et al.* have reported an extensive study of the effect of varying the spacer length as well as the solvent content on the mechanical properties of a solvent-swollen epoxy gel.[23] Skandani *et al.* showed that the material's stiffness and glass transition temperature were decreased when the length of the flexible aliphatic spacer in an azobenzene-functionalized liquid crystalline network was increased.[24]

Inspired by these works and our recent report on the synthesis of high-performance thermally responsive CANs, we synthesised different thiol-yne based covalent adaptable networks (CANs) that possess tunable thermomechanical properties in a straightforward two-step synthesis. First, a prepolymer was formed *via* the organobase-catalyzed reaction between a diynone and a commercially available dithiol. Subsequently, the pre-formed prepolymer was crosslinked using a multivalent thiol to form the dynamic network (CAN). In seeking to obtain materials with a wide range of thermomechanical properties, diynones containing different length aliphatic spacers were synthesised as well as diynone containing aromatic spacers in their composition.

Results and Discussion

Initially, we synthesised diynone monomers using a 2-step reaction. First, the respective difunctional Weinreb-Nahm amides[25] were synthesised from the reaction between diacid chloride and N,O-

dimethylhydroxylamine hydrochloride in the presence of a base. Then, each difunctional amide was reacted with 1-propynylmagnesium bromide to give the respective diynone monomer. The structures of the synthesised amides and ynone monomers were confirmed by ^{1}H NMR and ^{13}C NMR (Supplementary Information Figures S1-S12).

Prepolymers were synthesised by the addition of 1 equiv. of a diynone monomer (Y_6, Y_8, Y_{Ar}) to 0.85 eq. of a dithiol (T_{EG}, T_{TEG}, or T_8) using DCM in the presence of 0.05 eq. of DBU for 2 h to obtain the respective prepolymer (PrePol-Y_6-T_{EG}, PrePol-Y_6-T_{TEG}, PrePol-Y_6-T_8, PrePol-Y_8-T_{EG}, *etc.*). Subsequently, the formed prepolymers were mixed with 0.1 eq. of trimethylolpropane tris(3-mercaptopropionate), (TMPTP) to form the desired CAN *i.e.,* CAN- Y_6-T_{TEG}, CAN- Y_6-T_8, *etc.* (Figure 1). It is worthy note that, as a consequence of the presence of a residual catalyst (DBU) in the prepolymers, no additional catalyst was needed to from the network. Also, for all synthesised CANs, we maintained the optimal diynone:dithiol:crosslinker ratio (1:0.85:0.10) that was observed in our previous work, chapter 2 of this thesis.

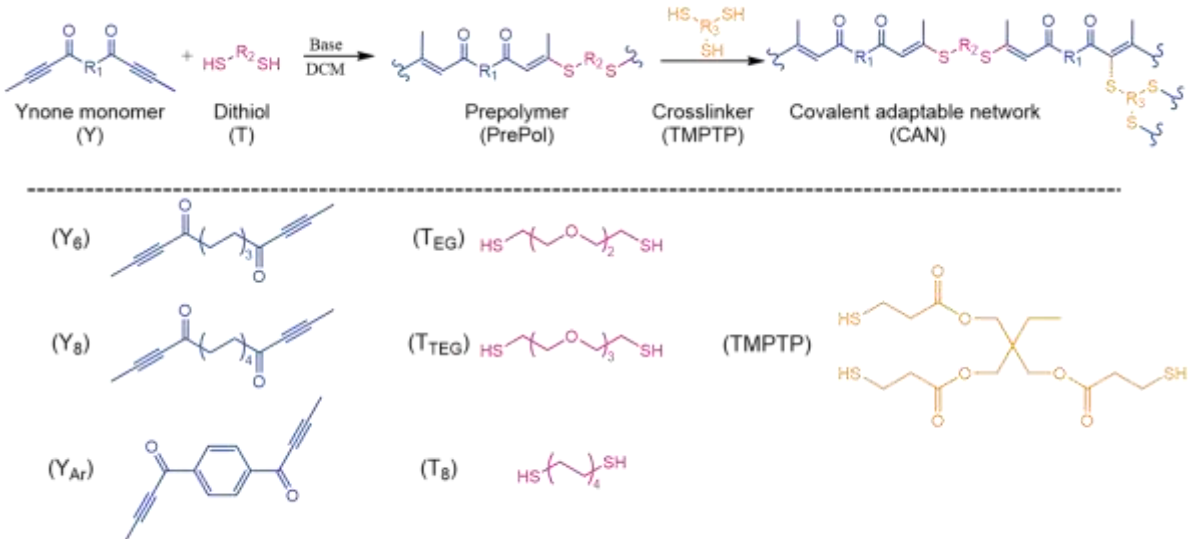

Figure 1. Two-step synthesis of linear prepolymers (PrePol) *via* the base-catalysed addition of dithiols to diynones, followed by the addition of a multi-valent thiol crosslinker (TMPTP) to form the covalent adaptable networks (CANs).

We initially synthesised CAN-Y_{Ar}-T_{EG} composed of aromatic alkyl-based diynone (Y_{Ar}) and 2,2'-(ethylenedioxy)diethanethiol, (T_{EG}) dithiol, which was further crosslinked with the multivalent thiol

(TMPTP). Uniaxial tensile testing revealed that the CAN had moderate stress and strain properties (*UTS* = 3.84 ± 0.5 MPa, elongation at break (ε_b) = 424.2 ± 59%), and a Young's modulus of 38.6 MPa (Figure 2a and Table 1). To further investigate the effect of composition on mechanical properties, the dithiol was replaced with a more flexible tetra(ethylene glycol) substitute (T_{TEG}) in order to reduce the rigidity of the prepolymer and thus improve its elongation and ultimate tensile strength. As expected, a large improvement (over 75%) in the elongation was observed; however, this improvement was at the expense of the ultimate tensile strength (*UTS* = 2.50 ± 0.1 MPa, ε_b = 717.6 ± 8.3%) (Figure 2a and Table 1). Finally, in seeking to enhance both Young's modulus and tensile stress, a less flexible dithiol (T_8) was used to build the network, however, the obtained material was a powdery brittle network (Supplementary Information, Figure S15), thus no mechanical or rheological analyses could be performed.

Following the investigation of the chemical composition effect on mechanical properties, a short aliphatic alkyl-based diynone (Y_6) was used for prepolymer formation with each dithiol (T_{EG}, T_{TEG}, and T_8), prior to crosslinking with TMPTP. Similarly to the previous findings, a higher tensile strength was found in CAN-Y_6-T_{EG} (*UTS* = 2.52 ± 0.3, ε_b = 954.7 ± 123%), but longer elongation was observed for CAN-Y_6-T_{TEG} (*UTS* = 1.14 ± 0.1 MPa, ε_b = 1783.6 ± 28%) (Figure 2b and Table 1). The increase of elongation and the reduction of strength that were observed for CAN-Y_6-T_{TEG} could be attributed to the presence of ethereal carbon-oxygen bonds in the respective dithiol, which increase the material flexibility. In an attempt to improve the tensile strength, the less flexible dithiol (T_8) was used which previously was shown to form stiff CANs. As expected, the ultimate tensile strength for CAN-Y_6-T_8 increased to 10.13 ± 0.4 MPa, yet the elongation at break was significantly decreased to 196.2 ± 10% (Table 1, Figure 2b). The high tensile strength observed in CAN-Y_6-T_8 may be driven by the crystallinity of the network as evidenced by the presence of both melting and crystallisation temperature. Overall, CANs formed from Y_6 monomer showed better elongation than the ones using Y_{Ar} across the different dithiols. However, noticeable decline of the tensile strength was observed when using Y_6 as opposed to Y_{Ar} diynone. This remarkable strength of Y_{Ar} CANs could be accredited to the presence of aromatic ring within the polymer backbone which confer chain rigidity.

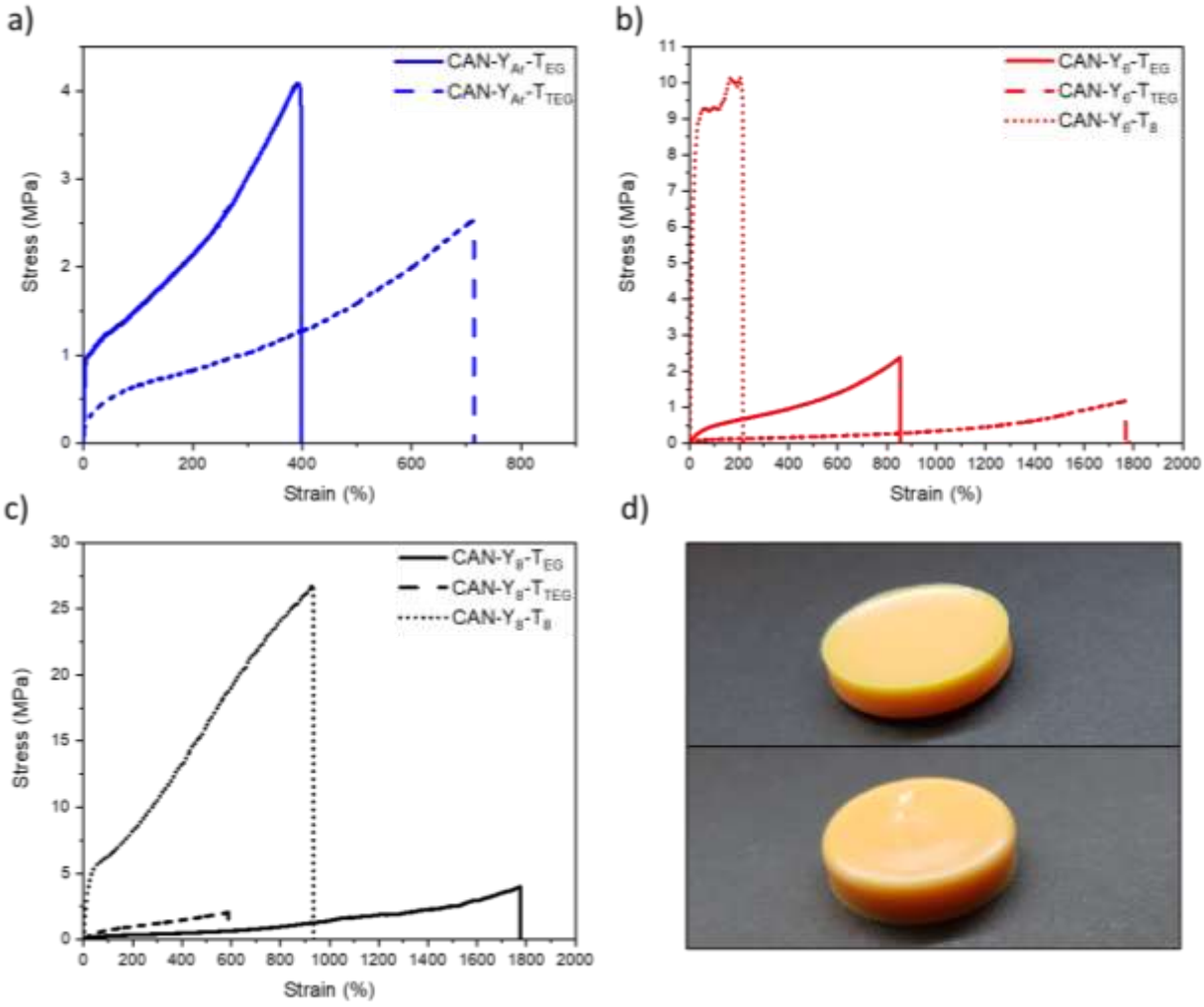

Figure 2. Representative tensile curves of CANs based on (a) Y_{Ar} (b) Y_6 and (c) Y_8 diynone monomers. d) Top and bottom image of C_8Y-T_8 film, measuring 25 mm in diameter.

Finally, the length of the aliphatic spacer in the diynone was increased from 6 to 8 carbons (Y_8) in order to lower the stiffness of the prepolymer and improve its tensile strength and elongation. Unlike all previously tested diynones, Y_8 did not follow the same trend when building CANs using T_{EG} and T_{TEG}. Surprisingly, CAN-Y_8-T_{TEG}, showed lower elongation at break (582 ± 24%) than CAN-Y_8-T_{EG} (1552 ± 202%), even though T_{TEG} contains an extra ethereal bond and thus being more flexible than T_{EG}. We attributed this deviation to the fact that Y_8 is generally more flexible, but stronger than Y_6 as evidenced by its higher UTS and lower glass transition temperature (T_g). As a result, the addition of a less flexible dithiol (T_{EG}) to Y_8 contribute to its strength and overall toughness better than a flexible dithiol (T_{TEG}). On the other hand, both Y_{Ar} and Y_6 are stiffer, thus a flexible dithiol (T_{TEG}) will improve chain flexibility and

the overall toughness better than a stiffer dithiol (T_{EG}). Remarkably; however, the use of T_8 as dithiol in CAN-Y_8-T_8 increased the ultimate tensile strength dramatically to 26 ± 0.8 MPa, while maintaining an excellent elongation 965.3 ± 34% (Figure 2c and Table 1). This excellent performance of CAN-Y_8-T_8 could be attributed to both the flexibility of Y_8 as well as a better chain packing among Y_8 CANs which demonstrated by the observed melting temperature at 65 °C.

Table 1. Thermal and mechanical properties for CANs with different compositions.

	CAN	[a] Thermal Transitions (°C)			[b] UTS (MPa)	[b] Strain at break (%)
		T_g	T_c	T_m		
Previous study	CAN-Y_{10}-T_{EG}	-10	-	-	23.6 ± 6	992 ± 138
This study	CAN-Y_8-T_{EG}	-11	-	-	3.83 ± 0.4	1552 ± 202
	CAN-Y_8-T_{TEG}	-22	-	-	2.02 ± 0.0	582 ± 24
	CAN-Y_8-T_8	-5	-	65	26.9 ± 0.8	965 ± 34
	CAN-Y_6-T_{EG}	-7	-	-	2.52 ± 0.3	955 ± 123
	CAN-Y_6-T_{TEG}	-16	-	-	1.14 ± 0.0	1784 ± 28
	CAN-Y_6-T_8	-6	35	95	10.1 ± 0.4	196 ± 10
	CAN-Y_{Ar}-T_{EG}	34	-	-	3.84 ± 0.5	424 ± 59
	CAN-Y_{Ar}-T_{TEG}	20	-	-	2.50 ± 0.0	718 ± 8
	CAN-Y_{Ar}-T_8	34	-	-	-	-

[a]Obtained from the 2nd DSC heating/cooling cycle. [b]Ultimate tensile strength and elongation at break determined from uniaxial tensile testing at 22 °C, 10 mm min^{-1} strain rate.

In order to investigate the effect of chemical composition on the thermal properties of the formed CANs, Differential Scanning Calorimetry (DSC) was performed to measure their thermal transitions (Table 1). General trend of glass transition temperature (T_g) was observed between ynones, where CANs synthesised from aromatic ynone Y_{Ar} showed the highest T_g compared to the other ynones, when using the same dithiol, followed by moderate T_g observed for Y_6, while CANs composed from the longest ynone (Y_8) showed the lowest T_g. The only exception to this trend is CAN-Y_8-T_8 and CAN-Y_6-T_8, where they showed similar T_g (Supplementary Information, Figures S23-S25). For example, when using T_{EG} dithiol, the T_g observed were (34 °C, −7 °C, −11 °C) for CAN-Y_{Ar}-T_{EG}, CAN-Y_6-T_{EG}, and CAN-Y_8-T_{EG},

respectively. Similarly, when using T_{TEG} dithiol, the T_g observed were (20 °C, −16 °C, −22 °C) for CAN-Y_{Ar}-T_{TEG}, CAN-Y_6-T_{TEG}, and CAN-Y_8-T_{TEG}, respectively. Finally, when using T_8 dithiol, CAN-Y_{Ar}-T_8 showed the highest T_g of (34 °C) while no difference in T_g was observed between CAN-Y_6-T_8 and CAN-Y_8-T_8 (-6 °C, -5 °C, respectively). In addition, melting temperature (T_m) was observed for CAN-Y_8-T_8 (T_m = 65 °C), while CAN-Y_6-T_8, showed both melting temperature (T_m = 95 °C) as well as crystallisation temperature (T_c) above room temperature (T_c = 35 °C), both results correlate well with the high stiffness observed in the tensile curve for both CANs.

The viscoelastic properties of the dynamic networks were assessed by performing stress relaxation measurements using 1% strain. The stress relaxation of the CANs was tested at 140 °C, 80 °C, and 25 °C starting at high temperature. Overall, there was no obvious trend across the three CANs. However, CAN-Y_6 showed faster relaxation than CAN-Y_8 for every dithiol. Furthermore, with the exception of CAN-Y_8-T_{EG} and CAN-Y_{Ar}-T_{TEG}, all CANs showed a moderate relaxation time at 140 °C *i.e.,* relaxation time < 7 minutes. It is worth noting however, that CAN-Y_6-T_{EG} and CAN-Y_6-T_8 showed unpredictable relaxation at 25 °C. This relaxation could be attributed to the effect of the thermal history and overall poor thermal stability of these CANs. Stress relaxation results for the best performing CANs (CAN-Y_8-T_8) are shown in Figure 3a, and the remaining can be found in SI (Supplementary Information, Figure S26−S33).

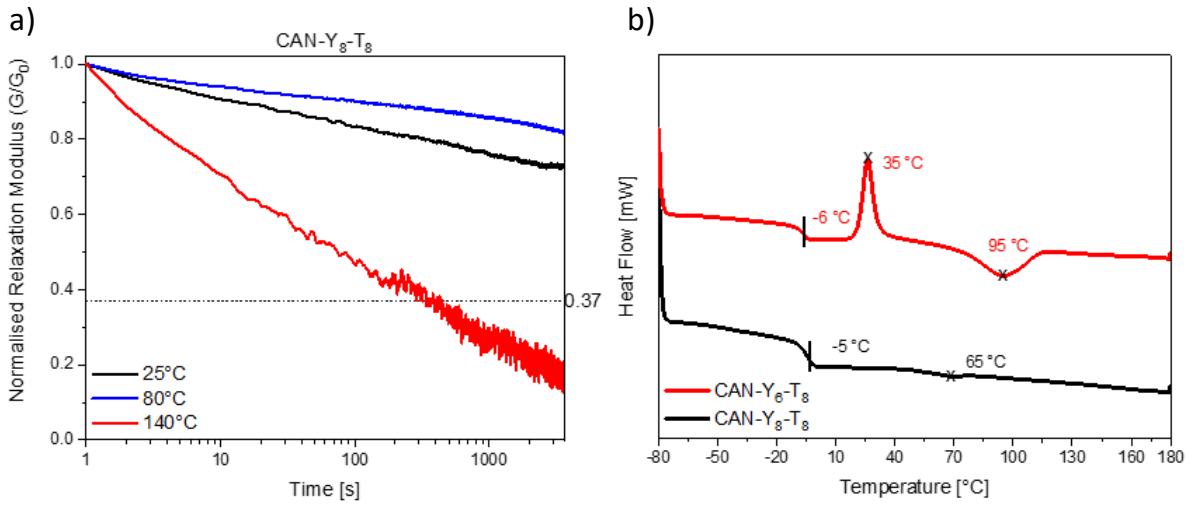

Figure 3. a) Representative stress relaxation of the best performing CAN (C_8Y-T_8) at various temperatures. b) DSC thermogram of semi-crystalline CANs (C_6Y-T_8 and C_8Y-T_8).

Conclusion

A series of dynamic networks based on thiol-yne chemistry were designed using different composition of ynone monomers and dithiol chain extenders. CANs with a wide range of thermomechanical properties could be obtained by altering the functionalities of the prepolymer. For example, while short aliphatic prepolymer (from Y_6 diynone) formed stiffer networks, longer aliphatic prepolymers (from Y_8 diynone) resulted in materials with decreased stiffness. Also, more rigid materials could be designed by replacing the aliphatic alkyl spacer with an aromatic one (Y_{Ar}). By screening different diynones and chain extenders, we were able to synthesise a very robust material (CAN-Y_8-T_8) that presented superior thermomechanical properties to all available CANs (*UTS* = 26 ± 0.8 MPa, ε_b = 965.3 ± 34%). Although the tensile strength and elongation were similar to the previously reported CAN-Y_{10}-T_{EG}, CAN-Y_8-T_8 presented a higher overall stiffness and Young's modulus (Supplementary Information, Figure S22). Further work anticipated also includes an extensive study on the effect of using multiple crosslinking system as well as varying the monomers' chemical structure.

References

1. J. Luo, Z. Demchuk, X. Zhao, T. Saito, M. Tian, A. P. Sokolov and P.-F. Cao, *Matter*, 2022, **5**, 1391-1422.
2. R. Yoda, *J. Biomater. Sci. Polym. Ed.*, 1998, **9**, 561-626.
3. M. Delahaye, J. M. Winne and F. E. Du Prez, *J. Am. Chem. Soc.*, 2019, **141**, 15277-15287.
4. N. Zheng, Y. Xu, Q. Zhao and T. Xie, *Chem. Rev.*, 2021, **121**, 1716-1745.
5. C. J. Kloxin, T. F. Scott, B. J. Adzima and C. N. Bowman, *Macromolecules*, 2010, **43**, 2643-2653.
6. C. J. Kloxin and C. N. Bowman, *Chem. Soc. Rev.*, 2013, **42**, 7161-7173.
7. Y. Wu, Y. Wei and Y. Ji, *Polym. Chem.*, 2020, **11**, 5297-5320.
8. M. Podgórski, B. D. Fairbanks, B. E. Kirkpatrick, M. McBride, A. Martinez, A. Dobson, N. J. Bongiardina and C. N. Bowman, *Adv. Mater.*, 2020, **32**, 1906876.
9. F. Van Lijsebetten, T. Debsharma, J. M. Winne and F. E. Du Prez, *Angew. Chem., Int. Ed.*, **n/a**, e202210405.
10. Z. Yang, Q. Wang and T. Wang, *ACS Appl. Mater. Interfaces*, 2016, **8**, 21691-21699.
11. J. L. Swartz, R. L. Li and W. R. Dichtel, *ACS Appl. Mater. Interfaces*, 2020, **12**, 44110-44116.
12. B. Akkus, B. Kiskan and Y. Yagci, *Polym. Chem.*, 2019, **10**, 5743-5750.

13. B. Zhang, J. Ke, J. R. Vakil, S. C. Cummings, Z. A. Digby, J. L. Sparks, Z. Ye, M. B. Zanjani and D. Konkolewicz, *Polym. Chem.*, 2019, **10**, 6290-6304.

14. J. S. Bermejo and C. M. Ugarte, *Macromol. Theory Simul.*, 2009, **18**, 317-327.

15. K. Yu, P. Taynton, W. Zhang, M. L. Dunn and H. J. Qi, *RSC Adv.*, 2014, **4**, 48682-48690.

16. A. Duval, G. Couture, S. Caillol and L. Avérous, *ACS Sustain. Chem. Eng.*, 2017, **5**, 1199-1207.

17. A. Jourdain, R. Asbai, O. Anaya, M. M. Chehimi, E. Drockenmuller and D. Montarnal, *Macromolecules*, 2020, **53**, 1884-1900.

18. S. K. Schoustra, T. Groeneveld and M. M. Smulders, *Polym. Chem.*, 2021, **12**, 1635-1642.

19. O. Anaya, A. Jourdain, I. Antoniuk, H. Ben Romdhane, D. Montarnal and E. Drockenmuller, *Macromolecules*, 2021, **54**, 3281-3292.

20. J. J. Lessard, G. M. Scheutz, S. H. Sung, K. A. Lantz, T. H. Epps, III and B. S. Sumerlin, *J. Am. Chem. Soc.*, 2020, **142**, 283-289.

21. J. S. A. Ishibashi, I. C. Pierce, A. B. Chang, A. Zografos, B. M. El-Zaatari, Y. Fang, S. J. Weigand, F. S. Bates and J. A. Kalow, *Macromolecules*, 2021, **54**, 3972-3986.

22. R. L. Snyder, C. A. Lidston, G. X. De Hoe, M. J. Parvulescu, M. A. Hillmyer and G. W. Coates, *Polym. Chem.*, 2020, **11**, 5346-5355.

23. R. A. Mrozek, D. B. Knorr, S. W. Spangler, P. J. Cole and J. L. Lenhart, *Soft Matter*, 2012, **8**, 11185-11192.

24. A. Skandani, J. A. Clement, S. Tristram-Nagle and M. R. Shankar, *Polymer*, 2017, **133**, 30-39.

25. S. Nahm and S. M. Weinreb, *Tetrahedron Lett.*, 1981, **22**, 3815-3818.

3.2 Supporting Information

Using composition to tune thermomechanical properties of thiol-yne covalent adaptable networks

Maher A. Alraddadi[§], Joshua C. Worch[§], Andrew P. Dove[*§]

[§]School of Chemistry, University of Birmingham, Edgbaston, Birmingham, B15 2TT (UK)

Table of Contents

General Materials and Methods

Materials: Unless stated otherwise, all chemicals and solvents were purchased from VWR Chemicals, Sigma-Aldrich, Fisher Scientific, or Apollo Scientific and were used as received without any further purifications. All air-sensitive compounds were handled under a nitrogen environment using Schlenk techniques. Dry Tetrahydrofuran (THF) was used from a drying and degassing solvent tower directly.

NMR Spectroscopic Analysis: All NMR spectroscopy experiments were conducted on a Bruker DPX-300 and DPX-400 NMR instrument. All chemical shifts were reported in ppm and referenced to the residual solvent signal $CDCl_3$ at δ= 7.26 ppm and ^{13}C NMR spectra are referenced to the residual solvent signal $CDCl_3$ at δ = 77.16. The multiplicity of the peaks was described as s= singlet, d=doublet, t=triplet, q=quartet, qu=quintet, m=multiplet.

Mass Spectrometry: Mass Spectrometry was conducted by the School of Chemistry at University of Birmingham on a Waters Xevo G2-XS Quadrupole Time-of-Flight (QTof) mass spectrometer.

Fourier-transform Infared spectroscopy (FTIR): All FTIR analysis were carried out using Cary 630 FTIR spectrometer from Agilent Technologies Inc. 16 Scans from 600 to 4000 cm^{-1} were recorded at a resolution of 2 cm^{-1}. All spectra were corrected against background absorbance.

Differential scanning calorimetry (DSC): All thermal transitions were determined using STARe system DSC3 from Mettler-Toledo. All samples, unless otherwise stated, were tested under nitrogen from -80 to 180°C at heating rate of 10 K min^{-1} for two heating/cooling cycles. The glass transition temperature was calculated from the inflection point of the second heating cycle.

Rheology: All flow characteristics of the polymer networks were conducted using Anton Paar MCR302 rheometer with Peltier controlled heating. All tests were performed on a disk-shape samples of 8 mm in diameter using parallel plates. All stress relaxation experiments were performed at 1% constant strain which is within the linear viscoelastic region of the polymer network at 140 °C.

Tensile testing: All uniaxial tensile measurements were performed at room temperature and strain rate of 10 mm/min on a Testometric M350-5CT tensometer equipped with a load cell of 5 kgF. Using custom ASTM Die D-638 Type 5 (Neck dimensions 7.11 × 1.70) and a hand press, polymer films were cut into dumbbell-shaped samples with a width of about 1.7 mm and about 0.2 mm in thickness while the gauge

length was set to 7.1 mm. Minimum of n = 3 specimens were tested for each film, unless otherwise stated. The average values and standard deviations were reported.

Film casting: A 100 mL Polytetrafluoroethylene (PTFE) beaker “Teflon beaker” charged with the respective prepolymer and equipped with a stirring bar was cooled to −70 °C (dry ice/acetone bath) for 30 seconds. The proper amount of crosslinker was added to the beaker and stirred for 5 seconds. The beaker was then removed from the cooling bath and placed inside a fume hood overnight to allow solvent to be evaporated. The film was casted at the bottom of the beaker. Note: for better film, a larger glass beaker is placed “upside-down” above the Teflon beaker to slow down the evaporation process. To increase the thickness of the film, a smaller Teflon beaker (50 mL) was use with same reactants amount Figure S35, on page S27.

Synthesis

General procedure for Weinreb amide synthesis

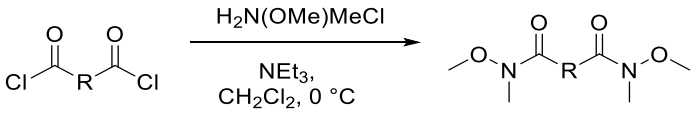

The procedure was adapted from literature.[1, 2] A 3-neck round-bottom flask, attached to a dropping funnel and equipped with a magnetic stirrer, was charged with 1 equiv. of the diacid chloride of interest and dissolved in dichloromethane to make 1 M solution. The mixture was cooled in brine-ice bath to −10 °C. N,O-dimethylhydroxylamine hydrochloride (2.1 equiv.) was added in one portion to the mixture. Triethylamine (NEt_3) (4.2 equiv.) was added to the dropping funnel and slowly dropwise over 20-30 minutes into the reaction mixture. Note: reaction was exothermic and ammonium salt by-product (white precipitate) was produced. After completing the addition of the NEt_3, the mixture was stirred at ambient temperature for 1 h. The mixture was diluted with dichloromethane (20% v/v) and transferred to a separatory funnel. The organic layer was then washed with 1 M HCl, saturated $NaHCO_3$, water, and brine, respectively. Finally, the combined organic layer was dried over $MgSO_4$ and concentrated with a rotary evaporator. Unless otherwise specified, the crude product was used directly without additional purification.

N^1,N^8-dimethoxy-N^1,N^8-dimethyloctanediamide (C_6-Amide)

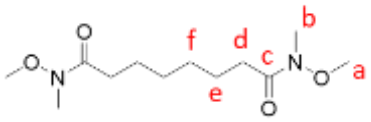

Using the general procedure specified above and octanedioyl dichloride as diacid chloride, a transparent oil product (27.10 g, 85% yield) was synthesised. ^{1}H NMR (300 MHz, Chloroform-d) δ 3.66 (s, 6H, H^a), 3.15 (s, 6H, H^b), 2.39 (t, J = 7.6 Hz, 4H, H^d), 1.70 – 1.54 (m, 4H, H^e), 1.40 – 1.29 (m, 4H, H^f). ^{13}C NMR (75 MHz, $CDCl_3$) δ 195.75 (C^C), 61.30 (C^a), 32.28 (C^b), 31.93 (C^d), 29.32 (C^e), 24.62 (C^f). FTIR: 1649 cm^{-1} (C=O Amide). HRMS (TOF MS ASAP+) (m/z): $[M + H]^+$ calculated for $C_{12}H_{24}N_2O_4$, 359.2950; found, 359.2950. Anal. Calcd for $C_{12}H_{24}N_2O_4$: C, 55.36; H, 9.29; N, 10.76. Found: C, 64.18; H, 6.8; N, 12.72. FT-IR: 1649 cm^{-1} (C=O amide).

N^1,N^{10}-dimethoxy-N^1,N^{10}-dimethyldecanediamide (C_8-Amide)

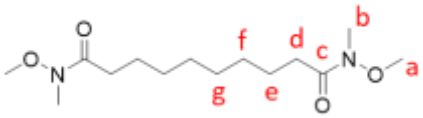

Using decanedioyl dichloride as the diacid chloride for the general procedure mentioned above, an off-white solid (30.88 g, 86% yield) was synthesised, ^{1}H NMR (300 MHz, Chloroform-*d*) δ 3.67 (s, 6H, H^a), 3.16 (s, 6H, H^b), 2.39 (t, *J* = 7.6 Hz, 4H, H^d), 1.61 (p, *J* = 6.7 Hz, 4H, H^e), 1.37 – 1.25 (m, 8H, $H^{f,g}$). ^{13}C NMR (101 MHz, $CDCl_3$) δ 174.94 (C^c), 61.33 (C^a), 32.29 (C^b), 32.02, (29.52, 29.39 ($C^{d,e,f}$), 24.75 (C^g). TOF MS ASAP+ (m/z): $[M + H]^+$ calculated for $C_{14}H_{28}N_2O_4$, 289.2128; found, 289.2127. Anal. Calcd for $C_{14}H_{28}N_2O_4$: C, 58.31; H, 9.79; N,9.71. Found: C, 58.19; H, 9.9; N,9.62. FT-IR: 1650 cm^{-1} (C=O amide).

N^1,N^4-dimethoxy-N^1,N^4-dimethylterephthalamide (C_{Ar}-Amide)

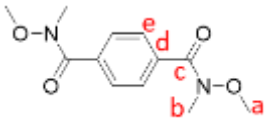

Using terephthaloyl dichloride as the diacid chloride in the above generic procedure, a white solid (24.30 g, 79% yield) was synthesised, ^{1}H NMR (400 MHz, Chloroform-d) δ 7.69 (s, 4H, H^c), 3.52 (s, 6H, H^a), 3.35 (s, 6H, H^b). ^{13}C NMR (101 MHz, $CDCl_3$) δ 169.26 (C^c), 136.16 (C^d), 127.95 (C^e), 61.30 (C^a), 33.69 (C^b). TOF MS ASAP+ (m/z): $[M + H]^+$ calculated for $C_{12}H_{16}N_2O_4$, 253.1188; found, 253.1191 Anal. Calcd for $C_{12}H_{16}N_2O_4$: C, 57.13; H, 6.39; N,11.10 . Found: C, 56.66; H, 6.37; N,11.51. FT-IR:1625 cm^{-1} (C=O amide).

General procedure for ynone/diynone synthesis

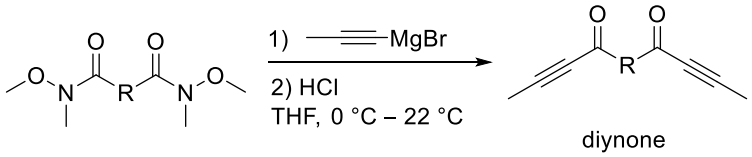

The Weinreb amide (1.0 equiv.) was added to an oven-dried, 2-neck round bottom flask under N_2 atmosphere using standard Schlenk technique and diluted with dry THF to make 1 M solution *via* cannula transfer. The solution was then cooled to 0 °C and 1.4 equiv. of 1-propynylmagnesium bromide solution (0.5 M in THF) was added *via* cannula to the reaction mixture slowly (over 30 min) while stirring the mixture. After the completion of addition, the reaction mixture was stirred for another 30 min in the cooling bath and then warmed to 22 °C and stirred overnight (about 16 h). The reaction mixture was cooled back to 0 °C, then quenched with 1 M HCl (25% v/v) *via* slow addition. The crude mixture was transferred to a separatory funnel. The aqueous layer was extracted with ethyl acetate. The organic layer was collected and combined with the previous organic layer collected from THF. The combined organic layers were then washed with brine, dried over magnesium sulfate, concentrated *in vacuo* and purified using silica gel column chromatography and/or recrystallized (see individual compound for details).

Synthesis of tetradeca-2,12-diyne-4,11-dione (Y_6)

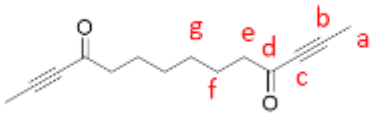

A transparent light-yellow oil was obtained (5.23 g, 67% yield) after purification by silica gel column chromatography (hexane/ethyl acetate 4/1, R_f = 0.4). ^{1}H NMR (400 MHz, $CDCl_3$) δ 2.50 (t, J = 7.4 Hz, 4H, H^e), 2.01 (s, 6H, H^a), 1.69 – 1.59 (m, 4H, H^f), 1.37 – 1.28 (m, 4H, H^g). ^{13}C NMR (101 MHz, $CDCl_3$) δ 188.35 (C^d), 90.08 (C^b), 80.33 (C^c), 45.39 (C^e), 28.73 (C^f), 23.90 (C^g), 4.17 (C^a). HRMS (TOF-MS-ES$^+$) (m/z): $[M + Na]^+$ calculated for $C_{14}H_{18}O_2$, 241.1204; found, 241.1210. Anal. Calcd for $C_{14}H_{18}O_2$: C, 77.03; H, 8.31; Found: C, 81.75; H, 8.22. FT-IR: 1667 cm^{-1} (C=O ketone), 2213 cm^{-1} (C≡C).

Synthesis of hexadeca-2,14-diyne-4,13-dione (Y_8)

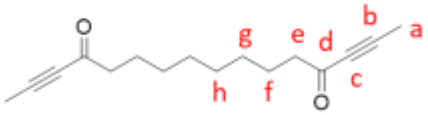

Off-white oil was obtained (3.59 g, 70% yield) after purification by silica gel column chromatography (hexane/ethyl acetate 3/1, R_f = 0.6). ^{1}H NMR (400 MHz, $CDCl_3$) δ 2.51 (t, J = 7.4 Hz, 4H, H^e), 2.01 (s, 6H, H^a), 1.64 (t, J = 7.3 Hz, 4H, H^f), 1.29 (s, 8H, H^{gh}). ^{13}C NMR (101 MHz, $CDCl_3$) δ 188.59 (C^d), 90.01 (C^b), 80.40 (C^c), 45.55 (C^e), 29.23 ($C^{f,g}$), 24.14 (C^h), 4.21 (C^a). HRMS (TOF-MS-ES$^+$) (m/z): [M + Na]$^+$ calculated for $C_{16}H_{22}O_2$, 269.1517; found, 269.1525. Anal. Calcd for $C_{16}H_{22}O_2$: C, 78.01; H, 9.00. Found: C, 73.19; H, 8.38. FT-IR: 1667 cm^{-1} (C=O ketone), 2213 cm^{-1} (C≡C).

Synthesis of 1,1'-(1,4-phenylene)bis(but-2-yn-1-one) (Y_{Ar})

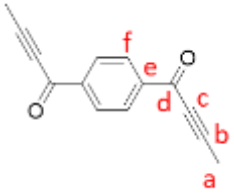

White powder was obtained (2.77 g, 65% yield) after purification by recrystallization with ethanol (100%). ^{1}H NMR (400 MHz, $CDCl_3$) δ 8.22 (s, 4H, H^f), 2.19 (s, 6H, H^a). ^{13}C NMR (101 MHz, $CDCl_3$) δ 177.47 (C^d), 140.46 (C^e), 129.70 (C^f), 94.11 (C^b), 79.14 (C^c), 4.59 (C^a). HRMS (TOF-MS-ES$^+$) (m/z): [M + H]$^+$ calculated for $C_{14}H_{10}O_2$, 211.0759; found, 211.0759. Anal. Calcd for $C_{14}H_{10}O_2$: C, 79.98; H, 4.79. Found: C, 78.66; H, 4.65. FT-IR: 1633 cm^{-1} (C=O ketone), 2205 cm^{-1} (C≡C).

Representative synthesis of Prepolymers

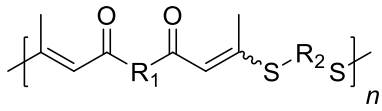

The following protocol was used for the synthesis of the propolymers, 1 equiv. of diynone monomer (Y_{10}, Y_8, Y_6, or Y_{Ar}) was added into a flask and dissolved in dichloromethane (30 wt%). Next, 0.85 equiv. of the diethanethiol (T_{EG}, T_{TEG}, or T_8) was added to the mixture. The reaction mixture was stirred for 5 minutes and cooled to −70 °C (dry ice/acetone bath). 0.05 equiv. of 1,8-diazabicyclo[5.4.0]undec-7-ene (DBU) was added and the reaction mixture was removed from the cooling bath and stirred at ambient temperature for 2 h. The reaction mixture was then cooled to −70 °C (dry ice/acetone bath), and 0.10

equiv. of trimethylolpropane tris(3-mercaptopropionate) was added. The reaction mixture was removed from the cooling bath, stirred for 30 s and poured into a mould.

NMR Spectra

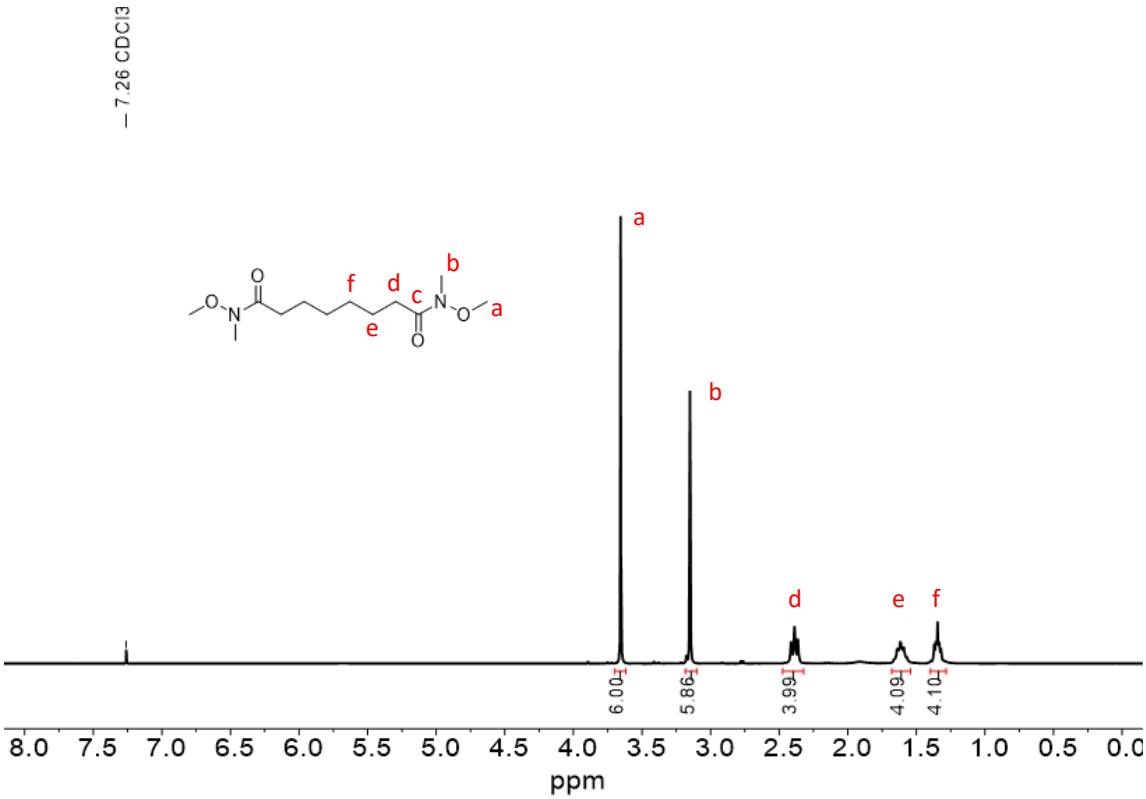

Figure S1. ^{1}H NMR Spectrum of C_6-Amide (300 MHz; 298 K; $CDCl_3$).

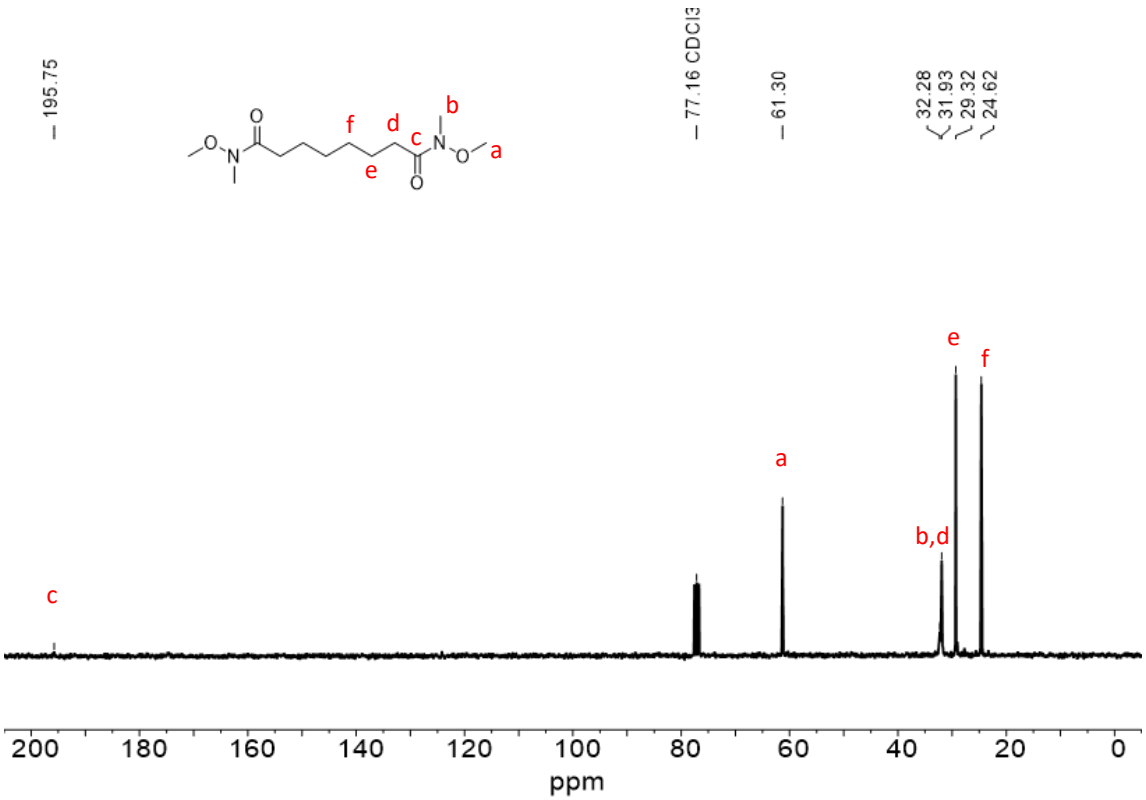

Figure S2. ^{13}C NMR Spectrum of C_6-Amide (75 MHz; 298 K; $CDCl_3$).

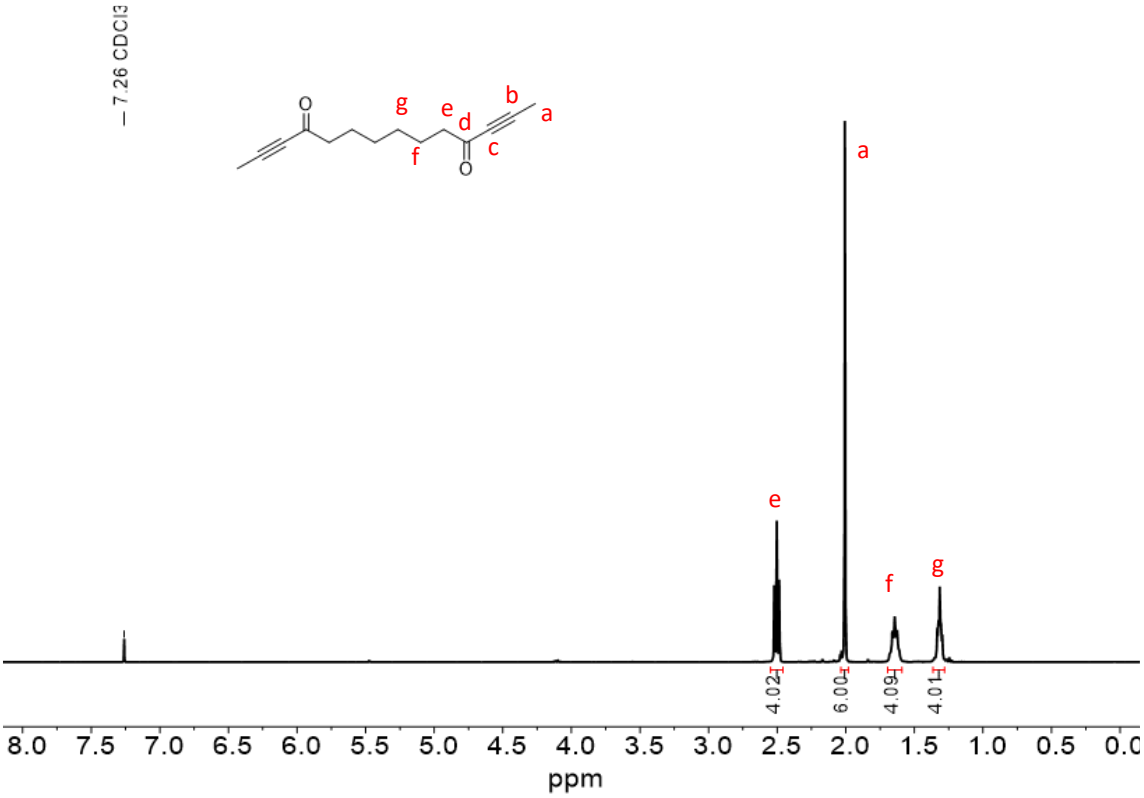

Figure S3. ^{1}H NMR Spectrum of "Y_6" ynone monomer (400 MHz; 298 K; $CDCl_3$).

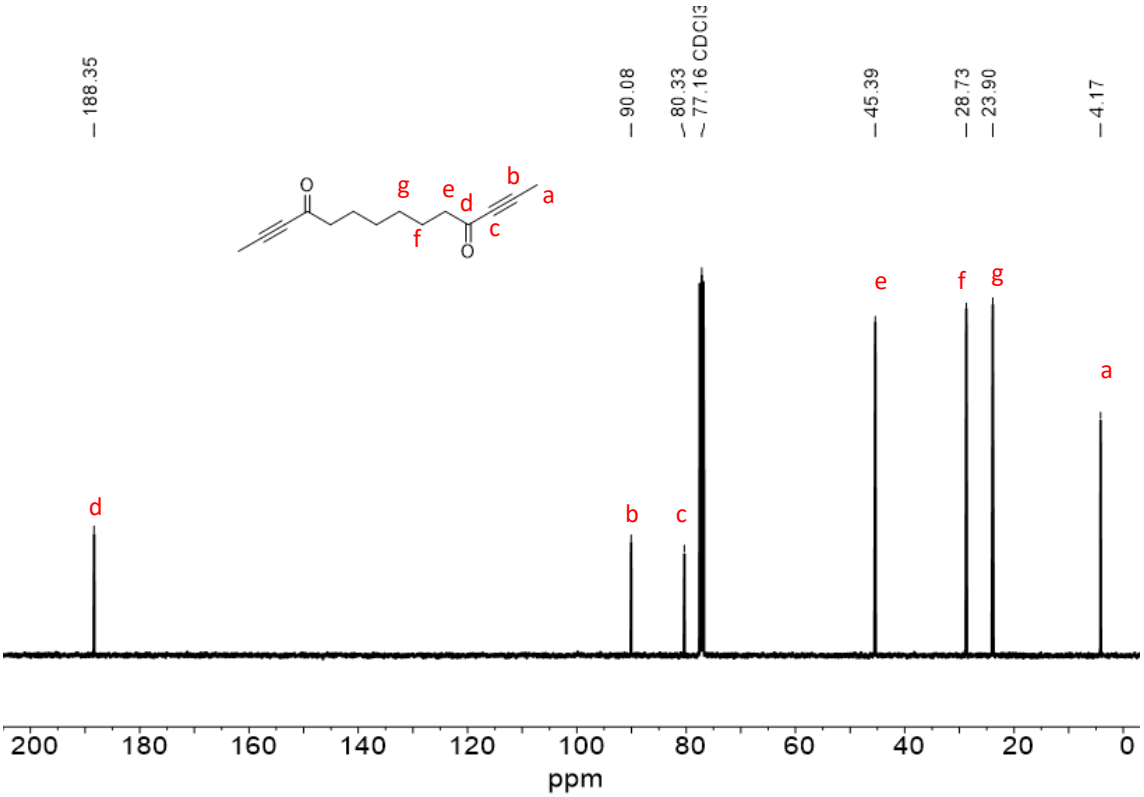

Figure S4. ^{13}C NMR Spectrum of "Y_6" ynone monomer (101 MHz; 298 K; $CDCl_3$).

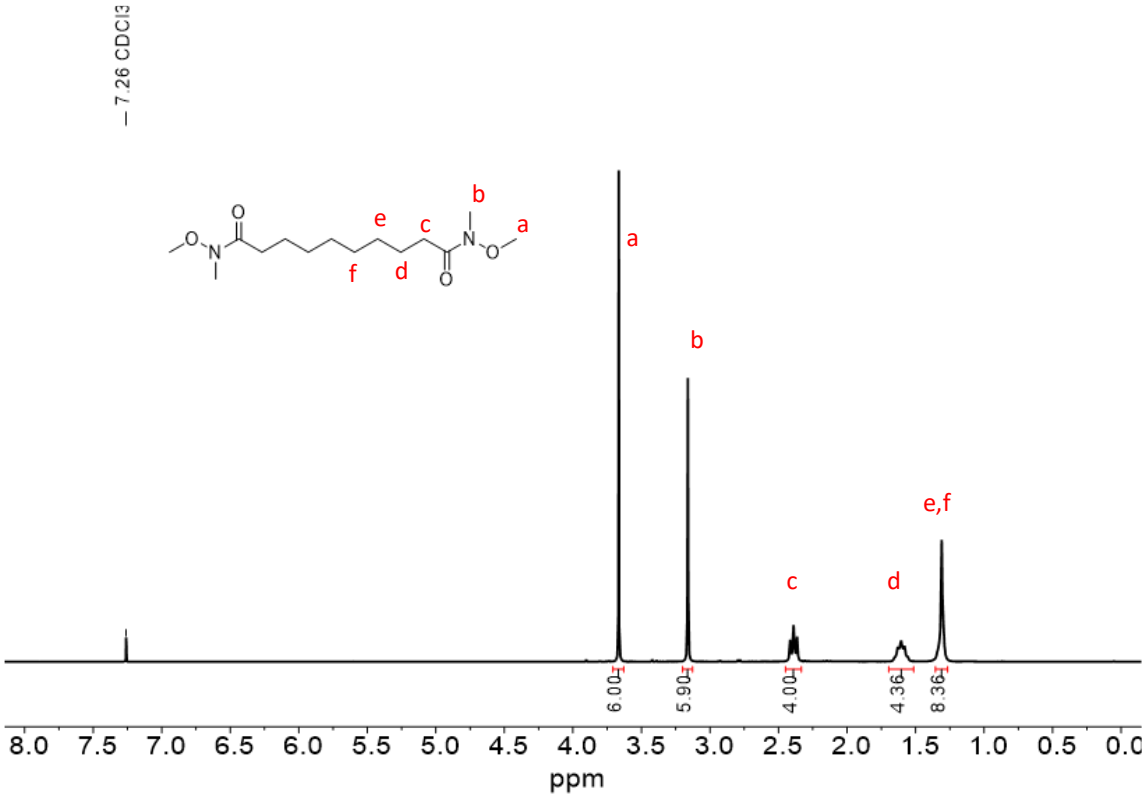

Figure S5. ^{1}H NMR Spectrum of C_8-Amide (300 MHz; 298 K; $CDCl_3$).

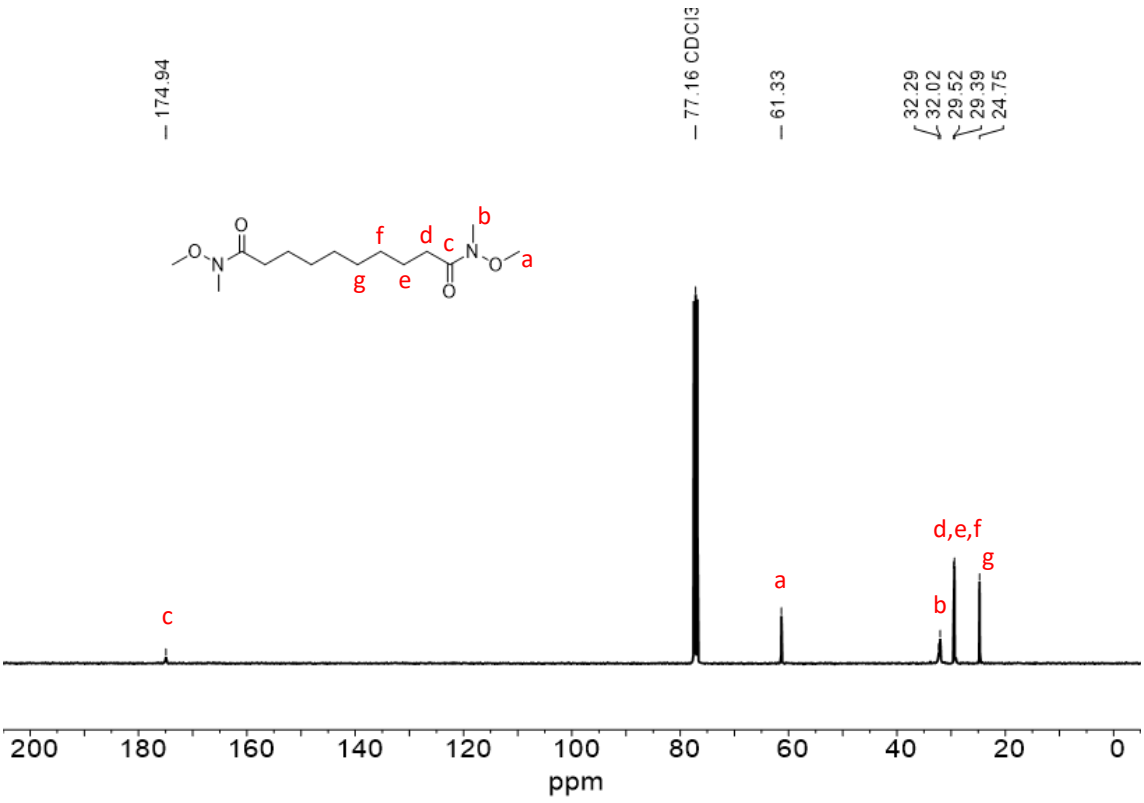

Figure S6. ^{13}C NMR Spectrum of C_8-Amide (101 MHz; 298 K; $CDCl_3$).

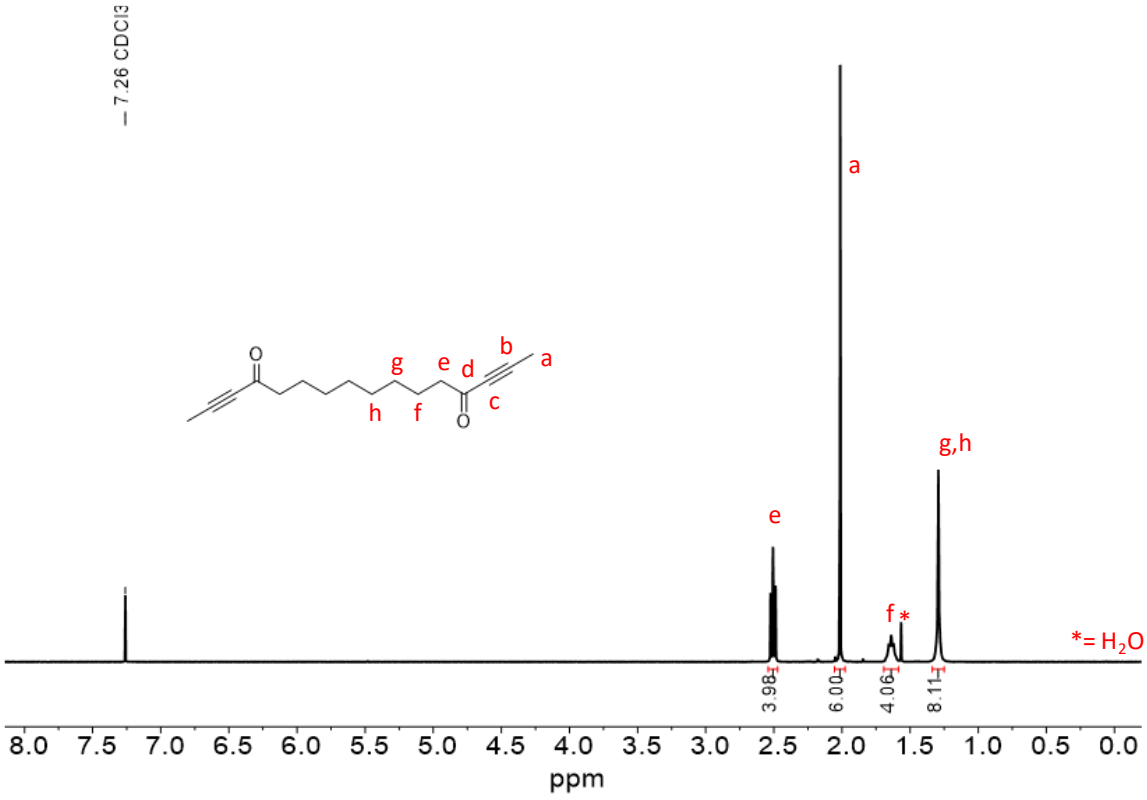

Figure S 7. ^{1}H NMR Spectrum of "Y_8" ynone monomer (400 MHz; 298 K; $CDCl_3$).

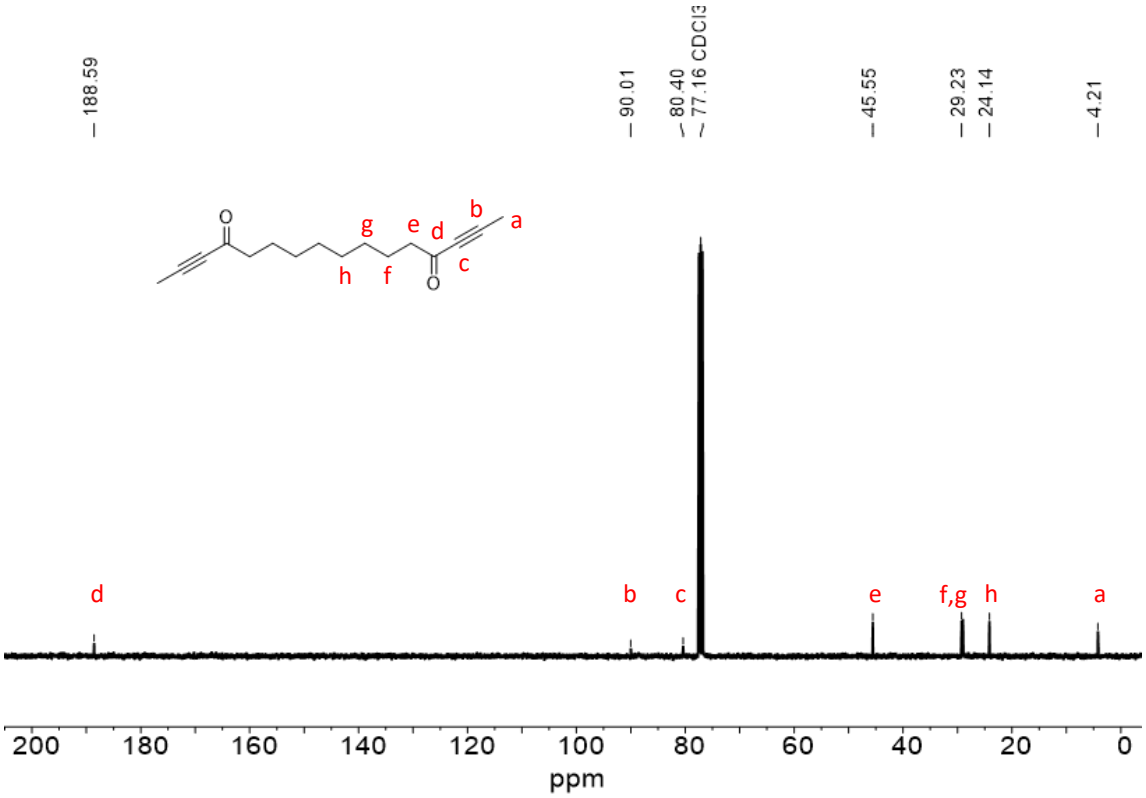

Figure S8. ^{13}C NMR Spectrum of of "Y_8" ynone monomer (101 MHz; 298 K; $CDCl_3$).

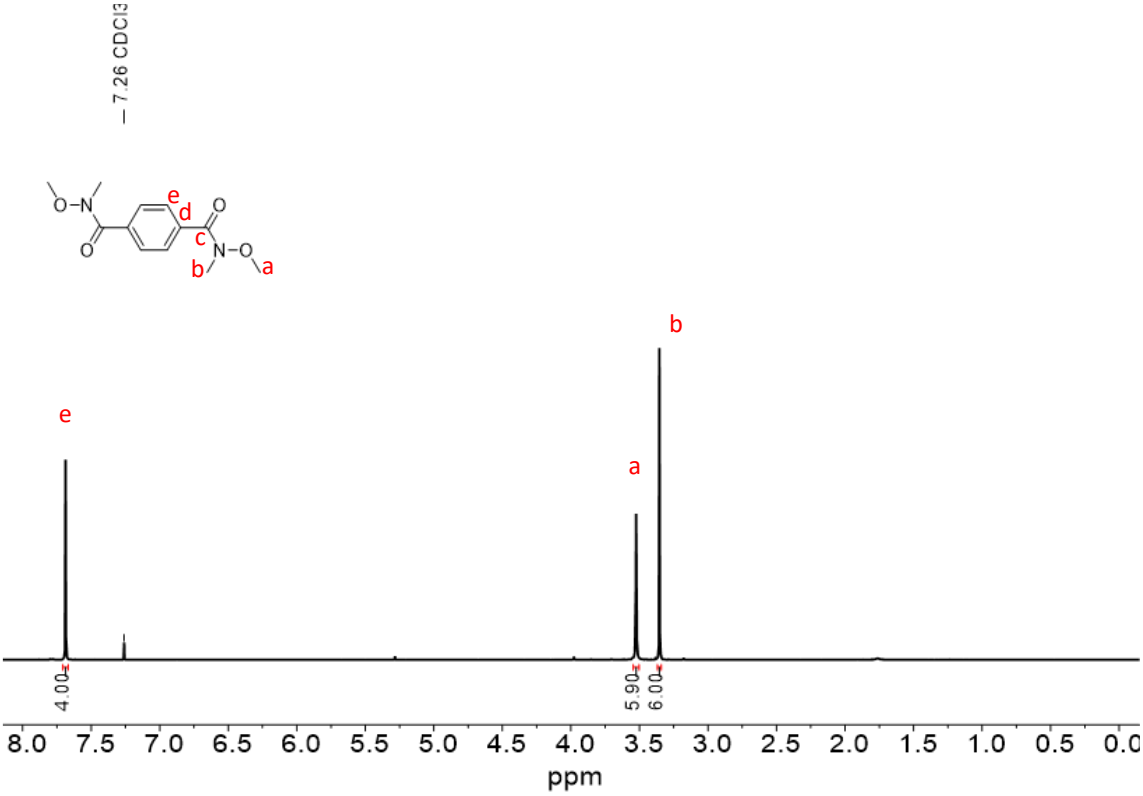

Figure S9. ^{1}H NMR Spectrum of C_{Ar}-Amide (400 MHz; 298 K; $CDCl_3$).

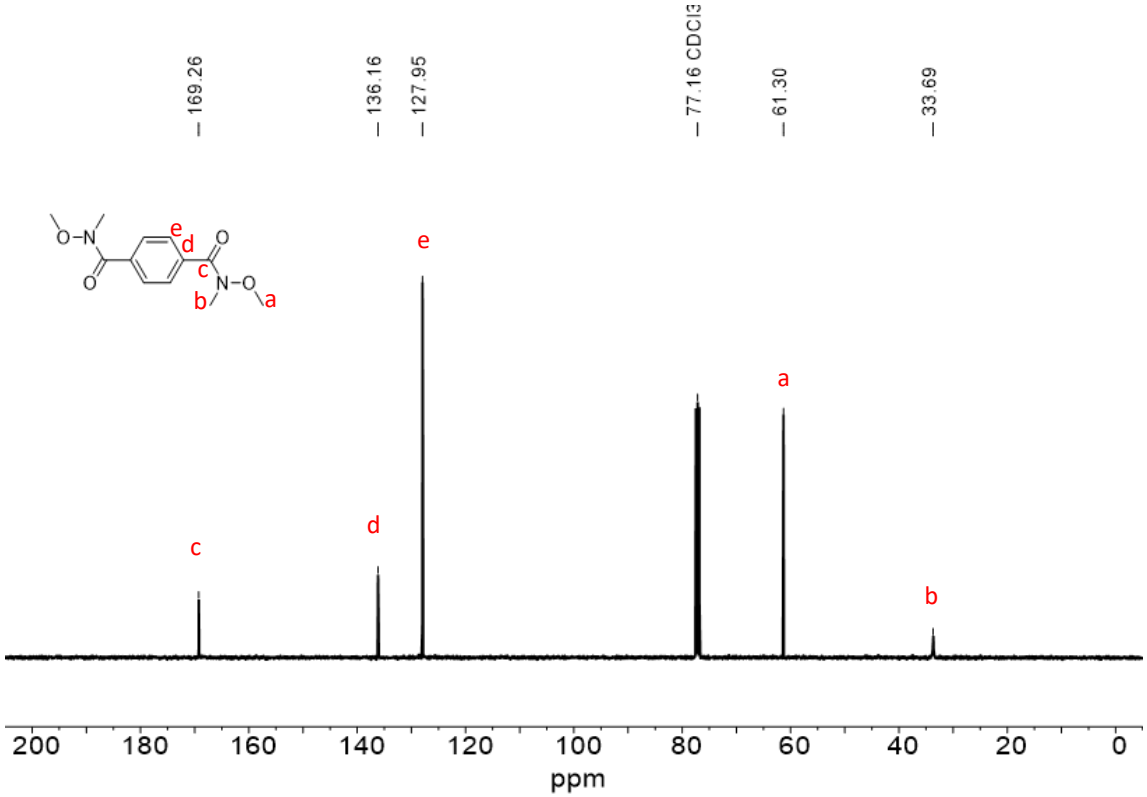

Figure S10. ^{13}C NMR Spectrum of C_{Ar}-Amide (101 MHz; 298 K; $CDCl_3$).

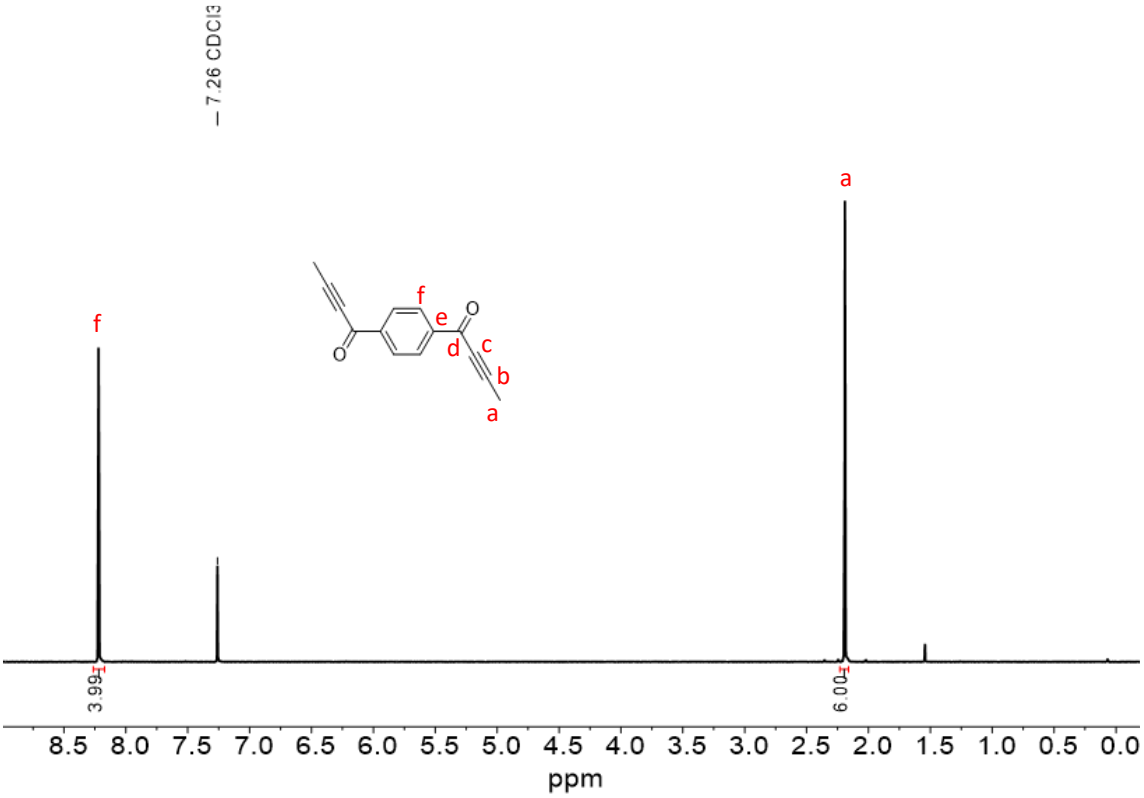

Figure S11. ^{1}H NMR Spectrum of "Y_{Ar}" ynone monomer (400 MHz; 298 K; $CDCl_3$).

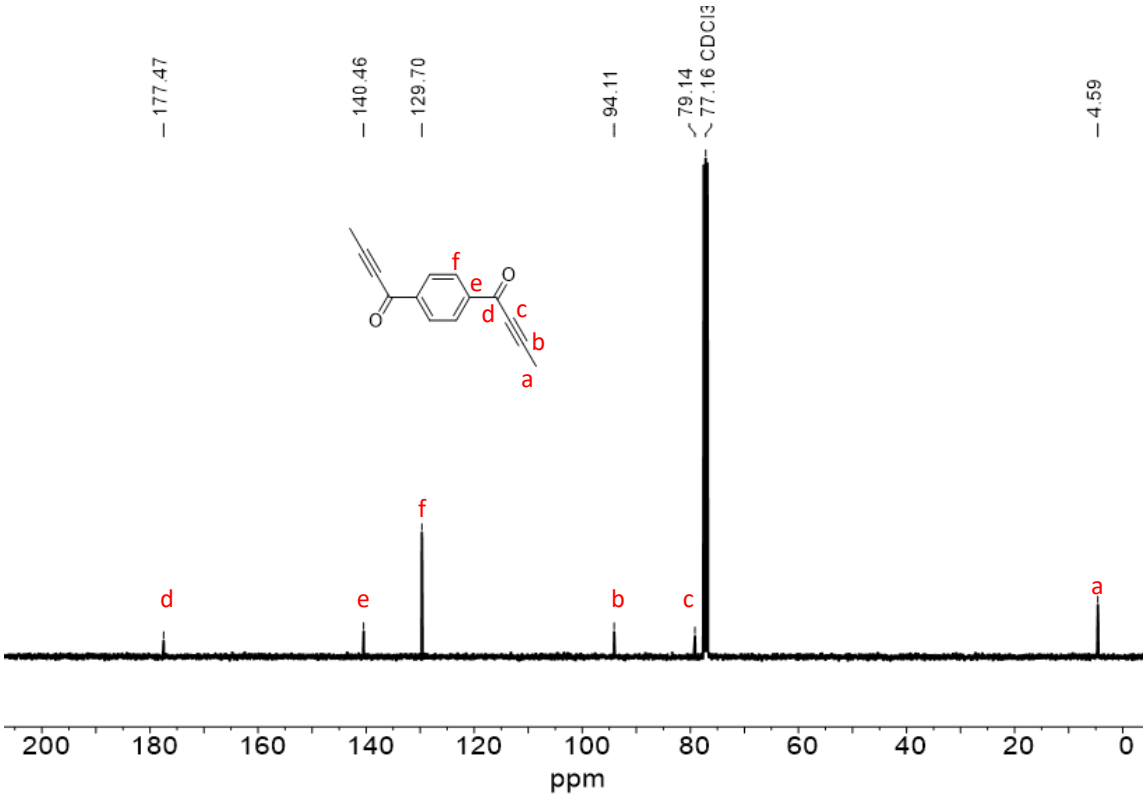

Figure S12. ^{13}C NMR Spectrum of "Y_{Ar}" ynone monomer (101 MHz; 298 K; $CDCl_3$).

Tensile Testing

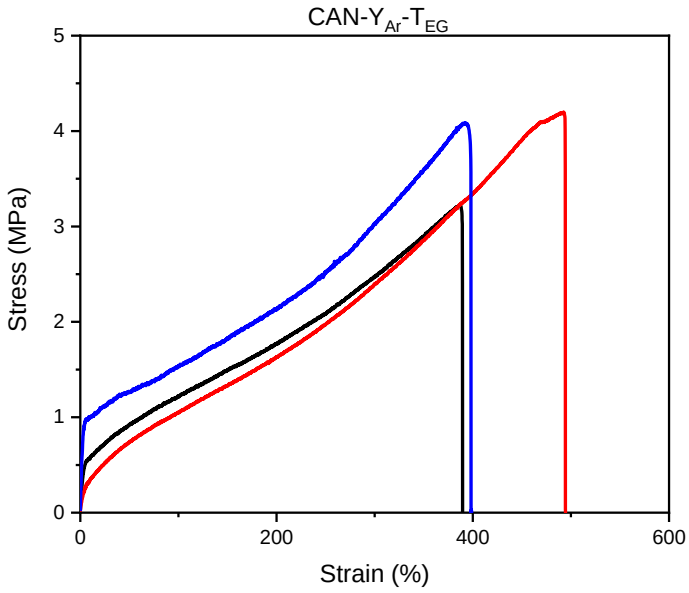

Figure S13. Stress vs strain curve of CAN-Y_{Ar}-T_{EG}.

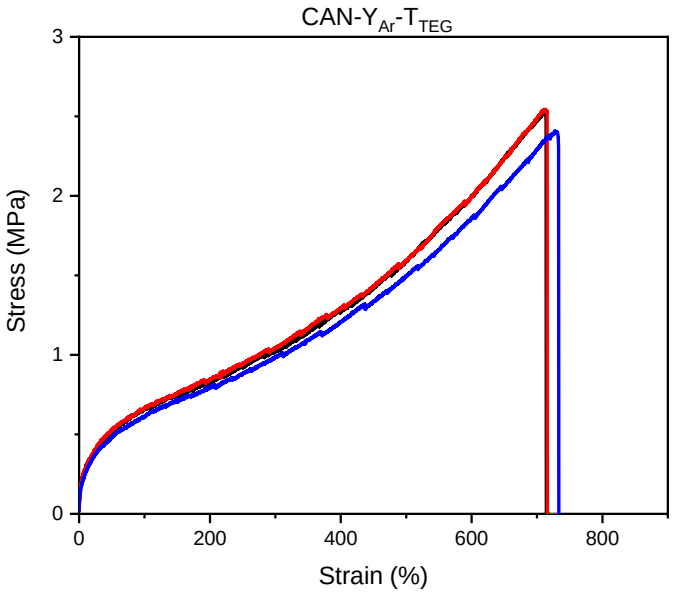

Figure S14. Stress vs strain curve of CAN-Y_{Ar}-T_{TEG}.

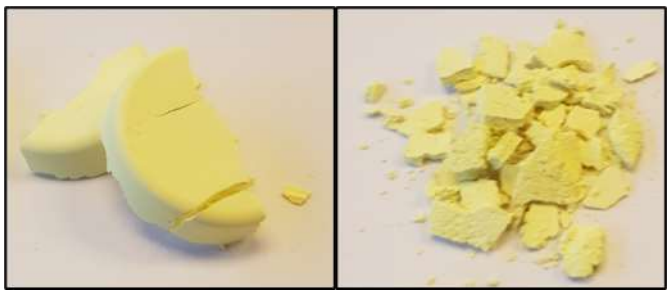

Figure S15. Fracture of CAN-Y_{Ar}-T_8

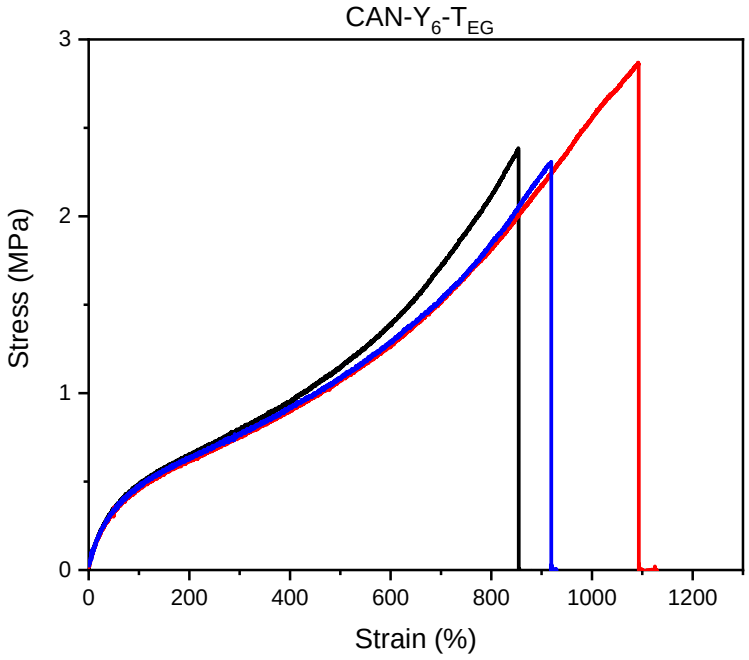

Figure S16. Stress vs strain curve of CAN-Y_6-T_{EG}.

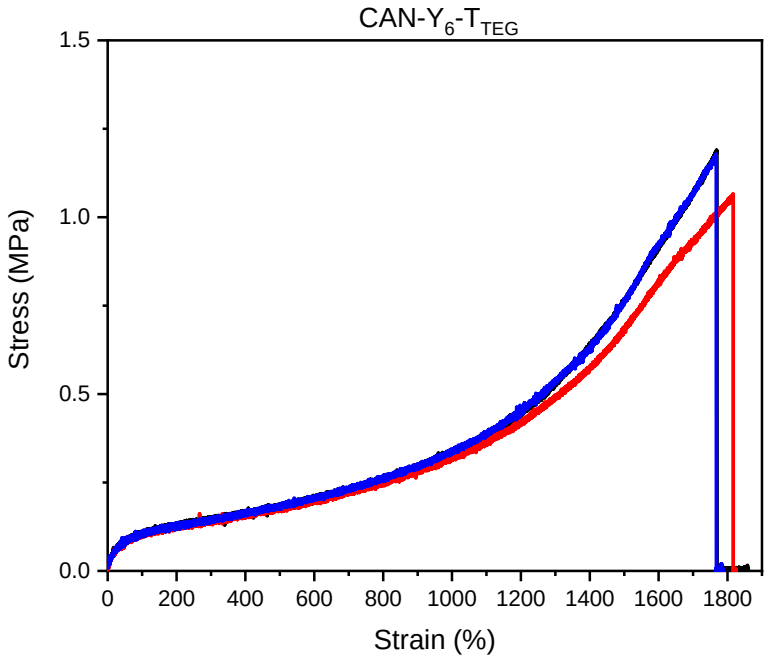

Figure S17. Stress vs strain curve of CAN-Y_6-T_{TEG}.

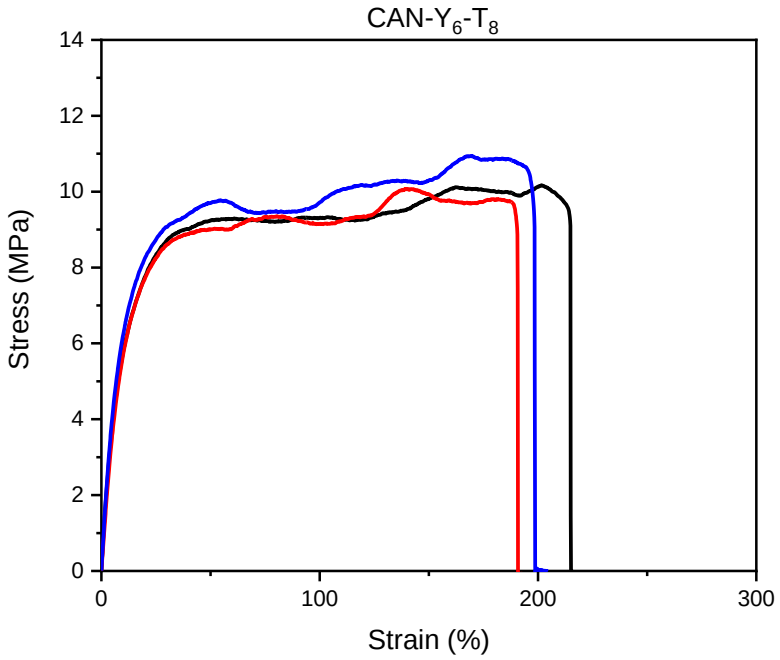

Figure S18. Stress vs strain curve of CAN-Y_6-T_8.

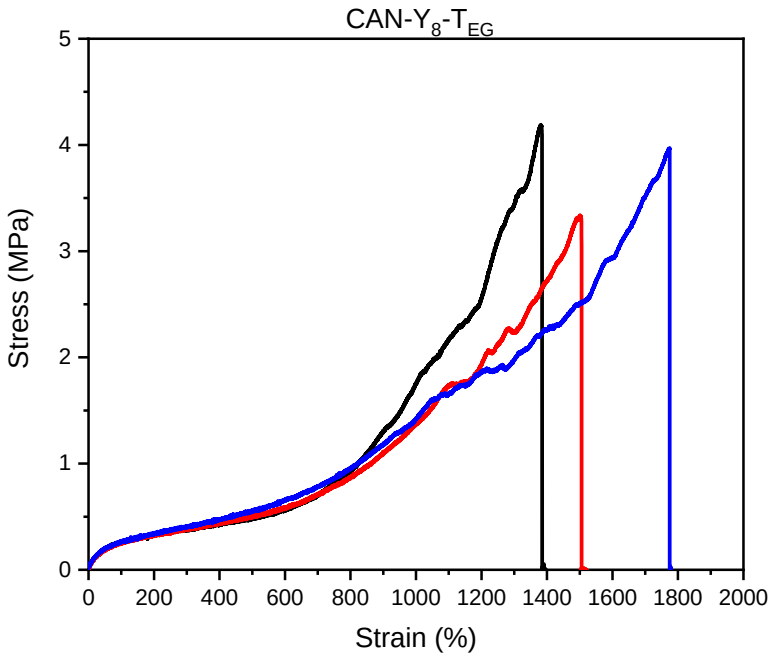

Figure S19. Stress vs strain curve of CAN-Y_8-T_{EG}.

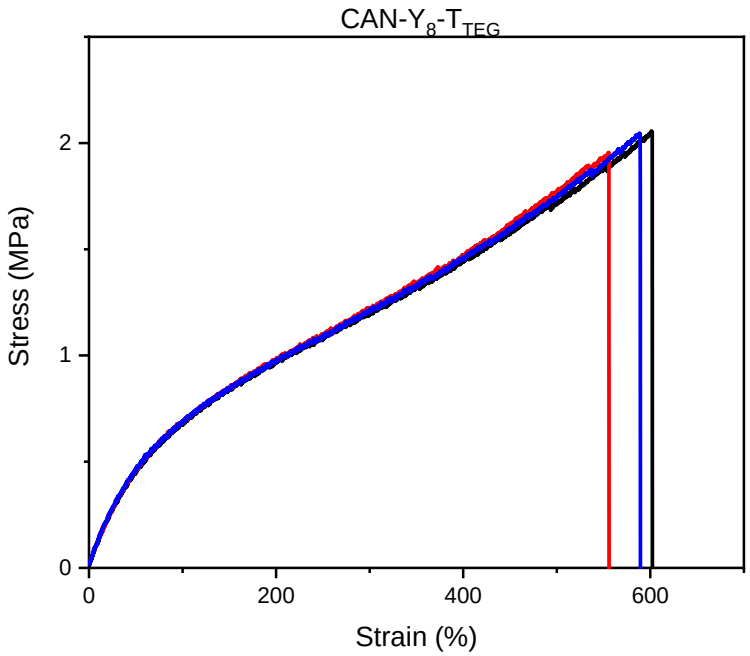

Figure S20. Stress vs strain curve of CAN-Y_8-T_{TEG}.

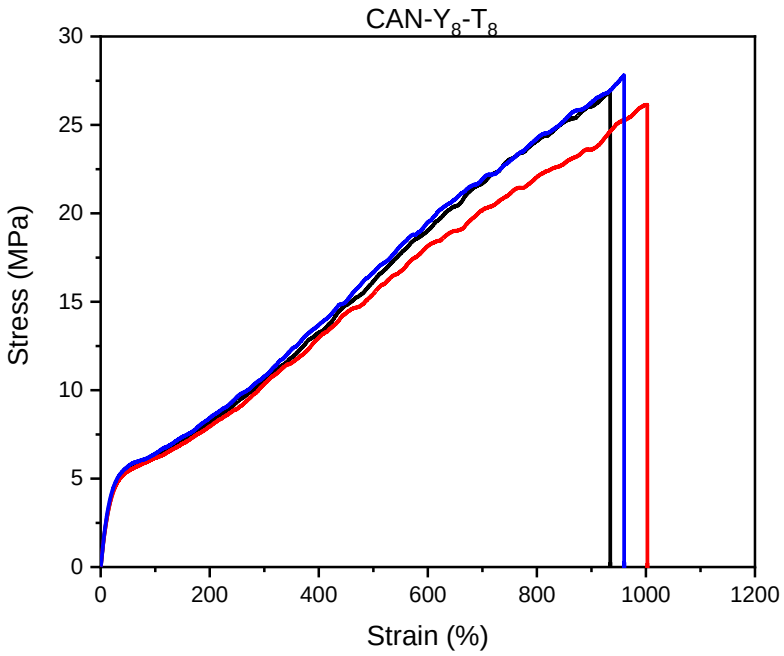

Figure S21. Stress vs strain curve of CAN-Y_8-T_8.

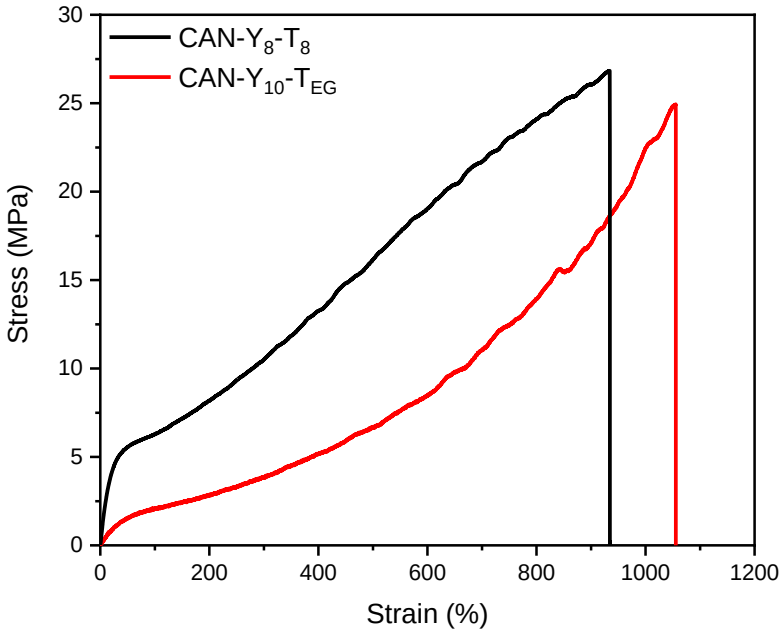

Figure S22. Stress vs strain curve of CAN-Y_8-T_8 and CAN-Y_{10}-T_{EG}.

DSC data

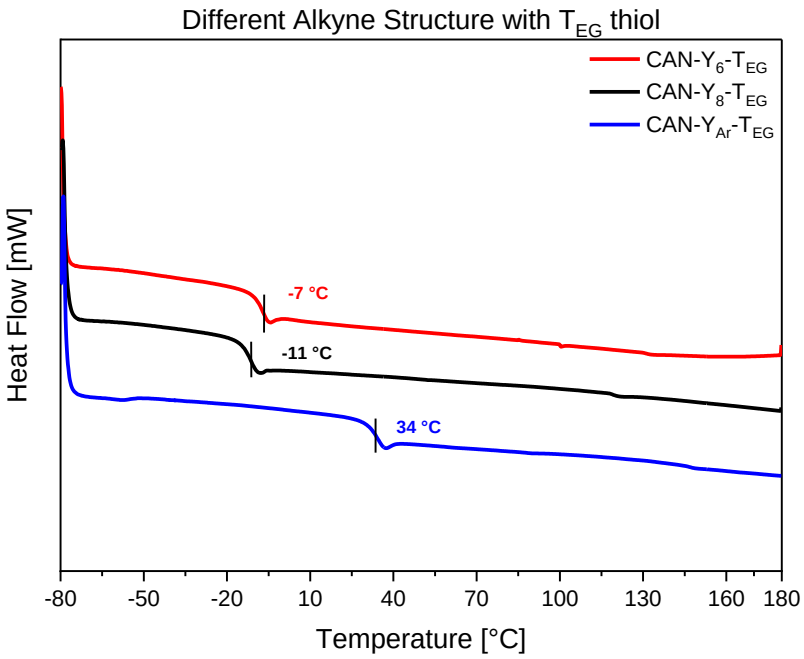

Figure S23. DSC thermograms of different alkyne spacer with T_{EG}.

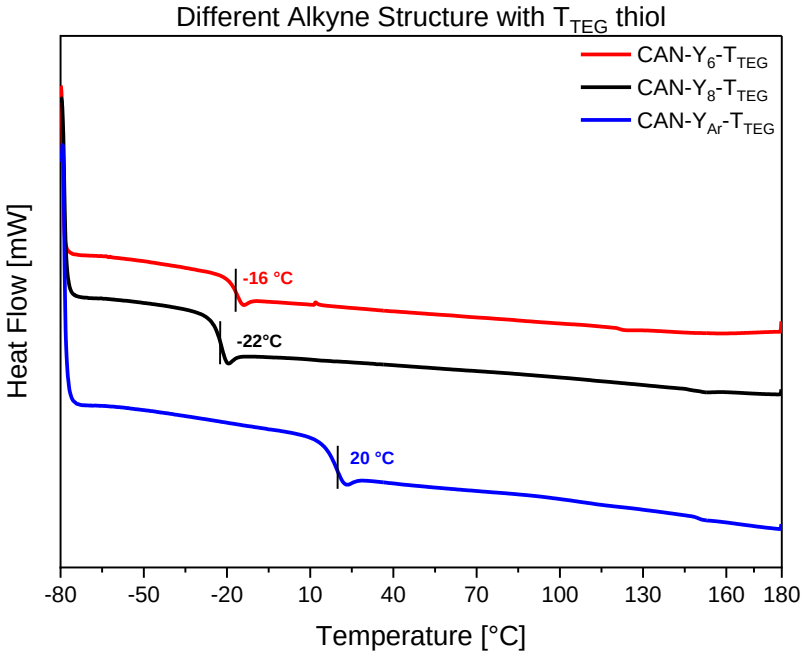

Figure S24. DSC thermograms of different alkyne spacer with T_{TEG}.

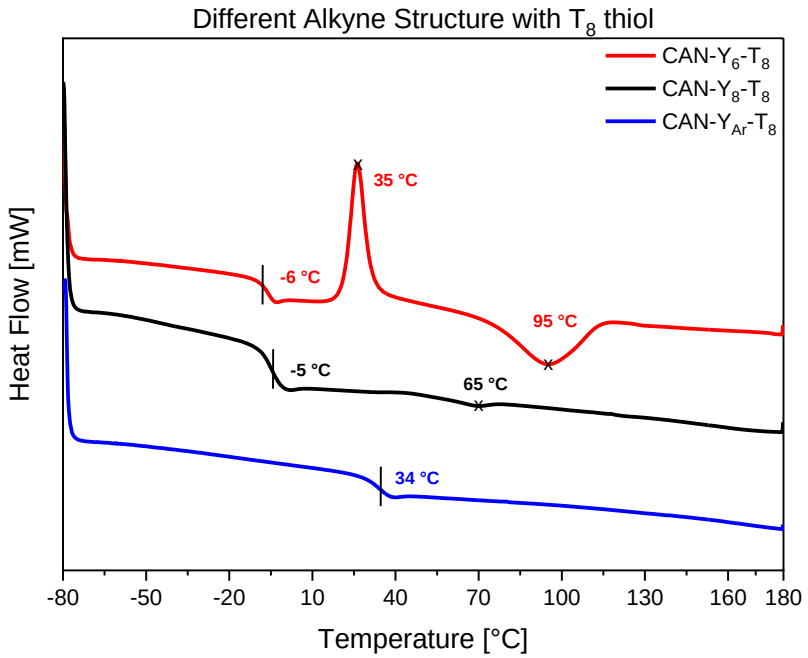

Figure S25. DSC thermograms of different alkyne spacer with T_8.

Rheology

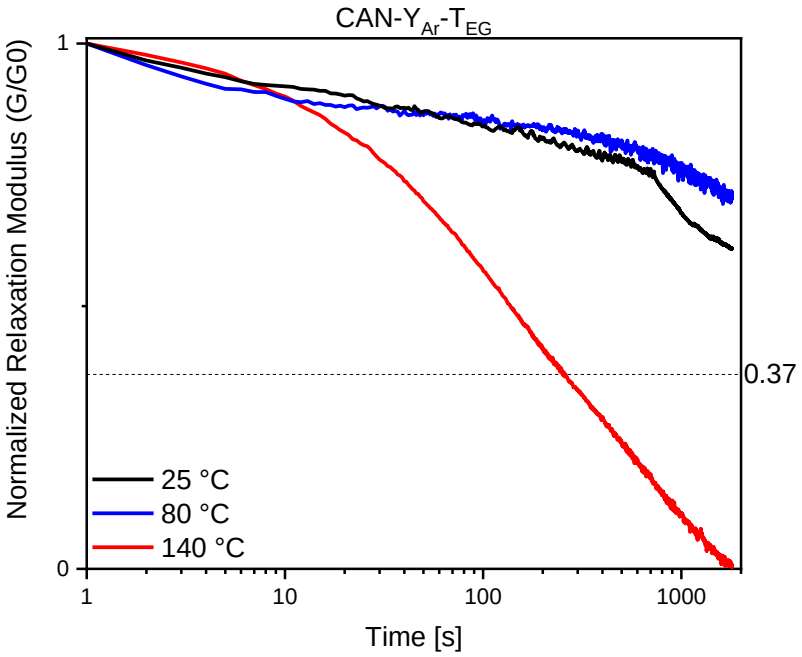

Figure S26. Stress relaxation for CAN-Y_{Ar}-T_{EG} at 140 °C, 80 °C, and 25 °C, respectively.

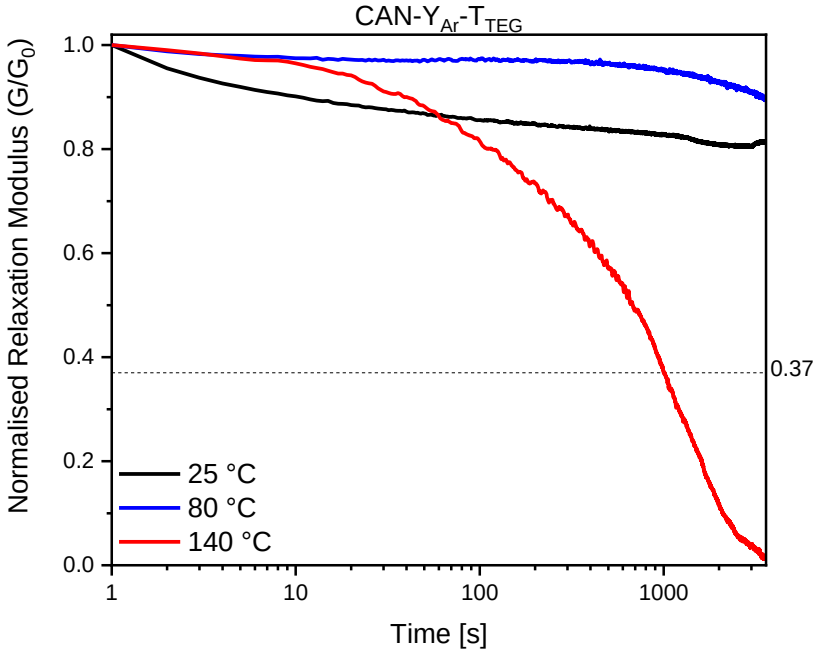

Figure S27. Stress relaxation for CAN-Y_{Ar}-T_{TEG} at 140 °C, 80 °C, and 25 °C, respectively.

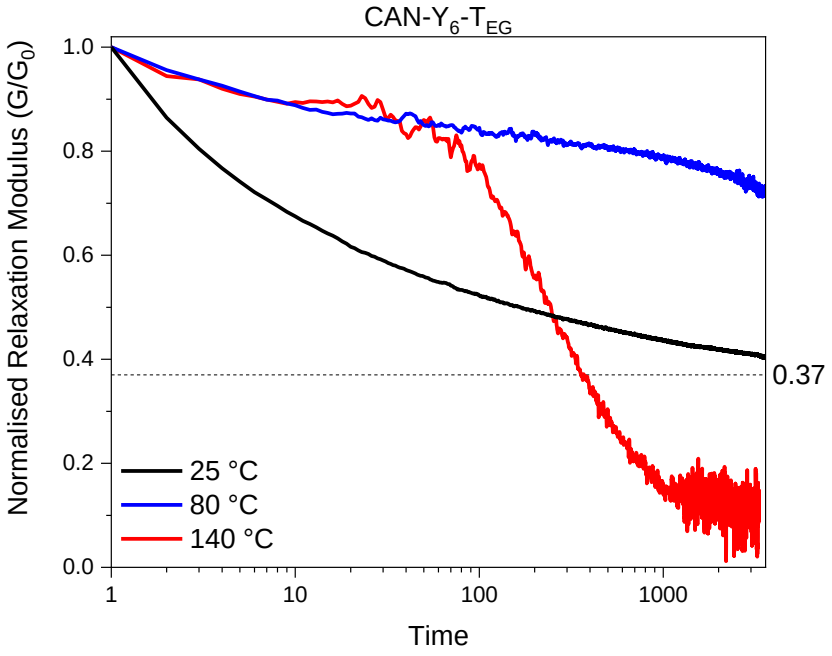

Figure S28. Stress relaxation for CAN-Y_6-T_{EG} in at 140 °C, 80 °C, and 25 °C, respectively.

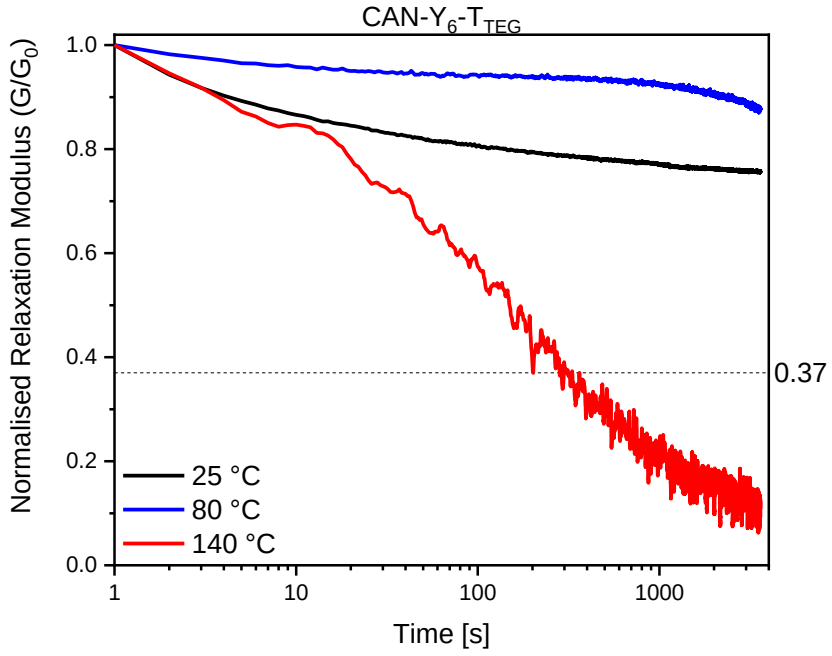

Figure S29. Stress relaxation for CAN-Y_6-T_{TEG} in at 140 °C, 80 °C, and 25 °C, respectively.

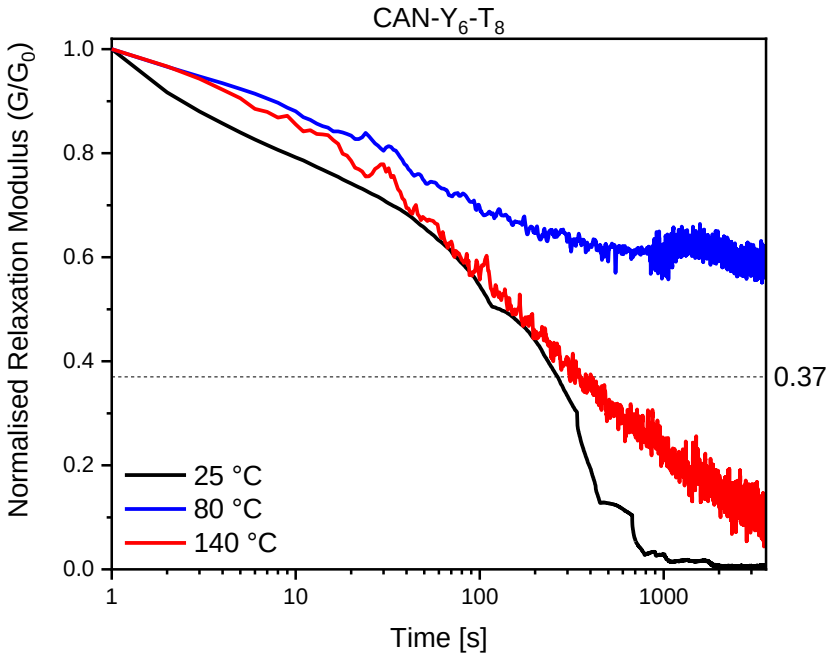

Figure S30. Stress relaxation for CAN-Y_6-T_8 in at 140 °C, 80 °C, and 25 °C, respectively.

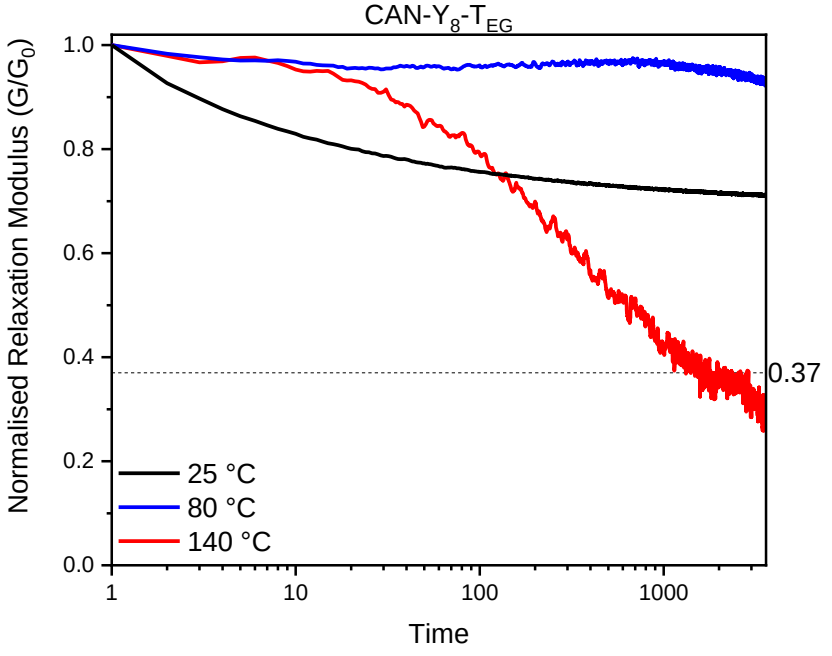

Figure S31. Stress relaxation for CAN-Y_8-T_{EG} in at 140 °C, 80 °C, and 25 °C, respectively.

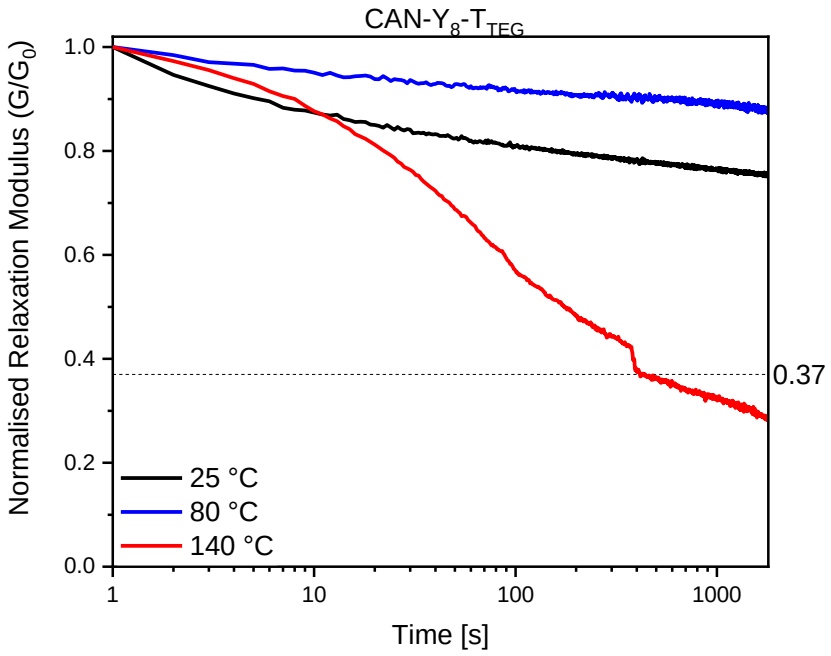

Figure S32. Stress relaxation for CAN-Y_8-T_{TEG} in at 140 °C, 80 °C, and 25 °C, respectively.

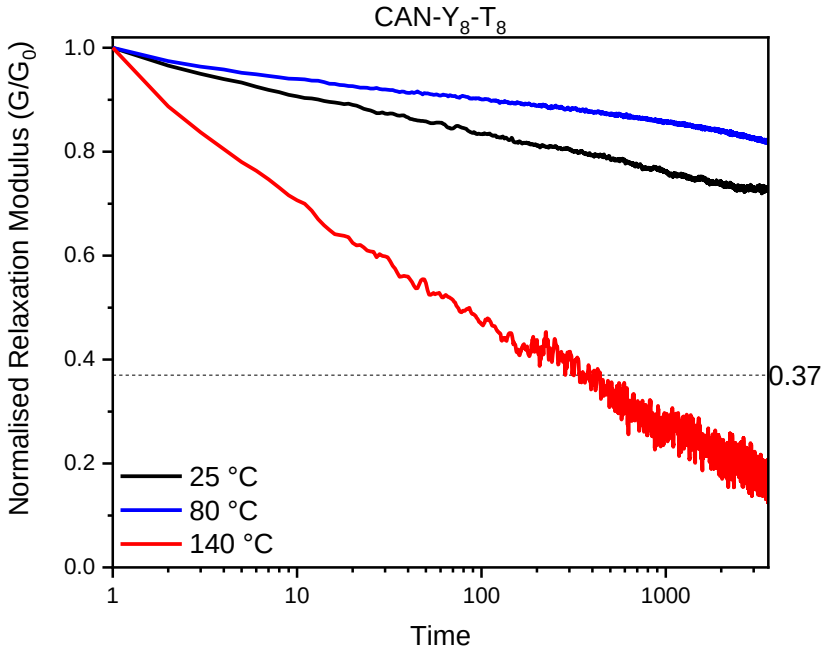

Figure S33. Stress relaxation for CAN-Y_8-T_8 in at 140 °C, 80 °C, and 25 °C, respectively.

FTIR

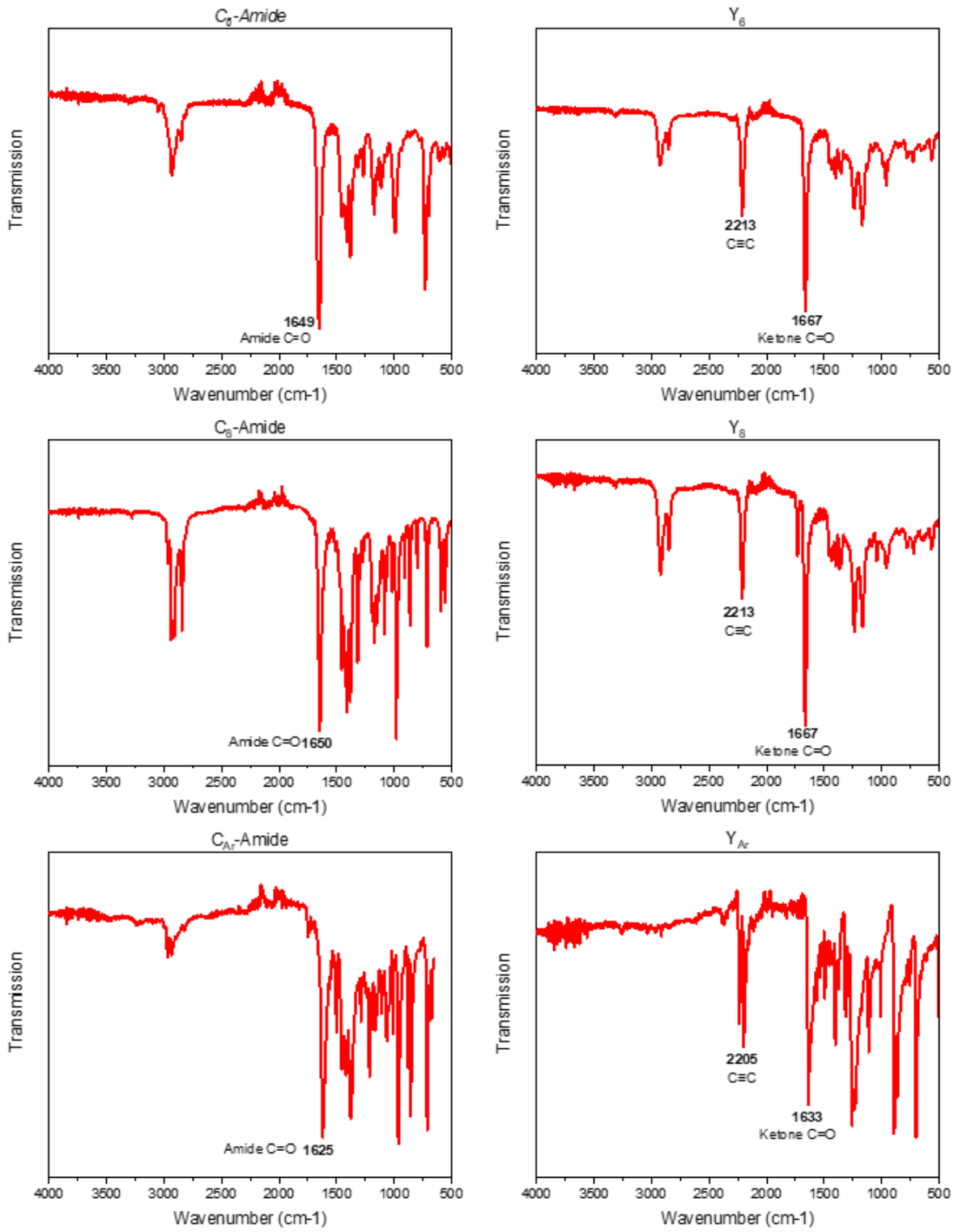

Figure S34. Infared-Spectra of Weinreb amide and ynone monomers.

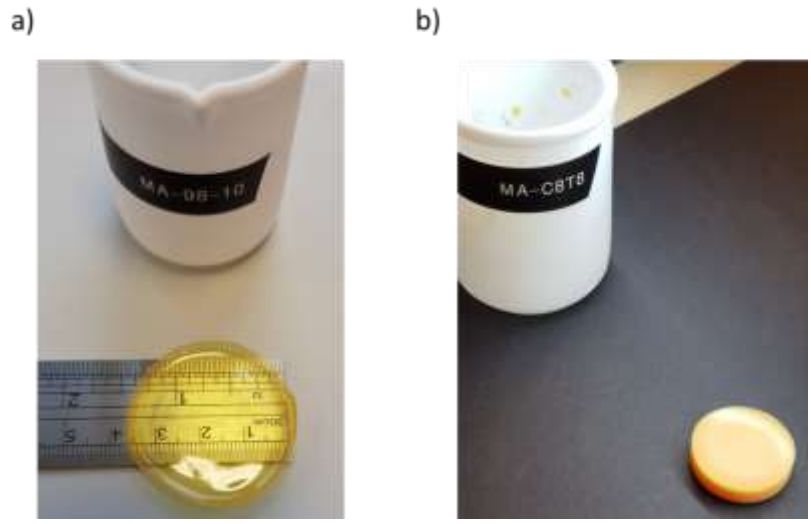

Figure S35. Film casting using Teflon beaker a) 100 mL beaker for large film “ideal for cutting dog-bone samples” b) 50 mL beaker for thicker but smaller film “ideal for cutting disks sample for rheology tests”.

References

1. F. Pilathottathil, D. Vineet Kumar and A. Kaliyamoorthy, *Synth. Commun.*, 2020, **50**, 1622-1632.
2. S. J. Wagh, R. Chowdhury, S. Mukhopadhyay and S. K. Ghosh, *J. Label. Compd. Radiopharm.*, 2013, **56**, 649-654.
3. T. Nishio and Y. Omote, J. Chem. Soc., Perkin Trans. 1, 1981, 934-938.

CHAPTER 4: RENEWABLE AND RECYCLABLE COVALENT ADAPTABLE NETWORKS BASED ON BIO-DERIVED LIPOIC ACID

4.1 Manuscript and overview

Title: Renewable and recyclable covalent adaptable networks based on bio-derived lipoic acid

Authors: **Maher A. Alraddadi**‡[1], Viviane Chiaradia‡[1], Connor J. Stubbs[1], Joshua C. Worch[1*] and Andrew P. Dove[1*]

‡denotes equal contribution

Affiliations: [1] School of Chemistry, The University of Birmingham, Edgbaston, Birmingham, B15 2TT, UK.

Journal: Polymer Chemistry

Year: 2021

Volume: 12

Page numbers: 5796-5802

DOI: 10.1039/d1py00754h

Submitted: 4th of June 2021

Published: 17th of September 2021

Permissions: This article and its supporting information are available, free of charge, at https://doi.org/10.1039/d1py00754h

Co-author contributions: Dr. Connor J. Stubbs (University of Birmingham) performed TGA and FTIR analysis. Dr. Viviane Chiaradia (University of Birmingham) synthesised the networks and performed rheology, DSC, and tensile experiments. Dr. Josh C. Worch (University of Birmingham) and Prof. Andrew P. Dove (University of Birmingham) conceived the material synthesis and designed the project idea. The manuscript was written through contributions of J. C. W and A. P. D.

Overview:

The aim of this chapter is to investigate alternative dynamic bonds from renewable resources. Previous reports in the field of CANs have mainly been focused on constructing CANs from non-sustainable feedstocks. Furthermore, the synthesis of monomers may require multiple steps to functionalise monomers and permit dynamic covalent bonding. The utilisation of sustainable feedstocks that contain functional group capable of dynamic bonding improves both the recyclability and the sustainability of thermosets. In this chapter, the dynamic disulfide bond of the bio-mass derived lipoic acid (LA) was utilised to synthesise CANs with tunable mechanical properties. First, a series of bifunctional monomers were synthesised in facile one-step synthesis from lipoic acid (LA). Next, these monomers were then cross-linked using multivalent thiol to afford disulfide based CANs. Furthermore, CANs with tunable thermal and rheological properties were easily access by altering the cyclic disulfide

monomer to thiol ratio. Similarly, varying the composition of the disulfide monomers afford CANs with large range of properties. Most importantly, a rapid stress relaxation at 100 °C were observed for many of these CANs, which denotes a potential reprocessability. Moreover, an optimised formulation was chemically recycled, or depolymerized, under mild conditions by simple dilution with a solvent containing small amount of catalytic organobase.

Polymer Chemistry

ROYAL SOCIETY OF CHEMISTRY

PAPER

View Article Online
View Journal | View Issue

Cite this: *Polym. Chem.*, 2021, **12**, 5796

Renewable and recyclable covalent adaptable networks based on bio-derived lipoic acid†

Maher A. Alraddadi,‡ Viviane Chiaradia,‡ Connor J. Stubbs, Joshua C. Worch * and Andrew P. Dove *

The modern materials economy is inefficient since most products are principally derived from non-renewable feedstocks and largely single-use in nature. Conventional thermoset materials are often inherently unreprocessable due to their irreversible covalent crosslinks and hence are challenging to recycle and/or reprocess. Covalent adaptable networks (CAN)s, which incorporate reversible or dynamic covalent bonding, have emerged as an efficient means to afford reprocessable crosslinked materials and increasing the feedstock sustainability of CANs is a developing aim. In this study, the biomass-derived lipoic acid, which possesses a dynamic cyclic disulfide moiety, was transformed into a series of bifunctional monomers *via* a one-step esterification or amidation reaction and reacted with a commercially available multivalent thiol in the presence of an organobase catalyst to afford dynamically crosslinked networks. Large differences in material properties, such as storage modulus and glass transition temperature, were observed when the ratio of the lipoic acid-based monomer to thiol (from 1 : 1 to 16 : 1) and the composition of the monomer were changed to modify the network architecture. The thermomechanical properties of an optimised formulation were investigated more thoroughly to reveal a moderately strong rubber (ultimate tensile strength = 1.8 ± 0.4 MPa) possessing a large rubbery plateau (from 0 to 150 °C) which provides an adaptable material with a wide operational temperature range. Finally, the chemical recycling, or depolymerisation, of the optimised network was also demonstrated by simply solvating the material in the presence of an organobase catalyst.

Received 4th June 2021,
Accepted 17th September 2021

DOI: 10.1039/d1py00754h

rsc.li/polymers

Introduction

Developing materials that are more compatible for reprocessing and/or reformulation is central to addressing the global environmental challenges linked to the abundant use of modern plastics and thermosets. Covalent adaptable network (CAN) materials,[1–4] which feature dynamic covalent bonding[5–7] at crosslinking sites, seek to combine the reprocessibility advantage that is inherent to thermoplastics with the mechanical robustness of conventional thermosets. However, the implementation of sustainable feedstocks is also needed in order to transition from petroleum-derived platform chemicals that have dominated the modern materials economy, alongside research in the CAN material space.[8] Progress on this front has relied on the derivatisation of bio-derived chemicals to enable dynamic bonding with the most common examples of bio-derived CAN materials featuring imine[9–16] and epoxy[17–23] chemistries. On the other hand, the use of a renewably sourced monomer that possesses inherent dynamic functionality is a more attractive feature for next-generation CAN materials since synthetic costs could be mitigated and overall sustainability improved.

Thioctic acid, or lipoic acid, is a naturally occurring carboxylic acid that contains a 5-membered cyclic disulfide which can be polymerised into a polydisulfide by ring-opening polymerisation (ROP).[24] The ROP of various strained cyclic disulfides to afford linear polydisulfides is well established and versatile as exemplified by numerous reaction pathways – such as thermal,[25] radical[26,27] or anionic (*via* thiolate).[28–34] An exemplary feature of strained cyclic disulfides is their dynamic nature that results from facile thiol-disulfide exchange[35–38] and has been exploited to reversibly depolymerise (or chemically recycle) some of the aforementioned polydisulfides[27,29–31,33] or to create functional supramolecular cyclic structures.[39]

Very recently, the bifunctionality and dynamicity of lipoic acid has been investigated to synthesise supramolecular crosslinked polymers by first polymerising through the cyclic disulfide (*i.e.* ROP) and then crosslinking the material *via* metal coordination/complexation of the carboxylate moiety.[40–46] Other studies have also modified the carboxylic acid of lipoic

School of Chemistry, University of Birmingham, Edgbaston B15 2TT, UK.
E-mail: j.worch@bham.ac.uk, a.dove@bham.ac.uk

†Electronic supplementary information (ESI) available. See DOI: 10.1039/d1py00754h

‡These authors contributed equally.

acid with dopamine[47] or *N*-hydroxy succinimide[48] to produce self-healing supramolecular adhesives. Additionally, dynamic cyclic disulfides have also featured in degradable nanoparticles[49,50] and adaptable hydrogels,[51–54] although in the gel examples the disulfide features as a reactive polymer pendant group or chain-end and thus the systems are synthetically non-trivial and more complex. To date, the creation of a simple, non-swollen dynamic material where the crosslinking is both driven by the thiol-disulfide exchange and features the disulfides in the polymer backbone has not been reported. However, this approach should offer easy access to mechanically robust and highly tunable dynamic materials.

Herein, we created a series of structurally simple disulfide CANs by employing synthetically accessible dimerised lipoic acid monomers directly in the crosslinking step during material formulation. The synthesis of networks with a range of properties were conveniently accessed by simply mixing a multivalent thiol, a difunctional lipoic acid-based monomer and organobase in solution under ambient conditions before pouring the mixture onto a flat surface or mould to produce a stable crosslinked film after the solvent evaporated. The dynamic networks were all amorphous with glass transition temperatures well below ambient environments, affording rubbery behaviour. Finally, the networks could be efficiently degraded (or chemically recycled) by simple dilution in solvent containing catalytic organobase.

Results and discussion

We initially synthesised a dimerised ester-based monomer (C_6E) *via* an EDC coupling of the carboxylic acid group on lipoic acid that was inspired by a recent report on similar structures for the synthesis of nanoparticles (ESI, Fig. S1 and 2†).[49] The organobase-catalysed reaction of C_6E with a commercial tri-armed thiol (3T) (at cyclic disulfide : thiol 1 : 1) in dichloromethane (DCM) afforded a free-standing crosslinked film (C_6E-3T-1 : 1) after the solvent evaporated (Fig. 1).

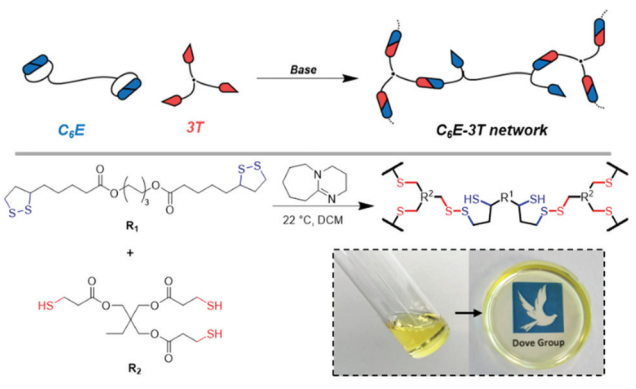

Fig. 1 Schematic illustrating the synthesis of disulfide-based CAN (C_6E-3T) assuming 1 : 1 disulfide to thiol. Inset shows photograph of monomer solution and subsequent crosslinking to afford homogeneous film after solvent evaporation.

This process is analogous to previous observations regarding the anionic ROP of lipoic acid[31] and other disulfides[33] that suggest the equilibrium between monomer and polymer is highly dependent upon reaction concentration. Here, the monomer is favoured under dilute conditions whereas the crosslinked material is favoured under more concentrated conditions, *i.e.* as the solvent evaporates. This process is also easily reversible for this system and networks can be chemically recycled (or depolymerised) by the addition of solvent that contains DBU (ESI, Table S1, Videos S1 and 2†). Moreover, our disulfide network was stable under ambient conditions without any further treatment. Previous studies have noted poor stability for polydisulfides unless the propagating thiolate species is protonated,[33] quenched with an electrophile[31] or the thiyl radical chain-end is reacted with a capping agent[41,46–48] to form a new S–C bond. However, in our system we only employ 1 mol% base (relative to the disulfide) so not all crosslink sites could be expected to be in their ring-opened thiolate form which may explain the observed behaviour here. Fourier transform infrared spectroscopy (FTIR) experiments do not, however, indicate any S–H species in the materials (absence of absorption near 2500 cm^{-1}, ESI, Fig. S9–11†).

Although the gelation times were rapid (under 60 s) when employing NEt_3 or DBU (ranging from 1–5 mol% relative to the thiol) the films produced from NEt_3 were tacky in nature, even after the solvent had fully evaporated, and thus DBU (1 mol% loading) was selected as the optimal catalyst (Fig. 2a). This observation was corroborated by the frequency sweep rheological analysis of two films synthesised using either DBU or NEt_3. Regarding the material obtained from NEt_3, some storage modulus-frequency dependence was apparent, especially at higher rates, which suggests a less solid-like structure (Fig. 2b). Dimethyl carbonate, which is a greener and more polar solvent,[55,56] was also screened but the gelation occurred almost instantly. Nevertheless, a wide range of solvents were found to facilitate the reaction and lowering the amount of base catalyst could allow for better film formation when using polar (and/or greener) solvents. When using chloroform or DCM, the films had similar physical appearance and gelation times so the latter solvent was preferred since it has a lower boiling point.

After optimising the reaction conditions for the synthesis of the 1 : 1 disulfide network, we set out to expand the material library. By altering the relative ratio of disulfide to thiol, it was possible to change the crosslinking density which is an important design consideration in dynamic material synthesis.[57,58] By increasing the stoichiometry of disulfide to thiol, oligomeric units could theoretically form (assuming idealised reactivity where each thiol initiates a disulfide monomer to form a new thiolate species). This could be expected to lead to longer chains between crosslinks and/or increased branching in the network, and thus tune the bulk properties of the materials. Using the optimised reaction conditions (disulfide 1 M in DCM, 1 mol% DBU), all synthesised networks exhibited rapid gelation times (under 60 s) and formed homogenous films. Expanding upon the initial system (C_6E-3T-1 : 1), we produced networks with higher disulfide contents (C_6E-3T-4 : 1,

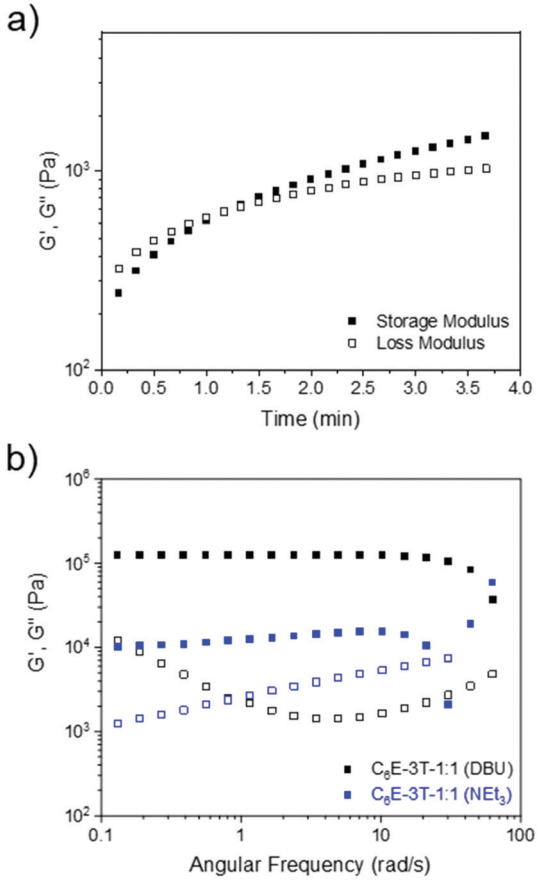

Fig. 2 (a) Rheology time sweep (10% strain, frequency of 1 Hz) at 25 °C to characterise gelation time of C_6E-3T-1 : 1 using 1 mol% DBU. (b) Frequency sweep analysis showing storage and loss modulus *versus* frequency for networks synthesized using DBU or NEt_3 at 25 °C (1% strain from 0.1 to 10 Hz, or 0.06 to 62 rad s^{-1}).

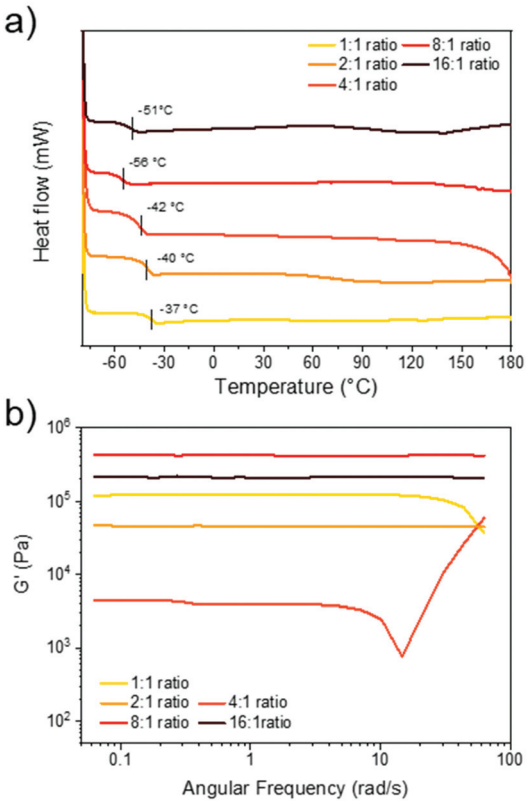

Fig. 3 Thermal and rheological properties of C_6E-3T networks. (a) DSC thermograms of the 2nd heating cycle from −80 to 180 °C, 10 °C min^{-1}. (b) Frequency sweep analysis of films showing storage modulus *versus* frequency at 25 °C (1% strain from 0.1 to 10 Hz, or 0.06 to 62 rad s^{-1}).

C_6E-3T-8 : 1) and compared the thermal properties of these films to C_6E-3T-1 : 1 using differential scanning calorimetry (DSC) (Fig. 3a). All materials were amorphous and in the rubbery regime under ambient conditions as evidenced by their low glass transition temperatures (T_g = −37 °C to −56 °C). The most densely crosslinked material (1 : 1 disulfide to thiol) exhibited the highest T_g. In general, the T_g decreased as the ratio of disulfide to thiol increased but C_6E-3T-16 : 1 had a slightly higher value than C_6E-3T-8 : 1. The DSC data suggests that the overall network topology was significantly modulated by adjusting monomer stoichiometry, although the precise network structure cannot be elucidated. Branching architectures may contribute to lowering the glass transition temperature in addition to overall crosslinking density.

The rheological properties of the various C_6E-3T networks were also investigated. Using a frequency sweep analysis at 25 °C, the 16 : 1, 8 : 1, and 2 : 1 ratios displayed unchanging elastic (solid-like) behaviour (Fig. 3b). However, the 1 : 1 and 4 : 1 ratios exhibited some frequency dependence, suggesting more fluid-like behaviour (Fig. 3b). Strain sweep experiments of the 4 : 1 ratio also suggest poor structural integrity of the film since the storage modulus is highly strain-dependent (ESI, Fig. S16†). The storage modulus of the samples differed by an order of magnitude according to their stoichiometry and the 4 : 1 ratio (C_6E-3T-4 : 1 = 4.4 kPa) was lower than the initial 1 : 1 ratio (C_6E-3T-1 : 1 = 120 kPa), but increased significantly for the 8 : 1 ratio material (C_6E-3T-8 : 1 = 431 kPa). Again, these results suggest that for C_6E-3T-4 : 1 system there is relatively inefficient crosslinking, *i.e.* poor network topology. Interestingly, the modulus for C_6E-3T-2 : 1 (47 kPa) was also lower than C_6E-3T-1 : 1, with a similar trend observed for C_6E-3T-16 : 1 (213 kPa) compared to C_6E-3T-8 : 1 (Fig. 3b). Together these data, along with thermal characteristics, indicate that the material properties can be significantly changed by adjusting relative stoichiometry of the disulfide to thiol. We are still investigating the superior properties that were observed in the 8 : 1 ratio material. There could be a 'Goldilocks zone' for this CAN system when the disulfide to thiol ratio is near 8 : 1, *i.e.* the 1 : 2 and 1 : 4 materials were relatively poor and the 16 : 1 ratio network was slightly less robust in comparison. A possible explanation points toward an advantageous effect from branching, up to a certain extent, likely somewhere between the 8 : 1 and 16 : 1 formulations.

Next, we investigated other dimeric monomers which were also synthesised in one step from lipoic acid using an EDC

coupling strategy. An analogous amide to C_6E was synthesised from 1,6-hexanediamine (C_6A) in addition to derivatives containing more flexible ether units formed from triethylene glycol ($C_{TEG}E$) and 1,8-diamino-3,6-dioxaoctane ($C_{TEG}A$) (Fig. 4a and ESI, Fig. S3–8†). However, we were unable to produce films from C_6A due to its poor solubility. These compositionally distinct networks were also synthesised at various ratios (1 : 1, 4 : 1, 8 : 1) to directly compare with materials from the alkyl monomer (C_6E) series. For the glycol ester-based materials ($C_{TEG}E$-3T), the 1 : 1 ratio network had a similar glass transition temperature to the C_6E-3T analogue, but there was little variation according to monomer stoichiometry (ΔT_g = 6 °C) and $C_{TEG}E$-3T-8 : 1 had the highest T_g of −33 °C within the series (ESI, Fig. S12†). The amide-based materials ($C_{TEG}A$-3T) provided some H-bonding character to the network which likely contributes to higher glass transition temperatures (T_g = −28 °C to 4 °C) compared to the ester variants, with the 1 : 1 ratio material also presenting with the highest value (ESI, Fig. S12†). The H-bonding is supported by a broad absorption near 3290 cm^{-1} with a small shoulder signal (3070 cm^{-1}) in the FTIR spectra for the series (ESI, Fig. S11†). As such, it is difficult to define any general trends in the thermal properties among networks with different compositions. However, all of the CANs displayed high thermal stabilities with decomposition temperatures ($T_{d,5\%}$) ranging from 234–277 °C (ESI, Fig. S13–15†). The disulfide monomer content was also positively correlated to the decomposition temperatures (Table S2†).

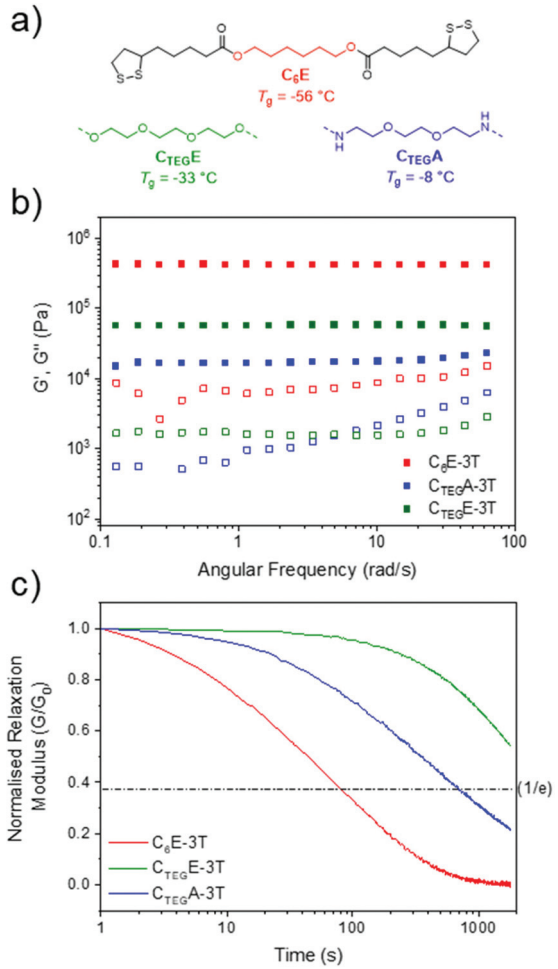

Fig. 4 (a) Structures of monomers to make networks at 8 : 1 ratio. (b) Rheology frequency sweep of networks at 25 °C (1% strain from 0.1 to 10 Hz, or 0.06 to 62 rad s^{-1}). (c) Stress relaxation experiments at 2% strain, 100 °C.

Comparing the three different monomer systems at the same ratio (8 : 1) offers striking differences in their rheological behaviour (Fig. 4). When investigating the analogous glycol monomer ($C_{TEG}E$-3T-8 : 1), the material was considerably less stiff as compared to the initial system (C_6E-3T-8 : 1) as evidenced by a lower storage modulus (56 kPa) (Fig. 4b). However, the amide version ($C_{TEG}A$-3T-8 : 1) possessed the lowest modulus in the series, at only 15 kPa, which is a contrast to what might be expected on account of the presence of H-bonding interactions. It is possible that the H-bonding may be disturbed by the complexity of the material topology. Interestingly, the C_6E and $C_{TEG}A$ networks both exhibited rapid stress relaxation at 100 °C which alludes to their reprocessibility (Fig. 4c). Full stress relaxation is observed for both CANs as a result of base-assisted disulfide bond exchange and/or reversible formation of the cyclic disulfide. Moreover, C_6E-3T-8 : 1 shows a full relaxation time (*i.e.* where the material may theoretically flow for reprocessing) of only 80 s at 100 °C. The full relaxation time is determined to be the time corresponding to (1/*e*) or ~37% of the initial stress value on normalised relaxation modulus (G/G_0) based on the Maxwell model.[59] At the same temperature, the $C_{TEG}A$ network relaxed approximately an order of magnitude slower (full relaxation time ≈ 700 s), which could be due to additional H-bonding interactions from the amide moiety. The higher T_g's observed in the amide networks also supports this observation (ESI, Fig. S12†). However, the $C_{TEG}E$ material had the slowest relaxation kinetics of the series and full relaxation was not observed within the experimental time frame (Fig. 4c). When compared to the amide structure, this result is surprising considering the relatively low T_g and lack of obvious additional H-bonding interactions. It is possible that the rate of the disulfide exchange or formation of the cyclic disulfide, and thus the overall dynamicity of the system, is influenced by the nature of the linking group (*i.e.* alkyl *vs.* ether and/or ester *vs.* amide). Finally, the trend in rheological properties within each respective class of materials also differed according to stoichiometry. For example, in the $C_{TEG}E$ system the 4 : 1 ratio had a higher modulus than the 1 : 1 ratio and the amides ($C_{TEG}A$-3T) generally followed the same trend, although both were disimilar to the C_6E networks (ESI, Fig. S20–24†).

After screening various disulfide CANs, we selected C_6E-3T-8 : 1 for further investigation based on its optimal thermal (lowest T_g) and rheological (highest storage modulus and excellent relaxation behaviour) properties. The mechanical properties were initially investigated using uniaxial tensile testing (Fig. 5a). The synthesised material can best be

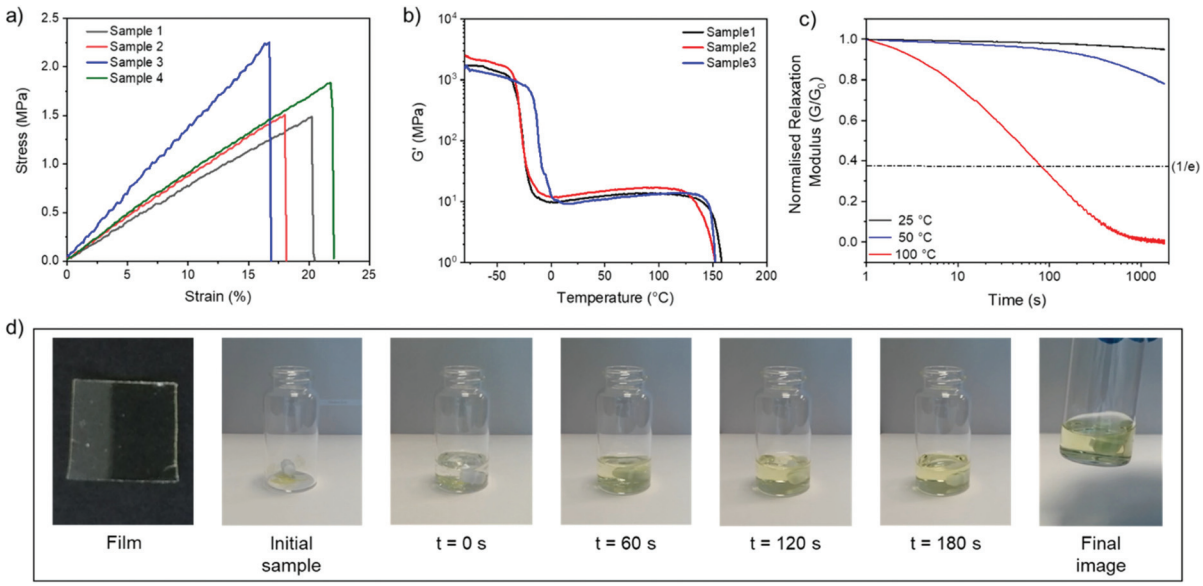

Fig. 5 Thermomechanical and physical data for C6E-3T-8 : 1. (a) Uniaxial tensile testing at 22 °C, 10 mm min^{-1} strain rate. (b) DMA temperature sweep from −80 to 180 °C, 5 °C min^{-1}. (C) Stress relaxation experiments at 2% strain (25 °C, 50 °C, and 100 °C). (d) Chemical recycling of as-synthesised film cut into small pieces (200 mg film in 5 mL DCM solution, 0.01 M DBU).

described as a rubber (Young's modulus = 9.1 ± 1.9 MPa) with moderate ultimate tensile strength (UTS = 1.8 ± 0.4 MPa) and a modest elongation at break (19 ± 2%) (Table S3†). The material properties *versus* temperature were then studied using dynamic mechanical analysis (DMA), revealing a large rubbery plateau before bulk flow of the material was observed near 150 °C (Fig. 5b and ESI, Fig. S28†). Additional stress relaxation experiments conducted at various temperatures revealed that the material was relatively stable at low to moderate temperatures (25 °C or 50 °C), but exhibited a sharp decrease in viscosity at 100 °C (Fig. 5c, see ESI† for other networks at various temperatures).

The dynamic behaviour was further probed by thermally reprocessing the material at 180 °C. Even though the material flowed to form a new homogeneous film after cooling, it was tacky in nature (ESI, Fig. S27†) indicating that the network did not completely reform. At elevated temperatures, each linear disulfide unit at a crosslink point can likely react by either direct exchange or reversion to the cyclic disulfide (Fig. 6). Then, reformation of an idealised linear disulfide network could be realised *via* a nucleophilic ring-opening route due to the presence of residual DBU within the system. However, it is possible that the DBU was thermally degraded at 180 °C and thus the bulk material had inadequate catalyst to facilitate the subsequent reformation of the crosslinked structure. A photomediated radical exchange mechanism is unlikely since a high intensity UV-light source (≥60 mW cm^{-2}) was required to enable dynamic exchange in another lipoic acid-based polymer.[27] Furthermore, our materials were observed to be stable under ambient light over a period of at least several weeks. Nevertheless, efficient chemical recycling of the network was demonstrated by adding a solution of DCM containing DBU to the film, thus showcasing its adaptive nature (Fig. 5d, ESI, Table S1, Videos S1 and 2†). The network briefly swelled in the solvent, but was fully dissolved within 3 min after adding 0.01 M DBU solution.

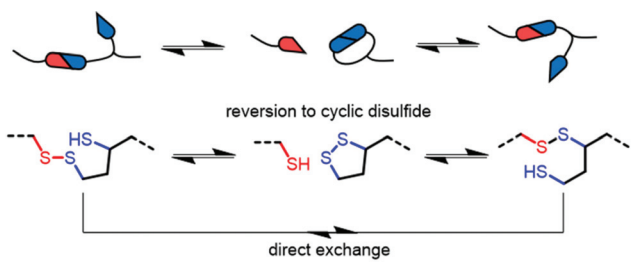

Fig. 6 Possible base-catalysed disulfide reaction pathways in networks.

Conclusions

A library of dynamic networks based on disulfide chemistry were prepared from synthetically accessible bifunctional lipoic acid-derived monomers. By varying network composition *via* monomer exchange and crosslinking ratios, we were able to obtain materials with divergent thermal and rheological properties. However, when adjusting the stoichiometry to alter the crosslinking density, the trends in material performance differed significantly depending on the starting monomer which precluded any universal structure–property relationships for this study. Future experiments are underway to more thoroughly investigate the network topologies which appear to be complex (*i.e.* non-idealised) and could be obfuscated by

branching regions. Nevertheless, all synthesised materials can be characterised as soft and rubbery with good structural integrity at ambient temperatures. C_6E_8-3T was found to exhibit optimal material properties and more in-depth thermo-mechanical analysis using DMA and tensile testing revealed a moderately strong rubber with a rubbery plateau extending out to around 150 °C. Although thermal reprocessing of the film revealed a tacky material, this is likely a result of inefficient reformation of the network due to thermal degradation of the amine base. Future experiments are underway to enhance the thermal reprocessability of these dynamic networks. Finally, base-promoted chemical recycling of C_6E-3T samples was also demonstrated which highlights the versatility of the disulfide CANs as renewable dynamic materials.

Author contributions

J. C. W. and A. P. D. conceived the material synthesis and designed the project idea. J. C. W. synthesised monomers. C. J. S. performed TGA and FTIR analysis. M. A. and V. C. synthesised the networks and performed rheology, DSC, and tensile experiments. M. A. and V. C. contributed equally. The paper was written through contributions of J. C. W. and A. P. D. All authors have given approval to the final version of the paper.

Conflicts of interest

There are no conflicts to declare.

Acknowledgements

A. P. D., J. C. W. and C. J. S. acknowledge funding from the European Research Council (ERC) under the European Union's Horizon 2020 research and innovation programme under grant agreement no. 681559. V. C. acknowledges funding from Unilever. M. A. thanks The Royal Commission for Jubail and Yanbu (RCJY) for support funding.

Notes and references

1 M. Guerre, C. Taplan, J. M. Winne and F. E. Du Prez, *Chem. Sci.*, 2020, **11**, 4855–4870.
2 M. K. McBride, B. T. Worrell, T. Brown, L. M. Cox, N. Sowan, C. Wang, M. Podgorski, A. M. Martinez and C. N. Bowman, *Annu. Rev. Chem. Biomol. Eng.*, 2019, **10**, 175–198.
3 G. M. Scheutz, J. J. Lessard, M. B. Sims and B. S. Sumerlin, *J. Am. Chem. Soc.*, 2019, **141**, 16181–16196.
4 C. J. Kloxin, T. F. Scott, B. J. Adzima and C. N. Bowman, *Macromolecules*, 2010, **43**, 2643–2653.
5 P. Chakma and D. Konkolewicz, *Angew. Chem., Int. Ed.*, 2019, **58**, 9682–9695.
6 A. Wilson, G. Gasparini and S. Matile, *Chem. Soc. Rev.*, 2014, **43**, 1948–1962.
7 S. J. Rowan, S. J. Cantrill, G. R. L. Cousins, J. K. M. Sanders and J. F. Stoddart, *Angew. Chem., Int. Ed.*, 2002, **41**, 898–952.
8 Y. Jin, Z. Lei, P. Taynton, S. Huang and W. Zhang, *Matter*, 2019, **1**, 1456–1493.
9 W. Xie, S. Huang, S. Liu and J. Zhao, *Chem. Eng. J.*, 2021, **404**, 126598.
10 K. Liang, G. Zhang, J. Zhao, L. Shi, J. Cheng and J. Zhang, *ACS Sustainable Chem. Eng.*, 2021, **9**, 5673–5683.
11 J. C. Markwart, A. Battig, T. Urbaniak, K. Haag, K. Koschek, B. Schartel and F. R. Wurm, *Polym. Chem.*, 2020, **11**, 4933–4941.
12 F. Chen, F. Gao, J. Zhong, L. Shen and Y. Lin, *Mater. Chem. Front.*, 2020, **4**, 2723–2730.
13 F. Song, Z. Li, P. Jia, M. Zhang, C. Bo, G. Feng, L. Hu and Y. Zhou, *J. Mater. Chem. A*, 2019, **7**, 13400–13410.
14 K. Huang, S. Ma, S. Wang, Q. Li, Z. Wu, J. Liu, R. Liu and J. Zhu, *Green Chem.*, 2019, **21**, 4964–4970.
15 S. Dhers, G. Vantomme and L. Avérous, *Green Chem.*, 2019, **21**, 1596–1601.
16 S. Wang, S. Ma, Q. Li, W. Yuan, B. Wang and J. Zhu, *Macromolecules*, 2018, **51**, 8001–8012.
17 Y. Liu, B. Wang, S. Ma, X. Xu, J. Qiu, Q. Li, S. Wang, N. Lu, J. Ye and J. Zhu, *Eur. Polym. J.*, 2021, **144**, 110236.
18 J. Wu, X. Yu, H. Zhang, J. Guo, J. Hu and M.-H. Li, *ACS Sustainable Chem. Eng.*, 2020, **8**, 6479–6487.
19 R. Mo, L. Song, J. Hu, X. Sheng and X. Zhang, *Polym. Chem.*, 2020, **11**, 974–981.
20 H. Memon, H. Liu, M. A. Rashid, L. Chen, Q. Jiang, L. Zhang, Y. Wei, W. Liu and Y. Qiu, *Macromolecules*, 2020, **53**, 621–630.
21 X.-L. Zhao, Y.-Y. Liu, Y. Weng, Y.-D. Li and J.-B. Zeng, *ACS Sustainable Chem. Eng.*, 2020, **8**, 15020–15029.
22 J. Liu, J. Dai, S. Wang, Y. Peng, L. Cao and X. Liu, *Composites, Part B*, 2020, **190**, 107926.
23 S. Wang, S. Ma, Q. Li, X. Xu, B. Wang, W. Yuan, S. Zhou, S. You and J. Zhu, *Green Chem.*, 2019, **21**, 1484–1497.
24 R. C. Thomas and L. J. Reed, *J. Am. Chem. Soc.*, 1956, **78**, 6148–6149.
25 K. Endo and T. Yamanaka, *Macromolecules*, 2006, **39**, 4038–4043.
26 M. Raeisi and N. V. Tsarevsky, *J. Polym. Sci.*, 2021, **59**, 675–684.
27 C. Choi, J. L. Self, Y. Okayama, A. E. Levi, M. Gerst, J. C. Speros, C. J. Hawker, J. Read de Alaniz and C. M. Bates, *J. Am. Chem. Soc.*, 2021, **143**, 9866–9871.
28 J. Kollár, A. Popelka, J. Tkac, M. Žabka, J. Mosnáček and P. Kasak, *J. Colloid Interface Sci.*, 2021, **588**, 196–208.
29 J. Lu, H. Wang, Z. Tian, Y. Hou and H. Lu, *J. Am. Chem. Soc.*, 2020, **142**, 1217–1221.
30 S. Pal, A. Sommerfeldt, M. B. Davidsen, M. Hinge, S. U. Pedersen and K. Daasbjerg, *Macromolecules*, 2020, **53**, 4685–4691.
31 Y. Liu, Y. Jia, Q. Wu and J. S. Moore, *J. Am. Chem. Soc.*, 2019, **141**, 17075–17080.

32 G. S. Pulcu, N. S. Galenkamp, Y. Qing, G. Gasparini, E. Mikhailova, S. Matile and H. Bayley, *J. Am. Chem. Soc.*, 2019, **141**, 12444–12447.
33 F. N. Behrendt and H. Schlaad, *Macromol. Rapid Commun.*, 2018, **39**, 1700735.
34 E.-K. Bang, G. Gasparini, G. Molinard, A. Roux, N. Sakai and S. Matile, *J. Am. Chem. Soc.*, 2013, **135**, 2088–2091.
35 G. M. Scheutz, J. L. Rowell, F.-S. Wang, K. A. Abboud, C.-H. Peng and B. S. Sumerlin, *Org. Biomol. Chem.*, 2020, **18**, 6509–6513.
36 R. Singh and G. M. Whitesides, *J. Am. Chem. Soc.*, 1990, **112**, 6304–6309.
37 J. Houk and G. M. Whitesides, *J. Am. Chem. Soc.*, 1987, **109**, 6825–6836.
38 A. J. Parker and N. Kharasch, *Chem. Rev.*, 1959, **59**, 583–628.
39 S. P. Black, J. K. M. Sanders and A. R. Stefankiewicz, *Chem. Soc. Rev.*, 2014, **43**, 1861–1872.
40 Q. Zhang, Y. Deng, C.-Y. Shi, B. L. Feringa, H. Tian and D.-H. Qu, *Matter*, 2021, **4**, 1352–1364.
41 Y. Liu, J. Yuan, K. Zhang, K. Guo, L. Yuan, Y. Wu and C. Gao, *Prog. Org. Coat.*, 2020, **144**, 105661.
42 Y. Deng, Q. Zhang, B. L. Feringa, H. Tian and D.-H. Qu, *Angew. Chem.*, 2020, **59**, 5278–5283.
43 A. Khan, R. R. Kisannagar, C. Gouda, D. Gupta and H.-C. Lin, *J. Mater. Chem. A*, 2020, **8**, 19954–19964.
44 Q. Zhang, Y.-X. Deng, H.-X. Luo, C.-Y. Shi, G. M. Geise, B. L. Feringa, H. Tian and D.-H. Qu, *J. Am. Chem. Soc.*, 2019, **141**, 12804–12814.
45 C. Dang, M. Wang, J. Yu, Y. Chen, S. Zhou, X. Feng, D. Liu and H. Qi, *Adv. Funct. Mater.*, 2019, **29**, 1902467.
46 Q. Zhang, C.-Y. Shi, D.-H. Qu, Y.-T. Long, B. L. Feringa and H. Tian, *Sci. Adv.*, 2018, **4**, eaat8192.
47 J. Chen, D. Guo, S. Liang and Z. Liu, *Polym. Chem.*, 2020, **11**, 6670–6680.
48 J. Chen, T. Yuan and Z. Liu, *Biomater. Sci.*, 2020, **8**, 6235–6245.
49 J. W. Trzciński, L. Morillas-Becerril, S. Scarpa, M. Tannorella, F. Muraca, F. Rastrelli, C. Castellani, M. Fedrigo, A. Angelini, R. Tavano, E. Papini and F. Mancin, *Biomacromolecules*, 2021, **22**, 467–480.
50 Y. Liu, M. J. van Steenbergen, Z. Zhong, S. Oliveira, W. E. Hennink and C. F. van Nostrum, *Macromolecules*, 2020, **53**, 7009–7024.
51 X. Zhang and R. M. Waymouth, *J. Am. Chem. Soc.*, 2017, **139**, 3822–3833.
52 G. A. Barcan, X. Zhang and R. M. Waymouth, *J. Am. Chem. Soc.*, 2015, **137**, 5650–5653.
53 G. M. Scheutz, J. L. Rowell, S. T. Ellison, J. B. Garrison, T. E. Angelini and B. S. Sumerlin, *Macromolecules*, 2020, **53**, 4038–4046.
54 L. Song, B. Zhang, G. Gao, C. Xiao and G. Li, *Eur. Polym. J.*, 2019, **115**, 346–355.
55 P. Tundo and M. Selva, *Acc. Chem. Res.*, 2002, **35**, 706–716.
56 S.-H. Pyo, J. H. Park, T.-S. Chang and R. Hatti-Kaul, *Curr. Opin. Green Sustainable Chem.*, 2017, **5**, 61–66.
57 N. De Alwis Watuthanthrige, P. Chakma and D. Konkolewicz, *Trends Chem.*, 2021, **3**, 231–247.
58 S. J. Garcia, *Eur. Polym. J.*, 2014, **53**, 118–125.
59 B. M. El-Zaatari, J. S. A. Ishibashi and J. A. Kalow, *Polym. Chem.*, 2020, **11**, 5339–5345.

4.2 Supporting Information

Electronic Supplementary Material (ESI) for Polymer Chemistry.

Renewable covalent adaptable networks based on bio-derived lipoic acid

Maher A. Alraddadi†[a], Viviane Chiaradia†[a], Connor J. Stubbs[a], Joshua C. Worch*[a] and Andrew P. Dove*[a]

[a] *School of Chemistry, University of Birmingham, Edgbaston B15 2TT, United Kingdom*

Corresponding Authors: adove@bham.ac.uk; jworch@bham.ac.uk

Table of Contents

General Materials and Methods. All compounds, unless otherwise indicated, were purchased from commercial sources and used as received. All solvents and chemicals used for recrystallisation were used as received. All films were prepared under ambient conditions and left overnight *ca.* 16 h in order to remove residual solvent before testing.

NMR Spectroscopic Analysis. All NMR spectroscopy experiments were performed at 298 K on a Bruker DPX-400 NMR instrument equipped operating at 400 MHz for ^{1}H (100.57 MHz for ^{13}C). ^{1}H NMR spectra are referenced to residual protio solvent (δ = 7.26 for $CDCl_3$) and ^{13}C NMR spectra are referenced to the

solvent signal (δ = 77.16 for $CDCl_3$). The resonance multiplicities are described as s (singlet), d (doublet), t (triplet), q (quartet) or m (multiplet).

Mass Spectrometry. High Resolution Electrospray Ionization Mass Spectrometry was performed in the School of Chemistry at University of Birmingham on a Waters Xevo G2-XS QTof Quadrupole Time-of-Flight mass spectrometer.

Differential Scanning Calorimetry (DSC). The thermal characteristics of the polymers were determined using differential scanning calorimetry (STARe system DSC3, Mettler Toledo) from −80 to 180 °C at a heating rate of 10 °C min^{-1} for two heating/cooling cycles unless otherwise specified. The glass transition temperature (T_g) was determined from the inflection point in the second heating cycle of DSC.

Thermogravimetric Analysis (TGA). TGA thermograms were obtained using a TGA/DSC 1 - Thermogravimetric Analyzer (Mettler Toledo). Thermograms were recorded under an N_2 atmosphere at a heating rate of 10 °C min^{-1}, from 10 − 600 °C, with an average sample weight of *ca*. 10 mg. Aluminium pans were used for all samples. Decomposition temperatures were reported as the 5% weight loss temperature ($T_{d\,5\%}$).

Fourier-transform infrared (FTIR) spectroscopy. FTIR spectra were collected out using an Agilent Technologies Cary 630 FTIR spectrometer. 16 Scans from 600 to 4000 cm^{-1} were taken at a resolution of 4 cm^{-1}, and the spectra were corrected for background transmittance.

Rheology. Rheological measurements were performed on an Anton Paar MCR 302 using Anton Paar PP8 parallel-plate, a diameter of 8 mm. Temperature was controlled with a P-PTD 200/AIR Peltier and a P-PTD 200 hood. Gelation time was monitored at 10% strain, frequency of 1 Hz and 0 N of normal force. Frequency sweeps were performed at 1% strain from 0.01 to 10 Hz (0.06 to 62 rad/s). Amplitude sweeps were performed at 1 Hz from 0.01 to 500%. Stress relaxation tests were performed at 2% strain at 25 °C, 50 °C, and 100 °C. Sample thickness was approximately 1 mm.

Dynamic Mechanical Analysis (DMA). Dynamic mechanical thermal analysis (DMTA) data were obtained using a Mettler Toledo DMA 1 star system and analyzed using the software package STARe V13.00a (build 6917). Thermal sweeps were conducted using films (L x W x thickness = 15.08 mm x 6.16 mm x 0.30 mm) cooled to −80°C and held isothermally for *ca*. 5 minutes. Storage and loss moduli, as well as the loss factor (ratio of *E"* and *E'*, tan δ) were probed as the temperature was swept from −80 to 180 °C, 5 °C min^{-1}, 1 Hz. Thermomechanical behavior was determined from three samples in this way.

Uniaxial Tensile Testing. Dumbbell-shaped samples were cut directly from the synthesized films using a custom ASTM Die D-638 Type V. Tensile tests at different stretching speed were carried out using a Testometric M350-5CT universal mechanical testing instrument fitted with a load cell of 5 kN at room temperature (22 ± 1 °C). The gauge length was set as 7.1 mm and the crosshead speed was set 10 mm min^{-1}. The dimensions of the neck of the specimens were 7.1 mm in length, 1.6 mm in width and 0.2 mm in thickness. The reported results are average values from at least three individual measurements (n ≥ 3).

Chemical recycling studies. The network film was manually cut into small pieces, placed into 20 mL scintillation vial equipped with a stirrer bar and then diluted with DCM containing DBU. For reactions using 0.01 M DBU solution, 200 mg of sample was diluted with 5 mL of solution. For reactions using 0.05 M DBU solution, 150 mg of sample was diluted with 3.75 mL of solution. The reaction mixture was then stirred at ambient temperature (22 ± 1 °C) and the degradation of the network was monitored using video recording until the solution was homogeneous.

Experimental Procedures

C_6E Synthesis

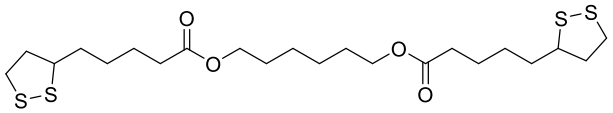

Lipoic acid (10 g, 2 equiv., 48.4 mmol), 1,6-hexanediol (2.86 g, 1 equiv., 24.2 mmol), DMAP (5.91 g, 1 equiv., 48.4 mmol) were placed in an oven-dried 250 mL 2-neck round-bottom flask and back-filled with N_2. DCM (100 mL) was added to the flask and the mixture was stirred until all reagents were dissolved (*ca.* 10 min). Note: the DCM did not have to be rigorously dried and reagent grade solvent was adequate for the reaction. The reaction mixture was then cooled to 0 °C in an ice-water bath and EDC·HCl (9.28 g, 1 equiv., 48.4 mmol) was added portion-wise over 5 min. After the addition was complete, the reaction was stirred for 15 min at 0 °C, then removed from the ice-bath. The flask was wrapped in aluminum foil to protect from ambient light and stirred overnight at ambient temperature (*ca.* 16 h at 22 °C). The reaction mixture was transferred to a 250 mL round-bottom flask and concentrated *in vacuo*. The crude mixture was purified directly using silica gel column chromatography, eluting with $CHCl_3$/MeOH 40/1 (R_f ≈ 0.7 $CHCl_3$/MeOH, 40/1) to afford a yellow oil after concentration *in vacuo* (yield = 9.72 g, 81%). ^{1}H NMR (400 MHz, Chloroform-*d*) δ 4.04 (t, J = 6.7 Hz, 4H), 3.55 (m, 2H), 3.27 – 2.98 (m, 4H), 2.56 – 2.35 (m, 2H), 2.29 (t, J = 7.4, 2H), 1.89 (m, 2H), 1.79 – 1.53 (m, 6H), 1.55 – 1.13 (m, 4H). ^{13}C NMR (101 MHz, Chloroform-*d*) δ 173.61, 77.48, 77.16, 76.84, 64.34, 56.42, 40.30, 38.57, 34.68, 34.17, 28.84, 28.61, 25.69, 24.78. HRMS (ESI-TOF) (*m/z*): [M + H] calculated for $C_{22}H_{38}O_4S_4$ H 495.1731; found 495.1729. Note: sometimes undesirable crosslinking was observed upon concentration of the purified product, but this can be significantly mitigated by adding butylated hydroxytoluene (BHT) (~ 50 mg) to the solution before concentrating.

$C_{TEG}E$ Synthesis

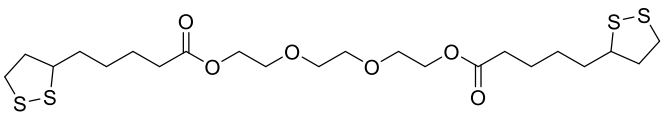

Lipoic acid (10 g, 2 equiv., 48.4 mmol), triethylene glycol (3.62 g, 1 equiv., 24.2 mmol), DMAP (5.91 g, 1 equiv., 48.4 mmol) were placed in an oven-dried 250 mL 2-neck round-bottom flask and back-filled with N_2. DCM (100 mL) was added to the flask and the mixture was stirred until all reagents were dissolved (*ca.* 10 mins). Note: the DCM did not have to be rigorously dried and reagent grade solvent was adequate for the reaction. The

reaction mixture was then cooled to 0 °C in an ice-water bath and EDC·HCl (9.28 g, 1 equiv., 48.4 mmol) was added portion-wise over 5 min. After the addition was complete, the reaction was stirred for 15 min at 0 °C, then removed from the ice-bath. The flask was wrapped in aluminum foil to protect from ambient light and stirred overnight at ambient temperature (*ca.* 16 h at 22 °C). The reaction mixture was transferred to a 250 mL round-bottom flask and concentrated *in vacuo*. The crude mixture was purified directly using silica gel column chromatography, eluting with $CHCl_3$/MeOH 20/1 ($R_f \approx 0.6$ $CHCl_3$/MeOH, 20/1) to afford a yellow oil after concentration *in vacuo* (yield = 13.05 g, quantitative). ^{1}H NMR (400 MHz, Chloroform-*d*) *δ* 4.26 – 4.14 (m, 4H), 3.70 – 3.65 (m, 4H), 3.63 (s, 4H), 3.54 (m, 2H), 3.23 – 3.02 (m, 4H), 2.43 (m, 2H), 2.32 (t, J = 7.4 Hz, 4H), 1.88 (m, 2H), 1.75 – 1.56 (m, 8H), 1.54 – 1.34 (m, 4H). ^{13}C NMR (101 MHz, Chloroform-*d*) *δ* 173.46, 77.48, 77.36, 77.16, 76.84, 70.59, 69.26, 63.45, 56.39, 40.27, 38.54, 34.64, 33.98, 28.77, 24.66. HRMS (ESI-TOF) (*m/z*): [M + H] calculated for $C_{22}H_{38}O_6S_4$ H 527.1630; found 527.1641. Note: sometimes undesirable crosslinking was observed upon concentration of the purified product, but this can be significantly mitigated by adding butylated hydroxytoluene (BHT) (~ 50 mg) to the solution before concentrating.

C_6A Synthesis

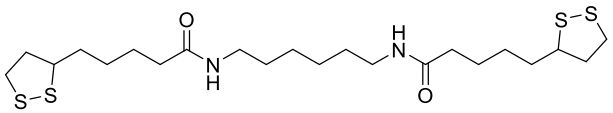

Lipoic acid (10 g, 2 equiv., 48.4 mmol), 1,6-hexanediamine (2.81 g, 1 equiv., 24.2 mmol), DMAP (5.91 g, 1 equiv., 48.4 mmol) were placed in an oven-dried 250 mL 2-neck round-bottom flask and back-filled with N_2. DCM (100 mL) was added to the flask and the mixture was stirred for *ca.* 10 min. Note: the DCM did not have to be rigorously dried and reagent grade solvent was adequate for the reaction. The reaction mixture was then cooled to 0 °C in an ice-water bath and EDC·HCl (9.28 g, 1 equiv., 48.4 mmol) was added portion-wise over 5 min. During the addition, white precipitate formed and after the addition was complete, the reaction was stirred at 0 °C, slowly warming in the bath overnight (c.a. 16 h). The reaction mixture was transferred to a 1 L separatory funnel and diluted with ~ 500 mL $CHCl_3$ (since solubility in DCM is poorer) to adequately dissolve the amide product. The organic layer was washed with 1 M HCl (3 x 200 mL), water (1 x 200 mL), saturated $NaHCO_3$ solution (3 x 200 mL), water (1 x 200 mL), and brine (1 x 200 mL). The organic layer was dried using $MgSO_4$ and concentrated *in vacuo* to reveal the title compound as a white solid (yield = 10.62 g, 89%). No further purification was necessary. ^{1}H NMR (400 MHz, Chloroform-*d*) *δ* 5.68 (s, 2H), 3.63 – 3.52 (m, 2H), 3.25 (q, J = 6.6 Hz, 4H), 3.22 – 3.06 (m, 4H), 2.46 (m, 2H), 2.26 – 2.16 (m, 4H), 1.91 (m, 2H), 1.76 – 1.61 (m, 8H), 1.54 – 1.40 (m, 8H), 1.35 (m, 4H). ^{13}C NMR (101 MHz, Chloroform-*d*) *δ* 172.91, 77.48, 77.16, 76.84, 56.63, 40.40, 39.05, 38.61, 36.67, 34.77, 29.61, 29.05, 26.05, 25.61. HRMS (ESI-TOF) (*m/z*): [M + H] calculated for $C_{22}H_{40}N_2O_2S_4$ H 493.2051; found 493.2061.

C_{TEG}A Synthesis

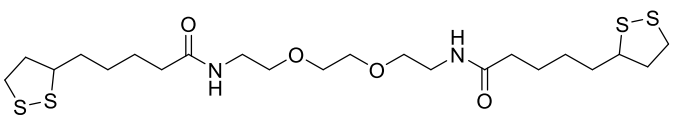

Lipoic acid (10 g, 2 equiv., 48.4 mmol), 1,8-diamino-3,6-dioxaoctane (3.58 g, 1 equiv., 24.2 mmol), DMAP (5.91 g, 1 equiv., 48.4 mmol)

were placed in an oven-dried 250 mL 2-neck round-bottom flask and back-filled with N_2. DCM (100 mL) was added to the flask and the mixture was stirred for *ca.* 10 min. Note: the DCM did not have to be rigorously dried and reagent grade solvent was adequate for the reaction. The reaction mixture was then cooled to 0 °C in an ice-water bath and EDC·HCl (9.28 g, 1 equiv., 48.4 mmol) was added portion-wise over 5 min. During the addition, white precipitate formed and after the addition was complete, the reaction was stirred at 0 °C, slowly warming in the bath overnight (c.a. 16 h). The reaction mixture was transferred to a 1 L separatory funnel and diluted with ~ 500 mL $CHCl_3$ (since solubility in DCM is poorer) to adequately dissolve the amide product. The organic layer was washed with 1 M HCl (3 x 200 mL), water (1 x 200 mL), saturated $NaHCO_3$ solution (3 x 200 mL), water (1 x 200 mL), and brine (1 x 200 mL). The organic layer was dried using $MgSO_4$ and concentrated *in vacuo* to reveal the title compound as a white solid (yield = 10.2 g, 80%). No further purification was necessary. ^{1}H NMR (400 MHz, Chloroform-*d*) δ 5.98 (s, 2H), 3.62 (s, 4H), 3.59 – 3.52 (m, 6H overlap), 3.46 (q, J = 5.2 Hz, 4H), 3.25 – 3.04 (m, 4H), 2.52 – 2.41 (m, 2H), 2.20 (t, J = 7.5 Hz, 4H), 1.97 – 1.86 (m, 2H), 1.79 – 1.59 (m, 8H), 1.59 – 1.35 (m, 4H). ^{13}C NMR (101 MHz, Chloroform-*d*) δ 172.94, 77.48, 77.16, 76.84, 70.33, 70.03, 56.54, 40.35, 39.24, 38.57, 36.48, 34.73, 28.99, 25.46. HRMS (ESI-TOF) (*m/z*): [M + H] calculated for $C_{22}H_{40}N_2O_4S_4$ H 525.1949; found 525.1960.

Synthesis of networks

Representative synthesis of C_6E-3T 1:1 using DBU

Trimethylolpropane tris(3-mercaptopropionate) (0.266 g, 1.00 molar equiv., 0.67 mmol) was weighed into a 20 mL scintillation vial. A 1.0 mL stock solution of disulfide monomer (1.0 mL, 1.50 molar equiv., 1.00 mmol) was added to the vial and the mixture was lightly mixed. A 100 mg·mL^{-1} stock solution of DBU (10.2 µL, 0.01 molar equiv., 0.067 mmol) was added in one portion, the mixture was vigorously shaken for 5-10 s and then poured onto a glass slide (L × W = 75 mm × 25 mm) to obtain thin films (c.a. 0.1 mm thickness). The film was left overnight (c.a. 16 h) to ensure solvent removal and then peeled off the substrate for analysis. In order to obtain thicker films (c.a. 1 mm thickness), the reaction was proportionally scaled up 3-fold (i.e. 3.0 mL of disulfide stock solution was used), mixed and left in the 20 mL scintillation vial. The vial was covered with an evaporating dish to ensure slower evaporation of the solvent (for more homogeneous film formation) and left overnight (c.a. 16 h) to dry.

Representative synthesis of C_6E-3T 8:1 using DBU

Trimethylolpropane tris(3-mercaptopropionate) (0.033 g, 1.00 molar equiv., 0.083 mmol) was weighed into a 20 mL scintillation vial. A 1.0 mL stock solution of disulfide monomer (1.0 mL, 12.00 molar equiv., 1.00 mmol) was added to the vial and the mixture was lightly mixed. A 100 mg·mL^{-1} stock solution of DBU (1.26 µL, 0.01 molar equiv., 0.00083 mmol) was added in one portion, the mixture was vigorously shaken for 5-10 s and then poured onto a glass slide (L × W = 75 mm × 25 mm). The film was left overnight (*ca*. 16 h) and then peeled off the substrate for analysis.

C_6E-3T Networks

Ratio 1:1 T_g (DSC) = -37 °C. $T_{d,5\%}$ (TGA) = 254 °C. FTIR 1726 cm^{-1} (C=O ester)

Ratio 2:1 T_g (DSC) = -40 °C. $T_{d,5\%}$ (TGA) = 264 °C. FTIR 1726 cm^{-1} (C=O ester)

Ratio 4:1 T_g (DSC) = -42 °C. $T_{d,5\%}$ (TGA) = 275 °C. FTIR 1726 cm^{-1} (C=O ester)

Ratio 8:1 T_g (DSC) = -56 °C. $T_{d,5\%}$ (TGA) = 274 °C. FTIR 1726 cm^{-1} (C=O ester)

Ratio 16:1 T_g (DSC) = -51 °C. $T_{d,5\%}$ (TGA) = 277 °C. FTIR 1726 cm^{-1} (C=O ester)

C_{TEG}E-3T Networks

Ratio 1:1 T_g (DSC) = -39 °C. $T_{d,5\%}$ (TGA) = 234 °C. FTIR 1726 cm^{-1} (C=O ester)

Ratio 4:1 T_g (DSC) = -39 °C. $T_{d,5\%}$ (TGA) = 272 °C. FTIR 1726 cm^{-1} (C=O ester)

Ratio 8:1 T_g (DSC) = -33 °C. $T_{d,5\%}$ (TGA) = 277 °C. FTIR 1726 cm^{-1} (C=O ester)

C_{TEG}A-3T Networks

Ratio 1:1 T_g (DSC) = -28 °C. $T_{d,5\%}$ (TGA) = 263 °C. FTIR 1732 cm^{-1} (C=O ester) 1644 cm^{-1} (C=O Amide) 3294 cm^{-1} (N-H)

Ratio 4:1 T_g (DSC) = 4 °C. $T_{d,5\%}$ (TGA) = 265 °C. FTIR 1732 cm^{-1} (C=O ester) 1637 cm^{-1} (C=O Amide) 3297 cm^{-1} (N-H)

Ratio 8:1 T_g (DSC) = -8 °C. $T_{d,5\%}$ (TGA) = 266 °C. FTIR 1729 cm^{-1} (C=O ester) 1640 cm^{-1} (C=O Amide) 3292 cm^{-1} (N-H)

NMR Spectra Collected for Monomers

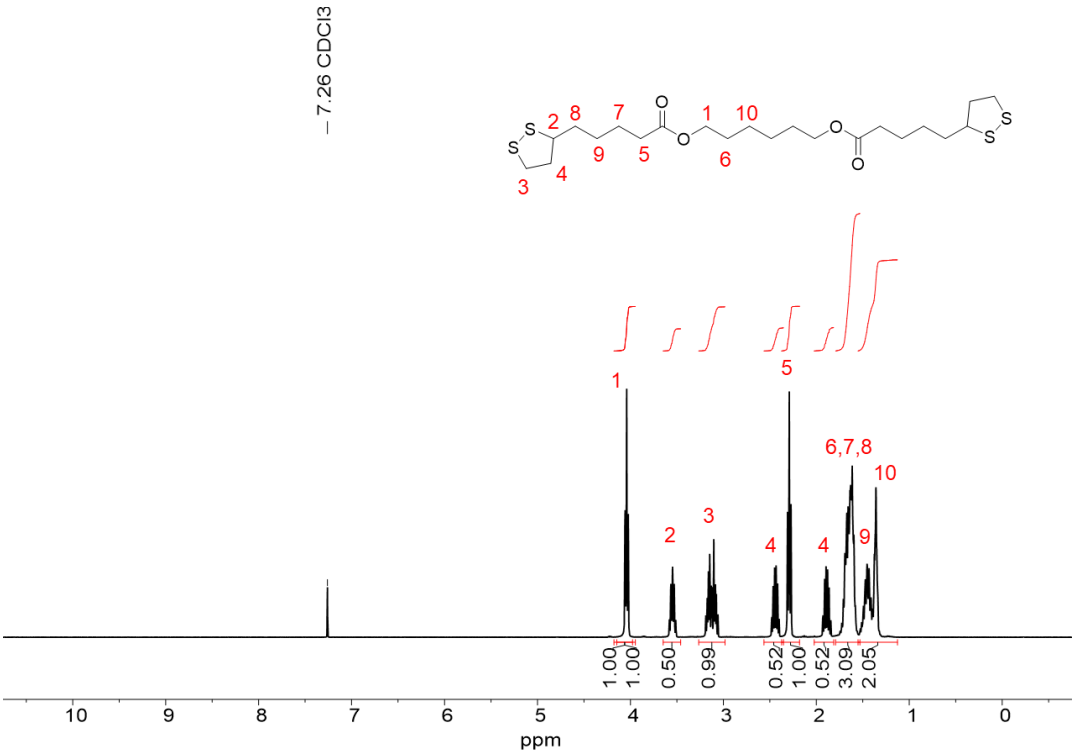

Figure S1. ^{1}H NMR Spectrum of C_6E (400 MHz, 298 K, $CDCl_3$).

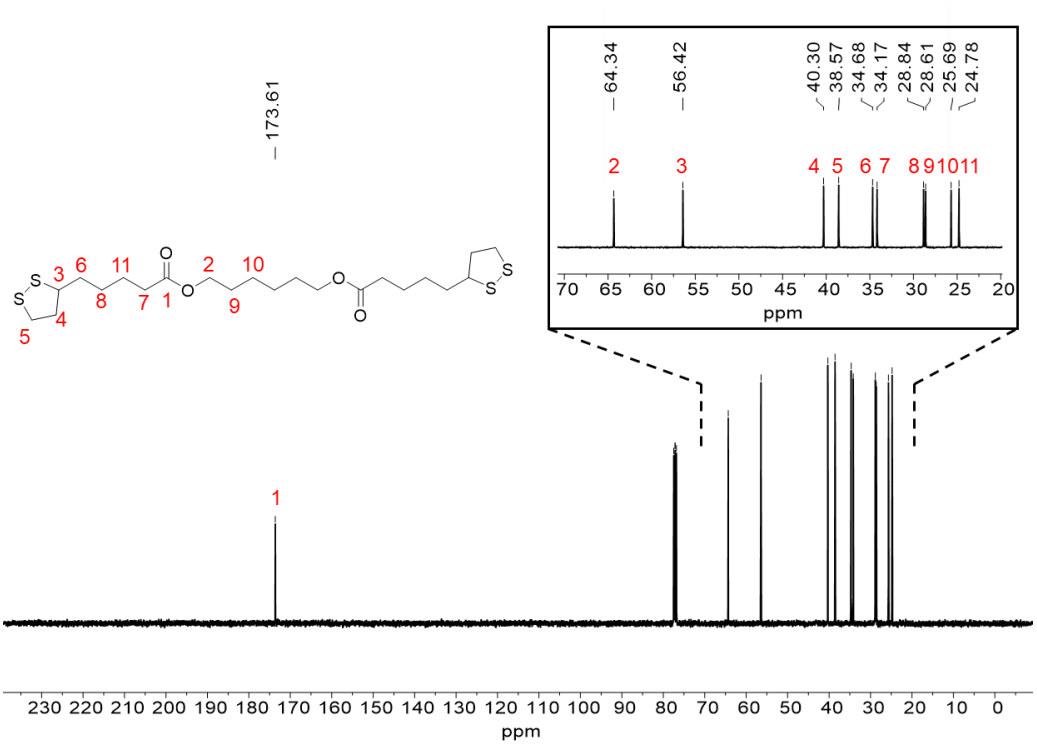

Figure S2. ^{13}C NMR Spectrum of C_6E (101 MHz, 298 K, $CDCl_3$).

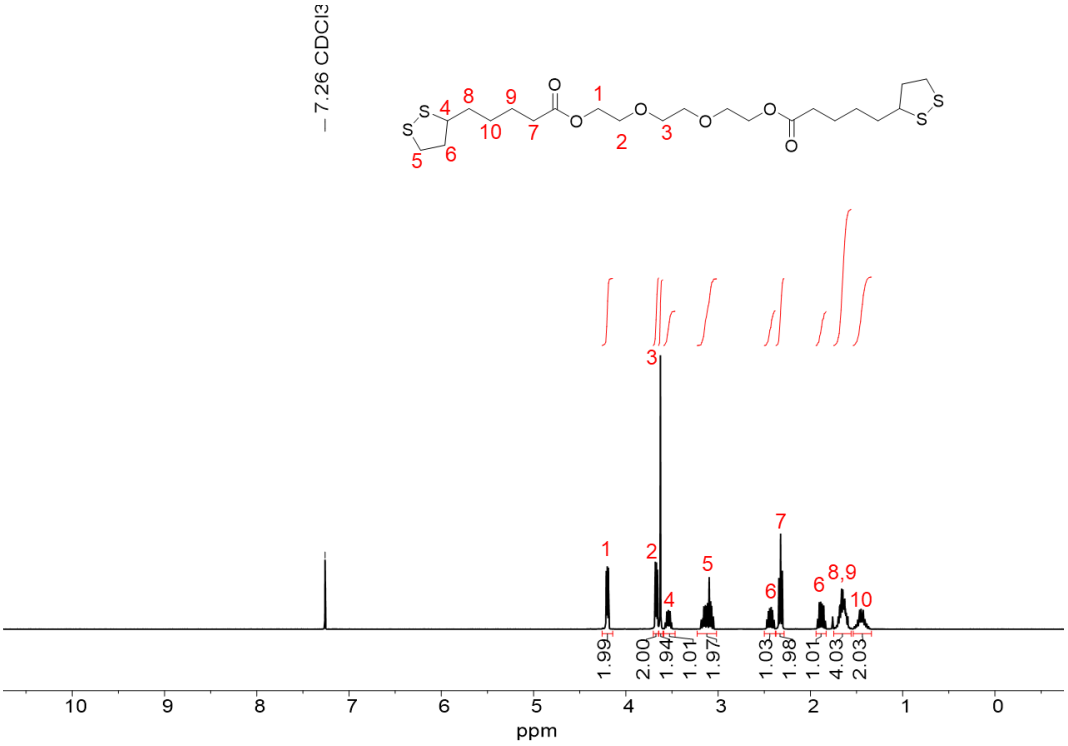

Figure S3. ^{1}H NMR Spectrum of $C_{TEG}E$ (400 MHz, 298 K, $CDCl_3$).

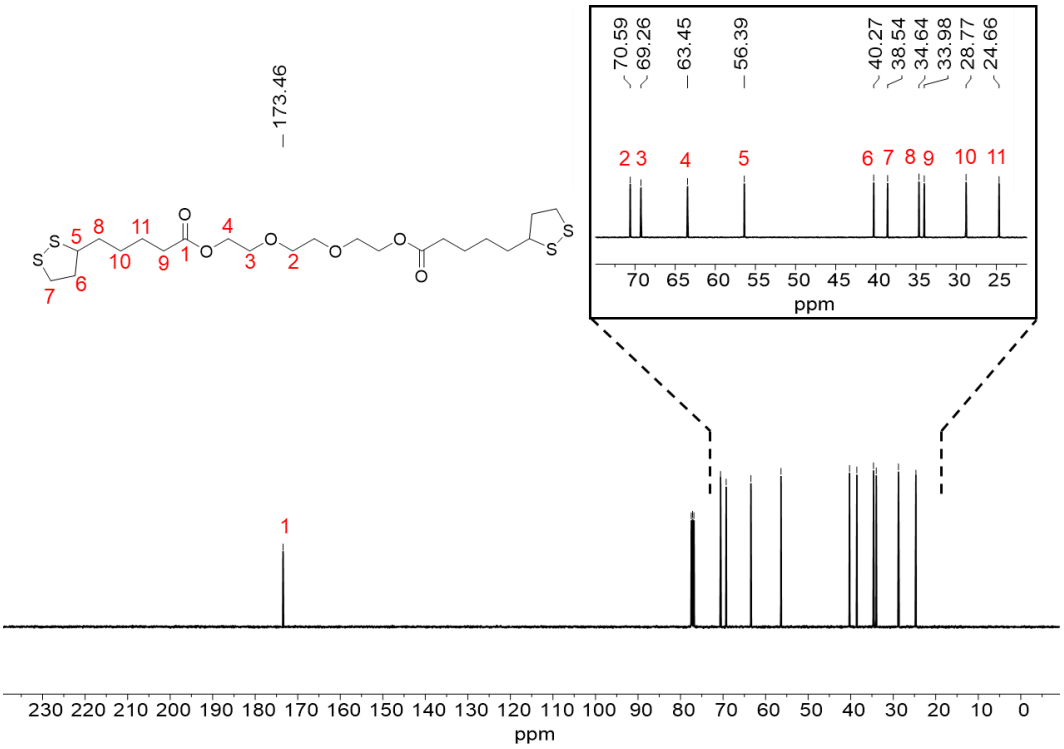

Figure S4. ^{13}C NMR Spectrum of $C_{TEG}E$ (101 MHz, 298 K, $CDCl_3$).

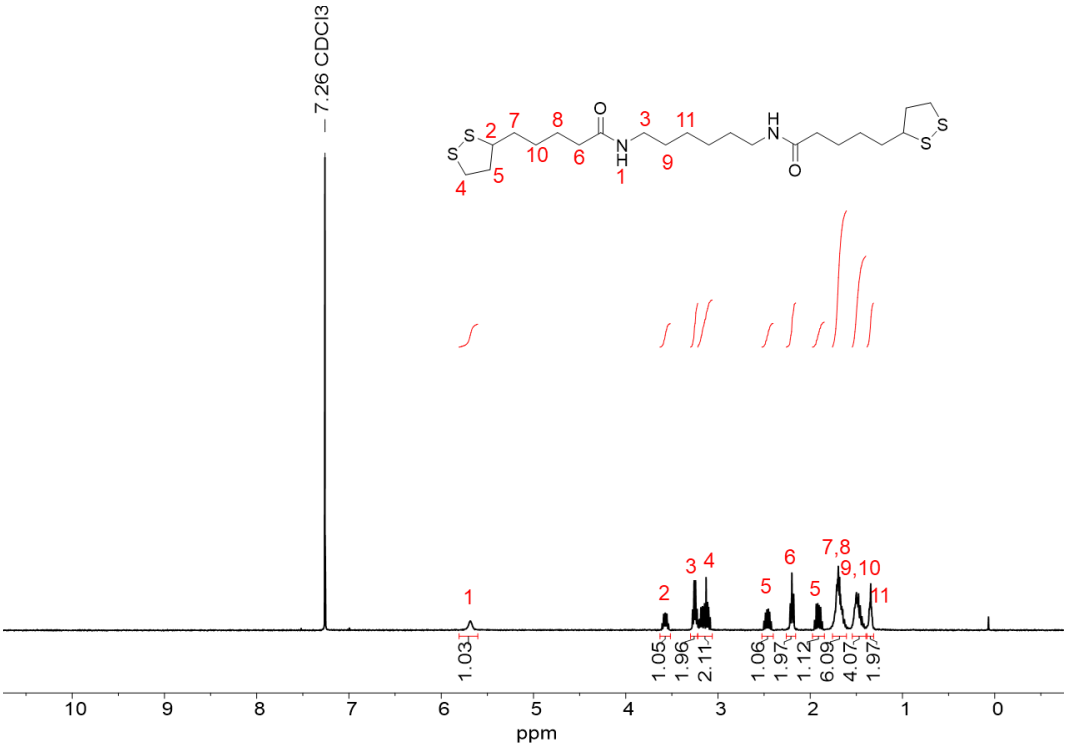

Figure S5. ^{1}H NMR Spectrum of C_6A (400 MHz, 298 K, $CDCl_3$).

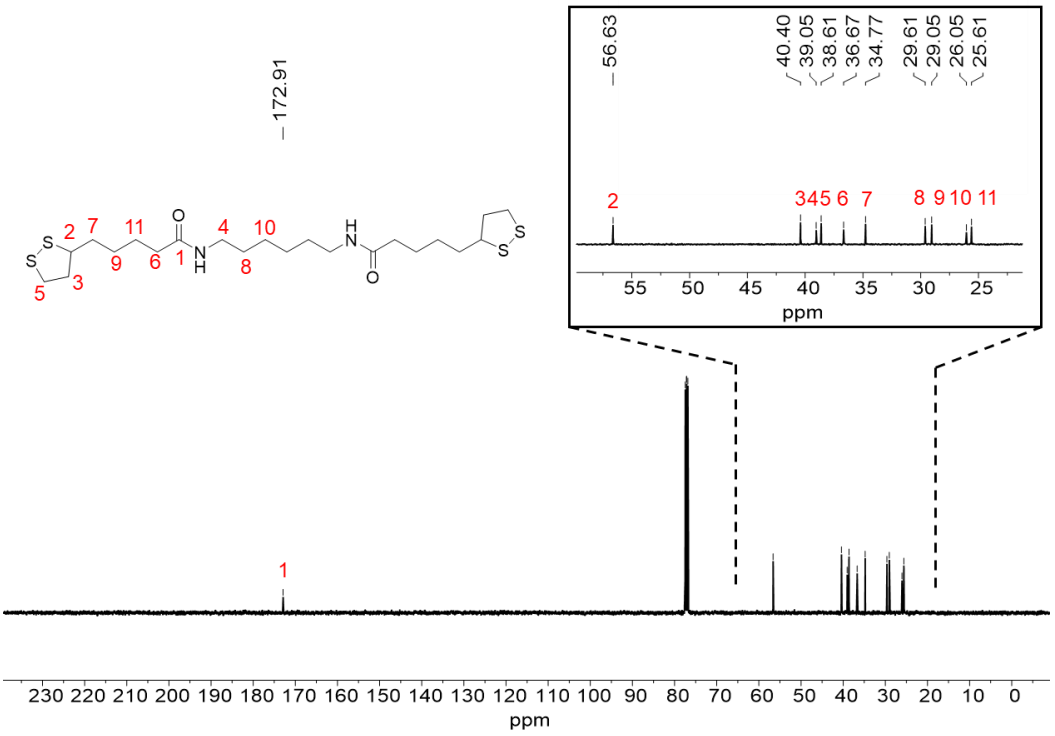

Figure S6. ^{13}C NMR Spectrum of C_6A (101 MHz, 298 K, $CDCl_3$).

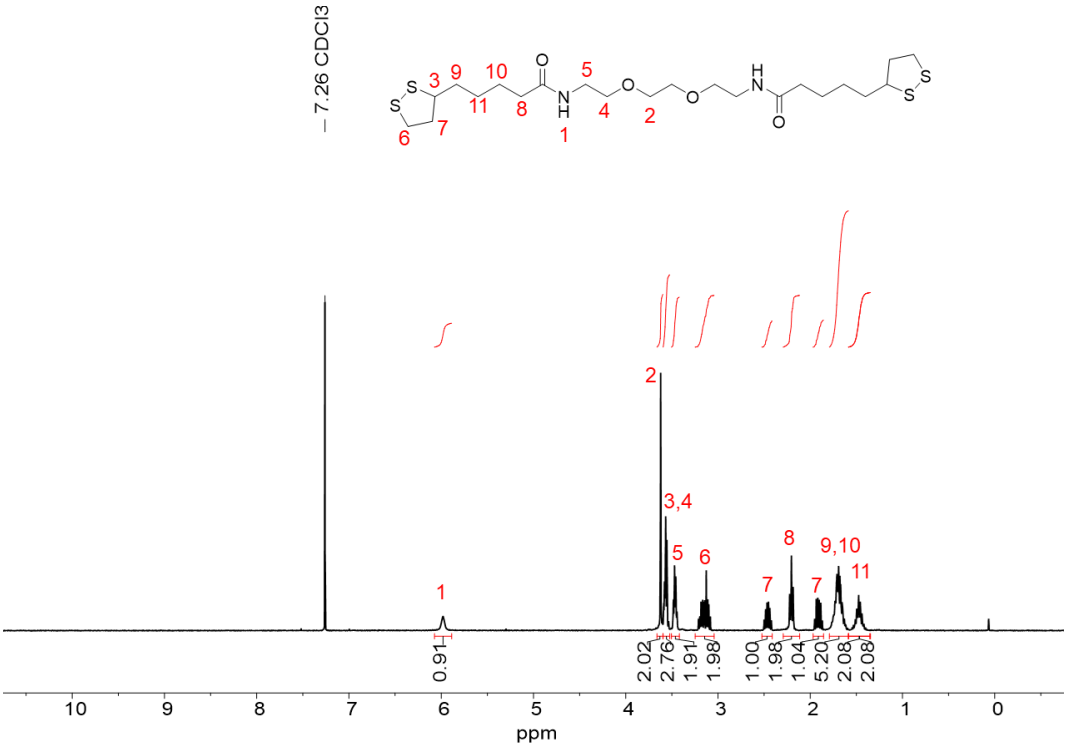

Figure S7. ^{1}H NMR Spectrum of $C_{TEG}A$ (400 MHz, 298 K, $CDCl_3$).

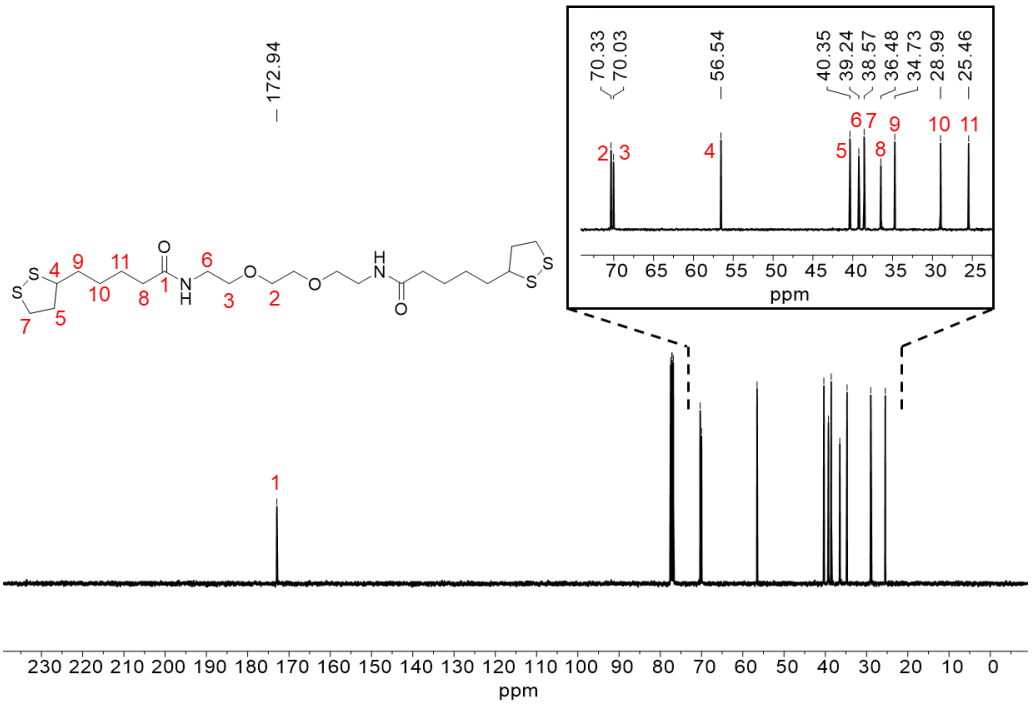

Figure S8. ^{13}C NMR Spectrum of $C_{TEG}A$ (101 MHz, 298 K, $CDCl_3$).

FTIR Data

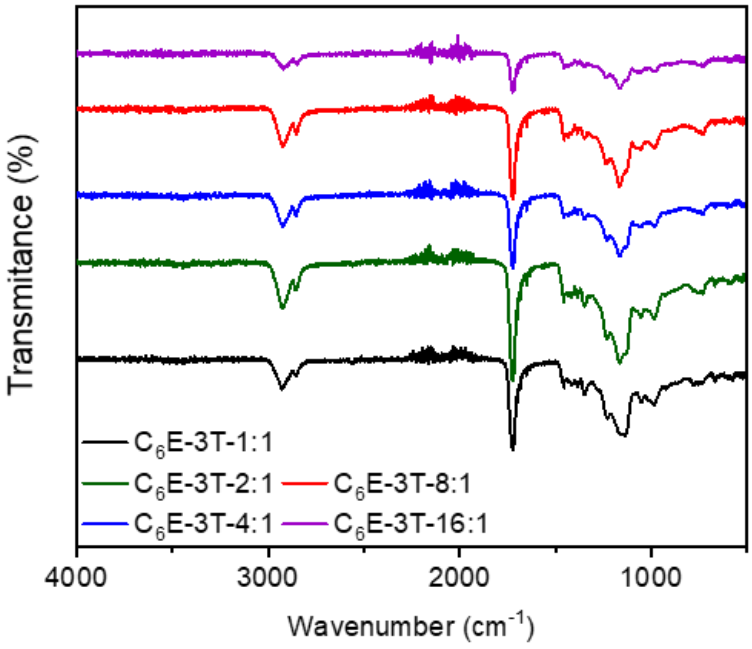

Figure S9. FTIR spectra of C_6E-3T networks.

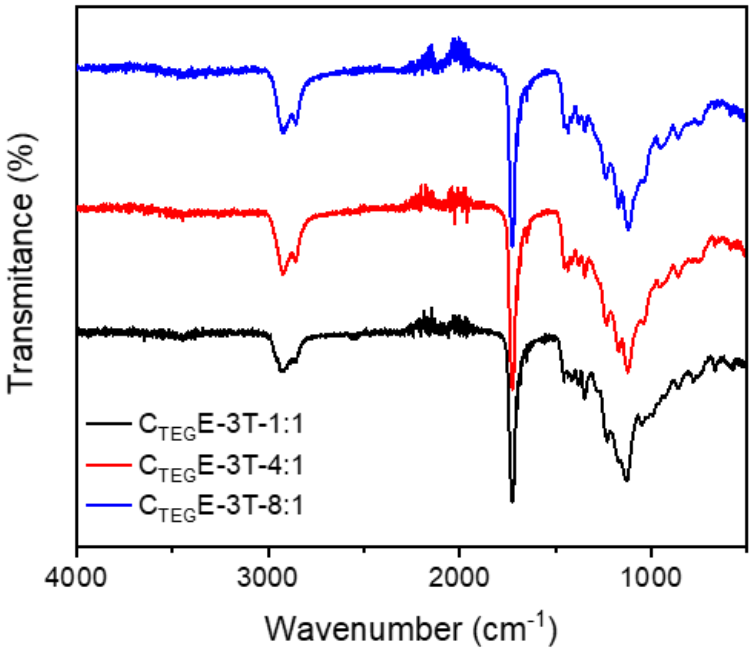

Figure S10. FTIR spectra of C_{TEG}E-3T networks.

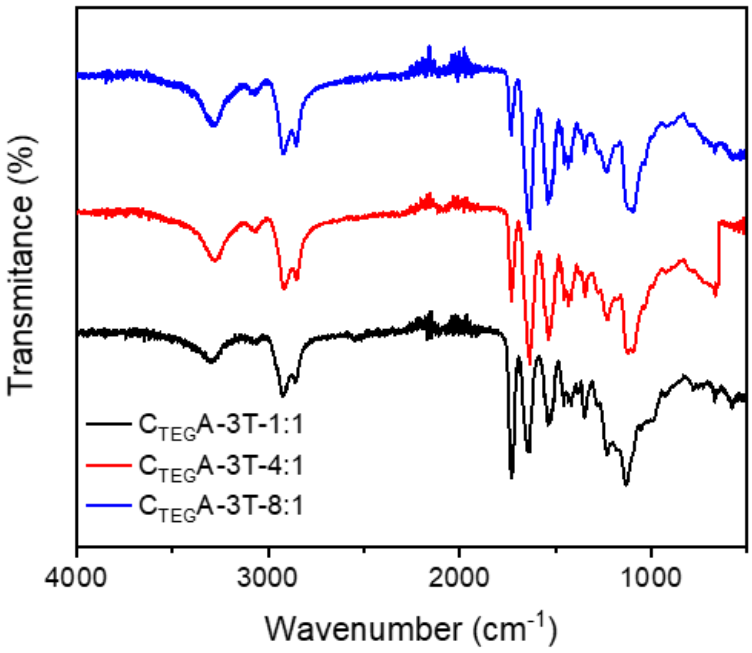

Figure S11. FTIR spectra of C_{TEG}A-3T networks.

DSC Data

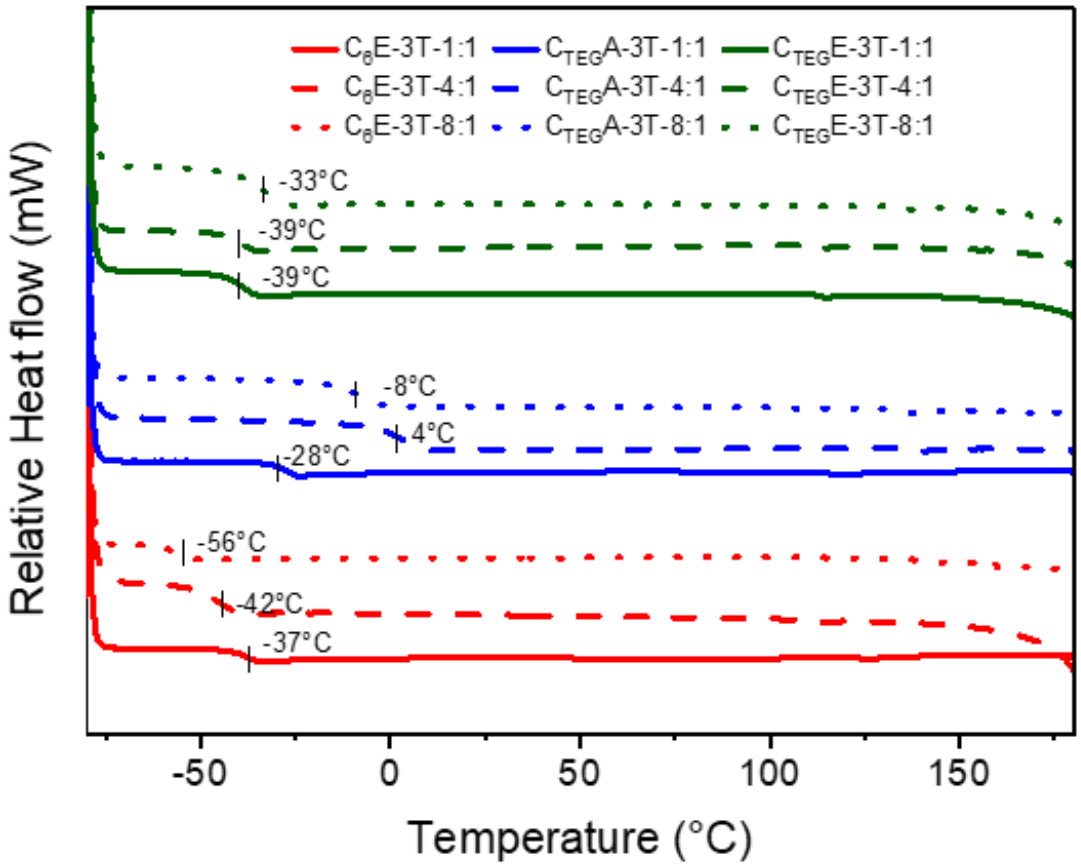

Figure S12. DSC thermograms of 2nd heating cycles for all networks at various ratios from −80 to 180 °C, 10 °C min^{-1}.

TGA Data

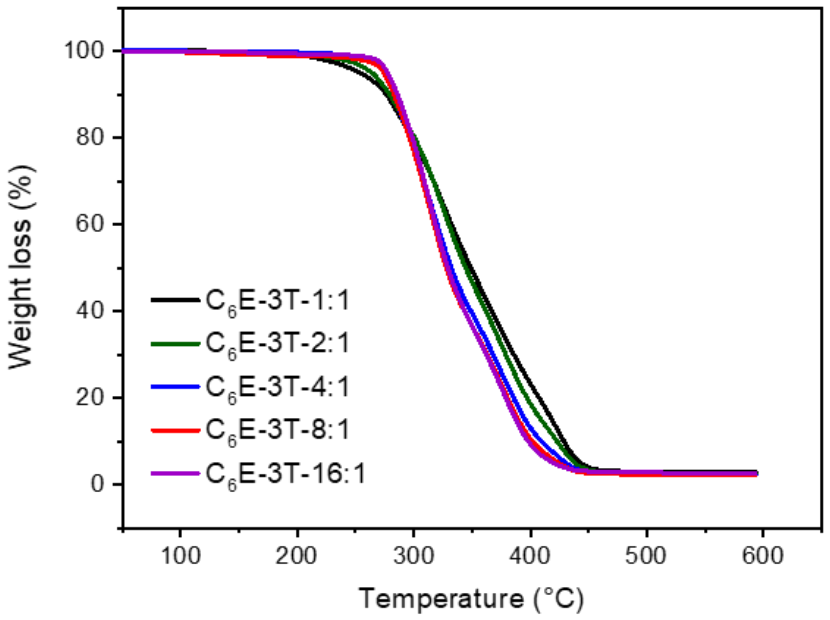

Figure S13. TGA thermograms of C_6E-3T networks.

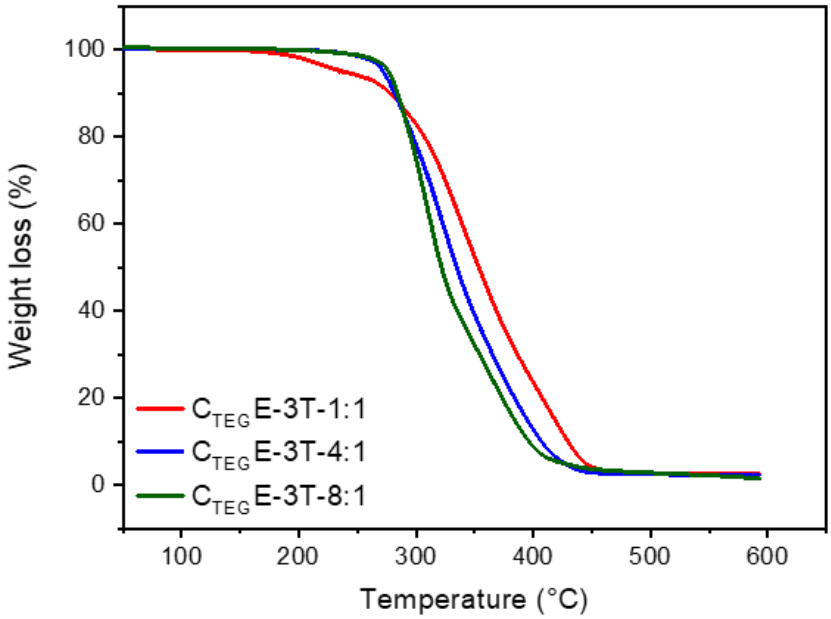

Figure S14. TGA thermograms of C_{TEG}E-3T networks.

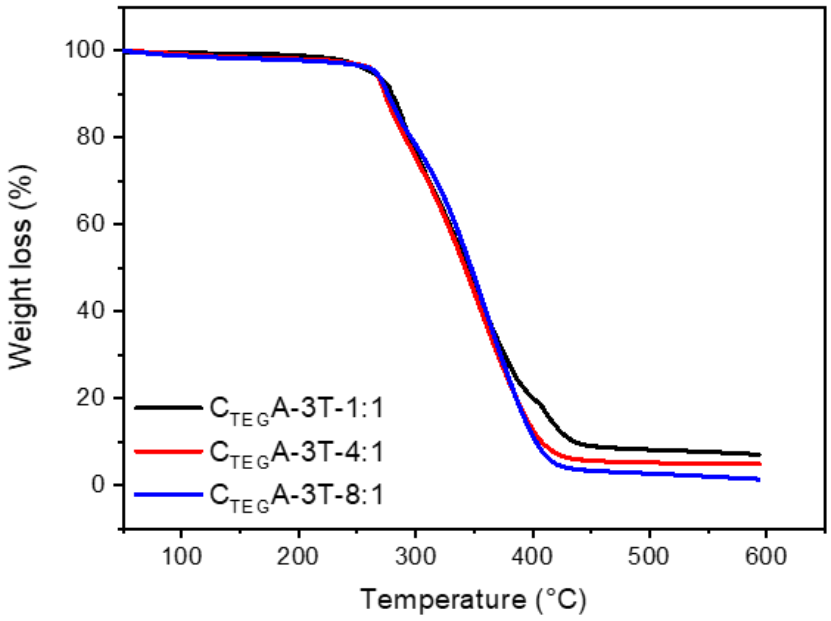

Figure S15. TGA thermograms of C_{TEG}A-3T networks.

Rheology Data

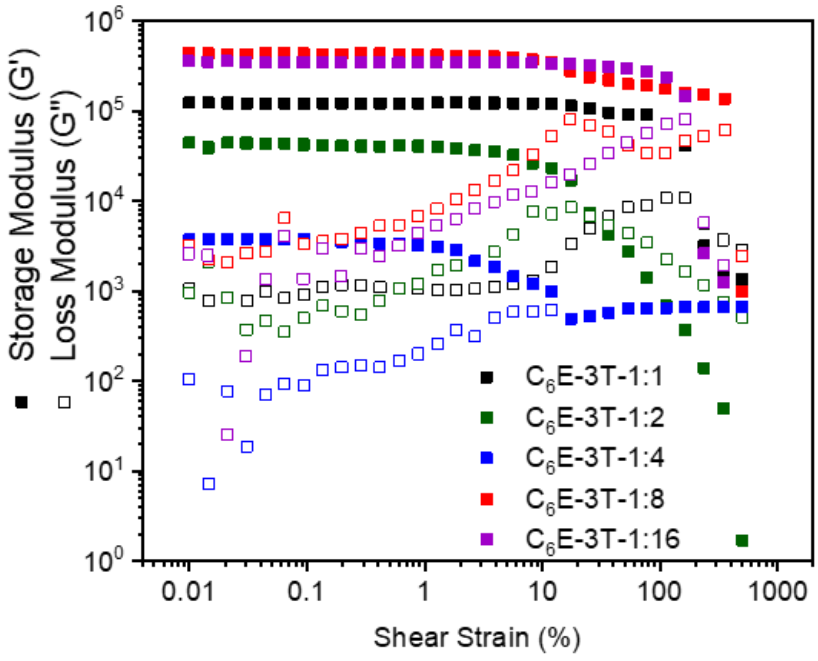

Figure S16. Strain sweeps of C_6E-3T networks.

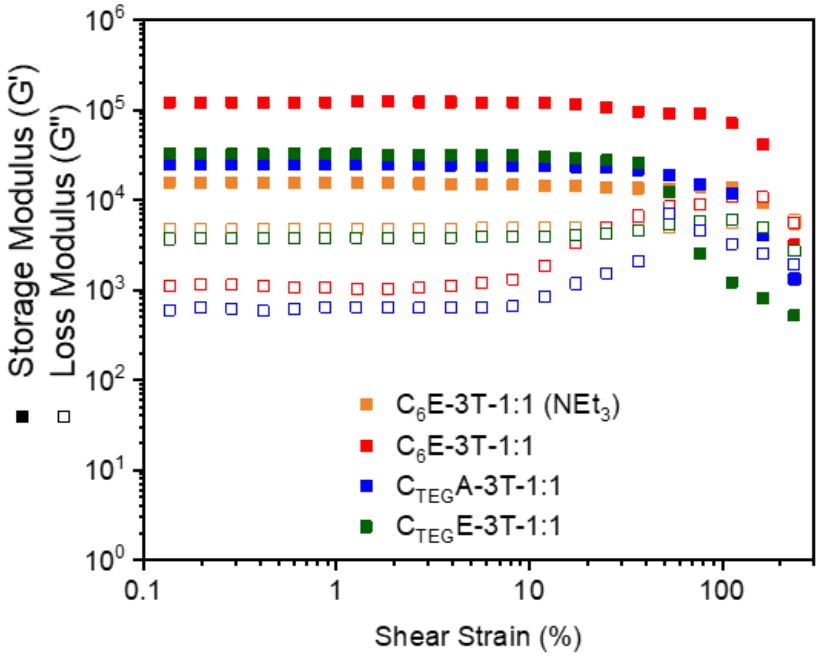

Figure S17. Strain sweeps of all networks at 1:1 ratio.

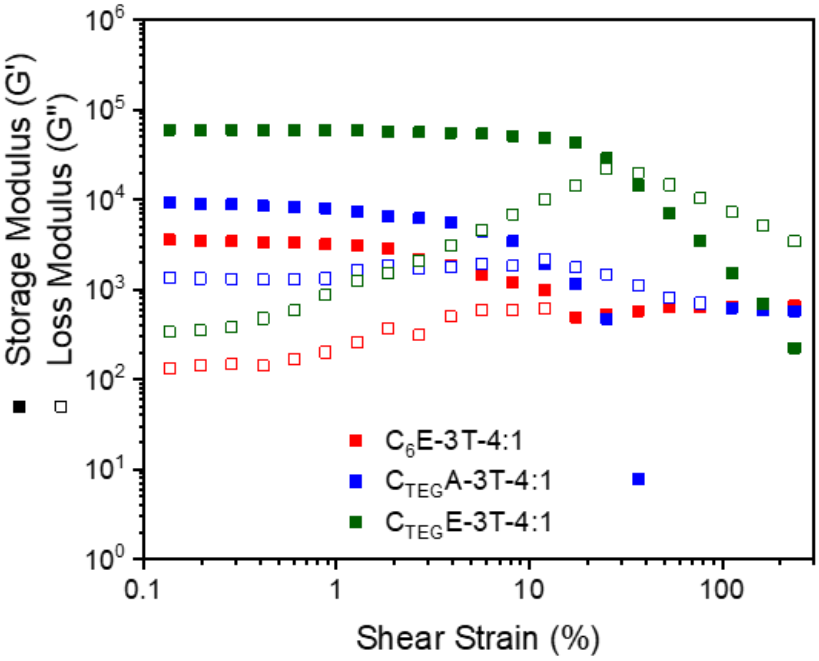

Figure S18. Strain sweeps of all networks at 4:1 ratio.

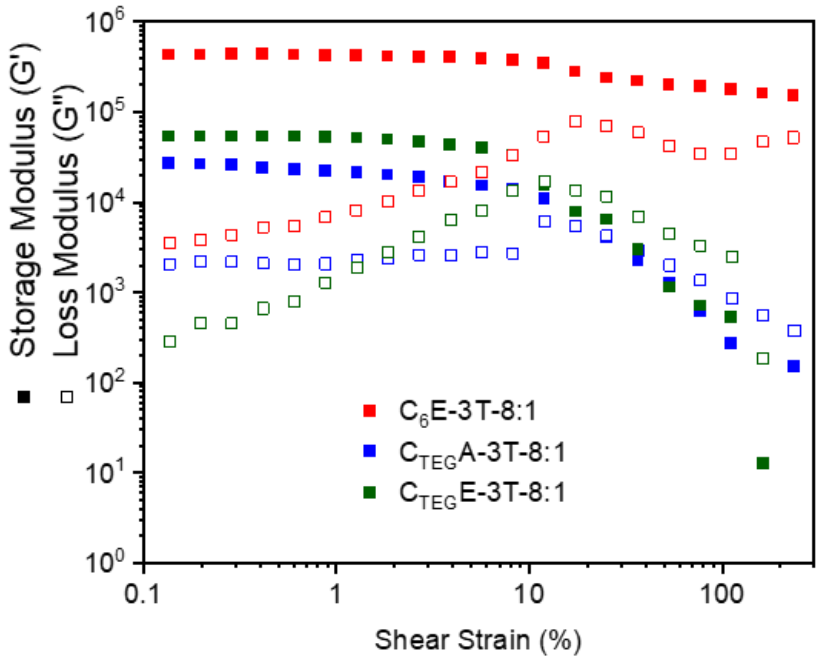

Figure S19. Strain sweeps of all networks at 8:1 ratio.

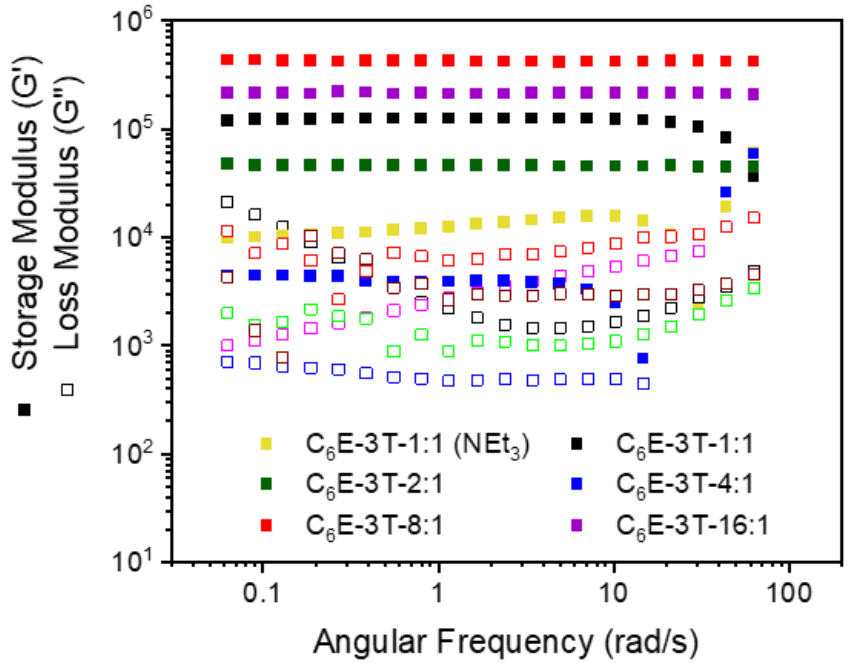

Figure S20. Frequency sweeps of all C_6E-3T networks.

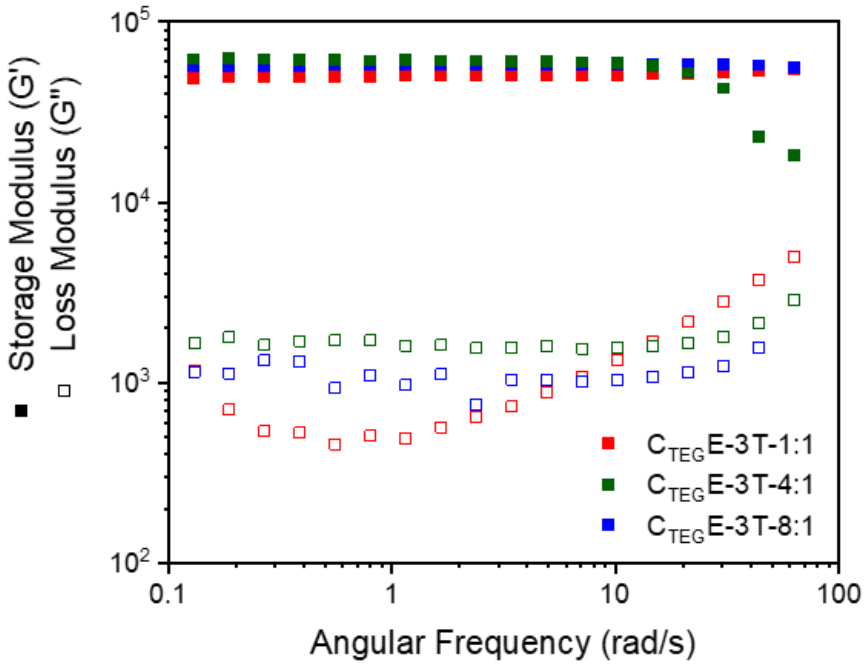

Figure S21. Frequency sweeps of C_{TEG}E-3T networks.

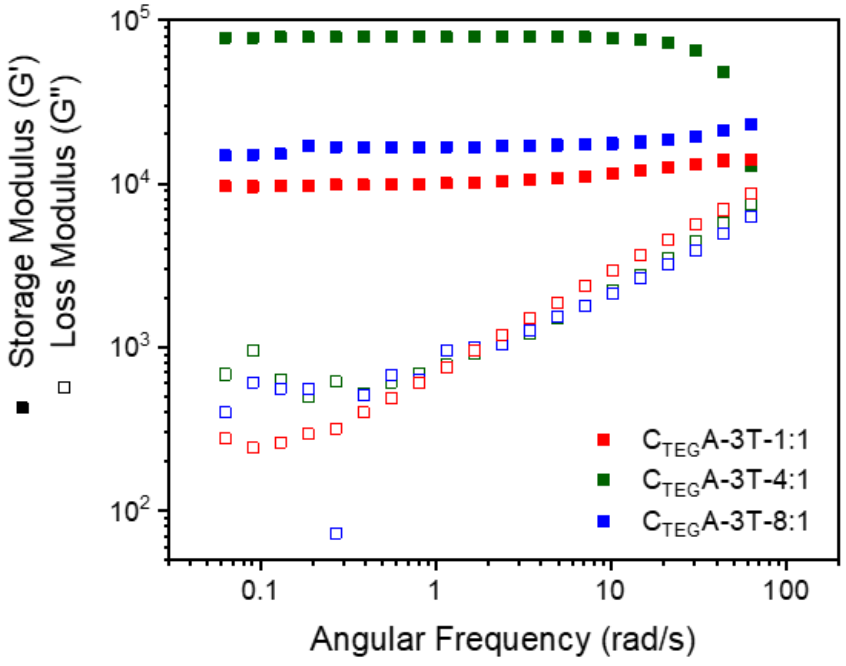

Figure S22. Frequency sweeps of C_{TEG}A-3T networks.

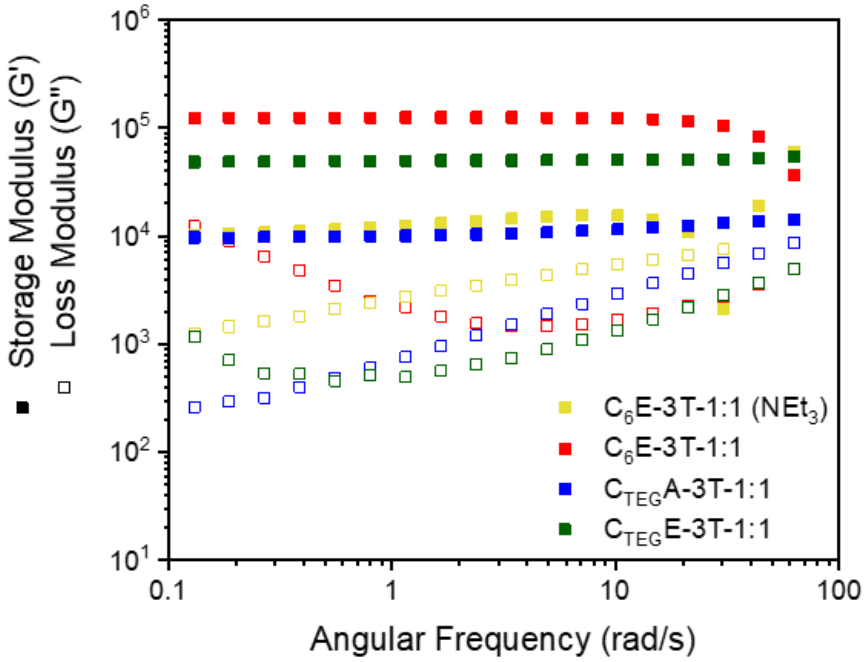

Figure S23. Frequency sweeps of all networks at 1:1 ratio.

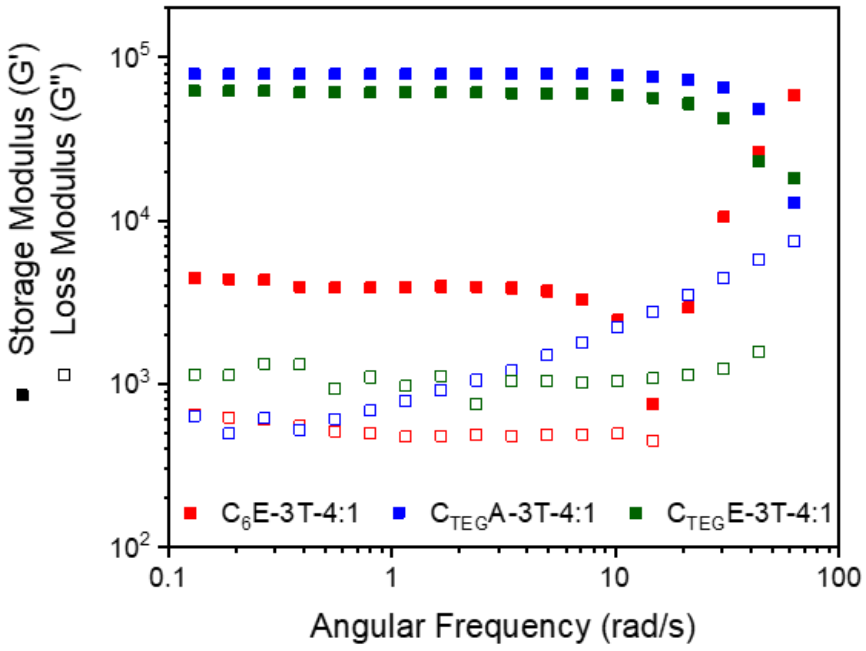

Figure S24. Frequency sweeps of all networks at 4:1 ratio.

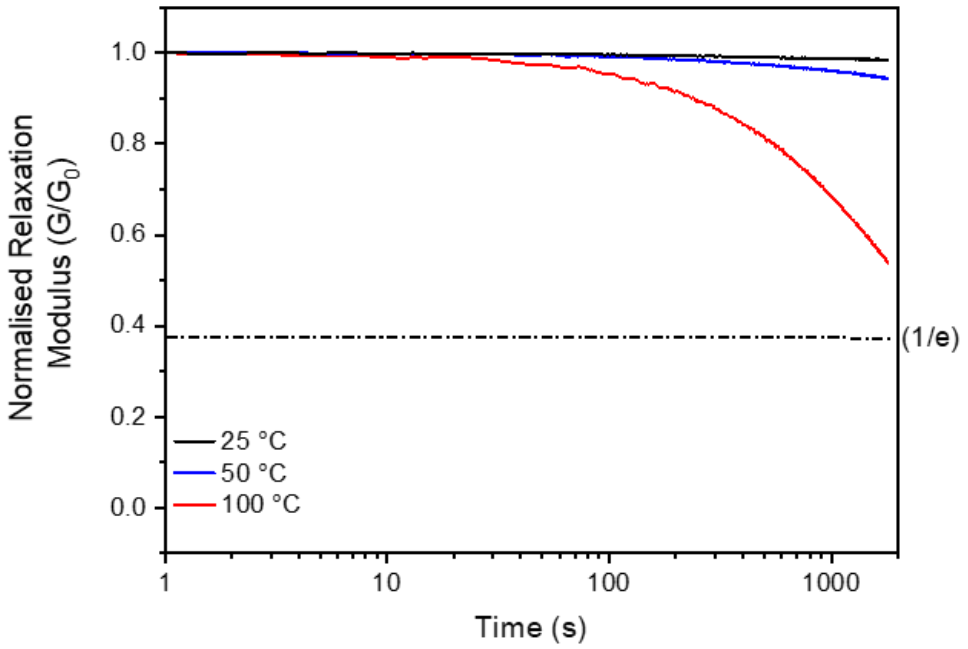

Figure S25. Stress relaxation of the C_{TEG}E-3T-8:1 network at various temperatures.

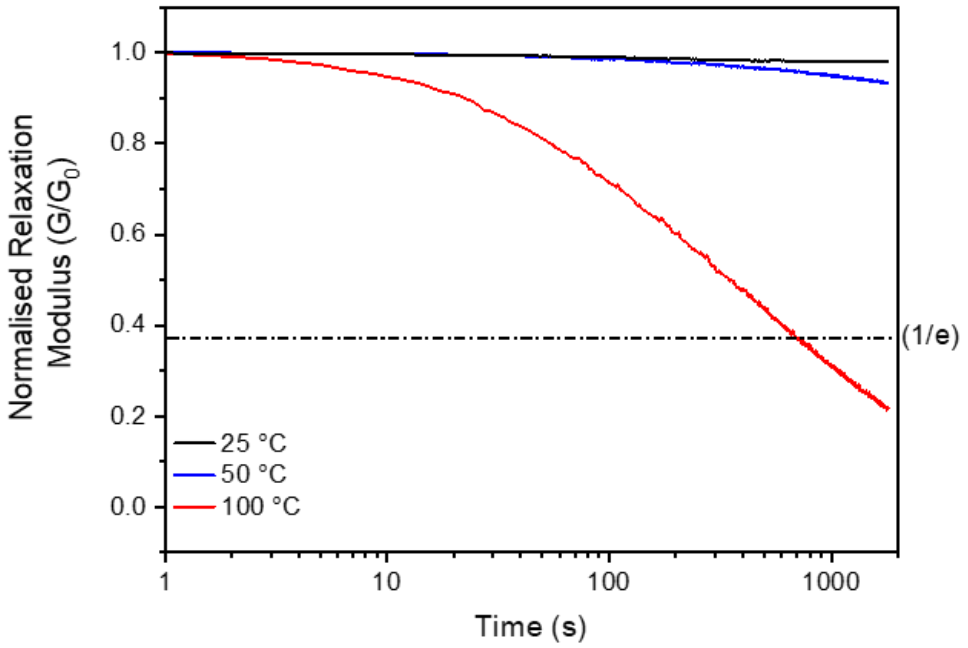

Figure S26. Stress relaxation of the C_{TEG}A-3T-8:1 network at various temperatures.

Thermal reprocessing of films

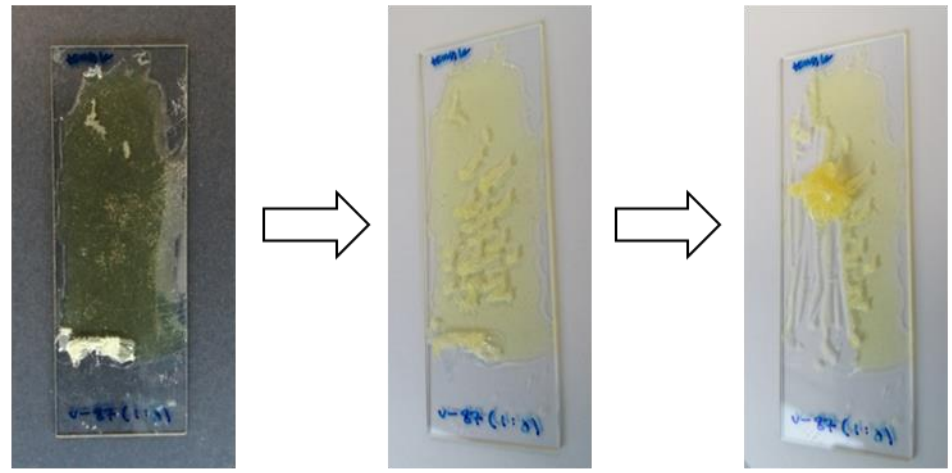

Figure S27. Photographs of C_6A-3T-8:1 network that was thermally reprocessed at 180 °C.

Chemical recycling of films

Table S1. Summary of chemical recycling experiments for C_6E-3T networks at 22 °C (40 mg/mL).

Network ratio (disulfide:thiol)	Mass (mg)	[a]Volume of solution (mL)	Concentration of solution (M)	[b]Approximate time for full dissolution (s)
1:1	200	5	0.01	210
1:1	150	3.75	0.05	95
8:1	200	5	0.01	180
8:1	150	3.75	0.05	90
8:1 (reprocessed film)	150	3.75	0.05	130

[a]Volume was adjusted for experiments to ensure same overall concentration of network relative to solvent. [b]Estimated time at which no network particles were visible.

DMA Data

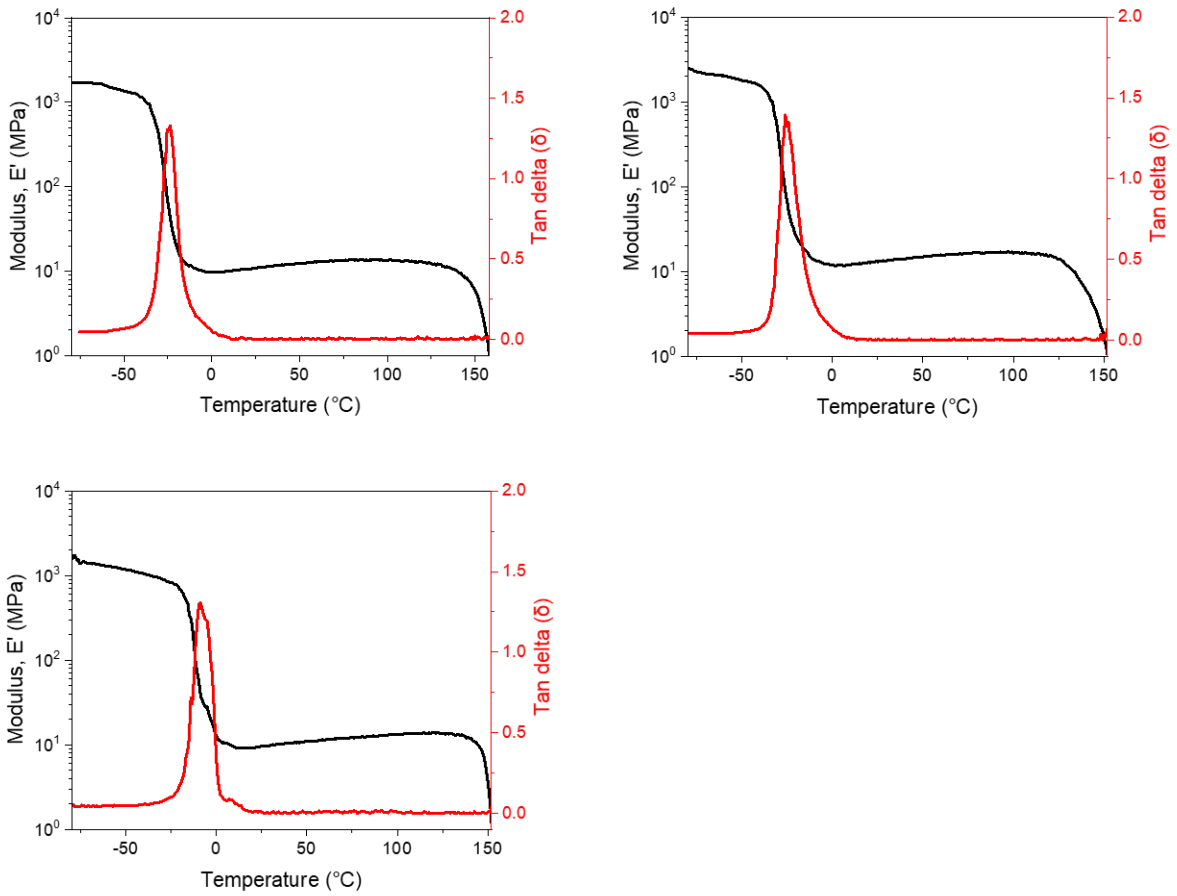

Figure S28. DMA temperature sweep for C_6E-3T-8:1 (n = 3). Summary of results are shown in Table S3.

Summary of Network Properties

Table S2. Physical, thermal and mechanical properties for networks with varied compositions.

Network	Ratio	[a]T_g (DSC)	[b]T_d (5% loss)	[c]τ at 50 °C (s)	[c]τ at 100 °C (s)	[d]Storage Modulus (kPa)
C_6E-3T	1:1	−37	254			120
	2:1	−40	264			47
	4:1	−42	275			4.4
	8:1	−56	274	**	80	431
	16:1	−51	277			213
C_{TEG}E-3T	1:1	−39	234			48
	4:1	−39	272			62
	8:1	−33	277	**	**	56
C_{TEG}A-3T	1:1	−28	263			9.6
	4:1	4	265			78
	8:1	−8	266	**	708	15

[a]Glass transition temperature determined from 2nd DSC heating run. [b]Thermal degradation temperature at 5% weight loss determined from TGA [c]Relaxation time determined to be the time required to reach 37% (1/e) of the initial stress value on normalized relaxation modulus (G/G_0) based on Maxwell model[1] (**relaxation time was not reached within 1800s). [d]Storage modulus determined from the dynamic strain sweep on rheometer.

Table S3. Summary of DMA and tensile data for C_6E-3T-8:1 network.

Network	Ratio	[a]T_g (DMA)	[b]Storage Modulus, *E'*, (MPa) at −70 °C	[b]Storage Modulus, *E'*, (MPa) at 25 °C	[c]Flow Temp. (°C)	[d]Youngs Modulus (MPa)	[d]Strain at break (%)	[d]Stress at break (MPa)
C_6E-3T	8:1	−20 ± 8	1748 ± 294	11.2 ± 1.2	145 ± 8	9.1 ± 1.9	19 ± 2.2	1.8 ± 0.4

[a]Glass transition temperature determined from tan δ of DMA temperature sweep from −80 to 180 °C, 5 °C min^{-1}. [b]Storage modulus determined during DMA temperature sweep at −70 °C and 25 °C. [c]Flow temperature determined from DMA temperature sweep and calculated by the 1st derivative of the modulus versus temperature after the rubbery plateau region. [d] Young's modulus, strain at break and stress at break determined from uniaxial tensile testing at 22 °C, 10 mm min^{-1} strain rate. All uncertainties are reported as 1 S.D.

References

1. B. M. El-Zaatari, J. S. A. Ishibashi and J. A. Kalow, *Polym. Chem.*, 2020, **11**, 5339-5345.

CHAPTER 5: CONCLUSION AND OUTLOOK

The aim of this thesis was to develop a framework to investigate methods and techniques for improving the reprocessability and recyclability of thermosets using covalent adaptable networks (CANs) instead of the typical permanent crosslinks. The use of dynamic covalent bonds to create CANs is known to come with the risk of sacrificing the polymer mechanical properties. Hence, the investigations made in this thesis have focused on developing novel CANs with tunable thermomechanical properties.

In chapter 2, we initially explored the reversibility of nucleophilic thiol-yne addition reaction as a selected platform for our investigation, initially in small molecule studies between unsaturated internal ynone substrates and monofunctional thiols. One of the key findings of this study was that there was dynamic exchange between the single-addition products of thiol-yne addition reaction. The proposed thiol-yne reaction was then extended to material synthesis by reacting diynone monomers with commercially available dithiols to create linear prepolymers, which were subsequently crosslinked using a multivalent thiol to form the desired CANs. Furthermore, changing the crosslink density as well as the dithiol structure allowed easy access to a large range of properties. Most importantly, one of these CANs has shown excellent mechanical properties, superior to those of available elastomers *i.e.,* tensile strength above 24 MPa and elongation at break near 1000%, with rapid relaxation time of 43 s at relatively low temperature (140 °C). As a result of its versatility and excellent dynamicity, the proposed reaction was adapted in chapter 3 to further explore different ways of tuning the thermomechanical properties of CANs.

In chapter 3, our investigation of improving the reprocessability and recyclability of CANs has extended to explore the effects of varying the chemical composition of ynone

monomers and dithiol chain extenders. The synthesis procedure was conceptually built on a similar approach to chapter 2 where a straightforward reaction between diynone and dithiol is conducted to create a linear prepolymer, which is then crosslinked using multivalent thiol. However, herein ynone monomers of different aliphatic length as well as an aromatic ynone were synthesised and copolymerised with a commercially available dithiol using same crosslink density. The study concluded that short aliphatic ynone spacer forms stiffer network, while increasing the length of the aliphatic ynone spacer decrease the network stiffness. Moreover, the use of aromatic ynone instead of aliphatic increase the stiffness to a large extent. As a result of screening various compositions, a robust CAN (ultimate tensile strength = 26 ± 0.8 MPa, elongation at break = 965.3 ± 34%) was successfully synthesised and characterised.

Finally, in order to improve both the recyclability and the sustainability of CANs, bio-mass derived lipoic acid (LA) was used to synthesise CANs with tunable mechanical properties in chapter 4. First, the lipoic acid (LA) was converted into a series of bifunctional monomers that contained the dynamic cyclic disulfide moiety. These monomers were then directly crosslinked using commercially available multivalent thiol in the presence of a base catalyst to form simple disulfide-based CANs. Furthermore, varying the cyclic disulfide monomer to thiol ratio gave an easy access to CANs with different thermal and rheological properties. Similarly, changing the composition of the disulfide monomers also provided CANs with different properties. In general, all CANs were soft and rubbery at room temperature as a result of their very low glass transition temperatures ≤ -37 °C with one CAN being relatively a strong rubber (ultimate tensile strength = 1.8 ± 0.4 MPa). Lastly, chemical recycling of the best performed CAN was

also conducted by simple dilution of the network in a solvent containing organo-base catalyst.

The dynamicity of thiol-yne addition and disulfide reaction has paved the way for the development of CANs. While both of these reactions have been implemented in dynamic networks, they are still being used actively in this area and have the potential to significantly enrich the field of CANs. The results obtained throughout this thesis justify further study in developing the recyclability of thermosets using CANs. More specifically, enhancing the stability of the reprocessed CANs as well maintaining their thermomechanical properties. Moreover, consequential effort to expand the library of dynamic biomass-derived monomers is also anticipated.

The advantages of having an extra double bond available for further functionalisation and/or tunning the thermomechanical properties, the simplicity, and the efficiency of the reaction positions thiol-yne addition reaction as a promising versatile reaction in the field of CANs. As a result, wide potential applications for thiol-yne addition in the field of dynamic network is anticipated including automotive, biomedical, painting and coating, along with others. On the other hand, the versatility and facile thiol-disulfide exchange have caused considerable interest within the research community with wide applications includes biomedical, 3D-printing, and others. While both thiol-yne addition and thiol-disulfide reactions have many interesting features that enrich the library of suitable dynamic network, there is still room for improvement and a noticeable trend in the filed on dynamic network is moving toward synthesising CANs from sustainable feedstock. Achieving dynamic network with reasonable thermomechanical properties from sustainable feedstock will have the potential to replace many commercially available crosslinked polymers.